GEORGIA INSTITUTE OF TECHNOLOGY
OFFICE OF CONTRACT ADMINISTRATION
SPONSORED PROJECT INITIATION

Date: 10/29/79

Project Title: A Generalized Wake-Integral Approach for Drag Determination in Three-Dimensional Flows

Project No: E-16-655

Project Director: Dr. James C. Wu

Sponsor: National Science Foundation

Agreement Period: From 9/15/79 Until ~~2/28/82~~ 6/30/82
(Grant Period - includes 6-months unfunded flexibility period)

Type Agreement: Grant No. ENG - 7900891

Amount: $156,747 (NSF)
3,083 (GIT E-16-341)
$159,830 TOTAL

Reports Required: Annual Progress Report; Final Project Report

Sponsor Contact Person (s):

Technical Matters

George K. Lea
National Science Foundation
Washington, D.C. 20550
Phone: 202/632-5787

Contractual Matters
(thru OCA)

Aileen Buie
National Science Foundation
Washington, D.C. 20550
Phone: 202/632-5965

Defense Priority Rating: N/A

Assigned to: Aerospace Engineering (School/Laboratory)

COPIES TO:

Project Director
Division Chief (EES)
School/Laboratory Director
Dean/Director–EES
Accounting Office
Procurement Office
Security Coordinator (OCA)
Reports Coordinator (OCA)
Library, Technical Reports Section
EES Information Office
EES Reports & Procedures
Project File (OCA)
Project Code (GTRI)
Other C. E. Smith

GEORGIA INSTITUTE OF TECHNOLOGY OFFICE OF CONTRACT ADMINISTRATION

SPONSORED PROJECT TERMINATION SHEET

2 - SR449

Date 8/24/82

Project Title: A Generalized Wake-Integral Approach for Drag Determination in Three-Dimensional Flows

Project No: E-16-655

Project Director: Dr. J. C. Wu

Sponsor: National Science Foundation

Effective Termination Date: 6/30/82

Clearance of Accounting Charges: 6/30/82

Grant/Contract Closeout Actions Remaining:

- [x] Final Invoice and Closing Documents
- [ ] Final Fiscal Report
- [x] Final Report of Inventions (only if positive)
- [x] Govt. Property Inventory & Related Certificate
- [ ] Classified Material Certificate
- [ ] Other _____

Assigned to: Aerospace Eng. (School/Laboratory)

COPIES TO:

Administrative Coordinator	Research Security Services	EES Public Relations (2)
Research Property Management	Reports Coordinator (OCA)	Computer Input
Accounting	Legal Services (OCA)	Project File
Procurement/EES Supply Services	Library	Other _____

FORM OCA 10:781

NATIONAL SCIENCE FOUNDATION
Washington, D.C. 20550

FINAL PROJECT REPORT
NSF FORM 98A

PLEASE READ INSTRUCTIONS ON REVERSE BEFORE COMPLETING

PART I–PROJECT IDENTIFICATION INFORMATION

1. Institution and Address	2. NSF Program	3. NSF Award Number
School of Aerospace Engineering Georgia Institute of Technology Atlanta, Georgia 30332	Fluid Mechanics	CME-7900891 A01 (formerly ENG-7900891)
	4. Award Period From 9/15/79 To 2/28/82	5. Cumulative Award Amount $156,747

6. Project Title

A Generalized Wake-Integral Approach for Drag Determination in Three-Dimensional Flows

PART II–SUMMARY OF COMPLETED PROJECT *(FOR PUBLIC USE)*

A generalized theory relating the drag force acting on a three-dimensional body in a wind tunnel to properties of the vortical wake downstream of the body has been developed. In the theory of Betz, only the profile drag is expressed as a wake integral. The present theory shows that, under quite general circumstances, the total drag can be decomposed into several components, each of the components is accurately determined by a wake integral. The generalized theory offers some insight to the interplay between the drag components and the wake characteristics.

Comprehensive wake survey data have been obtained by researchers at the Lockheed-Georgia Company for tests upon a wing and a car model. These data have been analyzed. The results show that the wake-integral approach determines the total drag with a high degree of precision. In this report, descriptions of the general wake-integral theory and the experimental program are given. Several open questions concerning the wake-integrals are discussed.

PART III–TECHNICAL INFORMATION *(FOR PROGRAM MANAGEMENT USES)*

1. ITEM *(Check appropriate blocks)*	NONE	ATTACHED	PREVIOUSLY FURNISHED	TO BE FURNISHED SEPARATELY TO PROGR	
				Check (✓)	Approx. Da
a. Abstracts of Theses					
b. Publication Citations					
c. Data on Scientific Collaborators					
d. Information on Inventions					
e. Technical Description of Project and Results					
f. Other *(specify)*					

2. Principal Investigator/Project Director Name *(Typed)*	3. Principal Investigator/Project Director Signature	4. Date
James C. Wu		7/29/82

NSF Form 98A (9-78) Supersedes Previous Editions — Form Approved OMB No.

E-16-655

FINAL REPORT

A GENERALIZED WAKE–INTEGRAL APPROACH FOR DRAG DETERMINATION IN THREE–DIMENSIONAL FLOWS

By

J. C. Wu, Principal Investigator

Prepared for

NATIONAL SCIENCE FOUNDATION

Under

Grant No. ENG 79–00891

July 1982

GEORGIA INSTITUTE OF TECHNOLOGY
A UNIT OF THE UNIVERSITY SYSTEM OF GEORGIA
SCHOOL OF AEROSPACE ENGINEERING
ATLANTA, GEORGIA 30332

Final Report

on National Science Foundation
Grant No. ENG 79-00891

entitled

A GENERALIZED WAKE-INTEGRAL APPROACH FOR DRAG DETERMINATION IN THREE-DIMENSIONAL FLOWS

Prepared by

J. C. Wu, Principal Investigator
School of Aerospace Engineering
Georgia Institute of Technology

TABLE OF CONTENTS

SUMMARY

A generalized theory relating the drag force acting on a three-dimensional body in a wind tunnel to properties of the vortical wake downstream of the body has been developed. In the theory of Betz, only the profile drag is expressed as a wake integral. The present theory shows that, under quite general circumstances, the total drag can be decomposed into several components, each of the components is accurately determined by a wake integral. The generalized theory offers some insight to the interplay between the drag components and the wake characteristics.

Comprehensive wake survey data have been obtained by researchers at the Lockheed-Georgia Company for tests upon a wing and a car model. These data have been analyzed. The results show that the wake-integral approach determines the total drag with a high degree of precision. In this report, descriptions of the general wake-integral theory and the experimental program are given. Several open questions concerning the wake-integrals are discussed.

ACKNOWLEDGEMENT

The principal investigator wishes to express his thanks to:

Dr. J. E. Hackett, who initiated the wake-integral study at the Lockheed-Georgia Company, directed the experimental program reported in Appendix B, and provided helpful comments and discussions on many occasions.

D. E. Lilley, who prepared the computer program presented in Appendix B.

Dr. M. M. El Refaee, who obtained the results presented in Table 1.

Dr. A. Sugavanam and K. Nohra, who participated in the theoretical studies.

J. Smith , who typed the manuscript.

I. INTRODUCTION

In 1925, A. Betz[1] presented a theory for the determination of drag forces acting on lifting bodies in free flight. In this theory, the total drag is resolved into a profile drag component and an induced drag component. The profile drag is expressed by Betz as a wake integral, i.e., an integral over the vortical wake region in a transverse plane downstream of the body. The experimental determination of the profile drag using Betz' theory is convenient and efficient since measurements need to be made only in the vortical wake region of one plane. The induced drag is expressed by Betz as the difference between the integrated kinetic energy associated with the transverse velocity components at two transverse planes, one downstream and the other upstream of the lifting body. The determination of the induced drag using Betz's formula presents serious experimental difficulties in cost as well as in accuracy since transverse velocity components need to be measured over a large region, including areas far from the vortical wake where the transverse velocities are too small for measurements with good accuracy. The preferred approach is clearly to recast the induced drag formula into a wake integral.

In 1973, E. C. Maskell[2] developed a formula for the drag acting on a lifting body placed in a wind tunnel. Maskell found, for this wind-tunnel application, an additional term to Betz's formula. By employing the devices of vortex filaments, source-sink singularities, and their images, Maskell obtained a wake-integral expression for the induced drag. This formula is expected to be valid under certain restricted circumstances.

In 1974, J. E. Hackett initiated a research program at the Lockheed-Georgia Company with the aim of further developing the wake-integral method for the determination of the induced drag. Pilot experiments conducted during the

initial stage of the program showed that the wake-integral approach accurately determines the drag for wings at low angles of attack. These experiments also identified several significant theoretical and experimental difficulties that need to be resolved. The principal investigator, in cooperation with Lockheed researchers, developed a generalized wake-integral theory for drag in 1976[3]. This theory expresses the induced drag, as defined by Betz, as the sum of two integrals. These two integrals represent separately the contributions of the axial and the transverse components of the wake vorticity. The axial vorticity integral is a wake integral. The transverse vorticity integral is an integral over the entire wind-tunnel cross-section. This generalized theory shows that, provided that the transverse vorticity integral is small compared with the axial vorticity integral, the induced drag is accurately determined by the measurement of axial vorticity in the wake only.

Subsequent to the development of the generalized wake-integral theory, D.E. Lilley prepared a computer code[5] which evaluates the wake-integral of the induced drag using measured transverse velocities in the wake. This computer code was used to analyze experimental data obtained at Lockheed-Georgia Company with a simple semispan wing. The results, together with a detailed description of the wake-integral theory[4], was presented in 1979. Also in 1979, the Lockheed-Georgia Company and the Georgia Institute of Technology initiated a joint research effort under the support of the National Science Foundation to further develop the wake-integral approach. In this report, results of this research effort are summarized and discussed. In order to make this report self-contained, two appendices are included. The first appendix is Reference 4 of this report and is a 1979 paper presented at the 17th Aerospace Sciences Meeting of the American Institute of Aeronautics and Astronautics. In this paper, the generalized wake-integral approach is presented together with some results of the pilot experimental

study. The second appendix is Reference 5 of this report and is a 1981 Lockheed-Georgia Company report. This Lockheed report presents detailed descriptions of the experimental program, data reduction technique, together with comprehensive wake traverse data and a listing of Lilley's computer program. In the main text of this report, frequent references to these two appendices are made.

II. GENERALIZED WAKE-INTEGRAL THEORY

The total drag D acting on a solid body placed in a wind tunnel with a uniform effective cross section is expressible as a sum of three terms as follows (Eq. (19) of Appendix A):

$$D = \iint_W \left[(H_o - H_2) + \frac{\rho}{2}(u_2^* - u_2)(u_2^* + u_2 - 2u_o)\right] dy\, dz$$

$$+ \frac{1}{2}\rho \iint_A \left[(v_2^2 + w_2^2) - (v_1^2 + w_1^2)\right] dy\, dz$$

$$- \frac{1}{2}\rho \iint_A (u''^2_2 - u''^2_1)\, dy\, dz \qquad (1)$$

where a Cartesian coordinate system (x, y, z) with the x-axis in the undisturbed tunnel flow direction, is used; u, v, and w are respectively the x-, y-, and z-components of the actual flow velocity; the subscript "o" designates the undisturbed tunnel flow conditions; the subscript "1" designates an upstream measurement station $x = x_1$; the subscript "2" designates a downstream measurement station $x = x_2$; W indicates an integration over the vortical wake region; A indicates an integration over the entire cross section of the tunnel ρ; is the fluid density; H is the total head of the flow; u^* is a reference velocity; and u'' is the deviation of u^* from the undisturbed tunnel flow velocity u_o. The quantities H, u^*, and u'' are defined as follows:

$$H = p + \frac{1}{2}\rho(u^2 + v^2 + w^2) \qquad (2)$$

$$u^* = \left[\frac{2}{\rho}(H_o - H) + u^2\right]^{1/2} \qquad (3)$$

and

$$u'' = u^* - u_o \qquad (4)$$

The first integral on the right side of Eq. (1) was identified by Betz [1] as the profile drag acting on a body in free flight. The second integral was similarly identified by Betz as the induced drag. The third integral was interpreted by Maskell[2] as a correction due to constraints placed on the flow by the presence of wind-tunnel walls.

The total drag formula, Eq. (1), is a direct consequence of the Navier-Stokes equations (Appendix A). This formula is exact in the sense that no simplifying assumptions other than those contained in the Navier-Stokes equations have been introduced in deriving it. The division of the total drag into three components, each with its own significance, is important. Indeed, such a division is essential to a reasonable understanding of the physical mechanisms responsible for aerodynamic drag and to the development of methods for drag reduction. It should be recognized, however, that the identification of the three integrals in Eq. (1) individually as the profile drag, the induce drag, and the tunnel correction term is not exact. Indeed, there are interchanges between these integrals and, as a result, the value of each integral is dependent upon the location of the measurement plane and is not unique. Under reasonably general circumstances, however, this dependency on the location of the measurement plane is weak and the physical significance ascribed to each of the three integrals is meaningful. This viewpoint is elaborated later in this paper on the basis of theoretical and experimental evidences.

It has been shown (Appendix A) that

$$\iint_A (v_1^2 + w_1^2 - u''^2_1)\,dy\,dz = 0 \qquad (5)$$

The quantities involving measurements at the upstream station $x = x_1$ in Eq. (1) may therefore be omitted without changing the exactness of the total drag

expression. Since the three drag components are not uniquely defined and the omitted quantities are small, it is logical to continue to associate the three integrals in Eq. (1), with the upstream quantities removed, individually with the profile drag, the induced drag, and the correction term.

The profile drag integral in Eq. (1) can be rewritten as

$$D_p = 2\iint_W (H_o - H_2)dy\,dz - 2\rho u_o u_b A \qquad (6)$$

where A is the cross-sectional area of the wind tunnel, and u_b is a wake blockage velocity defined by

$$u_b = \frac{1}{2A}\iint_W (u_2^* - u_2)dy\,dz \qquad (7)$$

It is known that the generation of lift in three-dimensional flows is linked to the process of continual shedding of vortices trailing from the lifting body moving relative to the fluids. Since shed vortices are accompanied by some increase in the kinetic energy of the fluid, power input is required to produce these vortices even if friction work is left out of account. This power input is provided through work performed by the induced drag. The word "induced" is used in the aerodynamics community to differentiate the drag component that is associated with lift generation from the profile drag which provides the frictional work. In many applications, shedding of trailing vortices may take place around bluff bodies with no net generation of lift. For such applications, the second term of Eq. (1) is not "induced" by a generation of lift. Maskell[2] used the expression "vortex drag" in place of the expression induced drag. In reality, however, vortex shedding is responsible for both the induced and the profile component of drag. Trailing vortices are elements of the well-known horseshoe vortex systems that must produce lift or side force. For applications with no net lift production, the geometry of the horseshoe vortex system is such that the lift (or side force)

associated with some of the horseshoe vortices are directed opposite to the negative lift force associated with other horseshoe vortices. The vortices shed in connection with the profile drag, on the other hand, do not produce lift. These vortices do not trail the body. They are shed as rings or loops, lying more or less in the transverse plane. Since these loop vortices induce velocity disturbances that are primarily in the axial direction, the first term in Eq. (1) is closely related to the profile drag. Since the trailing vortices are more or less parallel to the undisturbed tunnel flow direction, they are largely responsible for the velocity disturbances (v and w) in the transverse plane. In consequence, the second term in Eq. (1) is closely related to what is usually known as the induced drag. In the remainder of this report, this drag component is called the crossflow drag D_c.

The crossflow drag can be rewritten as (Appendix A)

$$D_c = \frac{1}{2}\iint_W \psi\xi \, dy \, dz - \frac{1}{2}\iint_A \phi_2\sigma_2 \, dy \, dz \tag{8}$$

where

$$\xi = \frac{\partial w}{\partial y} - \frac{\partial v}{\partial z} \tag{9}$$

$$\sigma = \frac{\partial v}{\partial y} + \frac{\partial w}{\partial y} \tag{10}$$

ψ and ϕ satisfy the Poisson's equations

$$\frac{\partial^2 \psi}{\partial y^2} + \frac{\partial^2 \psi}{\partial z^2} = -\xi \tag{11}$$

$$\frac{\partial^2 \phi}{\partial y^2} + \frac{\partial^2 \phi}{\partial z^2} = \sigma \tag{12}$$

and are subject to the no-slip boundary conditions at the wind-tunnel wall.

In Eq. (8), ξ is the axial component of the vorticity field and ψ may be interpreted as a stream function associated ξ in a two-dimensional flow in the y-z plane. Similarly, σ may be viewed as a source term in the two-dimensional flow and ϕ the scalar potential associated with σ . If, at the measurement plane $x = x_2$, the rate of change of the flow with x is very slow, then σ is small (Note that $\sigma = -\frac{\partial u}{\partial x}$ because of the continuity equation) and the second integral in Eq. (8) may be neglected.

Equation (8) contains a wake integral and an integral over the entire wind-tunnel cross section. It is of interest to note (Appendix A) that the crossflow drag contains not only a contribution of the axial component ξ of the vorticity field but also a contribution of the transverse components η and ζ of the vorticity. The former is obviously represented by the wake integral of Eq. (8). The latter is represented by the second integral of Eq. (8), as shown in Appendix A.

Maskell[2] considered an array of singular flow elements - horseshoe vortices, sources and sinks - - to construct a hypothetical flow. This array includes flow elements inside a tunnel with a rectangular cross section and the images of these elements outside the tunnel. The bound-vortex element of the horseshoe vortex in the tunnel is placed together with the sources along a center line of the wind-tunnel cross section. This center line represents the span of the wing. The trailing vortex lines are straight and are placed at equal distances from the center of the tunnel. The sinks are placed far downstream. Maskell utilized the symmetry properties of his hypothetical flow to obtain an approximate expression for the crossflow drag of the form

$$D_c = \frac{1}{2}\rho \iint_W \psi \xi \, dy \, dz \qquad (13)$$

In Eq. (13), the second integral of Eq. (8) is absent. In many applications, the actual flow in the tunnel may differ substantially from the hypothetical flow considered in Reference 2. For example, for a flow past an asymmetric body such as a road vehicle and a flow involving massive separation such as a stalled wing, the symmetric properties utilized in the derivation of Eq. (13) are not even approximately correct. Also, in many other applications, it may be desirable to make measurements in a traverse plane near the solid body, where the flow is rapidly varying with the axial location. For these applications, the use of Eq. (13) to determine the crossflow drag may be questionable. The use of Eq. (8) in such applications, however, is appropriate since it is completely equivalent to the second integral in Eq. (3) with the term $v_1^2 + w_1^2$ omitted. Indeed, with Eq. (8), it is possible in principle to determine the crossflow drag accurately through wake measurements at a traverse plane very near the body. It is noted in passing that the derivation of Eq. (13) given in Reference 2 is restricted to a wind tunnel with a rectangular cross section. Eq. (8), however, is valid for all tunnel cross-sectional shapes and is not restricted to rectangular tunnels.

Maskell[2] has shown that the third term on the right side of Eq. (1), designated D_W here, may be approximated by

$$D_W = -2\rho A u_b^2 \qquad (14)$$

Eq. (14) and (13) are derived using the same simplifying assumptions. Since the term D_w is expected to be small in wind-tunnel applications, the use of Eq. (14) is more generally acceptable than the use of Eq. (13).

The total drag acting on any solid body placed in the wind tunnel can be determined by evaluating individually the three drag components D_p, D_c and D_w and summing the results. The three drag components are given respectively by Eqs. (6), (8), and (14). With the exception of the second integral in Eq. (8), all the

integrals present in the expressions for the drag components are wake integrals. The second integral in Eq. (8) is an integral over the entire traverse plane of the wind tunnel. However, since the gradient of v and w are extremely small outside the vortical wake, by the definition of σ, Eq. (10), the important region of integration for the second integral in Eq. (8) is similar in extent to the vortical wake. In practice, therefore, this integral is replaced by a wake integral with the same integrand.

III. CROSSFLOW DRAG

The crossflow velocity components v and w at the measurement plane may be viewed as constituting a two-dimensional flow in the crossflow plane y-z. The two integrals in Eq. (8) contains flow quantities that are derived from the crossflow velocities v and w. For convenience, the first integral in Eq. (8) containing the axial vorticity ξ , is referred to as the vorticity integral and the second integral, containing the source σ , as the source integral. In reality, a source distribution does not exist in an incompressible flow. The source integral in fact represents the contribution of the transverse vorticity components to the crossflow drag (Appendix A). Physically, σ connects the three-dimensional effects to the crossflow drag (Appendix A). By virtue of the continuity equation, Eq. (10) can be rewritten as

$$\sigma = - \frac{\partial u}{\partial x} \qquad (15)$$

Therefore the quantity σ is a measure of the three-dimensionality of the local flow, i.e., the axial gradient of the velocity field. If, at the measurement plane, the local three-dimensionality effect is unimportant (for example, at measurement planes not too close to the model), then the second integral in Eq. (8) is negligible. If, on the other hand, the measurement plane is placed close to the model where the three-dimensionality of the local flow is important, then the neglect of the second integral may be suspect.

In the earlier studies of the wake-integral approach for drag determination[2,4], the measurement station was carefully chosen so as to ensure small three-dimensional effects, and the source integral in Eq. (8) was neglected in the computation of the drag. In the present work, an extensive experimental program was carried out. For each test, several wake surveys at different axial locations, including one wake survey very close to the model in each test, were

made. For some of these measurements, the neglect of the source integral is not justifiable. Nevertheless, as discussed below, the computer code previously prepared (Appendix B) for the evaluation of the vorticity integral is directly applicable also for the evaluation of the source integral. No new computer program was therefore needed in obtaining the source integral values reported in this paper.

It is well-known that a differentiable vector field can be decomposed into a solenoidal part expressible as the curl of a vector potential and an irrotational part expressible as the gradient of a scalar potential. For the crossflow velocity field, the scalar potential is ϕ , defined by Eq. (12) and an appropriate boundary condition. The vector potential reduces to the stream function ψ , defined by Eq. (11) and an appropriate boundary condition. This stream function is associated with the crossflow and is a constant on the wind-tunnel wall. The decomposition of the crossflow velocity field yields, consistent with Eqs. (9) to (12), the following expressions:

$$v = \frac{\partial \phi}{\partial y} + \frac{\partial \psi}{\partial z} \tag{16}$$

$$w = \frac{\partial \phi}{\partial z} - \frac{\partial \psi}{\partial y} \tag{17}$$

Since the normal component of the velocity is zero on the wind tunnel wall, one has, using Eqs. (16) and (17), the following equation on the wall

$$\frac{\partial \phi}{\partial n} - \frac{\partial \psi}{\partial t} = 0 \tag{18}$$

where n and t are respectively the normal and the tangential directions of the wall.

If one lets ψ be a constant on the wall, then, on the wall

$$\frac{\partial \psi}{\partial t} = 0 \tag{19}$$

Equations (18) and (19) give

$$\frac{\partial \phi}{\partial n} = 0 \qquad \text{on the wall,} \qquad (20)$$

Equations (19) and (20), together with Eqs. (11) and (12), defines ψ and ϕ to within an arbitrary constant. For an incompressible flow, the integration of σ over the wind-tunnel cross-section must be equal to zero. In consequence, the arbitrary constant contained in ϕ does not contribute to the value of the source integral. The no-slip condition on the wind-tunnel wall requires that the integration of ξ over the wind-tunnel cross-section to be zero. In consequence, the arbitrary constant in ψ does not contribute to the value of the vorticity integral. For convenience, the values of the arbitrary constants are assigned by requiring ψ and ϕ to be zero at the wall of the wind tunnel. It is of importance to note that the flow under consideration is neither irrotational nor solenoidal. The functions ϕ and ψ therefore do not form the complex potential.

IV. EVALUATION OF WAKE INTEGRALS

The general procedure for the evaluation of the vorticity integral consists of the following three steps:

a) Beginning with a set of experimentally obtained values of v and w in a measurement plane, the values of ξ in this measurement plane are determined using Eq. (9).

b) Using the values of ξ obtained in Step (1), a set of ψ values is then established by solving the Poisson's equation, Eq. (11), subject to the homogeneous boundary condition, Eq. (19).

c) The values of ξ and ψ are used in the evaluation of the vorticity integral.

In the general procedure just described, the input data are the experimental values of v and w. The output information is the value of the vorticity integral. If the experimental values of w are used as input data in place of v and the values of -v are used in place of w, then the general procedure produces the value of the source integral in place of the value of the vorticity integral. This conclusion is reached by comparing the set of equations (9), (11), and (19) with the set (10), (12), and (20). It is easy to see that, with the replacements just stated, the right side of Eq. (9) gives $-\sigma$ in place of ξ. Therefore Step (a) of the general procedure yields values of $-\sigma$ in place of ξ. Using these values of $-\sigma$ in Step (b), values of ϕ are obtained in place of values of ψ since, with the replacement of v and w by w and -v, the homogeneous Dirichlet boundary condition, Eq. (19), is transformed into a homogeneous Neumann's boundary condition Eq. (20). Since Steps (a) and (b) now yield $-\sigma$ and ϕ in place of ξ and ψ, step (c) gives the negative value of the source integral in place of the vorticity integral.

In preparing a computer code following the general procedure outlined earlier, it is clear that Steps (a) and (c) of the procedure can be easily accomplished

by the application of simple numerical differentiation and numerical quadrature methods. These methods are straightforward and are outlined in Appendix A. For Step (b), a large number of competing methods, including various forms of finite-difference and finite-element methods, exist. The method selected for the present work is based upon the integral representation approach developed by the principal investigator and his coworkers[6] at the Georgia Institute of Technology. This method offers certain distinctive advantages in accuracy and computation efficiency.

It has been shown[7] that Eq. (11) can be recast into an integral representation for the stream function ψ. Alternatively, the solenoidal part of the crossflow velocity defined by

$$v_s = \frac{\partial \psi}{\partial z} \tag{21}$$

$$w_s = -\frac{\partial \psi}{\partial y} \tag{22}$$

can be expressed as integral representations[6]

$$v_s = \frac{1}{2\pi}\iint_A \frac{\xi_o (z_o - z)}{(y_o - y)^2 + (z_o - z)^2}\, dy_o\, dz_o \quad \frac{1}{2\pi}\oint_B \frac{\left(\frac{\partial \psi}{\partial n}\right)_o (z_o - z)}{(y_o - y)^2 + (z_o - z)^2}\, db_o \tag{23}$$

and

$$w_s = -\frac{1}{2\pi}\iint_A \frac{\xi_o (y_o - y)}{(y_o - y)^2 + (z_o - z)^2}\, dy_o dz_o + \frac{1}{2\pi}\oint_B \frac{\left(\frac{\partial \psi}{\partial n}\right)_o (y_o - y)}{(y_o - y)^2 + (z_o - z)^2}\, db_o \tag{24}$$

where B is the boundary of A, the subscript "o" indicates that a variable, its differentiation or its integration is in the $y_o - z_o$ space, e.g., ξ_o is the value of ξ at the point $y = y_o$ and $z = z_o$.

In obtaining the integral representations (23) and (24), the Dirichlet boundary condition, Eq. (19), has been used. The integral representations (23) and (24), however, contains also the Neumann condition, $\frac{\partial \psi}{\partial n}$, on the boundary B. In consequence the problem of finding ψ, described by the Poisson's equation, Eq. (11), appears to be overspecified. In reality, the problem is not overspecified[8]. The appearance of the Neumann condition in the integral representations (23) and (24) merely implies the presence of a vortex layer at the boundary[8]. This vortex layer represents a boundary layer of the crossflow at the wind-tunnel wall. Since the stream function value is zero at the wall, the vortex layer does not contribute directly to the vorticity integral in Eq. (8). However, since the presence of this vortex layer influences the values of the stream function inside the wind tunnel, the vortex layer does contribute indirectly to the vorticity integral through this influence. In order to accurately determine the value of the vorticity integral, the distribution of the vortex layer strength must be first accurately established. The unique advantages of using the integral representations (23) and (24) for the accurate determination of the vortex layer strength are discussed fully in Reference 8. Wahbah[9] established a highly efficient and highly accurate method for computing the vortex layer strength and the solenoidal crossflow velocity components v_s and w_s using the integral representation approach presented in References 6 and 8. On the basis of Reference 9, Lilley prepared a computer program (Appendix B) for the evaluation of the vorticity integral. In this program, the solenoidal velocity field v_s and w_s is computed using the integral representation approach. The stream function ψ is then computed by a simple integration using Eq. (21) or (22).

Lilley's computer program includes a subroutine for computing the profile drag D_p as defined by Eq. (6). The computation procedure is outlined in Reference 4 (Appendix A).

V. EXPERIMENTS

Previous studies of the wake-integral approach showed that the approach accurately determines the drag on an unstalled wing (Appendix A) with the wake survey plane not very near the model. The approach, however, was not verified for more complex flows involving massive flow separations or for survey planes near the model. The contribution of the source integral to the drag, which may be significant for complex flows, was not evaluated. Under the present research, an extensive experimental program was carried out by Lockheed-Georgia researchers with the objective of providing comprehensive wake survey data for drag determination under reasonably wide experimental circumstances. A semi-span semi wing model and a car model was tested using the 30" x 43" cross-section low speed Model Test Facility at Lockheed. The semi-span wing model was mounted vertically at quarter chord on a under-floor balance at the level of the tunnel floor, has a 12" chord, a 18" span, and an NACA 0012 section. Tests were carried out at 6-degrees angle of attack with wake surveys made at -6", 12", and 36" from the quarter chord, and at 18-degrees angle of attack with traverses at -6", 18", and 36" from the quarter chord. The car model was a 15.4 percent scale model of a "simple automotive shape" previously tested in the Lockheed-Georgia 16.25 x 32.25 foot low speed wind tunnel. The overall length of the model was 26.4 inches and the overall width was 10 inches. The car model was also mounted to the balance at the floor level. Tests were carried out at 0-degree and 12.5 degrees yaw, with wake surveys made at 18" and 36" aft of the model center. Wake surveys were carried out using five-holed pitch/yaw pressure probes. Pressure and velocity data needed for the wake analyses were obtained from the probe data. Drag forces were also directly measured using the platform balance on the wind tunnel.

Comprehensive wake survey data are presented in Appendix B for tests upon both the wing and the car models. These data are supplemented by limited

survey data ahead of the wing model. Balance measured aerodynamic forces and moments, including lift, drag, and pitching moment for the wing model and side force, drag and yawing moment for the car model are also given in Appendix B. Descriptions of the test facility, the probes, the test models, data quality and data reduction techniques for the wake surveys are presented in detail in Appendix B. In Section VI of this paper, selected experimental results are presented and interpreted using the generalized wake-integral theory.

VI. RESULTS AND DISCUSSIONS

The emphasis of the present research program has been on the development of the generalized wake-integral approach for drag determination. In order to accomplish this emphasis, a combined theoretical and experimental study, aimed at the resolution of several theoretical questions and the providing of definitive data under various experimental circumstances, has been undertaken. Considerable care was used both in gathering and in analyzing the wake survey data.

For the generalized wake-integral approach to be used with confidence, the drag values determined through the balance measurement must agree well with the wake-integral results. In addition, to gain insight into the interplay between the drag components and the wake characteristics, the wake survey data are invaluable.

Wake-survey data are presented at the end of Appendix B in the form of "MPs" (Machine Plots). A total of eighty wake survey plots are given, twenty plots for each of the four test cases. The four test cases are, as stated earlier, the wing at 6^{o} and 18^{o} angles of attack and the car at 0^{o} and 12.5^{o} yaw. For each test case, two sets of wake-surveys plots are presented, one set at a survey plane close to the model and the other set at a greater distance from the model. For the wing at 6^{o} angle of attack, the first survey plane is 12" aft of the wing's quarter chord. Since the wing chord is 12", this first survey plane is only 1/4 chord aft of the wing's trailing edge. The second survey plane, 36" aft of the wing's quarter chord, is 2¼ chord aft of the wing's trailing edge. For the wing at 18^{o} angle of attack, the first survey plane is moved to 18" aft of the wing's quarter chord, or 3/4 chord aft of the wing's trailing edge, in order to avoid the complicated flow region associated with the stall of the wing at this angle of attack. Even at this survey plane (18"), however, the flow is somewhat unsteady and the probes are operating near, and possibly beyond, their angle limit (Appendix B). In consequence, the wake-integral

results obtained from this set of wake-survey data do not possess the same high quality as do those obtained from other sets of data.

The first set of wake-survey plots, MPs 1 to 10, are for the wing at 6^{o} angle of attack and the 12" survey plane. MP1, which shows the crossflow velocity magnitude, clearly indicates the presence of a trailing vortex being shed from the wing's tip. MPs 2, 3, 8, and 9, showing the crossflow velocity components, as well as MPs 6 and 7, showing the crossflow kinetic energy and the axial vorticity distributions, confirm the existence of this tip vortex. In addition, MP7 also indicates the presence of some axial vortices along the trailing edge at the outboard portion of the wing, in the form of kinks in the otherwise more or less circular vorticity contours. For convenience, the axial vorticity associated with the kinks are designated "loop vortices". While the more or less circular contoured vortices are obviously tip trailing vortices associated with the well-known horseshoe vortex system that is connected to the lift force, the loop vortices appear to have their origin in the profile drag, as discussed below. Both types of vortices, however, obviously must contribute to the crossflow drag.

It is known that, since the vorticity field is solenoidal, vortex lines in three-dimensional flows do not begin or end in a fluid, but must form closed loops. The well-known horseshoe vortex system is composed of the bound vortex (the lifting line), the trailing vortex lines, and a starting vortex line which complete the loop. The starting vortex line moves with the freestream velocity relative to the wing. The horseshoe system therefore grows continually even in a steady flow[10]. The lift force and the induced drag acting on the wing is attributable to the growth of this system[10]. Co-existing with the horseshoe system are vortices originating from the boundary layers on the wing. Although the boundary-layer vortices are directed mainly along the wing-span direction, boundary-layer vortices are shed from the wing near the trailing edge in the form of loops because the vorticity field

is solenoidal. The vortices in the loop are transported with the fluid motion. In consequence, these loops distort after they leave the wing's trailing edge. Immediately downstream of the trailing edge, because of the downwash, the planes of the loops are inclined significantly from the survey plane. Therefore an axial component of the vorticity associated with the loops exists near the trailing edge. Further downstream, the downwash diminishes in magnitude (particularly within a tunnel) and the plane of the loops becomes nearly coincident with the survey plane. The axial component of the vorticity associated with the loops disappears, and the primary influence of the loops is the induction of an axial velocity deficit.

It is important to realize that the vortices in the fluid do not stay stationary relative to the wing even though the flow is steady. In reality, vorticity is continually being generated at the surface of the wing and subsequently being transported with the fluid. In a steady flow, the kinetic processes continually remove the vorticity locally and, at the same time, continually replenish the vorticity at the same rate. In this sense, one may consider a stationary distribution of vorticity in the region near the wing. However, the starting vortex, which is located at great distances from the wing, continues to move with the tunnel stream away from the wing and, in this process, elongates the trailing vortices connecting it to the bond vortex. The vortex loops originating from the steady-state boundary layers are not connected to the wing by trailing vortices. They leave the wing's trailing edge as self-contained loops. The loops form a tube of vortices with vortex lines tangential to the circumference of the tube. The starting vortex, like the loop vortices and other vortices in the fluid, is attenuated by viscous diffusion. However, the total amount of circulation in the starting vortex is conserved[10].

MPs 4 and 5 show the axial velocity ratio and the total pressure deficit. These two plots clearly exhibit two major wake features - the tip vortex region which is also evident in the plots discussed earlier and the wake originating from

the steady state boundary layer. The inboard boundary-layer wake is almost two-dimensional. That is, the variation of the flow variable in the span direction is small. Near the root of the wing, however, the flow interacts with the boundary layer on the wall of the wind tunnel and is highly three-dimensional. It is significant that the constant axial velocity and the constant total-pressure deficit contours associated with the boundary-layers end near the wing's tip at locations coinciding with the kinks of the axial vorticity contours. This fact clearly indicates that the loop vortices, as described earlier, have their origin in the profile drag.

MP 10, showing the crossflow streamlines, exhibits more or less circular streamlines centered near the wing's tip. These streamlines are elongated in the span direction inboard of the tip and possess rapid changes of slope at the outboard portion of the trailing edge, where the loop vortices are present.

A comparison of MPs 1 to 10, obtained from wake surveys at the 12" plane, with MPs 11 to 20, obtained at the 36" plane, reveals a number of significant features. The center of the tip vortex is shifted inboard and upward (MP 7 and 17). The axial component of the loop vortices (the kinks observed in MP 7) is not visible in MP 17, although its presence can still be observed in the streamline pattern (MP 20). The boundary-layer wake is evident in MP 15. This boundary-layer wake is shifted downward, as expected due to the downwash, and is significantly attenuated. The axial velocity in the tip vortex flow as well as in the boundary-layer wake has reached almost the freestream value, as shown in MP 14. The crossflow kinetic energy has diffused significantly. The core of the tip vortices, however, persisted with much slower attenuation.

The wake survey data have been used to evaluate the profile and crossflow components of the drag. The results are presented in Table 1, where the crossflow drag is expressed as two parts - - the vorticity integral drag and the source integral drag - - representing respectively the contributions of the vorticity integral and the source integral to drag.

Table 1. Drag Values Determined from Wake and Balance Measurements

Model	Angle of Attack or Yaw	Measurement Plane	WAKE INTEGRAL				Balance* Measured Total Drag
			Profile Drag	Vorticity Integral Drag	Source Integral Drag	Total Drag	
Wing	6^{o}	12"	0.0135	0.0130	0.0000	0.0265	0.0260
		36"	0.0148	0.0117	0.0000	0.0265	0.0260
	18^{o}	18"	0.2422	0.0482	0.0068	0.2972	0.2480
		36"	0.1981	0.0419	0.0004	0.2404	0.2480
Car	0^{o}	18"	0.4153	0.0056	-0.0005	0.4204	0.4120
		36"	0.4070	0.0258	-0.0208	0.4120	0.4120
	12.5^{o}	18"	0.5945	0.0912	-0.0162	0.6695	0.6650
		36"	0.6143	0.0578	-0.0009	0.6712	0.6650

* Balance measured total drag values are provided by Lockheed-Georgia and due to tunnel correction, are different from the values given in Appendix B.

For the wing at 6^{o} angle of attack, the profile drag and the crossflow drag determined from the wake survey at the 12" survey plane are comparable in value. There is an interchange between the two drag components between the survey planes of 12" and 36" (two chord lengths). The amount of this interchange is approximately 10% of the value of the drag components at the 12" station. In view of the flow features discussed earlier, the amount of this interchange is not unreasonable. The source integral drag is negligibly small at both survey planes. This observation confirms the theoretical conclusion (Appendix A) that the source integral is of secondary importance compared to the vorticity integral. In the present tests, although the flow is varying noticeably in the axial direction at the

12" survey plane, the "three-dimensional" effects on drag represented by the source integral is insignificant.

For the wing at 6° angle of attack, the values of the total drag obtained from the wake-survey data at the two different survey planes are in total agreement. Furthermore, the total drag value determined from the wake-integral approach is in excellent agreement with the balance data.

For the wing at 18° angle of attack, the value of the total drag obtained using the wake-survey data at the 18" survey plane differs substantially from the balance data. As discussed earlier, the probes are possibly operating beyond their angle limit. The discrepancy between the wake-survey result and the balance result is therefore attributed not to a flaw in the generalized wake-integral theory but to the suspected quality of the wake-survey data. The set of machine plots MPs 21 to 30, however, does reveal several flow features of interest. In these plots, the tip vortex is readily identifiable. As expected, the boundary-layer wake is absent. There exists, however, imboard of the tip vortex a distribution of axial vorticity, a part of which is directed opposite to the trailing vortex. An examination of MP 30 reveals that the circulation around this inboard distribution of axial vorticity is opposite to and has a much smaller magnitude than the circulation around the starting vortex. It is of interest to note that the center of the negative inboard axial vorticity nearly coincides with a region of minimum axial velocity. In this region, the flow angle is clearly large and the probe data are in doubt. The flow at this 18" survey plane is complex. The flow features just described persist, with expected attention, as shown in MPs 31 to 40. The center of the tip vortex shifts downward, as is consistent with the downwash induced by the imboard circulation. The inboard circulation persisted as is still visible at the 36". Thus, this circulation is expected to form an additional horseshoe system which generates a negative lift.

The total drag value determined from the wake-survey data at the 36" plane is in excellent agreement with the balance data. The total drag for this stalled wing (18^{o} angle of attack) is about a factor of nine greater than the total drag for the unstalled wing (6^{o} angle of attack). The profile drag and the crossflow drag increase respectively by factors of about 14 and 4. The increase in the crossflow drag suggests that the lift for the stalled wing is greater than that for the unstalled wing. According to classical aerodynamics, the factor of increase of the lift should be approximately the square root of the factor of increase of the crossflow drag. For the present case of a stalled wing, there exists an imboard trailing vortex producing a negative lift force. This imboard trailing vortex is much weaker than the tip vortex. In consequence, the factor of increase of lift for the stalled wing is expected to be somewhat smaller than 2 (the square root of 4). Indeed, Figure 3.2 of Appendix B shows that this factor is about 1.7 (0.60 0.35).

The two sets of plots, MPs 41 to 60, are for the car at 0^{o} angle of yaw at the 18" and 36" survey planes. Two pairs of counter-rotating vortices are recognized in MP 47 and MP 50, at the 18" plane. The four vortices lie roughly at the four corners of the car's trunk. The upper pair of vortices persists and are identified also in MP 57 and 60, at the 36" plane. This pair of vortices is relatively strong and represents trailing vortices contributing to a lift force on the car. The lower vortices are much weaker and are pushed outboard by the lateral flow associated with the upper pair of vortices (MP 57). In fact, MP 57 shows a complex pattern of vorticity, including a number of vortices originating from the tunnel floor. The senses of the lower vortices are opposite to those directly above them (MP 47). Therefore this lower pair of vortices is expected to yield a download, or a negative lift. Since this lower pair of vortices is relatively weak, the two pairs of vortices are expected to give rise to a net positive lift. This positive lift is consistent with the fact that the car's mean line is cambered. Because the "span" of the car is small, the trailing vortices are close together. In MP 46, the location

of maximum crossflow energy is seen to be near the center line of car body, where the effects of the upper two vortices reinforce each other. A comparison of MP 46 with MP 56 shows clearly that the wake flow is rapidly attenuated.

The total drag values determined from wake surveys at the two survey planes are both in excellent agreement with the balance data. The values obtained and given in Table 1 for the several drag components, however, are puzzling in three respects. First, the profile drag shows a small decrease from the 18" plane to the 36" plane. This is not expected since the "Loop vortices" described earlier in connection with the wing at 6° angle of attack is expected to be present in this case, and the effect of its presence is to make the profile drag increase in the downstream direction. Second, both the vorticity integral and the magnitude of the source integral increase in the downstream direction. This is unexpected since the source integral is supposed to diminish as the flow variation in the axial direction decreases. Also, the increase in the value of the vorticity-integral drag is contrary to the behavior of the loop vortices just described. Third, the vortices originating from the tunnel floor are expected to interfere with the accuracy of the wake approach. The excellent agreement between the total drag values determined from the wake surveys and the balance data were not expected.

The two sets of machine plots, MP 61 to MP 80, for the car at a yaw angle of 12.5° are markedly different from those for the car at zero yaw angle. A number of previously identified flow features, however, can be recognized. The two clockwise vortices for the zero yaw case (upper left and lower right) have merged. An additional clockwise vortex appears near the right-hand edge of the car's roof. The peak values of the vorticity are similar in the two cases with different yaw angles. The roof vortex has a strong influence on the flow.

The total drag values obtained from the two wake surveys at 12.5° yaw shown in Table 1 are again in excellent agreement with the balance data. The

profile drag increases while the vorticity integral and the magnitude of the source integral decrease in the downstream direction. These behaviors are expected, as described earlier.

A close examination of the machine plots for the car reveals that, at zero yaw angle, the upstream survey plane (18") contain regions where the axial velocity is relatively small and the crossflow velocity is relatively large. The remaining cases (the 12.5° yaw cases and the 36" survey plane with the 0° yaw case) appear to be free of these regions. It is possible, therefore, that the quality of the wake survey data for the 0° yaw case at the 18" survey plane is, like the stalled wing case at the 18" plane, adversely effected by the probe's angle limitation. Since the crossflow drag is of secondary importance compared to the profile drag for the car, which is not designed to generate lift, accurate determination of the crossflow drag is perhaps not crucial to the accuracy of the total drag value. In addition, the tunnel-wall constraint drag, defined by Eq. (14), is proportional to the square of the blockage velocity u_b, defined by Eq. (7). This blockage velocity is relatively large at the upstream survey plane. It's accurate evaluation and inclusion in the total drag determination may show that the total drag values for the car obtained from upstream wake-survey data (18" plane) are somewhat less accurate than those presented in Table 1. The wake integral results presented in Table 1 obtained from the downstream wake-survey data (36" plane), however, are considered to be of higher quality, although the question of the interference of vortices originating from the tunnel floor remains.

VII. CONCLUDING REMARKS

The subject of fluid dynamic drag has been traditionally a focal problem of aerodynamic research. A qualitative understanding of various physical processes contributing to aerodynamic drag has been available for many decades. This understanding, however, has been insufficient for quantifying the relative importance of the various features in three-dimensional flows. Developmental measurements have been usually restricted to total forces or surface pressure measurements. On such a basis, it has been difficult to distinguish between the contributions of various flow mechanisms to drag. In consequence, proposals for drag reduction have been assessed only through extensive experimentation, frequently and solely on the basis of total forces. The designer interested in drag reduction often has relied upon cut-and-try processes, utilizing the wind tunnel, to arrive at desired design compromises. These processes are time consuming and costly, often prohibitively so. In this regard, the generalized wake-integral approach described in this report presents an opportunity for systematic experimental studies leading to quantified knowledge about the importance of the various contributions to drag. This approach does distinguish the contributions of the various flow features and is more efficient than the previous alternatives since data collection is needed in only the vortical wake region of one survey plane. The availability of this approach is expected to substantially improve our understanding of drag and to lead to meaningful improvements in the design of airborne vehicles as well as road vehicles.

The theoretical foundation of the generalized wake-integral approach has been firmly established. On the basis of the theory, there is no doubt that the approach determines the total drag with a high degree of precision. With this generalized approach, there exists a wide latitude in the location of the wake-survey plane. Accurate total drag values are obtainable using wake data at survey

planes extremely close to the lifting body, provided that the quality of wake data is good, as well as at survey planes moderately distant from the body. The theory decomposes the total drag into the profile drag, the crossflow drag, and the tunnel-wall effect components, each with its own physical significance. There are interchanges between these integrals and, as a result, the value of each integral is dependent upon the location of the measurement plane. Under reasonably general circumstances, however, this dependency on the location of the measurement plane is weak and the physical significances ascribed to the individual drag components are meaningful.

The theory, as presented, is in the strict sense applicable only to vortical wakes completely surrounded by a potential region. In the case of a model mounted on a tunnel wall, the vortical wake of the model is connected to the vortical boundary layer on the tunnel wall. The problem of distinguishing the model-generated vortices and tunnel wall-generated vortices requires additional theoretical efforts. Also, the present theory is valid only for a tunnel with a constant effective cross section. The effect of axial variation of the tunnels' effective cross section caused either by a rapid growth of the tunnel boundary layer or by the tunnel design deserves attention. In addition to the drag formula, exact formulas for determining the lift and the side force are of great interest.

The computer program (Appendix B) now available for converting the wake data into drag values is satisfactory for the research reported here. It is recommended, however, that additional features be incorporated into the program to make it user-oriented and more generally applicable. The present program is designed specifically for use in conjunction with the Lockheed-Georgia Model Test Facility which has a 30" x 43" cross-section. Provisions should be introduced to permit the use of the program in other tunnels with different dimensions and cross-sectional shapes. Several contributions to the drag computation are considered to be of secondary importance and are omitted in the existing program. Among these

contributions are those associated with Eq. (14) and certain terms in the evaluation of the total pressure deficit. The inclusion of these contributions in the computer program will broaden its scope of application.

Excellent agreement between the total drag values obtained from wake surveys and those obtained from balance measu rements has been observed for various types of flows. For the case of unstalled wings, the present results reaffirm earlier conclusion (Appendix A) concerning the effectiveness and accuracy of the wake-integral approach. In addition, the theoretical prediction that the total drag value can be accurately determined through wake surveys close to the wing has been verified experimentally. The same conclusions apparently are also applicable to complex flows involving stalled wings and bluff bodies, although a more extensive data base than presently available is needed. In particular, the quality of the wake-survey data at planes very close to the model needs to be examined critically. Additional wake data obtained using non-intrusive instruments, such as lasers, that are not subject to flow angle limitations are of value. As expected, the present study has led to an improved understanding of the various physical processes contributing to aerodynamic drag. This improved understanding, although significant, is by no means complete. A thorough, quantitative and detailed understanding of the processes of drag production will certainly require extensive and persistent efforts over a number of years. The work reported here, however, is highly encouraging in that it lends support to the expectation that such an understanding is feasible.

REFERENCES

1. Betz, A. "Ein Verfahren zur direkten Ermittlung des Profilwiderstandes", Zeitschrift fur Flugtechnik und Motorluftschiffahrt", Vol. 3, 1925.

2. Maskell, E.C., "Progress Towards a Method for the Measurement of the Components of the Drag of Wing of Finite Span," Royal Aircraft Establishment Technical report 72232, 1973.

3. Wu, J.C., "Notes on Maskell's Method of Drag Measurement," Unpublished Notes, Georgia Institute of Technology, August 1976.

4. Wu, J.C., Hackett, J. E. and Lilley, D. E., "A Generalized Wake-Integral Approach for Drag Determination in Three-Dimensional Flows," AIAA Paper 79-279, 1979.

5. Hackett, J.E., Phillips, C. G., and Lilley, D.E., "Three-Dimensional Wake Flow Measurements for a Wing and a Bluff, Car-Like Body", Lockheed-Georgia Company, Report LG-81-ER 0201, August 1981.

6. Wu, J.C., "Problems of General Viscous Flows", Chapter 4 of Developments in Boundary Element Methods - 2, P. K. Banerjee and R. P. Shaw, Editors, Applied Sciences Publishers, Ltd.

7. Wu, J.C. and Sampath, S., "A Numerical Study of Viscous Flows Around Airfoils," AIAA paper 76-337, American Institute of Aeronautics and Astronautics, 1976.

8. Wu, J.C., "Numerical Boundary Conditions for Viscous Flow Problems," AIAA Journal, Vol. 14, No. 8, pp. 1042-1049, 1976.

9. Wahbah, M.M., "Computation of Internal Flows with Arbitrary Boundaries Using the Integral Representation Method," Georgia Institute of Technology Report, March, 1978.

10. Wu, J.C., "Aerodynamic Force and Moment in Steady and Time-Dependent Viscous Flows," AIAA Journal, Vol. 19, No. 4, pp. 432-441, 1981.

APPENDIX A

Development of Generalized Wake-Integral Theory

(AIAA Paper No. 79-0279)

by J. C. Wu, J. E. Hackett and D. E. Lilley

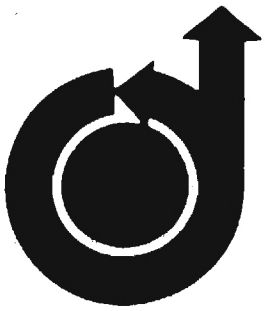

79-0279

A Generalized Wake-Integral Approach for Drag Determination in Three-Dimensional Flows

J.C. Wu, *Georgia Institute of Technology, Atlanta, Ga.; and* J.E. Hackett and D.E. Lilley, *Lockheed-Georgia Co., Marietta, Ga.*

17th AEROSPACE SCIENCES MEETING

New Orleans, La./January 15-17, 1979

A GENERALIZED WAKE-INTEGRAL APPROACH

FOR DRAG DETERMINATION IN THREE-DIMENSIONAL FLOWS

J. C. Wu*
Georgia Institute of Technology
Atlanta, Georgia

J. E. Hackett** and D. E. Lilley+
Lockheed-Georgia Company
Marietta, Georgia

Abstract

A generalized theory relating the drag on a three-dimensional lifting body in a wind tunnel to properties of the vortical wake downstream of the body is presented. In the well known theory of Betz, the profile drag is expressed as a wake integral, i.e., an integral over only the vortical wake region of a downstream section. The present theory shows that, under quite general circumstances, the induced drag is also determined accurately by a wake integral. The theory offers some insight to the interplay between the drag components and the wake characteristics. Results of an exploratory experimental study are presented in the paper. They show that wake measurements at sections near the lifting body can determine the induced drag with good accuracy.

1. Introduction

The subject of fluid dynamic drag has been traditionally a focal problem of aerodynamic research. A qualitative understanding of various physical processes contributing to aerodynamic drag has been available for many decades. Unfortunately, this understanding is often insufficient for quantifying the relative importance of the various features in three-dimenional flows. Developmental measurements are usually restricted to total forces, components forces, or surface pressure measurements. On such a basis, it is difficult to distinguish the contributions of various flow mechanisms to drag. In consequence, proposals for drag reduction at the present can be assessed accurately only through extensive experimentation. The designer interested in drag reduction often relies upon cut-and-try processes, utilizing the wind tunnel, to arrive at desired design compromises. These processes are time consuming and costly, often prohibitively so. New experimental procedures for drag determination that can distinguish the contributions of the various flow features and are more efficient than those in current use are therefore needed. The availability of such procedures will reduce design costs and will provide an opportunity for systematic experimental studies leading to quantified knowledge about the importance of the various flow features to drag.

The present research was initiated several years ago by the second author of this paper with the aim of establishing an efficient experimental procedure for drag analysis and interpretation in three-dimensional flows. In the course of this research, a generalized wake-integral theory for drag has been uncovered. This theory is an extension of the well known theory of Betz [1]. It is generally accepted that the total drag acting on a lifting body can be resolved into profile drag and induced drag components. Betz expressed the profile drag on a lifting body in free flight as a wake integral, i.e. an integral over only the vortical wake region of a transverse plane downstream of the body. The experimental determination of the profile drag using Betz's formula is convenient and efficient since measurements need to be made only in the vortical wake region of one plane. The determination of the induced drag in Betz's formula requires measurements of transverse velocity components over a large region and is not limited to the vortical wake. The transverse velocities are usually too small in regions outside the vortical wake for measurement with good accuracy. For these reasons, the determination of the induced drag presents serious difficulties in cost as well as in accuracy. The preferred approach is clearly to express the induced drag also as a wake integral.

The present generalized wake-integral theory expresses the induced drag as the sum of two integrals. These two integrals represent separately the contribution of the axial component of the wake vorticity and the contribution of the transverse components. The axial vorticity integral is a wake-integral. The transverse vorticity integral is usually negligible compared with the axial vorticity integral. In consequence, the induced drag is determined accurately under quite general circumstances by axial vorticity measurements in the vortical wake only.

Relatively recently, Maskell [2] found a correction term to the drag formula of Betz. The drag components usually referred to as the induced drag is called the vortex drag by Maskell. By employing the devices of vortex filaments and source-sink singularities to construct a hypothetical flow, Maskell succeded in expressing the vortex drag as a wake integral under certain specialized circumstances. The axial and transverse vorticity integrals for the vortex drag presented in this paper are generally valid. They are obtained from an exact analysis of the vorticity field of the wake, and no hypothetical flow is required. Of greater significance is the improvement of understanding made possible

* Professor of Aerospace Engineering, Associate Fellow AIAA.

** Scientist, Member AIAA

+ Senior Aerodynamics Engineer

by the present theory in the physical processes and wake characteristics associated with drag.

The purpose of this paper is twofold: (1) to describe the generalized wake-integral theory for drag determination in three-dimensional flows, and (2) to present selected experimental results substantiating major conclusions of the theory. It was anticipated that a thorough, quantitative, and detailed understanding of the various physical processes contributing to aerodynamic drag would require extensive and persistent efforts over a number of years. The work reported here represents only the present authours' first few steps in search of this understanding. In this context, the results obtained are encouraging in that they lend support to the expectations that the profile and vortex drags can be separately measured through wake integrals and that such measurements can provide quantified knowledge about the relative importance of various flow features to drag.

2. Betz-Maskell Formula

2.1. General Development

The continuity and Navier-Stokes equations for the steady incompressible flow of a fluid with a constant viscosity are expressible as

$$\vec{\nabla} H + \mu \vec{\nabla} \times \vec{\omega} = \rho \vec{q} \times \vec{\omega} \qquad (1)$$

and

$$\vec{\nabla} \cdot \vec{q} = 0 \qquad (2)$$

where μ is the absolute viscosity, ρ is the density, $\vec{q}$ is the velocity, $\vec{\omega}$ is the vorticity, and H is the total head of the fluid. H and $\vec{\omega}$ are defined by

$$H = p + \rho q^2/2 \qquad (3)$$

and

$$\vec{\omega} = \vec{\nabla} \times \vec{q} \qquad (4)$$

Integrating (1) over a singly connected region R of the fluid and using well known theorems of vector calculus to re-express the left-hand terms of the resulting equation in the form of boundary integrals, one obtains,

$$\oiint_B H \vec{n}\, dB - \mu \oiint_B \vec{\omega} \times \vec{n}\, ds = \rho \iiint_R \vec{q} \times \vec{\omega}\, dR \qquad (5)$$

where $\vec{n}$ is an unit normal vector directed outward from R.

The quantity $\vec{q} \times \vec{\omega}$ can be re-written as $\frac{1}{2}\vec{\nabla} q^2 - \vec{\nabla} \cdot (\vec{q}\vec{q})$. Therefore the right-hand side integral of (5) can also be expressed as boundary integral. The relation is

$$\iiint_R \vec{q} \times \vec{\omega}\, dR = \tfrac{1}{2} \oiint_B q^2 \vec{n}\, dS - \oiint_B \vec{q}\, (\vec{q} \cdot \vec{n})\, dS \qquad (6)$$

Consider a steady flow around a three-dimensional model placed in a wind tunnel with a uniform undisturbed stream. The boundary layer and separated regions near the model and the wake trailing the model are vortical. For high Reynolds number flows, the rate of spreading of the vortical wake is not large. There exists in the test section usually a potential flow region surrounding the vortical region. For the present study, the effective cross-section of the test section is assumed to be constant and supports effects, tunnel boundary layer effects, etc. are ignored.

Let R be a segment of the wind tunnel. In a Cartesian coordinate system (x,y,z), with the undisturbed tunnel stream in the x-direction, as shown in Figure 1, B is composed of two planes of constant x and the effective tunnel boundary between the two planes. In addition, if any part, or all, of the model is located between the two planes, then the boundary B includes the solid surface between the two planes. The contributions of the component surfaces to the left-hand side of (5) are now examined. For convenience, the constant x planes are designated by S_1, and S_2, where $x=x_1$, and $x=x_2$ respectively, and $x_1 < x_2$. The wind tunnel boundary between the two planes is designated S_b. The surface of the model between the two planes is designated S_s.

On S_s, the no-slip condition gives, according to (3), $H = p$ and $\tau = -\mu \vec{\omega} \times \vec{n}$, where τ is the shearing stress. The contributions of S_s to the two integrals on the left-hand side of (5) are respectively the pressure force and the skin friction on S_s. The sum of these two contributions is the total force on S_s. On the surface S_b, one has $H = H_o$, the undisturbed wind-tunnel-stream total head, and $\vec{\omega} = 0$. The contributions of S_b to the left hand side of (5) are therefore zero. On the surfaces S_1 and S_2, $\vec{n}$ is in the x-direction. Therefore the contributions of these two surfaces to the first integral are in the x-direction, and those to the second integral are perpendicular to the x-direction. The facts just described can be utilized to obtain from (5) a formula for the aerodynamic force acting on the surface S_s. The x-component of this force is the drag D and is given by

$$D = \iint_{S_1} H\, dydz - \iint_{S_2} H\, dydz + \rho \iiint_R (v\zeta - w\eta)\, dR \qquad (7)$$

where v and w are the y- and z- components of $\vec{q}$, respectively, and η and ζ are y-and z- components of $\vec{\omega}$, respectively.

It is easy to see that the contributions of S_b and S_s to the right-hand side of (6) are zero. Placing the x-component of (6) into (7) therefore yields the following alternative formula for D:

$$D = \iint_{S_1} \left[H + \tfrac{1}{2}\,(u^2 - v^2 - w^2)\right] dydz - \iint_{S_2} \left[H + \tfrac{1}{2}\,(u^2 - v^2 - w^2)\right] dydz \qquad (8)$$

where u is the x-component of $\vec{q}$.

Equation (8) is usually derived in a much simpler manner through an application of the momentum theorem and is well known. The derivation presented here, however, offers some useful information. It is worthy of note that this formula is valid whether or not the model is located between the stations $x=x_1$ and $x=x_2$. The drag force D is the force acting on S_s.

If R is an irrotational region of the flow where $\vec{\omega}$ is zero, then each term in (5) is clearly zero. If both the stations $x=x_1$ and $x=x_2$ are upstream of the vortical region associated with the model, then, since D=0, one has from (8)

$$\iint_A (u^2 - v^2 - w^2)\, dydz = C \qquad (9)$$

where C is a constant and A indicates an integration over the effective cross-section of the tunnel. It is obvious that

$$C = u_o^2 \; A$$

where u_o is the velocity of the undisturbed wind-tunnel stream and A is the effective cross-sectional area of the tunnel.

Consider the disturbance velocity field with components u', v and w, where

$$u' = u - u_o \qquad (10)$$

Placing (10) into (9) yields

$$\iint_A (u'^2 - v^2 - w^2)\, dydz + 2u_o \iint_A u'dydz + \iint_A u_o^2\, dydz = u_o^2 A \qquad (11)$$

The conservation of mass requires the second integral in (11) to be zero. The third integral gives $u_o^2 A$. Therefore one has

$$\iint_A (u'^2 - v^2 - w^2)\, dydz = 0 \qquad (12)$$

for all x-stations upstream of the model and its vortical region.

2.2. Modified Betz Formula

Consider now the case where the station $x=x_1$ is upstream of the model (and the vortical region) and the station $x=x_2$ is downstream of the model. D is in this case the total drag on the model. Following Betz, a velocity magnitude u*, defined by

$$H_o = p + \tfrac{1}{2}\rho(u^{*2} + v^2 + w^2), \qquad (13)$$

is introduced. Clearly, u* = u at $x=x_2$ outside of the vortical wake and also everywhere in the $x=x_1$ section. Let

$$u'' = u^* - u_o \qquad (14)$$

It is easy to show that

$$u^2 = u^2 - u^{*2} + u_o^2 + 2u_o\, u'' + u''^2 \qquad (15)$$

or

$$u^2 = u^2 - u^{*2} + u_o^2 + 2u_o\, u^* - 2u_o^2 + u''^2 \qquad (16)$$

The conservation of mass requires that

$$\iint_A (-2u_o^2)\, dydz = -2u_o \iint_A u_o dydz = -2u_o \iint_A udydz \qquad (17)$$

Integrating (16) and using (17), one obtains

$$\iint_A u^2 dydz = \iint_A (u-u^*)(u+u^* - 2u_o)dydz + \iint_A u''^2\, dydz + \iint_A u_o^2\, dydz \qquad (18)$$

Since $u \neq u^*$ only in the vortical wake, the first integral on the right-hand side of (18) is a wake integral. That is, this integral needs to be evaluated only over the vortical wake downstream of the model. Placing (18) into (8) and noting that $H \neq H_o$ only in the vortical wake, one obtains

$$D = \iint_W [(H_o - H_2) + \tfrac{1}{2}\rho\,(u^*_2 - u_2)(u^*_2 + u_2 - 2u_o)]dydz + \tfrac{1}{2}\rho \iint_A [(v_2^2 + w_2^2 - u_2''^2) - (v_1^2 + w_1^2 - u_1''^2)]\, dydz \qquad (19)$$

where W designates a wake integral, the subscripts 1 and 2 denote variables evaluated at stations $x=x_1$ and $x=x_2$ respectively.

Equation (19) was first obtained by Maskell [2]. The first integral in (19) was identified by Betz [1] as the profile drag in his study of an external flow past a finite solid in the absense of wind-tunnel walls. The quantity D_v, defined below, was identified as the induced drag [3,4], or the vortex drag, following the theory of Betz:

$$D_v = \tfrac{1}{2}\rho \iint [(v_2^2 + w_2^2) - (v_1^2 + w_1^2)]\, dydz \qquad (20)$$

where the integral is over the entire infinite planes at $x=x_1$ and $x=x_2$.

Equation (19) deviates from the theory of Betz only in that the integral for the vortex drag is over the finite cross-sections of the wind-tunnel and that the u'' terms are present.

Maskell showed that the contribution of the u'' terms can be expressed as a wake integral as follows:

$$\tfrac{1}{2}\rho \iint_A (u_1''^2 - u_2''^2)\, dydz = -\rho\, u_b \iint_W (u_2^* - u_2)\, dydz \qquad (21)$$

where u_b is a wake-blockage velocity defined by

$$u_b = \frac{1}{2A} \iint_W (u_2^* - u_2)\, dydz \qquad (22)$$

This contribution was interpreted by Maskell as a small correction due to constraints placed on the flow by the presence of wind-tunnel walls. This contribution is readily incorporated into the profile drag component, i.e., the first integral of (19). The result is an expression that differs from the profile drag formula of Betz only in that the freestream undisturbed velocity is replaced by the effective velocity of the wind-tunnel stream, u_e, defined as the sum of u_o and u_b.

2.3. Further Comments on Equation (19)

It can be shown that (19) is valid and exact for the external flow problem considered by Betz, provided that the magnitude of the disturbance velocity field (u', v, w) approaches zero as r^{-n}, r being a distance from the finite solid and n being greater than 2, for large r. It has been shown that this order condition for the asympotic behavior of the velocity vector is always satisfied [See, e.g., 5]. Strictly speaking, then, the contribution of the u" terms should not be interpreted wholly as a correction due to constraints placed on the flow by the presence of wind-tunnel, since it does not vanish for the infinite external flow problem. This fact can be shown by letting the station $x=x_1$ be sufficiently far upstream of the finite solid so that, according to the asymptotic behavior of the disturbance velocity field (note that $u_1" = u_1'$), the contribution of $u_1"$ to the left-hand side of (21) is zero. The correction, as given by the left-hand side of (21), is therefore finite since the term $u_2"^2$ is non-negative. This observation brings to attention the approximate nature of (21). The correction, as given by the right-hand side of (21), in zero for an infinite external flow since the blockage velocity u_b is zero for this case. Maskell suggested that the correction due to the u" terms is small. Further studies of this point is desirable.

It is important to note that the integral of (20) does not identify a drag component uniquely. The value of this integral depends on the stations $x=x_1$ and $x=x_2$ at which measurements are made. This dependency can be seen by first considering the limiting case where the station $x=x_1$ is far upstream of the model and next considering a case where the station $x=x_1$ is near the model. In the first case, v_1 and w_1 both go to zero and the contribution of the quantity $(v_1^2+w_1^2)$ to the integral vanishes. In the second case the contribution is finite since v_1 and w_1 are not vanishingly small everywhere and the quantity $(v_1^2 + w_1^2)$ is non-negative.

It is of interest to note that the second integral of (19) is independent of the measurement station $x=x_1$. In fact, since $u_1" = u_1'$, the contribution of $(v_1^2 + w_1^2 - u_1"^2)$ to this integral is zero according to (12). In the absence of a proof that the contribution of $(v_2^2 + w_2^2 - u_2"^2)$ to this integral is independent of the measurement station $x=x_2$, however, there is little reason to think that the second integral of (19) provides a better definition of a drag component than does (20).

The well accepted assumption that the total drag force acting on a three-dimensional lifting body can be resolved into distinct profile drag and vortex drag components is based on the understanding that two different physical processes are involved in the production of drag. The existence of the vortex drag component, the study of which is the primary concern of this paper, is based upon the notion of continual shedding of trailing vortices from a lifting body. Since shed vortices are accompanied by some kinetic energy of the fluid, power input is required to produce these vortices even if frictional work is left out of account. This power input is provided through work performed by the vortex drag. In a viscous flow, distributed vorticity exists instead of vortex filaments. A "diffused vortex system" trailing a lifting body is generally discernible in high Reynolds number flows, whether or not an appreciable region of recirculating flow (separation bubble) is present near the body. On this basis it is meaningful to accept the vortex drag as a definable component of the total drag for flows involving an appreciable recirculating region as well as for flows that does not contain such a region.

Based on the energy consideration just discussed, it is concluded that, because of the process of viscous dissipation occuring in the vortical wake, the identification of either the profile drag or the vortex drag with a wake integral cannot be precise. Indeed, such an identification must be non-unique, since viscous dissipation continually alter the energy content of the vortical wake. For a definition of the vortex drag, such as (20), to be meaningful, it is necessary for the rate of viscous dissipation to be very small in the vortical wake. If this necessary (though not sufficient) condition is met, then the possibility of defining the vortex drag accurately (though not precisely) by a wake integral exists. In a high Reynolds number flow, rapid viscous dissipation usually occurs only in boundary-layer regions near the model. The necessary condition just described is satisfied for most applications of practical importance.

3. Wake-Integral for Vortex Drag

3.1. General Expression for Vortex Drag

Consider the velocity components v and w in a transverse plane x=constant. These velocity components satisfy the following differential relations

$$\frac{\partial v}{\partial y} + \frac{\partial w}{\partial z} = f \tag{23}$$

$$\frac{\partial w}{\partial y} - \frac{\partial v}{\partial z} = \xi \tag{24}$$

where ξ is the x-component of the vorticity vector, and $f = -\partial u/\partial x$. Equation (23) follows from the continuity equation in three dismensions. Equation (24) is the axial (x) components of the vorticity definition equation. Both f and ξ are functions only of y and z in the transverse plane x=constant.

Let ψ and ϕ be two scalar functions of y and z satisfying the differential equations

$$\frac{\partial^2 \psi}{\partial y^2} + \frac{\partial^2 \psi}{\partial z^2} = -\xi \tag{25}$$

and

$$\frac{\partial^2 \phi}{\partial y^2} + \frac{\partial^2 \phi}{\partial z^2} = f \tag{26}$$

Equation (23) and (24) are satisfied if one lets

$$v = \frac{\partial \psi}{\partial z} + \frac{\partial \phi}{\partial y} \tag{27}$$

and

$$w = -\frac{\partial \psi}{\partial y} + \frac{\partial \phi}{\partial z} . \qquad (28)$$

Equation (25) and (26) are applied in the tunnel section A. With ξ and f known, these two equations do not by themselves uniquely determine ψ and ϕ. By prescribing appropriate boundary condition on the boundary of A, ψ and ϕ are rendered unique. For convenience, ψ is prescribed to be homogeneous on the boundary. Since the effective cross-section of the tunnel is uniform, the normal component of the velocity vector $v\vec{j} + w\vec{k}$ necessarily vanishes on the boundary. The homogeneous boundary condition for ψ then requires, on account of (27) and (28), the normal gradient of ϕ to be zero on the boundary.

From (23), (24), (27) and (28), one obtains

$$\iint_A (v^2 + w^2)\, dydz = -\iint_A \left[\frac{\partial}{\partial y}(\psi w) - \frac{\partial}{\partial z}(\psi v)\right] dydz$$

$$+\iint_A \left[\frac{\partial}{\partial y}(\phi v) + \frac{\partial}{\partial z}(\phi w)\right] dydz + \iint_A (\psi\xi - \phi f)\, dydz \qquad (29)$$

By the use of Stokes' theorem and the divergence theorem, the first two integrals on the right-hand side of (29) are re-expressed as line integrals:

$$-\oint_b \psi v_t\, ds + \oint_b \phi v_n\, ds$$

where b is the boundary of A, v_t and v_n are respectively the tangential and normal components of the velocity vector $v\vec{j} + w\vec{k}$ in the transverse section on b. The first integral above vanishes since ψ is zero on b. The second integral vanishes since v_n is zero on b. Equation (29) therefore reduces to

$$\iint_A (v^2 + w^2)\, dydz = \iint_A (\psi\xi - \phi f)\, dydz. \qquad (30)$$

Noting that ξ is non-zero only in the wake, one obtains the following expression for the vortex drag D_v, defined by (20):

$$D_v = \tfrac{1}{2}\rho \iint_W \psi_2 \xi_2\, dydz$$

$$+ \tfrac{1}{2}\rho \iint_A (\phi_1 f_1 - \phi_2 f_2)\, dydz \qquad (31)$$

3.2. Simplified Formula and Physical Significance

If the second integral in (31) vanishes, or is negligibly small compared to the first integral, then one obtains a simplified equation,

$$D_v = \tfrac{1}{2}\rho \iint_W \psi_2 \xi_2\, dydz \qquad (32)$$

and the vortex drag, like the profile drag, is determined by measurements only in the wake of a single transverse section.

There exist several circumstances under which (31) reduces to (32). Clearly, if the flow is essentially two-dimensional at the sections $x=x_1$ and $x=x_2$; i.e., it varies negligibly slowly with respect to x at these two stations, then both $f_1 = -(\partial u/\partial x)_1$, and $f_2 = (\partial u/\partial x)_2$ are negligible. Equation (32) is then valid. This occurs if the station $x=x_1$ and $x=x_2$ are sufficiently far from the model. It is, however, not practical to make measurements "sufficiently far" downstream of a model placed in the wind tunnel. Of greater practical importance are circumstances where the quantities $\phi_1 f_1$ and $\phi_2 f_2$ are individually not negligible, but are of nearly equal magnitude so that their difference is negligible. To examine these circumstances, it is necessary first to become familiar with the physical significance of the quantities ϕ, ψ, ξ, and f.

The vorticity field $\vec{\omega}$ surrounding the model in the wake downstream of the model is three-dimensional. In component form, one writes

$$\vec{\omega} = \xi\vec{i} + \eta\vec{j} + \zeta\vec{k} \qquad (33)$$

The velocity field in the tunnel is related to the vorticity field $\vec{\omega}$ kinematically through the continuity equation and the vorticity definition equation. With any given $\vec{\omega}$ distribution and appropriately prescribed velocity boundary conditions, the vector field $\vec{q}$ is uniquely determined. The contribution of the boundary condition to the velocity field $\vec{q}$ can be represented by image vorticity fields suitably placed outside the tunnel. Thus, one writes the following generalized Biot-Savart law for $\vec{q}$:

$$\vec{q}(x,y,z) =$$

$$-\frac{1}{4\pi}\iiint_V \frac{\vec{\omega}(x_o, y_o, z_o) \times (\vec{r}_o - \vec{r})}{\vec{r}_o - \vec{r}^{\,3}}\, dx_o dy_o dz_o \qquad (34)$$

where V is the region of non-zero vorticity, including the wake and all its images, $\vec{r} = x\vec{i} + y\vec{j} + z\vec{k}$ is the position vector, and the integration is performed in the $\vec{r}_o$ space. The vorticity field $\vec{\omega}$ now includes the actual vorticity in the tunnel and all its images.

It is obvious from the Biot-Savart law that an axial vorticity field, i.e. a vorticity field with only the ξ component non-zero, induces only transverse velocities. That is, the axial velocity component associated with an axial vorticity field is always zero.

For convenience, the vorticity field $\vec{\omega}$ is now decomposed into an axial vorticity field $\vec{\omega}_a$ and another vorticity field $\vec{\omega}_b$, with

$$\vec{\omega}_a = \xi_2 \vec{i} \qquad (35)$$

and

$$\vec{\omega}_b = (\xi - \xi_2)\vec{i} + \eta\vec{j} + \zeta\vec{k} \qquad (36)$$

where

$$\xi_2 = \xi(x_2, y, z). \qquad (37)$$

It is obvious from (25) that ψ_2 is a two-dimensional stream function associated with the axial vorticity field $\vec{\omega}_a = \xi_2 \vec{i}$. The first integral in (31) therefore represents a contribution of the axial vorticity field ω_a to the vortex drag. This integral in fact represents the total contribution of the axial vorticity field ω_a to the vortex drag, as shown below.

The field ϕ is uniquely determined by f, through (26), and the homogeneous Neumann boundary condition described earlier. Recalling that $f = -\partial u/\partial x$ and that the x-component of velocity associated with an axial vorticity field is zero, one concludes that f, and hence also ϕ, are dependent only on the transverse components, η and ζ, of $\vec{\omega}_b$. These components, moreover, are identical to the transverse components of the actual vorticity field $\vec{\omega}$ and its images. Thus, the first and second integral of (31) represents separately the contributions of the axial and transverse vorticity components of the vorticity field.

The quantity f may be interpreted as a source term in a two-dimensional continuity equation and the quantity ϕ may be interpreted as a scalar potential associated with f. Such interpretations, however, are not important for the purpose of estimating the relative importance of the two integrals in (31). By letting $\vec{\omega} = \omega_b$ in (34) and differentiating the x-component of the resulting equation, one obtains

$$f(x,y,z) = \frac{3}{4\pi} \iiint_V \frac{[\zeta_o(y_o - y) - \eta_o(z_o - z)](x_o - x)}{[(x_o - x)^2 + (y_o - y)^2 + (z_o - z)^2]^{5/2}} dx_o dy_o dz_o \qquad (38)$$

It is simple to show that if the transverse vorticity is compressed into a vortex sheet located at the section x=a, then $f(2a-x, y, z) = -f(x, y, z)$. Furthermore, with homogeneous Neumann condition for ϕ, (26) gives $\phi(2a-x,y,z) = -\phi(x, y, z)$. Therefore, $\phi_1 f_1 - \phi_2 f_2 = 0$ provided that one lets $x_1 = 2a - x_2$. In consequence, the second integral in (31) vanishes if the transverse vorticity is a vortex sheet located in a constant x section. In reality, the transverse vorticity components are small except in the neighborhood of the model. It is simple to show that, if the x=0 plane is placed at the center of pressure of the model, then (32) provides an accurate measure of the vortex drag as long as one selects x_2 such that $x_2 > 0$ (c/2), where c is the chordwise dimension of the model. The precise location of x_2 is unimportant as long as the above inequality holds.

3.3. Computation of ξ and ψ

With measured transverse velocity components v and w, the axial vorticity ξ is easily computed using (24) by numerical differentiation.

The stream function ψ can be computed by solving (25), subject to the homogeneous Dirichlet condition. It should be emphasized that ψ cannot be computed directly from measured values of v and w since, according to Equations (27) and (28), $\partial\psi/\partial z$ and $-\partial\psi/\partial y$ represent only a part (solenoidal part) of the transverse velocity. There exist a variety of methods for computing ψ by numerical solution of (25). A method which permits the ψ values to be computed only in the vortical wake, where they are needed, is described in section 4 of this paper. This method has been developed and used in the solution of viscous flow problems [6]. The method is highly efficient and highly accurate because of its unique ability to confine the computation of ψ to the wake region.

4. Application of the Generalized Wake-Integral Approach

4.1 Experimental Techniques

Experimental implementation of the above equations presents a substantial challenge both in experimental technique and in data handling and analysis. Pressure probe techniques have long been available for measuring flow velocity and direction over a suitable range (see ref. 8). However, the need to determine cross-flow derivatives places serious demands upon the accuracy of measurement at any given point while also requiring greater-than-usual point density across wakes or vortices. There is also a definite question whether a five-hole pitch-yaw probe, for example, as needed for cross-flow measurements is also inherently suitable for determining profile drag.

First-generation experiments in the Lockheed-Georgia 30" x 43" wind tunnel highlighted the practical difficulties mentioned above. For example, though the traverse gear had been adequate for other work, it introduced slight and (more importantly) nonrepeatable variations in probe alignment. Small irregularities in the tunnel flow also degraded the early results. These problems have now been overcome: a new, more robust and more accurate traverse gear is now used and a honeycomb has been installed in the wind tunnel. In addition, datum runs are now made with the tunnel empty which exactly repeat the test procedure. These are used to remove the effects of deflection, of probe wander and, to some degree, of tunnel flow irregularities.

Probe calibration has also been refined. The method currently used for the five-tube Conrad-type probes is basically the chart method described in reference 8. However, a number of modifications have been made including the use of minimum, rather than mean, side-tube pressure in the denominator of quantities such as $(p_3 - p_1)/(p_5 - p_m)$. This extends the usable angle ranges of the probes. A comprehensive calibration procedure is employed using a special, accurately-machined rig with complete sets of measurements made every five degrees in pitch and yaw over a ±40-degree range. Four calibration maps are produced for each of the seven rake probes and both calibration and data reduction procedures are highly automated. Inspection of the calibration maps has revealed nonlinearities, for simultaneous pitch and yaw, which make the above comprehensive approach mandatory in the present application. Contrary to the experience of some workers, the calibrations have remained repeatable over a period of years.

4.2 Calculation of Fundamental Flow Variables

Lateral and vertical components of velocity, total pressure and static pressure at the measurement points are determined on-line and presented at the tunnel console. The subsequent, off-line analyses for determination of vorticity, stream function, induced drag and profile drag will be described below.

All computations are made on a 'calculated' grid pattern which is offset by one half mesh from the measurement points.

Calculation of Vorticity, ξ, in the Wake. The circulation around each point on the calculation grid is determined using a simple circulation integral using velocity components at the nearest measurement points. Division by mesh area completes the vorticity calculation.

Calculation of Velocities due to Wake Vorticity. Since the divergence of the velocity field in the measurement plane, i.e., $\partial v/\partial y + \partial w/\partial z$, is in general non-zero, the stream function ψ in (32) cannot be uniquely determined directly from measured values of v and w. In the present study, the induced velocity field associated with the distributed wake vorticity ξ is first calculated. The algorithms utilized for this calculation are those reported in Reference 9. The procedures were verified by recomputing the vorticity values, using the calculated induced velocity values, and comparing the results with the original values of ξ.

Tunnel Boundary Correction. The measured transverse velocities included contributions associated with tunnel wall constraint. Field-point vorticity values obtained from the measured velocities reflect the boundary condition at the tunnel wall. The induced velocity values just calculated, however, do not reflect the effects of the boundary condition. These values in general do not give zero normal velocity at the tunnel boundary, a condition required by the physics of the problem. The induced velocities therefore must be corrected before being used to compute the stream function ψ. The procedure used in the present work is a "tunnel correction" in the limited sense that the normal velocity is rendered zero at the tunnel wall and transverse velocities at points within the tunnel reflects this fact. The procedure bears no relationship to tunnel corrections as usually understood.

In order to compute the present tunnel wall correction, a mesh of point vortices is arrayed around the boundary with intermediate collocation points. Normal velocities, due to the internal vorticity ξ, are calculated at these collocation points. A solution for the strength of the boundary vortices is then obtain by requiring the combined velocity field of the internal vorticity ξ and the boundary vortices to have zero normal component at the tunnel boundary. Velocities induced by the boundary vortices are calculated and added to that induced by the internal vorticity at points on the calculation mesh. This procedure is conceptually equivalent to the use of image vorticities outside the tunnel to satisfy the tunnel boundary condition. The procedure is relatively simple to execute. Its validity is shown in Reference 7.

Calculation of Stream Function. The combined velocity field just computed is free from flow divergence and satisfied the required tunnel boundary condition. The computation of a stream function associated with this velocity field is a straightforward matter of performing a line integral of transverse velocity from a convenient reference point to the field point.

4.3 Calculation of Lift and Drag

The traverses and axis systems of the present work are related to the tunnel centerline for drag and to the true vertical for lift. No attempt is made to correct to equivalent free air axes. Conventional axis notation is used.

Calculation of Lift Coefficient. Lift is readily obtained by considering each element of trailing vorticity as emanating from a bound vortex far upstream. Thus

$$C_L = \frac{2}{u_o S} \sum_W y_i(\xi_i \Delta y_i \Delta z_i) \qquad (39)$$

where individual values i are summed over the wake W. Δy and Δz are mesh dimensions. S is the lifting surface area.

Calculation of Induced-Drag Coefficient. Integration of Equation (32) is performed via a simple summation, namely

$$C_{D_i} = \frac{1}{u_o^2 S} \sum_W \psi_i \xi_i (\Delta y_i \Delta z_i) \qquad (40)$$

Figure 2 shows the distributions of ξ, ψ and their product for the flow behind a half-wing. Vorticity and stream function contours each show the anticipated form. In more recent experiments, with tighter grids normal to the wing trailing edge, inboard-going tongues are evident in the stream function contours in the viscous wake. In the distribution of the product $\xi\psi$, vorticity evidently has a dominant effect upon the contour shapes.

Calculation of Profile Drag Coefficient. This is evaluated using the standard method described by Betz[1] and later by Goldstein[3]. These authors identify the first integral in Equation (19) as the profile drag. In the experimentally-obtained flow variables H_o g_o H_{2i} and g_{2i}, this becomes

$$C_{D_p} = \frac{1}{S} \sum_W (H_{T_i} + H_{S_i})(\Delta y_i \Delta z_i) \qquad (41)$$

where $g = \frac{1}{2} \rho u^2$

$$H_{T_i} = \frac{H_o - H_i}{g_o}$$

$$H_{S_i} = \left[\left(\frac{u_{2i}^*}{u_o}\right) - \left(\frac{u_{2i}}{u_o}\right)\right]\left[\left(\frac{u_{2i}^*}{u_o}\right) + \left(\frac{u_{2i}}{u_o}\right) - 2\right]$$

and

$$\left(\frac{u_{2i}^*}{u_o}\right) = \left(\frac{H_o - (H_{2i} - g_{2i})}{g_o}\right)^{1/2}$$

$$\left(\frac{u_2^*}{u_o}\right) = \left(\frac{H_{2i} - (H_{2i} - g_{2i})}{g_o}\right)^{\frac{1}{2}}$$

In practice, it is found that the H_S term is relatively small, leaving the total pressure deficit integral as the main contributor to profile drag.

5. Experimental Results

5.1 Flow Measurements

A floor-mounted half-wing was set up in the Lockheed-Georgia 30" x 43" low-speed tunnel as shown in Figure 3. Wake surveys were carried out, using the techniques described in Section 4.1, at distances of 7 inches and 34 inches aft of the wing quarter-chord. Only results from the forward traverse position will be described here. Six horizontal sweeps were made through the wake with points taken at 0.1-inch intervals for the upstream traverse and 0.2 inches downstream. The spacing between the 7-probe sweeps was three inches vertically. Traverses were made at angles of attack of 0, 3, 6, 7½, 9 and 12 degrees. Tunnel floor boundary layer control was not applied.

Figure 4 shows typical measured cross-flow vectors at the higher angles of attack. For reproducibility, only every fourth vector is shown in the across-wing direction. The tip vortex and the velocity jump across the trailing vortex sheet are clearly visible. In addition, there is evidently a significant disturbance at the wing root where it intersects the floor. Ultimately, this develops into a root stall. Examination of the velocity jump in the wake shows a sign change (i.e. a load maximum) some 5½-inches outboard of the wing root. It remains at this location up to and including $\alpha = 7\frac{1}{2}^\circ$. At greater angles of attack, the maximum load point moves outboard as the lift curve departs from linearity.

Figure 5 shows contours of axial vorticity corresponding to the Figure 4 flow vectors. As a consequence of the non-square grid (0.1" x 0.5"), the tip vortex vorticity contours are flattened. This provides a good illustration of the tendency of simple averaging procedures to spread vorticity concentrations. Though gross quantities such as overall circulation are not affected, further study is needed to assess theoretically the impact upon wake integrals and to develop improved methods for non-square grids.

5.2 Force Integrations

Measured lift values (normal to the tunnel axis) agreed extremely well with wake integrations via Equation (39). However, drag measurements were inconsistent with the known performance of the wing, probably due to turntable tare forces. New tests are being made to investigate this. Comparisons will therefore be made against estimates made using standard procedures.

Lift Curve Slope. Reference 10 gives

$$a = k\,\frac{a_e}{1 + 57.3\,a_e/\pi AR} \qquad (42)$$

where a_e is based upon measured sectional data and includes Jones' edge correction factor. k is obtained from Reference 10. Conventional wind tunnel procedures are used to correct a for tunnel-induced upwash effects. Figure 6 shows excellent agreement in slope between the wake integral, (39), and (42) above. Departure from the theoretical line above 7½-degrees reflects inboard separation, mentioned previously.

Induced Drag Factor. For an untwisted wing induced drag is given by

$$C_{D_i} = \frac{C_L^2}{\pi AR\,e} \qquad (43)$$

where the induced drag factor e is obtained from standard texts. Reference 10 gives 0.976 for the the present wing. The broken line in Figure 7 reflects this value, suitably corrected for tunnel constraint. The experimental vortex drag values, determined from wake measurements via Equation (40), give a significantly lower "e" value than that obtained from Equation (43) after correction for tunnel constraint. However, there are obvious departures from full-span wing flow near the present wing root where there is evidence of premature flow separation in the vicinity of the floor boundary layer (see Figure 4). Fairing through this region produced good results for profile drag (see below) but this has not yet been done for vortex drag. Further, more detailed reviews of the existing data will clarify this situation. When new force data becomes available, this will also contribute, since total drag checks will then be possible.

Profile Drag. Figure 8 shows the distribution, across the wing wake, of the integrand of Equation (41). These are essentially total pressure contours. Once again, tip vortex contours are oval as a result of grid shape and the previous comments apply.

Figure 9 shows integrated profile drag, which is compared with sectional data [10] as a function of C_L^2. To facilitate this comparison, wing root effects (Figure 8) have been faired out. Figure 9 shows remarkably good agreement with sectional data in the 0 to 6-degree range. The wake integrations are approximately two counts higher than the two-dimensional values, an amount consistent with the Reynolds number difference involved. The departure from lift linearity is reflected in C_{D_p} above 7½-degrees angle of attack.

The present results suggest that there are no serious drawbacks in using five-hole probes for profile drag measurement.

6. Concluding Remarks

The present position of the authors' research program concerning theoretical, experimental, and verification aspects of a generalized wake-integral approach for drag determination in three-dimensional flows has been reviewed in this paper. Some results of detailed pitch/yaw pressure probe traverses behind a simple wing are also presented. It may be said that theoretical and experimental data acquisition aspects of the problem are reasonably well in hand. The exploratory studies presented here for a simple wing show good correlations with anticipated performance in lift and profile drag. The vortex drag determined by wake

measurements is higher than anticipated. Though this deviation may be a genuine reflection of a flow problem occuring where the wing root intersects the tunnel floor, the possibility is not excluded that integration techniques, for example, require further refinement. Isolated off-range data points also may have affected the results. Additional data analyses are being carried out to clarify this situation.

Theoretical studies suggested that the profile and vortex drags can be separately measured through wake integrals and such measurements can provide quantified knowledge about the relative importance of various flow features to drag. Furthermore, wake measurements are relatively insensitive to the downstream location of the measurement station. Experimental results lend substantial support to these expectations. Experiments and data analyses thus far have omitted several contributions to drag that are of secondard importance. Among these contributions are those due to the blockage velocity u_b, or alternatively u", due to the transverse vorticity integral, and due to the interchange between the total pressure deficit integral and the vorticity integrals as a result of viscous dissipation in the wake. Definitive experiments quantifying these secondary contributions are appropriate for the future.

Acknowledgement

This research was supported by the Lockheed-Georgia Company and by the Office of Naval Research, Contract No. N00014-75-C-0249. The authors wish to record their thanks and deep appreciation to Mr. R. A. Boles who painstakingly developed the experimental techniques and who also carried out the wake traverses presented in this paper.

References

1. Betz, A. "Ein Verfahren zur direkten Ermittlung des Profilwiderstandes", Zeitschrift fur Flugtechnik und Motorluftschiffahrt", Vol. 3, 1925.

2. Maskell, E. C., "Progress Towards a Method for the Measurement of the Components of the Drag of Wing of Finite Span," Royal Aircraft Establishment Technical Report 72232, 1973.

3. Goldstein, S., Editor, "Modern Developments in Fluid Dynamics", Vol. 1, pp. 258-260, Oxford University Press, 1938.

4. Prandtl, L., "Aerodynamic Theory, Edited by W. F. Durand", Vol. 3, pp. 202-207, Dover. 1963.

5. Wu, J. C., "A Theory for Aerodynamic Forces and Moments", Report under ONR Contract No. N00014-75-C-0249, Georgia Institute of Technology Report, June 1978.

6. Wu, J. C., and Thompson, J. F., "Numerical Solution of Time-Dependent Incompressible Navier-Stokes Equations Using an Integro-Differential Formulation," Journal of Computers and Fluids, Vol. 1, No. 2, pp. 197-215. 1973.

7. Wu, J. C., "Numerical Boundary Conditions for Viscous Flow Problems", AIAA Journal, Vol. 14, Aug. 1976, pp. 1042-1049.

8. Bryer, D. W.; and Pankhurst, R. C.: "The Determination of Wind Speed and Flow Direction by Pressure-Sensing Instruments," N.P.L. Note on Applied Science.

9. Wahbah, M. M.: "Computation of Internal Flows with Arbitrary Boundaries Using the Integral Representation Method." Technical Report Under ARO Grant No. DAAG29-75-6-0147.

10. Abbot, I. H.; and von Doonhoff, A. E.: "Theory of Wing Sections," Dover Publications. 1958.

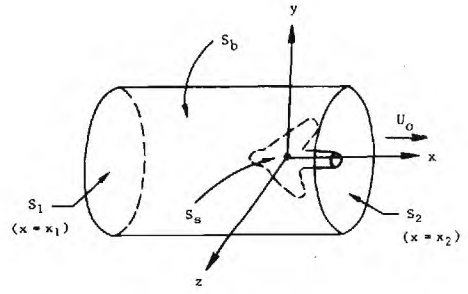

FIGURE 1 DEFINITION OF AXES AND INTEGRATION SURFACES

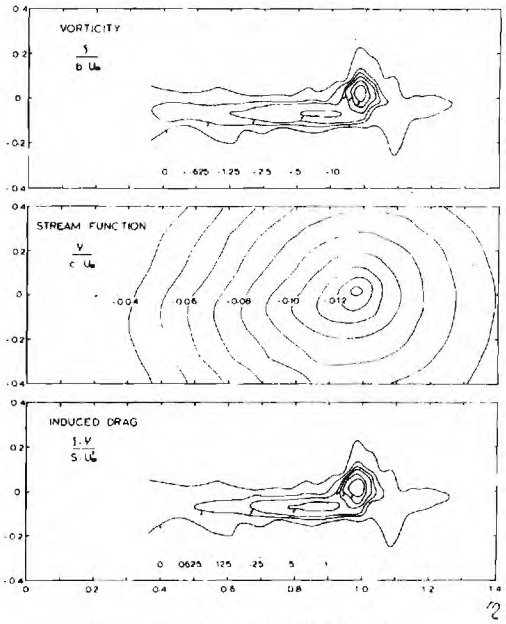

FIGURE 2 BUILDUP OF VORTEX DRAG INTEGRAND

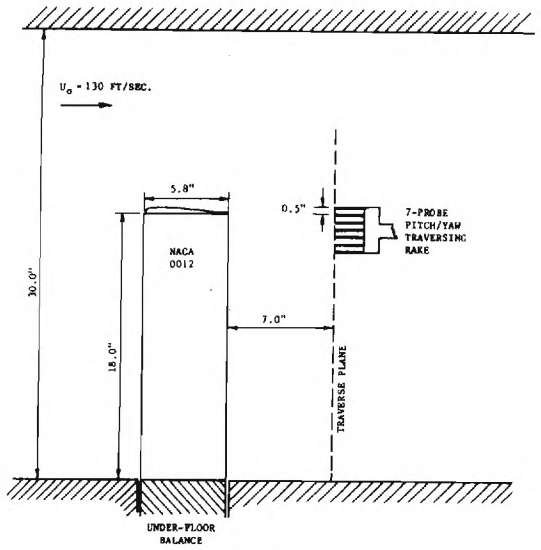

FIGURE 3 RECTANGULAR WING EXPERIMENT

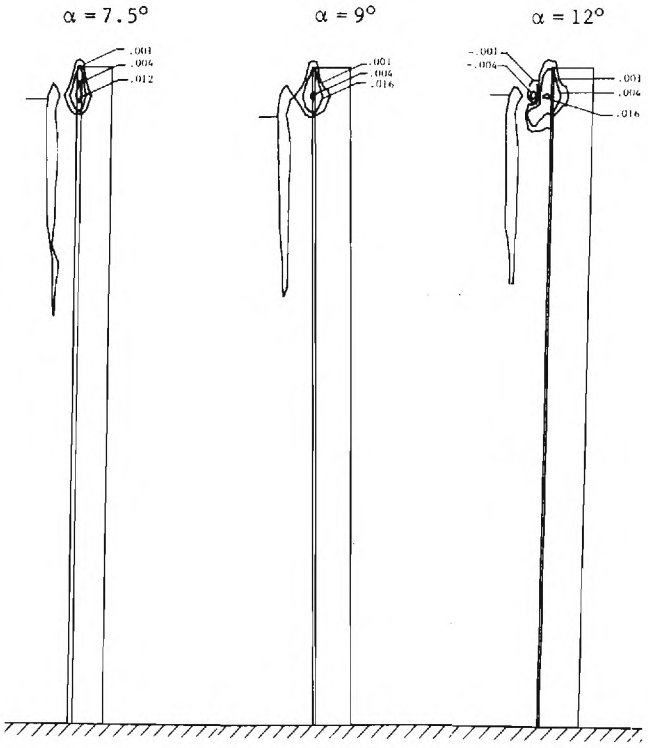

FIGURE 5 MEASURED AXIAL VORTICITY DISTRIBUTIONS FOR AR=6 WING AT VARIOUS ANGLES OF ATTACK

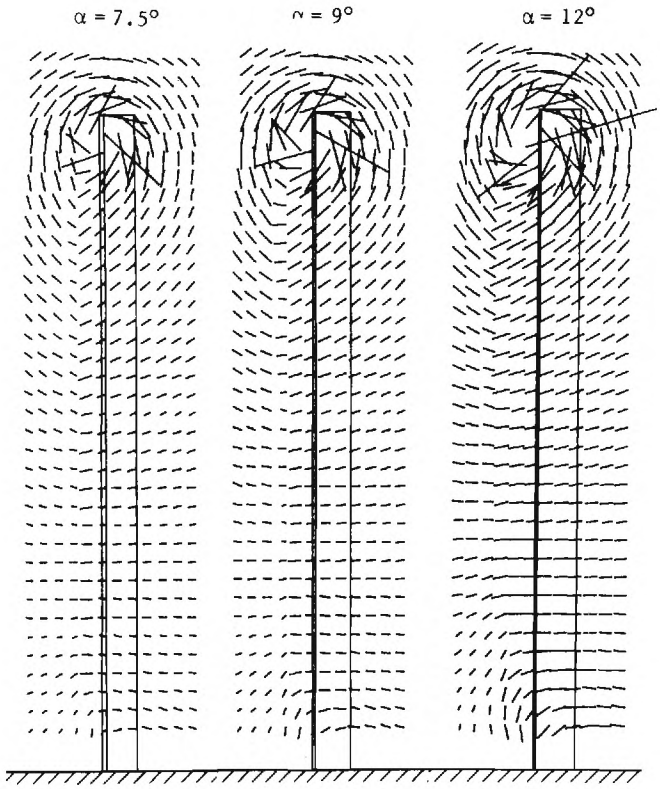

FIGURE 4 MEASURED FLOW VECTORS FOR AR=6 WING AT VARIOUS ANGLES OF ATTACK

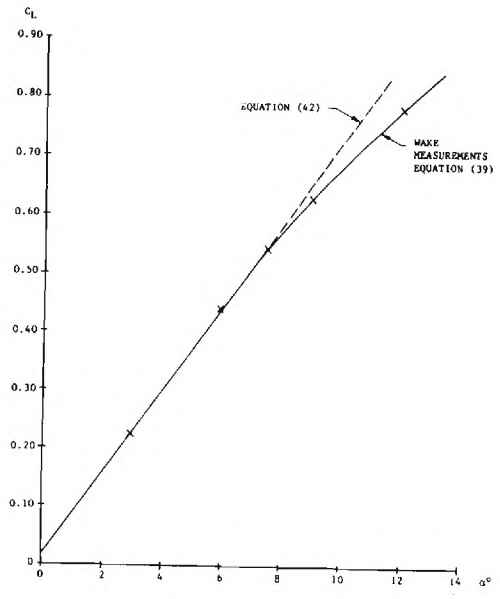

FIGURE 6 IN-TUNNEL LIFT FOR AR=6 WING

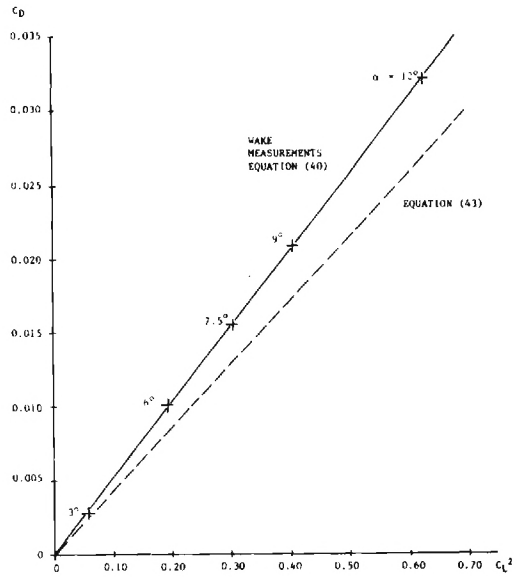

FIGURE 7 IN-TUNNEL VORTEX DRAG FOR AR=6 WING

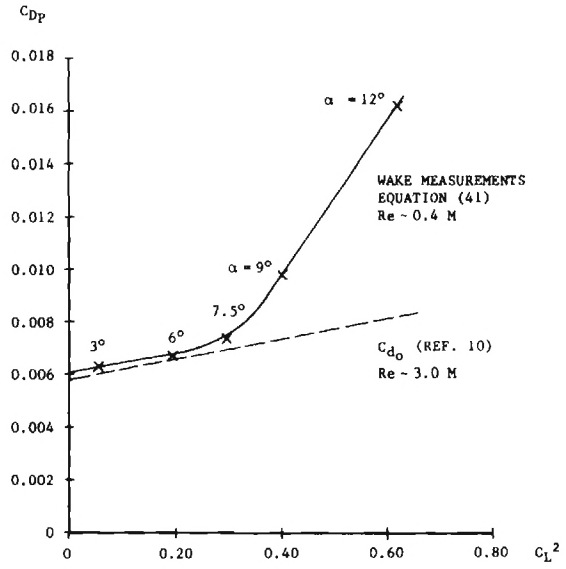

FIGURE 9 PROFILE DRAG FOR AR=6 WING

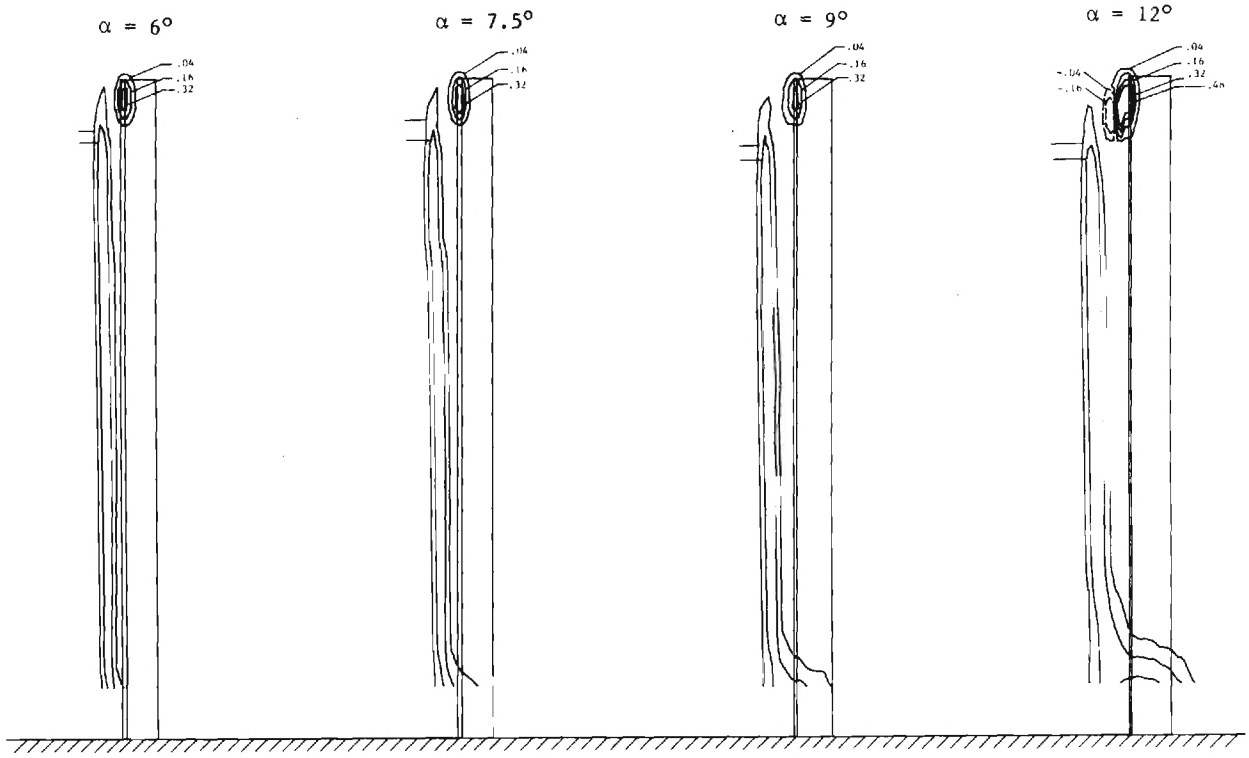

FIGURE 8 PROFILE DRAG INTEGRAND FOR AR=6 WING AT VARIOUS ANGLES OF ATTACK

APPENDIX B

Three-Dimensional Wake Flow Measurements

Lockheed-Georgia Report LG 81 ER 0201

by J. E. Hackett, C. G. Phillips and D. E. Lilley

LG 81 ER 0201

THREE-DIMENSIONAL WAKE FLOW MEASUREMENTS FOR A WING AND A BLUFF, CAR-LIKE BODY

BY

J. E. HACKETT

C. G. PHILLIPS

D. E. LILLEY

August 1981

Prepared for the Georgia Institute of Technology under Subcontract 1-E-16-655 as part of a collaborative study sponsored by the NSF via Grant No. ENG-7900891.

Lockheed-Georgia Company

Marietta, Georgia 30063

CONTENTS

CONTENTS (Cont'd)

LIST OF FIGURES

LIST OF FIGURES (Cont'd)

SUMMARY

Comprehensive wake traverse data are presented, with limited discussion, for tests upon a simple wing and a bluff, car-like model. These data are supplemented by limited traverse data ahead of the wing. All traverses were made with five-holed pitch/yaw pressure probes and suitable force data were acquired for correlation with wake integration, which shall be the subject of future work. The data have been transmitted to Professor J. C. Wu, of Georgia Tech, for this purpose.

The experimental and data reduction techniques for the wake traverses, which represent more than five years of development, are described in detail. The report also includes a review of some open questions concerning wake traverses, many of which arose during the present studies.

This report is identified as LG 81 ER 0201 for Lockheed internal control purposes.

ACKNOWLEDGEMENTS

The authors wish to express their sincere thanks to:

Sherry Bartley, who prepared many figures;

Shelby Christophers and Louise Ballew, who typed the text;

Ananthanarayanan Sugavanam, for his help in preparing Appendix II;

Professor J. C. Wu, for helpful comments and discussions on numerous occasions over the past two years.

The Ford Motor Company for permission to use the 'SAS' idealized car model design.

1. INTRODUCTION

1.1 General Background

In 1973 Maskell (ref. 1) described an integral method for determining vortex drag which represents a significant advance because measurements are needed only in a model's wake: direct cross-flow kinetic energy integrations, extending into the far field, are avoided. In 1978-9 the method was generalized by Wu, Hackett and Lilley (ref. 2). At about the same time Landahl (ref. 3) derived a similar result independently.

Though reference 2 shows the general method to be very successful for wake traverses aft of a simple wing with attached flow, the method has not been checked for more complex or for highly separated flows. In addition, certain integral terms found in the reference 2 studies were discarded in reference 1 at an early stage. It is not readily apparent when such neglect of the "source-term" integral is justified.

In September 1979 the Georgia Institute of Technology and the Lockheed-Georgia Company were awarded a joint grant by the National Science Foundation to study the questions just described. The present report gives the results of experiments carried out by the Advanced Flight Sciences Department at Lockheed-Georgia, in its "MTF", 30 x 43 inch low speed wind tunnel, under contract to Georgia Tech. Corresponding data, delivered on magnetic tape in early October 1980, is being analyzed at Georgia Tech to complete the joint program.

1.2 Selection of Test Models

To provide a thorough test of the new wake-integral method, a range of model characteristics was required which included both vortex-dominated and profile drag dominated wake characteristics. There was also an obvious need to examine the effectiveness of the method for complex wakes containing a number of vortices. The models agreed upon were a basic, aspect ratio three wing with NACA 0012 section (Figure 1.1), and an idealized car shape

(Figure 1.2). A major factor in choosing these models was that each had an extensive test background and its characteristics were well known.

The wing model had been the subject of wake flow investigations dating back to 1974. However, the original balsa wing was replaced by a more accurately made metal wing for the present test. Force and moment data for the new wing differed negligibly from those for the previous model.

Since a simple high-profile-drag wake can be generated by the wing at high-angle-of-attack, a more complex shape was chosen for the bluff body tests. The "simple automobile shape" selected exhibits a two-vortex pair wake pattern and has the additional advantage of an extensive test background (ref. 4). The shape was developed by Ford and Lockheed as a standard for preformance comparisons between wind tunnels. The new model was sized, for the "MTF", so that the model-to-test section relationship was the same as for the "full-scale" model when tested in the Lockheed-Georgia 16.25 x 23.25 foot tunnel.

Full details of the models and test facilities will be given in Section 2.

1.3 Test Instrumentation

Both the wing and the car model were mounted from a platform balance which measured forces and moments in a horizontal plane (i.e. lift, drag and pitch for the wing; sideforce, drag and yawing moment for the car). In addition, the wing was fitted with a root balance which measured root bending moment and normal load. The tunnel ceiling was equipped with a central row of pressure orifices which were used to determine tunnel blockage interference at the model location using the "wall pressure signature" method of reference 5.

The mainstay of the reference 2 flow measurements was a 5-holed probe rake used to measure total pressure and the three mean velocity components. While this instrument was evidently adequate for the largely attached flows investigated in reference 2, it was not apparent that equal success would be possible in the heavily separated, highly turbulent wakes of current interest. Accordingly emphasis was placed, at the proposal stage, on using a laser velocimeter.

Severe operational difficulties were encountered with the LV and its traverse gear. A number of unrelated mechanical and electronic failures occurred, including a laser tube failure. These difficulties were compounded by the fact that, to obtain three velocity components, two sets of two-dimensional measurements were needed, from different angles. The outcome of the LV problems was that a single, minimally intrusive, five hole pitch-yaw probe was used for measurements in an upstream plane: all wake measurements employed the rake of 5-holed probes, as previously.

1.4 Scope of Tests and Analysis

Each model was tested at two attitudes with traverses at up to three planes - upstream, near-wake and far-wake - for each attitude. The wing model was tested at 6-degrees and 18-degrees angle-of-attack with traverses at approximately -6" (i.e. ahead of quarter chord), 12" and 36" and -6", 18" and 36" respectively. The further-aft location for the near-wake traverse was used in the latter case to ensure that the separation bubble closed ahead of the traverse. The car model was tested at zero and 12.5-degrees yaw: traverses were at 18" and 36" aft of the model center.

Data quality was tested, as it was acquired, by using the original Lockheed analysis program to produce wake flow plots, including vorticity contours. At a later stage, stream function was computed and streamline plots were prepared. Details of these analyses are given in Section 4. The main results are presented in Sections 5 and 6, which includes comprehensive plots of both measured data and derived quantities.

2.0 TEST FACILITIES, MODELS AND PROBES

2.1 The Model Test Facility

The Model Test Facility (MTF) is a closed return low speed wind tunnel located at the Lockheed-Georgia Company Research Laboratory. The rectangular test section has a 30" x 43" cross-section and a usable length of 90". A three-component (sideforce, drag and yaw) strain gauge balance is located beneath the tunnel floor 30" from test section entry, leaving 60" of test section for wake observation and measurement.

The tunnel is driven by a constant speed 400 horse-power motor running at 1200 rpm. A 6 foot diameter fan is manually controlled via an eddy current variable speed unit. A motorized turntable on the underfloor balance permits easy selection of yaw angles (or pitch for half models) during a run.

An electrically driven 2-D traverse mechanism, which may be seen in Figures 1.1 and 1.2, can be mounted in the downstream portion of the test section to permit remote control of probe position during wake surveys. This mechanism is limited to an operational width of about 14", but can accommodate about 27" of the 30" tunnel height. The probe position is continually displayed to the operator, and automatically monitored by the data acquisition system.

The MTF data acquisition system can simultaneously acquire analog data from 32 channels. Currently, only 16 of these channels are equipped with signal conditioners and amplifiers and are used to monitor free stream conditions, internal and external balances, scani-valves and single unit pressure transducers. The remaining channels are used for self contained measurement devices such as hot-wire anenometers. Data can be acquired at rates up to 5000 samples/sec for a maximum of 32768 samples.

The heart of the system is a 32K Lockheed electronics MAC 16 mini-computer which is equipped with a dual "Floppy Disc" system, CRT input

and high speed line printer output. Data reduction is generally on-line, however, a 9-track magnetic tape unit is available to store the raw data to permit re-reduction with updated constants, or to permit a higher level of reduction on alternate computer systems.

2.2 Wing and Car Models

The wing model was an aluminum replica of the original balsa wood NACA 0012 section wing which has been used very successfully in previous tests. This semi-span model has 12" chord and 18" span and is mounted, at floor level, directly to the underfloor balance, which measures lift, drag and pitching moment. The wing tip is a half-body of revolution with a cross section matching the NACA 0012 wing section. The positions of the wing and the survey planes are shown in Figure 2.1.

The attachment to the balance is through a 1" diameter internal balance mounted in the quarter chord of the wing root. This eliminates the need for a rotatable floor section and also provides root bending moment, normal load and end load for the wing.

The car model was a wooden 15.4 percent scale model of the "full scale" standard automobile shape utilized in Lockheed's 16.25 x 32.25 foot low speed wind tunnel. It's major dimensions are shown in figure 2.2 together with the location of the survey planes. The car was attached to the underfloor balance by 0.25" diameter steel pegs in each wheel which, in turn, were attached to a metal plate mounted on the balance. Clearance holes were drilled in the floor of the tunnel, at each of the desired yaw positions, to accommodate these pegs.

The 19" to 22" width of the survey necessary to fully encompass the car's wake, required that the survey be completed in two halves because of the limited lateral probe movement. The traverse rig position was retained and the probe was offset in each direction to give about 2" of overlap between the two halves of the survey.

2.3 5-Holed Probes and Their Calibrations

The basic tool used to determine the flow conditions in the wake of either model, was the 5-holed pressure probe (Figure 2.3), so named because it consists of four inclined static pressure orifices mounted about a central total pressure orifice. The pressure differential between the opposing pairs of static pressure orifices is proportional to the pitch or yaw attitude of the probe, and the combination of the statics and the total orifice readings yields the true total and dynamic pressures, as a function of these attitudes.

The probe is calibrated, using the rig shown in Figure 2.4 by subjecting it to a combination of pitch and yaw attitudes in a known flow, and generating the plots typified by Figure 2.5. These maps are stored on the disc for each probe of the rake and are readily available to the computer. The terms F(A) and F(P) can be determined from the five measured pressures, noting that P_{min} is the minimum of the four static pressure orifices, not the average more commonly used. This procedure increases the angular range of the instrument. The attitudes, alpha and psi (pitch and yaw) can then be determined from the alpha-psi map. The total and dynamic pressure terms, F(H) and F(Q), are then obtained from their respective maps and the appropriate pressures and velocities are calculated.

This procedure, and the collation of the results for the entire survey, are beyond the capability of the on-line reduction program, and are handled off-line on a separate computer equipped with a larger disc memory, a scope and hard copy plot capabilities.

2.4 Test Conditions

In most tunnel tests involving force measurements, data is corrected for tunnel-induced axial flow effects, via 'blockage' corrections and for lift related tunnel-induced upwash, via angle-of-attack corrections. Both of these corrections increase in the downstream direction for unpowered

models, though blockage may pass through a peak in the vicinity of the model. In many cases, it is sufficient to use a single blockage and a single angle-of-attack correction, corresponding to the model location. However, blockage gradients must be recognized in the present work because of the substantial axial distances between the model and the traverse locations. Blockage effects are of two types; due to model/separation bubble volume - solid blockage - and due to the displacement effect of the viscous wake, which causes wake blockage.

Distributions of total blockage, i.e. solid-plus-wake, are shown in Figures 2.6 to 2.8 for the various model conditions and traverse locations employed in the present work. These will be discussed further below. Filled points in these figures depict temporary, on-line corrections which are mainly wake-related. There is one q-ratio per model condition/ traverse location and this ratio is used to correct both the force and the traverse data presented later in this report. These temporary, on-line corrections are employed subsequently in this report and will be discussed further in subsection 4.2.

Determination of Blockage Distributions

The method used, known as the "wall pressure signature method," is a developed version of a method invented at Lockheed-Georgia in 1975. It relies entirely upon pressure measurements at wind tunnel surfaces - along the tunnel ceiling for the car, and along a horizontal line opposite to the wing tip. These data are used as input to what is essentially an inverse solution which determines the strengths of an array of line sources representing the model (see References 5 and 7). Having determined these strengths, in the presence of the tunnel, calculation of tunnel effect is achieved by removing the central member of the image set.

Blockage Distributions for Wing Tests

Figure 2.6 shows the blockage distribution due to the wing and its wake with the effect of the traverse gear removed. The data were prepared

by subtracting wall velocities with only the traverse gear installed (at the 36-inch location) from corresponding wing-plus-gear data, then converting back to Cp.

At 6-degrees angle-of-attack, the blockage is very small, since the wing occupies only 3% of the tunnel cross section and flow is attached. Wake blockage, represented by the downstream asymptote, predominates over the solid blockage effect.

At 18-degrees, a stalled condition, there is a large increase in blockage which occurs mainly in the wake components. The solid blockage now reflects the occurrence of a large separation bubble behind the model. The large blockage asymptote is caused by the thick wake which develops subsequently.

Figures 2.7 and 2.8 represent the true test condition for the present work, with the traverse gear present. Though the normal-to-stream area of its components is not unduly large, the gear's aerodynamic shape is poor and comparison between Figures 2.6 and 2.7 shows that it causes a substantial blockage increase.

Vertical broken lines in Figures 2.7 and 2.8 depict the traverse planes of interest. It is apparent that the dynamic pressure rises by several percent between the model and the traverse planes. As the traverse gear is moved back to the 36" location (broken curves) its effect is reduced. A summary will be given, in a later figure, of the q-ratios relevent to specific traverses.

Blockage Distribution for Car Tests

Though the car's cross section is only about twice that of the wing, it is aerodynamically 'dirty'. Consequently its blockage effects (Figure 2.8) are comparable with the stalled wing. Yaw produces some increase in blockage due to the newly exposed leeward area of the car side. However the effect is not large.

Summary Table for Blockage Effects

Figure 2.9 is a tabulation of blockage dynamic pressure ratios at the model and traverse plane locations. The "on-line" data are those used during the preparation of force and flow field data presented in later sections. As noted previously, the same values are used at both model and traverse positions. The "off-line" data are taken from the full, wall-pressure signature results depicted in Figures 2.7 and 2.8 It is anticipated that the latter data will be needed to complete a proper momentum balance during wake analysis.

3. MEASURED FORCES AND MOMENTS

Force and Moment data for the wing and the car are tabulated Figure 3.1 for ready comparison with wake integral results to be derived using the new analyses being developed at Georgia Tech. For discussion purposes, corresponding data plots are also provided. Force and Moment data are presented in this report without correction for tunnel-induced upwash but with "on line" blockage corrections (see previous section). This procedure permits direct comparisons with wake integrals.

3.1 Lift, Drag and Pitching Moment for Wing Model

The initial slope of the C_L α ~ curve in Figure 3.2 agrees well with classical finite-wing theory, if modified suitably to include the present tunnel-induced upwash and blockage effects. (see Ref. 6) The middle part of the lift curve exhibits upward curvature, away from the theoretical slope, due to vortex lift at the wing tip. Subsequently, the curvature reverses as boundary layer thickening reduces the lift curve slope. Finally, a rapid stall occurs at about 16-degrees angle-of-attack. This is accompanied by pitch down (Figure 3.3) as the airfoil center-of-pressure moves aft.

The drag polar (Figure 3.2) also shows the expected behavior. Detailed analyses in Reference 6 includes a study of the induced drag factor `e` and shows that the measured value approximates well to the sum of the finite-wing, potential flow `e` and a constant representing the viscous sectional drag increase with C_L-squared.

3.2 Forces and Moments for the Car Model

As mentioned earlier, the platform balance on the MTF tunnel measured side force, drag and yawing moment directly in wind axes. No attempt was made to use the vertical balance, as for the wing, because of balance flexibility and the consequent potential for problems with wheel/floor fouling and with known drag sensitivity to small angle-of-attack changes. As the model was mounted from pins extending below the simulated wheels, continuous

variation of yaw was not possible and a series of individual runs was required. As for the wing, tunnel corrections were made only for blockage,using the "on-line" procedure.

The force tests with the car yawed were conducted at a late stage in the present work. Earlier it had been hoped to use the present zero yaw data as a check point and to rely upon existing data to supplement this. However, on reviewing the existing data, inconsistencies were revealed between tests at various model scales (Ref. 4) and it became evident that new tests were needed. This means that only sideforce, drag and yawing moment data are available directly. Other components may be estimated from Reference 4 using 100-inch wheelbase model data, since this is in best agreement with the present results for those components which were measured. It should be noted that much of the Reference 4 data is quoted in a body axis system which causes the drag characteristics, in particular, to look considerably different from those quoted here. Slight differences also exist between models, particularly in the omission of transverse underfloor beams on the present model. This omission was at the recommendation of the test engineer who supervised the large-scale tests. At 15.4-inch wheelbase scale, as for the present model, beam cross section would have been approximately 0.3-inches square. Comparison with Ref. 4 data shows that their omission reduced the zero-yaw drag coefficient by about 0.04.

The sideforce, drag and yawing moment coefficients are plotted against angle of attack in Figures 3.4, 3.5 and 3.6 respectively. The sideforce curve is surprisingly linear, considering the complexity of the flow, and the drag polar is very nearly parabolic up to 13-degrees angle-of-attack. Thereafter, a plot of C_L^2 vs. C_D reveals an upward offset (i.e. increase in C_L) accompanied by a sharp increase in dC_L^2/dC_D (i.e. increased effective car "aspect ratio", based upon height). It is speculated that this is caused by separation of the rear window, which would prevent the roof-line vortices from being swept downwards over the trunk. However, this is not entirely consistent with the very linear lift and yawing moment characteristics shown in Figures 3.4 and 3.6.

4.0 REDUCTION AND ANALYSIS OF WAKE DATA

Ten plots are described in Section 6 for each wake traverse. The first five comprise v-w vectors, v contours, w contours, axial velocity contours and total-pressure-deficit contours. These are essentially 'direct' measurements. Their work-up from probe readings and subsequent normalization will be described in subsection 4.1. The second five plots are derived data and comprise contours of cross-flow kinetic energy, axial vorticity, "corrected" v and w values (see below) and stream function. The associated derivations are given in subsection 4.2.

4.1 Axis Systems

Conventional wind axis systems are used in the present report for the presentation of car and wing data (see Figure 4.1). As it was desired to view the wing's suction surface through the LV window, on the right side of the tunnel looking upstream, the floor mounted half model becomes a left wing. Spanwise inflow, rather than outflow, is therefore positive in the present work. The convention for the car is similar: spanwise inflow is positive on the left side.

The primary traverse direction was parallel to the long side of the tunnel and the rake lay parallel to the short side in all tests. For this reason a tunnel-referenced, rather than a model-referenced, axis system was employed for data recording and transmittal on magnetic tape (see Figure 4.2). This gives reversed signs relative to the wing aerodynamic axes and a 90-degree rotation for the car.

4.2 Preparation of Velocity and Total Pressure Deficit Data

U, v and w components are normalized using blockage-corrected mainstream velocity. Data presented here employ a "on-line" correction*, described below. A single normalization velocity, for a given test condition is employed for both balance measurements and wake velocities

* The definition of 'on-line' correction used here reflects some special needs of the current study. This definition does not reflect current on-line practice at the 'MTF' tunnel.

"Off-line" corrections, which define the variation of blockage velocity along the tunnel axis, were described in subsection 2.4. For the present purposes, it was considered inadvisable to normalize via "off-line"-corrected velocities because they differ from plane-to-plane and between force and traverse measurements.

No attempt has been made to estimate or to apply angle-of-attack corrections, since comparisons between in-tunnel force measurements and in-tunnel wake integrations are to be made.

Normalization

The 'on-line' blockage correction reflects techniques reported in March 1976 in NASA CR 137857. Appendix I of the present report is an adaption of an Appendix in that NASA CR. Roughly speaking, the on-line method uses the mean of test section entry static pressure and the downstream 'breather' slot pressure as the effective static pressure at the model. Since total pressure is available, a corresponding dynamic pressure can be found. This technique responds to profile-drag-related blockage ('wake' blockage) but not to solid blockage, which is estimated independently (see Appendix). The newer, "off-line" method avoids the need to estimate solid blockage by employing more complete wall pressure data.

Application of 5-Holed Probe Calibrations

The five measured pressures from each probe are used to determine the non-dimensional parameters $(p_3 - p_1)/p_5 - p_{min})$, $(\equiv F(A))$, and $(p_2 - p_4)/(p_5 - p_{min})$, $(\equiv F(P))$. The values of pitch angle (α) and yaw angle (ψ) are then read off by a tabular look-up equivalent to the $\alpha \sim \psi$ map in Figure 2.5. These angles are used to find the dynamic and the total pressure deficit parameters from the F(Q) and the F(H) maps. Dimensional local dynamic pressure and total pressure deficit are then found from

$$q_o = \frac{p_5 - p_{min}}{F(Q)} \quad \text{and} \quad (H_o - p_5) = (p_5 - p_{min})\ F(H)$$

These pressures are normalized using the on-line 'q' value for the test concerned (Figure 2.9). The u-component of velocity is obtained directly from q_o. Other components are then obtained by using the angles α and ψ appropriately.

Removal of Model-Absent Zeros

Since the perturbation to the flow caused by the model is required, a set of datum traverses is performed with the model absent and the above procedures are executed in full to give datum distributions of normalized u, v, w and total pressure deficit. These data are subtracted, on a point-for-point basis, from the results of subsequent model - present tests. In the case of axial velocity, u, deviations from the nominal value are incremented.

It has been found that removal of model-absent zeros, as just described, markedly improves data smoothness and accuracy. In particular, some problems of probe alignment are eased and the spurious effects of probe deflection due to air loads are largely eliminated. Towards the edges of the traverse field, as model-induced perturbations become small, 'noise' due to small local imperfections in tunnel flow is reduced.

Preparation of Machine Plots

The machine plots are drawn against a background which includes a frame marked with 'ticks' at 1-inch intervals. The tunnel floor corresponds to the right hand edge of the plot for wing data and to the bottom edge for the car. A line through the model axis and a representation of the model are shown as seen from a location far downstream. The model outline is changed appropriately to show angle-of-attack or yaw. Negative contours are indicated by dashed lines and listings of contour values are provided.

4.3 Derived Quantities

Vortex drag may be determined as an integral of cross-flow quantities, either of cross flow kinetic energy over the entire field or of the product $\xi \cdot \psi$ over the viscous wake. Though it is possible to bound the kinetic energy integral, using Green's theorem, Maskell's wake integral formulation and developments from it (ref. 2) are of primary interest in the present work. The focus for derived quantities is therefore upon axial vorticity, ξ, and a related stream function ψ. No additional derivations from the basic data are required for the profile drag integral. The procedures for finding the five derived quantities, presented in machine plots 6 to 10 etc, are presented below.

Cross-Flow Kinetic Energy

These plots are intended to illustrate the location of shed cross-flow energy in the wake. Comparisons may be made between the regions for a direct K. E. integration and for a $\xi \cdot \psi$integration, which largely follows the ξ distribution. Like the other derived quantities, cross flow K.E. is determined on a grid shifted by half a cell (i.e. 0.25 - inches) vertically and horizontally relative to the measurement points. The K.E. data are based on measured v and w quantities, rather than reworked, "corrected" values used in subsequent plots (see below).

Axial Vorticity, ξ

The circulation around a typical cell is determined from

$$\Gamma_p = \tfrac{1}{2}\ (w_1 + w_2 - w_3 - w_4)\ dz + \tfrac{1}{2}\ (v_4 + v_1 - v_2 - v_3)dy$$

The vorticity at the central point, P, then follows from

$$\xi_p = \frac{\Gamma_p}{U\ dydz}$$

Vorticity-Induced Lateral and Vertical Velocities

As the measured velocity fields are three dimensional and viscous, divergence is present ("source" effect) and stream function, ψ, is not uniquely defined. This problem is overcome by recalculating the velocity field from the ξ_p distribution and integrating to obtain stream function.

The determination of vorticity-induced cross flow velocities is not straightforward because values are required within the vorticity field itself. Both Poisson solver and integral techniques have been tried: the integral techniques were found to be superior. For efficient computing, the integration domain for velocity at a particular point is divided into far-field, near field and sometimes intermediate regions. For the far field, simple point-vortex velocity equations may be used. For the near field, in which the "receiving" point is embedded, a fairly elaborate procedure is required involving eight neighboring vorticity grid points and graded vorticity (see Appendix II). If the measurement cells are thin rectangles, an intermediate region may be defined where vorticity is condensed to a central line following the long axis of the rectangle. For near-square cells, the usual procedure is to regard the receiving cell and the eight which surround it as the near field and the remaining cells, to the traverse boundary, as far field, The procedures and equations used are explained in more depth in Appendix II.

"Corrected" Lateral and Vertical Velocities

The velocity recalculation just described removes not only the unwanted

divergence effects, but also tunnel-induced velocities. Extension of the above calculation to include points on the tunnel boundary would reveal normal velocities there, which is incorrect. It is therefore necessary to determine a correction to the velocity field which returns normal to-wall components to zero. This is accomplished by calculating normal velocities at collocation points around the tunnel boundary and using these to determine a boundary vorticity distribution†. "Corrected" lateral and vertical velocities are then found by adding boundary-vorticity-induced increments to the velocities found previously.

A further potential difficulty, from $\xi \cdot \psi$ drag contributions associated with tunnel-wall vorticity, may be circumvented by arranging that $\psi = 0$ at the tunnel wall.

Stream Function

Stream function is determined as a line integral of normal-to-path corrected velocity. In the routine calculation, integration starts from a reference point at the center of the traverse and comprises first a wdy integral, at constant z, followed by a vdz integral at constant y. Positive and negative paths are included in both y and z directions to give a ψ distribution for the entire traverse field.

In order to rereference ψ to a tunnel wall zero, a further integration is made along a vertical line from the tunnel wall to the reference point. This yields a correction $\Delta\psi$. In cases where the traverse does not reach a tunnel boundary, additional calculations of corrected v or w may be necessary to accomplish this. Finally, $\Delta\psi$ is added to the previously-calculated stream function value and streamlines are mapped using suitable interpolation procedures.

† An array of two dimensional point vortices is used. As some traverses are less than one tunnel diameter aft of the model, some error may arise because the actual, tunnel surface axial vorticity tapers off to zero upstream of the model.

5.0 MEASUREMENTS AHEAD OF WING MODEL

5.1 General Comments

The need to conduct traverses upstream of the model, as well as in it's wake, arises because of some uncertainties about added source terms, in the wake integral, which were neglected by Maskell (ref. 1) but which are considered in analyses being performed at Georgia Tech, using the present data. The wake source integral concerned is the product (source strength x velocity potential) and is discussed further in Reference 2. Unlike the wake vorticity integral which it complements, it is a whole-field integral and it does exist ahead of the wing.

Maskell (ref. 1) avoids consideration of the source term for the wake by declaring that the traverse plane must be sufficiently far downstream for divergence to be negligible. This increases the traverse area and requires better measurement accuracy. For given instrumentation, better accuracy and greater experimental convenience are attainable for traverse planes closer to the model. Early analyses of the present wake data, at Georgia Tech, indicate that the source terms in the drag integral are not negligible for the traverse positions selected. The question which arises is whether these terms are offset by corresponding terms upstream of the model.

Recognizing that the perturbations upsteam of the wing are significantly smaller than those downstream of it, a plane 3-inches ahead of the wing leading edge (i.e. X = -6") was selected for the upstream measurements. It may be noted that the near field wake traverses were 3-inches (X = 12") and 9-inches (X = 18") aft of the trailing edge of the wing respectively for the 6- and 18-degree cases.

5.2 Flow Quality and Data Accuracy

The measurements were made with a single, minimally intrusive 5-holed pitch/yaw probe, similar to those used in the rake shown in Figure 2.4. All data to be shown here were meased at $X = -6''$. To place the flow data from upstream traverses in perspective, the apparent flow quality ahead of the wing, as perceived by this single probe, will be discussed first.

Figures 5.1 and 5.2 show contours of total pressure deficit with the wing at 6- and 18-degrees angle-of-attack respectively. Apart from a small, higher-energy region to the bottom right of each traverse, total pressure deviations are within ±0.5 percent. This is regarded as good for a general purpose tunnel such as the 'MTF'. Examination of the changes in the higher energy region (broken lines), on increasing from 6- to 18-degrees, reveals significant stretching and shifting of the pattern in an outward direction, as would be anticipated. However the -.004 region towards the top left of Figures 5.1 and 5.2 changes very little.

Ahead of the wing, no axial vorticity should be measurable. As a check of the overall accuracy of the measurement and reduction procedures, Figures 5.3 and 5.4 show the apparent vorticity calculated for the 6- an-18-degree cases. It will be noted that the values on the contours are very small. However, they do appear to be wing-related: there are no far-field contours. The contour shapes suggest that normal-to-wing cell size may be too large for the (implicit) assumption of linear velocity variation to be adequate.

5.3 Flow Data

Figures 5.5 and 5.6 show axial flow velocity and cross flow vectors for the 18-degree angle-of-attack setting. This is a stalled case and it is evident that the axial velocity distribution is dominated by wing blockage. Nonetheless strong upwash is present (Figure 5.6) and outflow is significant towards the wing tip. It may be seen from Figures 5.7 and 5.8 that the maximum upwash, located above the wing, is about twice as great as the maximum outflow, which occurs ahead of the wing tip. A small

inflow region may be noted in Figures 5.6 and 5.8, near the wing root. This is a manifestation of the root stall and is related to the negative lift gradients in this region.

Figure 5.9 shows the apparent source-sink strength distribution derived from the preceding cross flow data. It is important to note that the peak values are only about $2\frac{1}{2}$ times greater than the vorticity for the same case (Figure 5.4) - which is spurious. Nonetheless the source region is the more extensive and both the location and the trends normal to the wing are as anticipated.

The expected variations in source strength are best thought of in terms of $(-du/dX)$, the flow retardation, which appears as source strength in Figure 5.9. Normal-to-wing trends comprise blockage and lift-related components. The blockage part may be though of as induced by a spanwise line source at the wing location. This is a strong effect for the present case and produces a strong retardation immediately ahead of the wing (Figure 5.5) which declines above and below it. Lift effects, on the other hand, are vortex-related and give no u-component - and so no source effect - immediately ahead of the wing. There is, however, flow acceleration above the wing and retardation below it. Only the former is readily apparent in Figure 5.9.

The general trends for the 6-degree traverse (Figures 5.10 to 5.14) are very similar to those just described. As might be expected, the magnitude of the wing-induced flow is less than before and experimental errors may be more significant. As the wing is not stalled, the vortex-induced above-wing acceleration is more marked in relation to the retardation in front of the wing leading edge.

6. MEASUREMENTS IN MODEL WAKES

Because there are many, the 'production' data plots are placed last in the present report and are designated with separate figure numbers in an "MP" (i.e., Machine Plot) series. A cross reference table is provided in Figure 6.1. Eight complete traverses comprise two X-locations for each of two setting angles for both the wing and the car models. For each traverse, five measured and five derived quantities are provided giving a total of eighty machine plots. Details of plot conventions and derivations were given in Section 4. Some limited comments will be made below which highlight some of the more important features of the car and the wing wake traverses.

6.1 Wing data

The inboard wake

At an angle-of-attack of 6-degrees, total pressure deficit contours MP5 and MP15 show that the inboard viscous wake is almost two-dimensional. Due to viscous decay, the maximum total pressure deficit decreases from approximately 0.3 to about 0.1 between the 12- (MP5) and 36-inch stations (MP15). Examination of the streamlines in MP10 shows a kink in the viscous wake region where the spanwise flow changes sign across the trailing sheet. This kink moves down, with the wake, as may be seen in MP20, which is for the downstream location. In MP7 the vorticity responsible for the kink may be seen extending inboard from the wing tip. This vorticity has attenuated significantly at the 36-inch station (see MP17) though a remnant of the associated kink is still apparent in the streamline pattern (see MP20).

The wake for the 18-degree case is quite complicated, because the wing is stalled. As the probes are operating near, and possibly beyond their angle limits at the 18-inch station, it is appropriate to consider the 36-inch station first. Here, the total pressure deficit has dissipated substantially (see MP25 and 35) and only remnants of the previous negative vorticity are evident inboard of the mid semi-span (MP27 and 37). Axial velocity away from the vortex has recovered to no less than 0.7 to 0.8 of mainstream (MP34)

and the probes should be comfortably within their operating range.

A peculiar feature in MP40, which also appears in MP30 (but may be suspect there), is the appearance near to the wing root of a region having negative stream function. The implication of this is that an 'open' separation is present on the wing. The zero streamline in MP40 lies just left of the dashed streamline and must close to the wall. The similarity between the 18- and 30-inch zero streamline regions in MP30 and 40 suggests that the former is at least qualitatively correct. However, it should be emphasized that the streamlines are derived from the axial vorticity: convergence, such as that towards the wake near the wing root in MP21, is not recognized. It seems likely that a tracking type of streamline program would show spiral entrainment in the negative stream function region in MP30 and possibly also in MP40.

The vortex region

The most striking thing about the vortex is its persistence. Neither maximum total pressure deficit (e.g. MP5 vs. MP15) nor maximum vorticity (MP7 vs. MP17) decay appreciably in the axisymmetric part of the vortex. This may be because vorticity is fed in by the 'tail' (MP7), during completion of the roll-up process. For the 18-degree angle-of-attack case the comments are the same: maximum total pressure deficit (MP25 vs. MP35) and maximum vorticity (MP27 vs. MP37) remain almost unchanged between the 18- and 36-inch stations. This is perhaps more surprising for the 18 degree case, both because the vortex, being stronger, is non-dimensionally older and because of its proximity to a large stalled region of low energy air.

Though all of the plots just mentioned depict the vortex as approximately axisymmetric, more detailed traverses show a spiral structure. However, the results of pilot integrations (Ref. 2) suggest that such fine detail may not be needed for the present purposes.

6.2 Car data

The car wakes are dominated by viscous effects and vortex drag is secondary. The near-field viscous wake is large (MP45) and grows quite rapidly (MP55). As it grows, the maximum total pressure deficit is almost halved. During this process, cross flow velocity and consequently stream function are approximately halved (compare MP50 and MP60). Vorticity peaks, at X = 36" (MP57) are only about a quarter of their upstream intensity (MP47). This suggests that, as the wake decays, cross flow kinetic energy is converted by a mixing process into total pressure deficit, causing an apparent increase in the axial dissipation rate. It is anticipated that wake drag integrals for total drag will contain a greater "profile" component as X increases. Profile and induced drag consequently may not be uniquely defined.

Zero yaw (MP41 to 60)

Four strong vortices can be identified in the wake (MP47), together with a number of secondary cells. The strong vortices lie at the corners of a roughly rectangular wake which corresponds to the cross section in the vicinity of the trunk. Considering pairs of trailers, it is apparent that the joining lines represent forces on car surfaces. The upper vortex pair (MP47) may be roughly identified with lift on upward-facing surfaces while the side pairs correspond to body-side suctions which place the car body in sideways tension. As the lower vortex pair is somewhat weaker than the upper pair, some vortex lines must arch to the ground, via the wheels. The underbody download should therefore be smaller than the upper surface upload and net lift is anticipated. This can be predicted in other ways - from the fact that the car mean line is cambered in side view or from the knowledge that floor-mounted half-bodies experience lift. However, as some of the measured axial vorticity in MP47, for example, may originate at the floor (particularly in downstream traverses such as MP57), there are doubts whether it is theoretically feasible to estimate car lift from wake vorticity measurements. This example is a special case of the problem of estimating, from wake measurements, the individual forces on joined bodies. The topic requires further study.

The yawed case (MP61 to 80)

Though the trailing vorticity contours for the yawed case (MP67) are markedly different from before (MP47) a number of the previous features can be identified. The previous four vortices, behind the trunk, can still be identified, but the clockwise (i.e., positive) regions have joined. A new clockwise vortex is also evident in MP67 which almost certainly springs from the right hand edge of the roof.

The peak values of vorticity are generally similar in MP67 and MP47 but the greater contour areas, and the new vortex suggest that circulations and consequently self-deformation of the wake will increase for the yawed case. This is already fairly apparent at an upstream location (compare MP67 with MP47) but becomes very marked at X = 36" (MP77) where the yawed-wake case bears little resemblance to that for zero-yaw (MP57).

The roof vortex has an obvious influence upon the total pressure deficit profiles (MP65) which persists at the downstream station (MP75). Apart from this, the previous comments apply equally to the yawed case.

7. CONCLUSIONS

Scope of the present tests

The primary objective of the work described was to acquire wake traverse data as needed to evaluate the new wake integration methods described in Ref. 2. These are of great interest because the vortex drag integration includes only the viscous wake. New tests, made on various models, included flow measurements ahead of the model (Section 5) and in its wake (Section 6), balance measurements and tunnel surface pressures as needed to define the axial distribution of blockage velocity (Section 3). All of the data have been transmitted to Professor J. C. Wu, of Georgia Tech, for further analysis.

Test configurations included a simple semi-wing at low and high angles of attack and a bluff, car-like model at zero and 12.5-degrees of yaw. Wakes surveyed ranged in complexity from one with a single vortex and low profile drag to one with five major vortices and a large low total pressure region.

Near-field and far-field wake data are presented for all four test configurations. Sets of wake data plots, for each of the eight traverses, are presented in Appendix IV. Each set comprises u, v, w and total pressure-deficit contours; cross flow vectors, streamlines and kinetic energy; axial vorticity and the v and w distributions derived from it - a total of ten quantities per set. A cross reference table is given in Figure 6.1 and highlights of the data are discussed in Section 6.

Some limited traverses were made ahead of the wing. These data, which were gathered to aid the resolution of some theoretical questions, are described in Section 5.

Test and analysis procedures

Considerable care is needed in both gathering and analyzing wake traverse data if worthwhile results are to be obtained. The techniques used in the present work reflect more than five years of continuing development,

particularly of the software for reduction and analysis. The opportunity has been taken in Sections 2 and 4 to document these procedures.

Discussion of 'open' items

Though the present analyses extend only to the point where wake integrations can be performed, a review of the present situation with regard to wake investigations and of the data itself raises a number of questions which deserve further consideration. These will be discussed below.

1. The fact that most tests will inevitably involve a noticeable blockage gradient between model and traverse plane locations violates a common assumption of zero gradient. Appropriate terms should be retained in the analysis.

2. The importance of the "source term" in the wake integral, which was neglected by Maskell, should be evaluated.

3. Inspection of some of the present data suggests that, as a part of long term decay, a cascade process occurs in which cross-flow energy (vortex drag) dissipates via axial flow deficit in the early stages. Total drag in the wake thus contains an increasing proportion of profile drag at successive stations downstream. This means that profile and vortex drag are not uniquely defined.

4. With the present test grids, each vortex appears to be more or less homogenous and axisymmetric and the spiral structure which is known to exist in some cases is not acknowledged. The effect of this on wake integrals is unknown.

5. There is an open question, when recalculating crossflow velocities - and thence streamlines - from axial vorticity, concerning the tunnel wall effect. At present, the tunnel boundary condition is reestablished via the assumption of an array of point vortices disposed around the periphery. In reality, these vortices are finite in the upstream

direction. This may affect the stream function values and consequently the vortex drag integrals. The topic requires further attention.

6. The analyses conducted so far include the implicit assumption that traverses are made in a free wake with no connection to a tunnel surface. This can be true only with magnetic suspension. For the present half-wing model, it is not too difficult to 'bridge' the tunnel boundary layer when evaluating the wake integrals. However, it is much less clear that this is feasible, with reasonable validity, for the car. There appears to be a fundamental problem in distinguishing between model-generated and tunnel surface-generated trailing vorticities and total pressure deficits. The same problem would arise in analysis of the wakes of joined-bodies.

7. The emphasis in acquiring, analyzing and presenting the wake data described here has been upon its use for drag evaluation and analysis. It is clear that (at least for isolated wakes) other force and maybe moment integrations are possible, by taking suitable moments of vorticity. Evaluation of wing lift, in particular, appears to be relatively easy. For other configurations or for other force or moment components, such evaluations may be theoretically impossible or may suffer from the 'joined-body' difficulties just mentioned. A careful study of this subject appears to be well worthwhile.

8. REFERENCES

1. Maskell, E. C.: "Progress Towards a Method of Measurement of the Components of the Drag of a Wing of Finite Span." Royal Aircraft Establishment Technical Report 72232, January 1973.

2. Wu, J. C.; Hackett, J. E.; Lilley, D. E.: "A Generalized Wake Integral Approach for Drag Determination in a Three-Dimensional Flows." AIAA Paper Number 70-0279 (Revised), presented at the 17th Aerospace Sciences Meeting, January 1979.

3. Landahl, M. T.: "Numerical Modelling of Blunt-Body Flows - Problems and Prospects." - In "Aerodynamic Drag Mechanisms of Bluff Bodies and Road Vehicles." Plenum Press 1978.

4. Wilsden, D. J.: "A Low Speed Wind Tunnel Test Utilizing Simple Automobile Shape (S.A.S.) Model at 0.375, 0.475 and Full Scale in the 16.25 X 23.25 Foot Test Section." Lockheed-Georgia Company Report No. LSWT 303, December 1978.

5. Hackett, J. E.; Wilsden, D. J.; Stevens, W. A.: "A Review of the 'Wall Pressure Signature' and Other Tunnel Constraint Methods for High Angle-of-Attack Tests." Paper prepared for the AGARD Round Table Discussion on Wind Tunnel Corrections, Munich F.R.G., May 1980.

6. Hackett, J. E.; Phillips, C. G.: "Low Speed Tests on Various Wing Tip Devices for Drag Reduction." Lockheed-Georgia Company Engineering Report No. LG 80 ER 0049, March 1980.

7. Hackett, J. E.; Sampath, S. and Phillips, C. G.: "Determination of Wind Tunnel Constraint Effects by a Unified Wall Pressure Signature Method: Applications to Winged Configurations." NASA CR 166, 186, June 1981.

8. Hackett, J. E.; Boles, R. A.; and Lilley, D. E.: "Ground Simulation and Tunnel Blockage for a Jet-Flapped, Basic STOL Model Tested to Very High Lift Coefficients." NASA CR 137,857, March 1976.

9. Hackett, J. E.; and Boles, R. A.: "High Lift Testing in Closed Wind Tunnels." AIAA Paper No. 74-641, July 1974.

10. Wahbah, M. M.: "Computation of Internal Flows with Arbitrary Boundaries Using the Integral Representation Method." Technical Report, School of Aerospace Engineering, Georgia Institute of Technology, 1978. (ARO Grant No. DAAG29-75-G-0147).

FIGURES

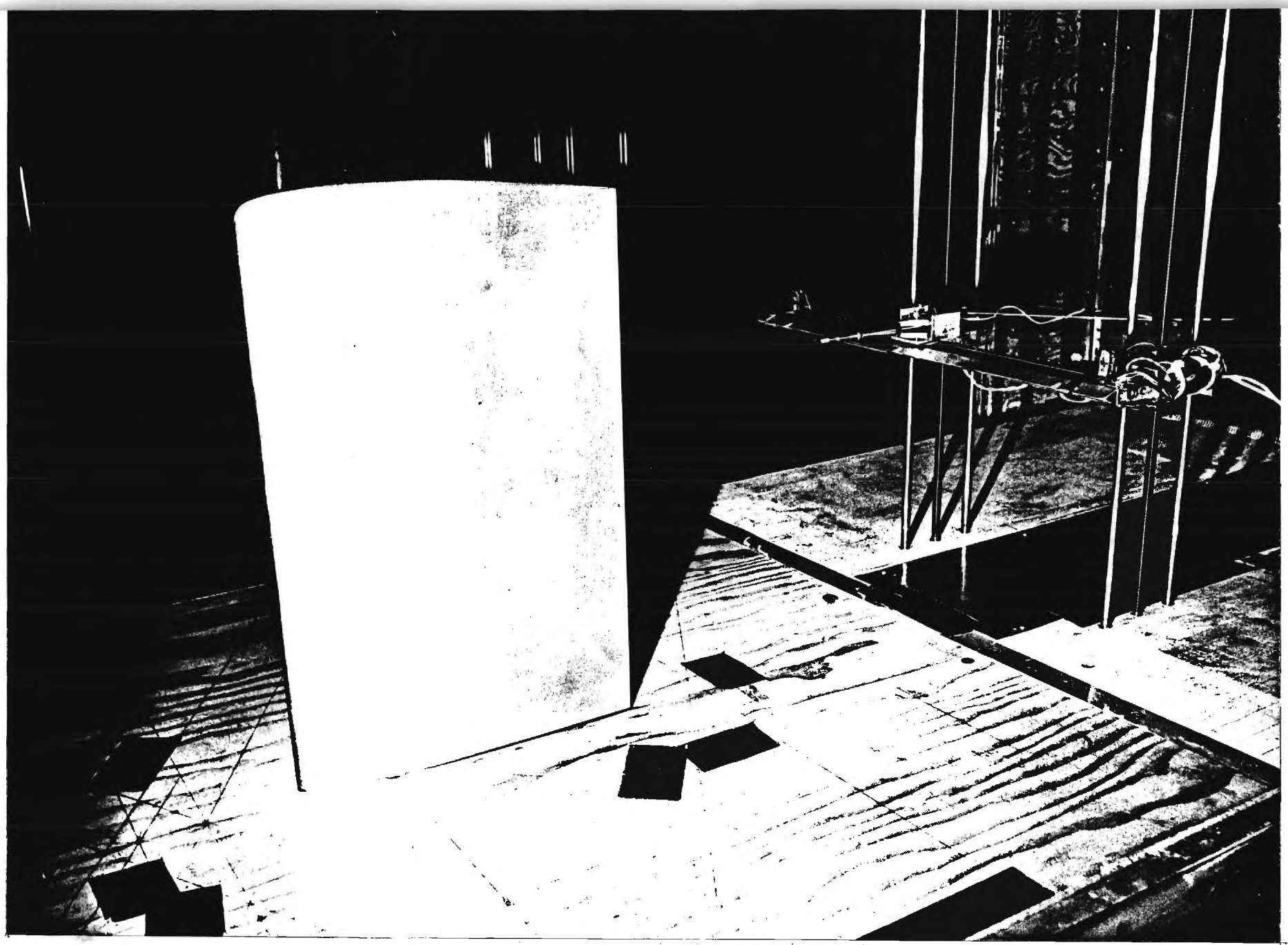

Figure 1.1 Wing Installed in MTF

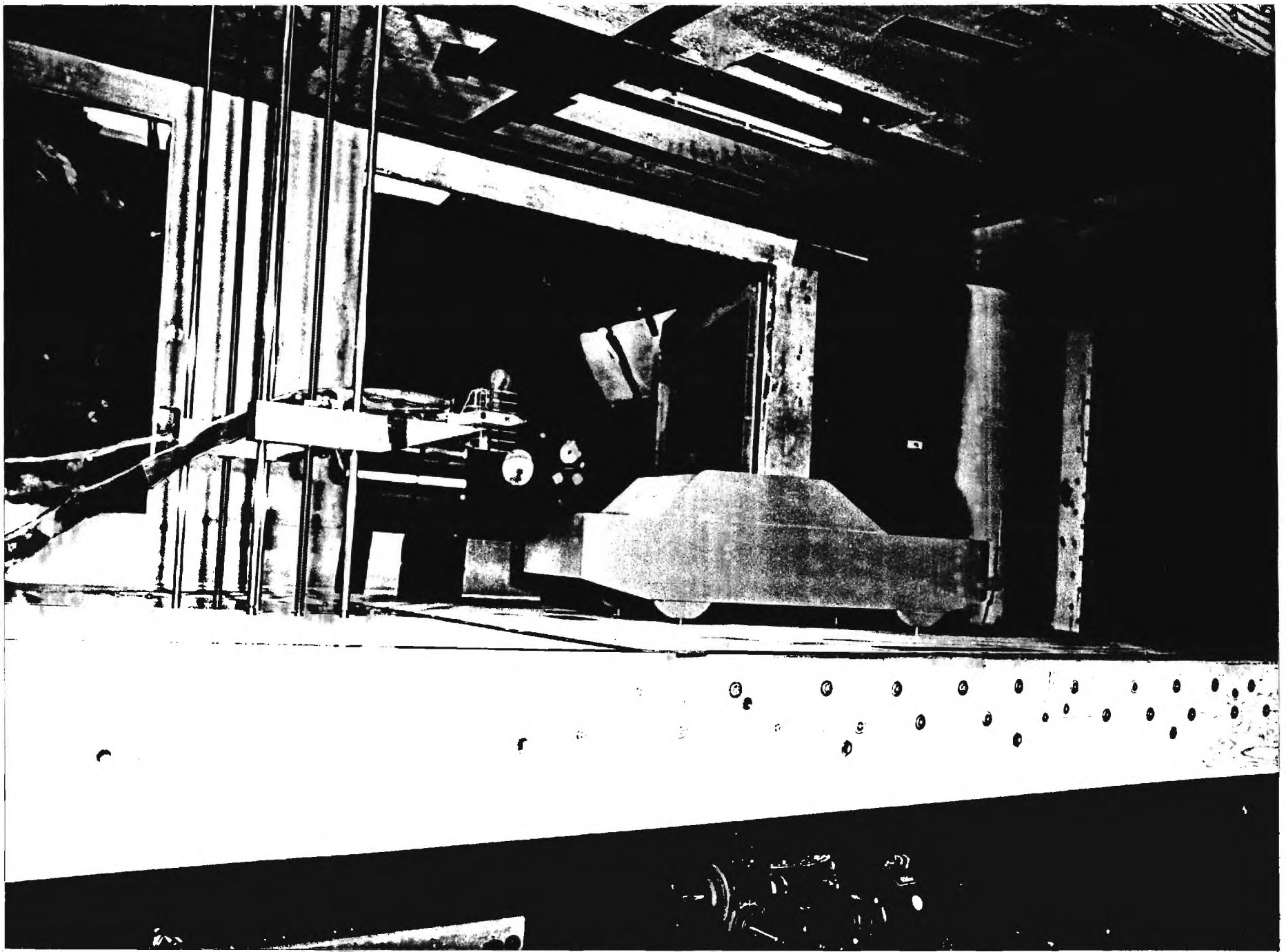

Figure 1.2 Car Installed in MTF

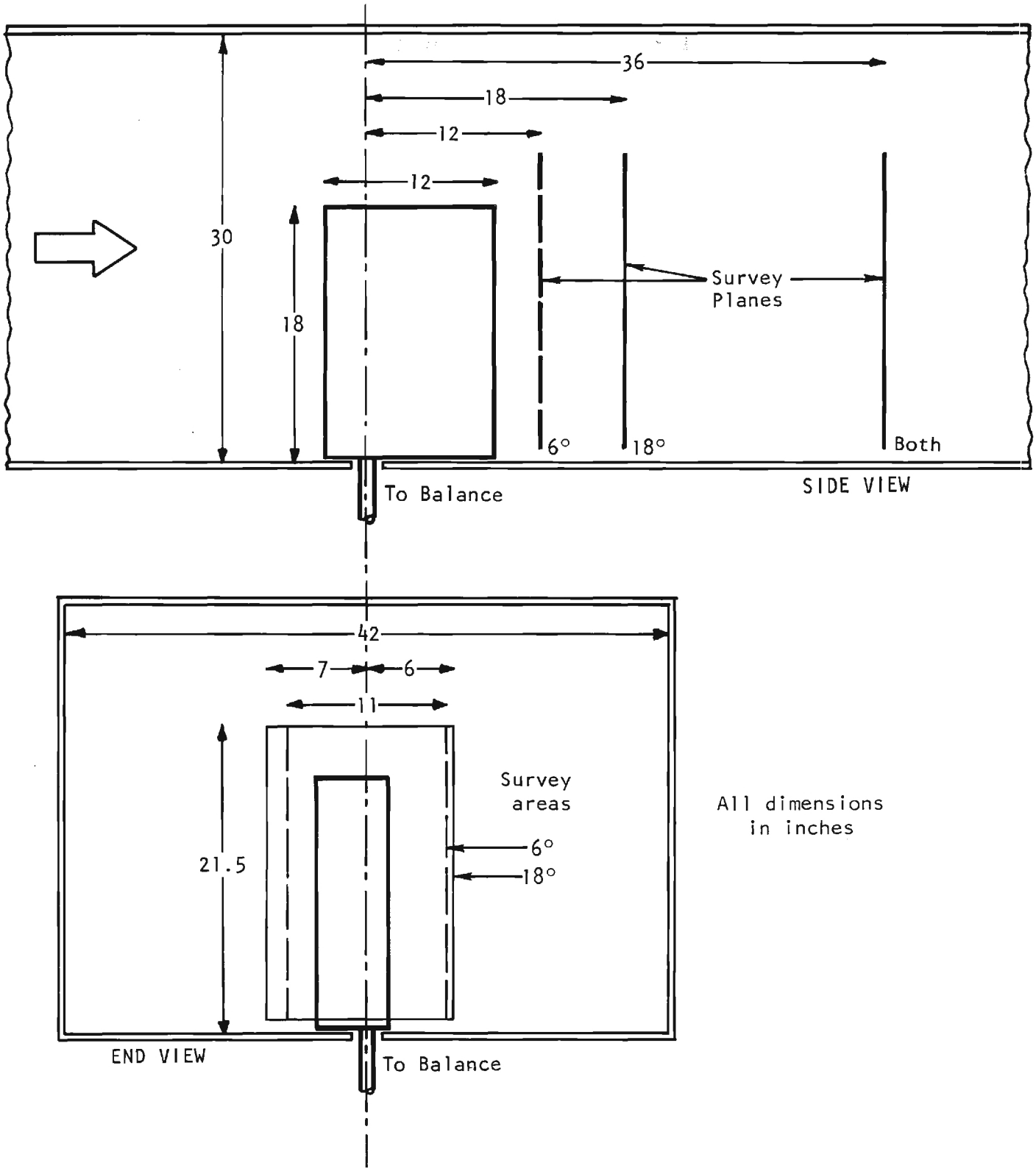

Figure 2.1 Wing Model - Dimensions & Traverse Locations

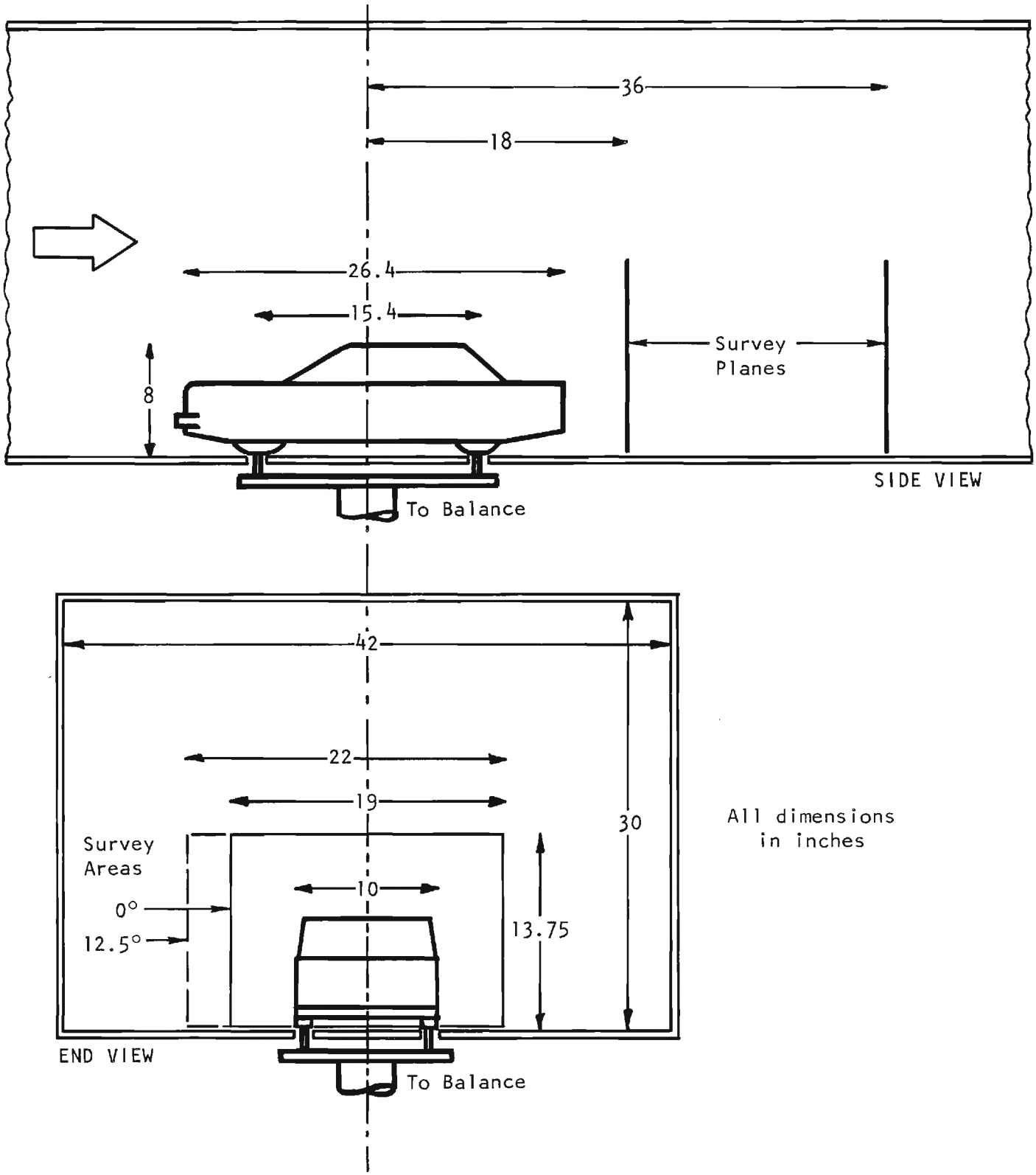

Figure 2.2 Car Model- Dimensions & Traverse Locations

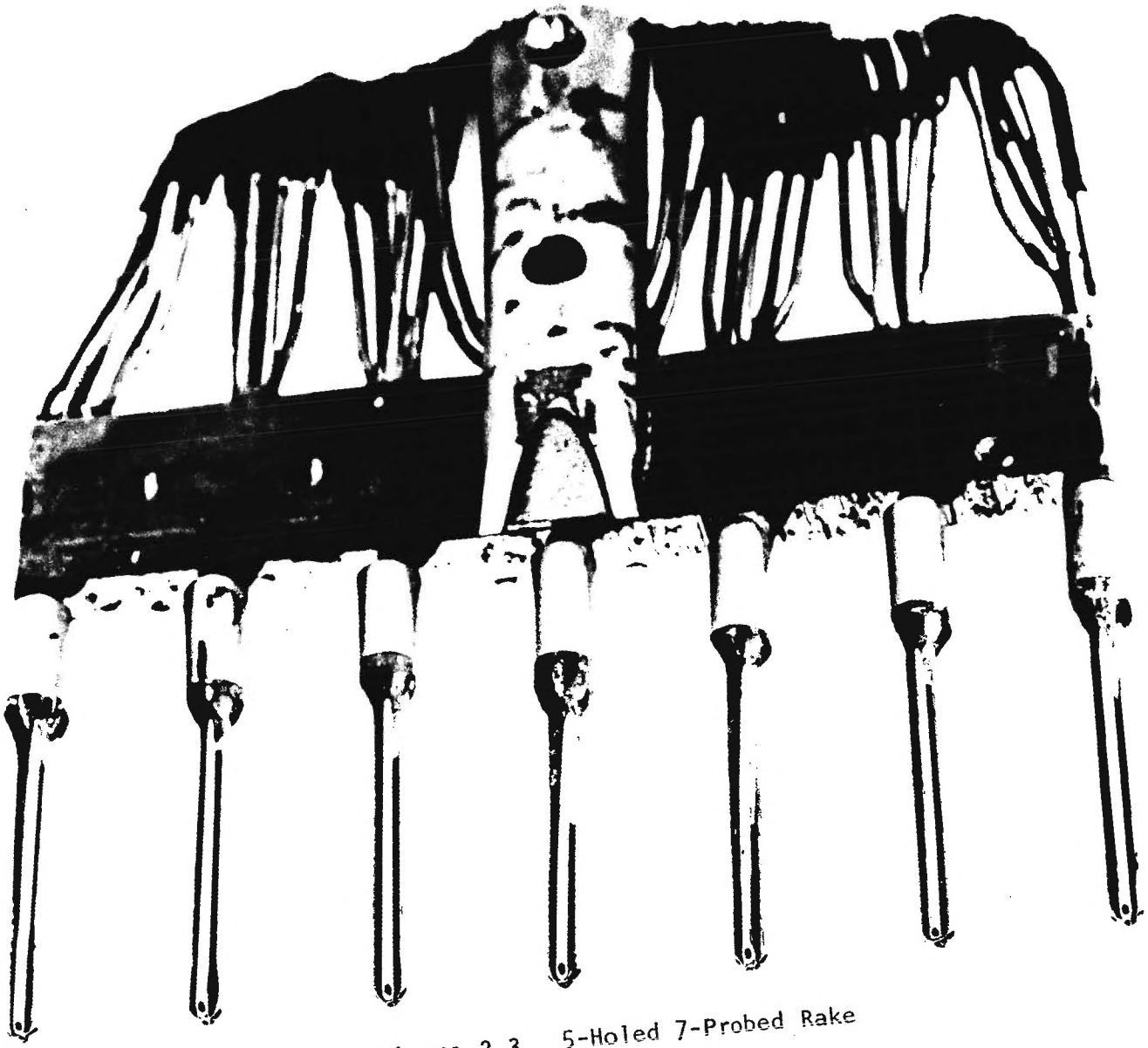

Figure 2.3 5-Holed 7-Probed Rake

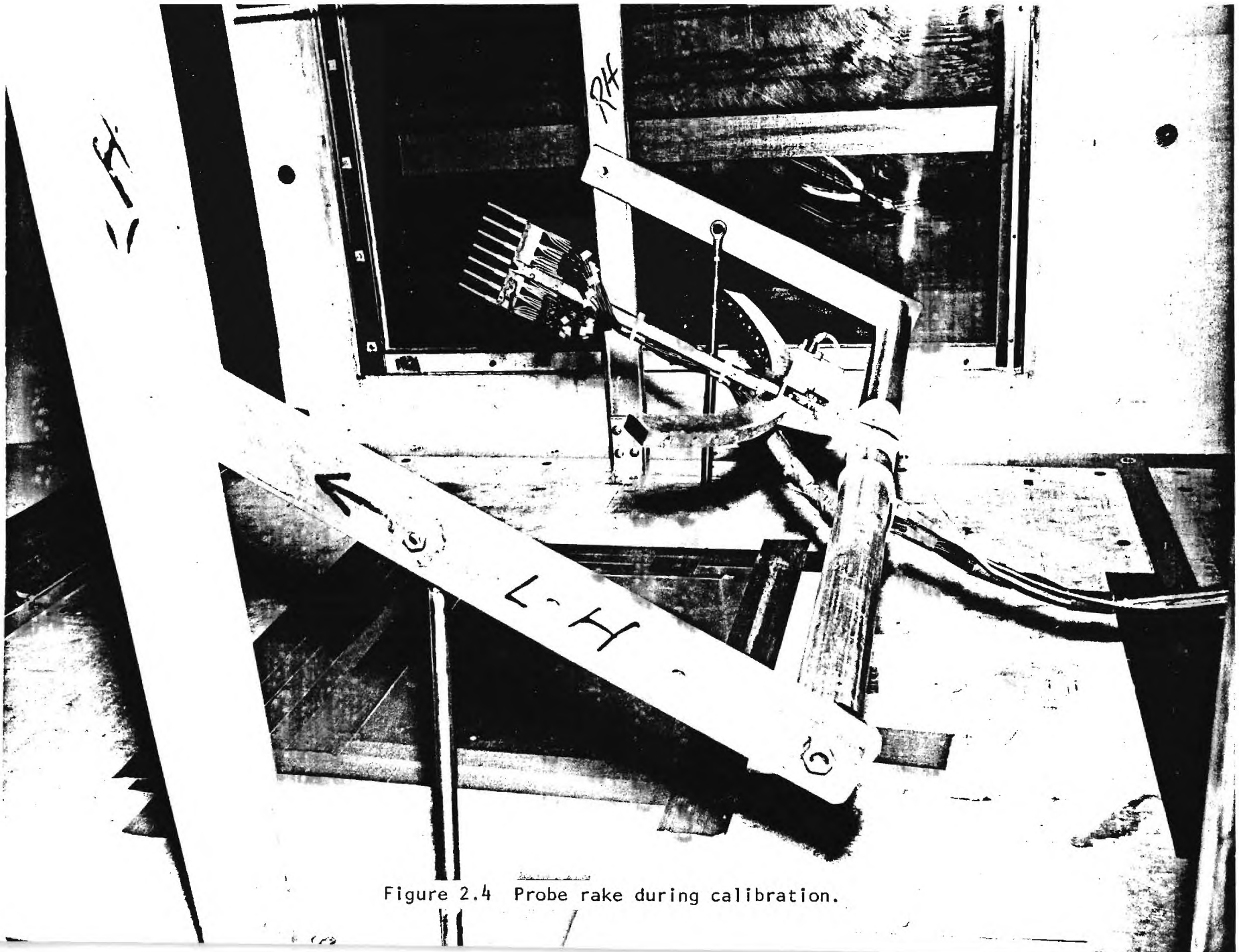

Figure 2.4 Probe rake during calibration.

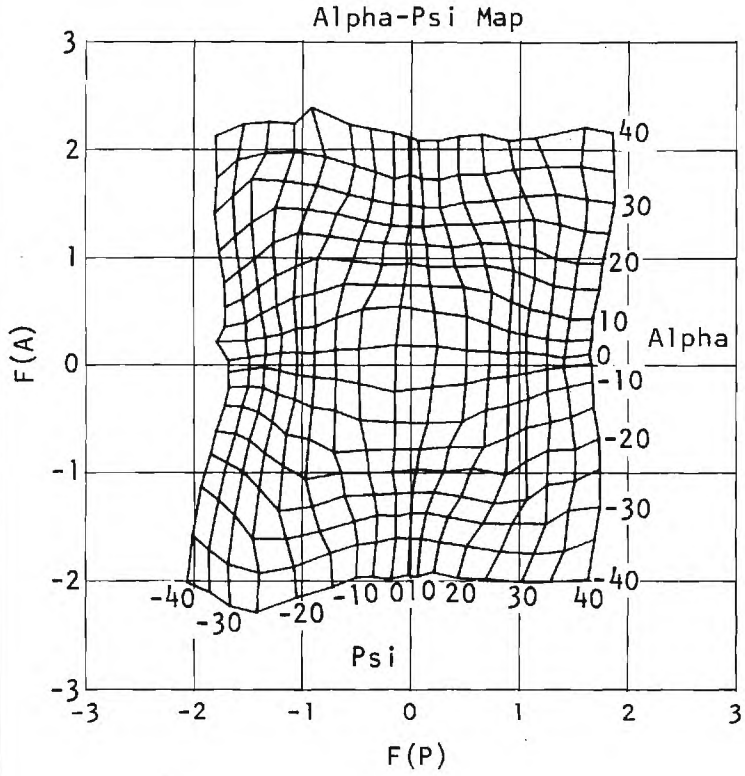

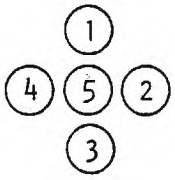

5-Holed Probe
(facing downstream)

Measure pressure p_1 thru p_5

Determine minimum press p_m

$$F(A) = \frac{P_3 - P_1}{P_5 - P_m} \qquad F(P) = \frac{P_2 - P_4}{P_5 - P_m}$$

$$F(Q) = \frac{P_5 - P_m}{q_o} \qquad F(H) = \frac{H_o - P_5}{P_5 - P_m}$$

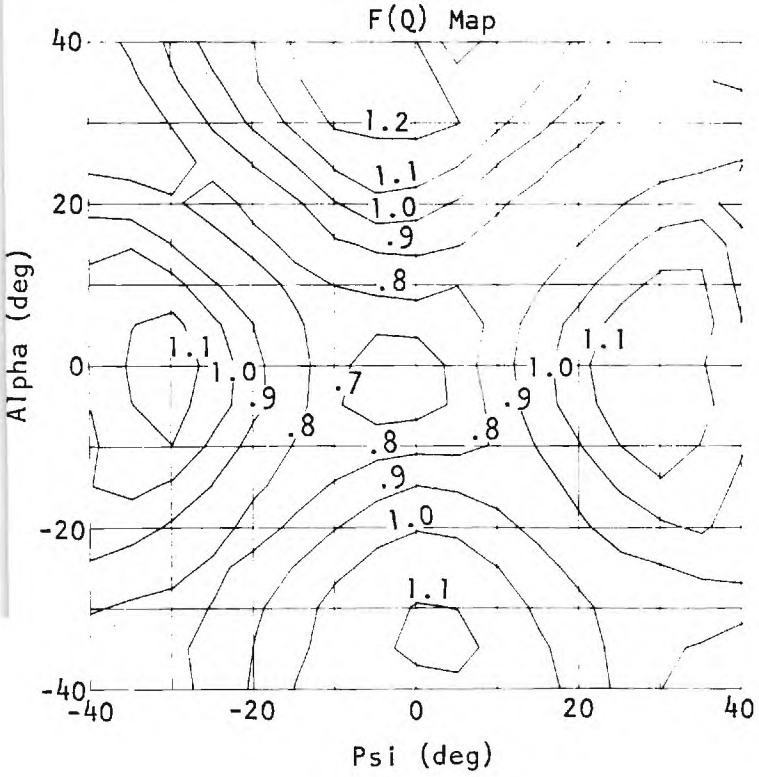

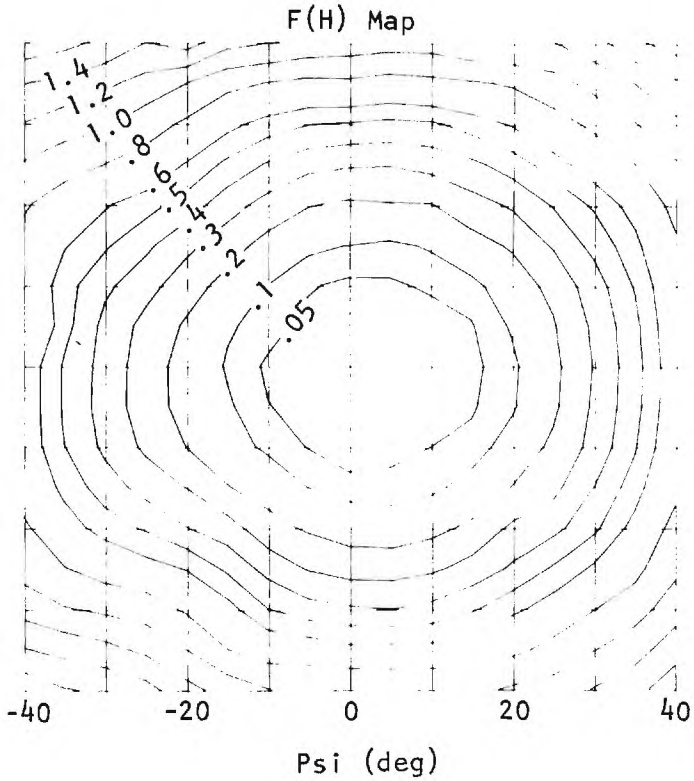

Figure 2.5 Sample 5-Holed Probe Calibration Maps

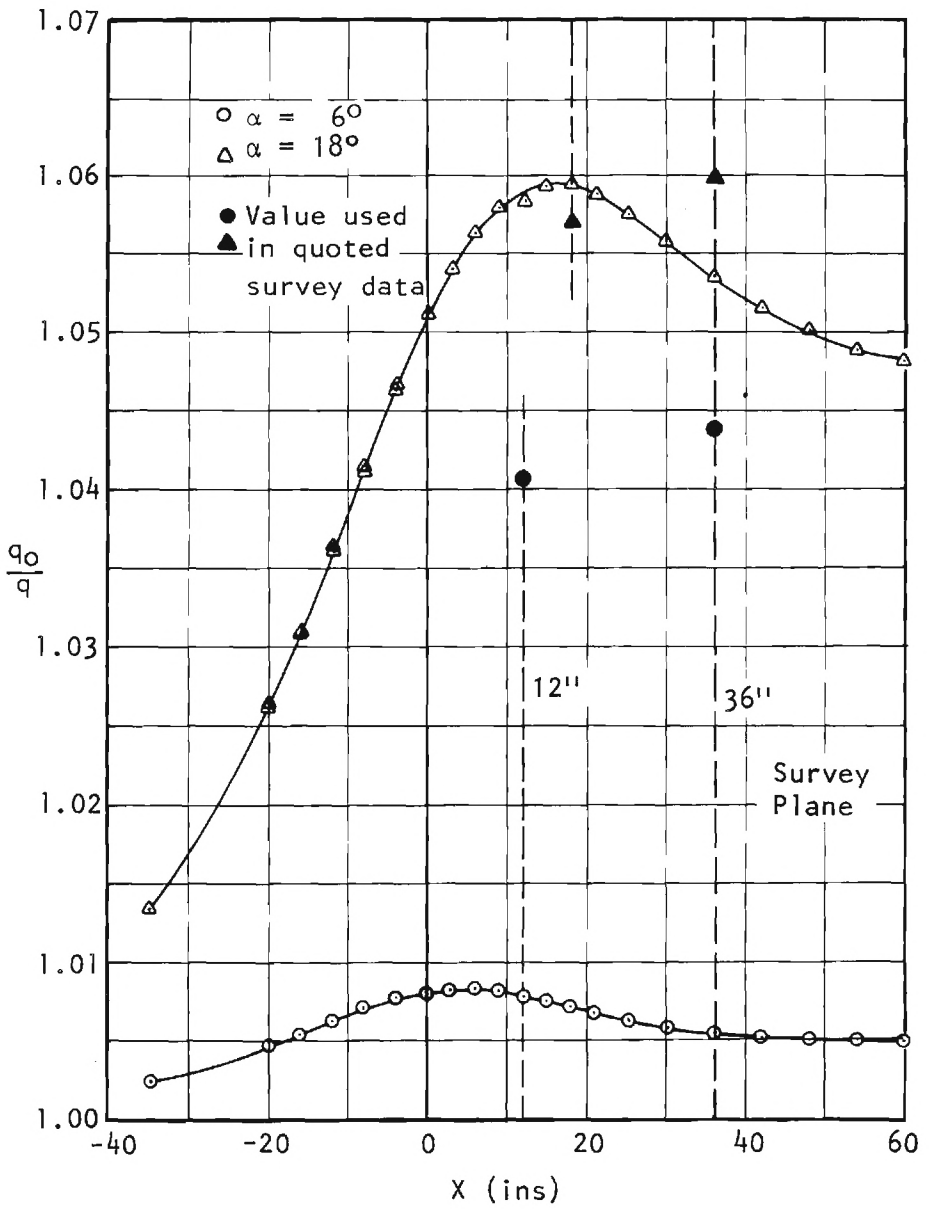

Figure 2.6 Blockage-corrected dynamic pressure distribution along the x-axis for the wing model with the effects of the traverse gear removed.

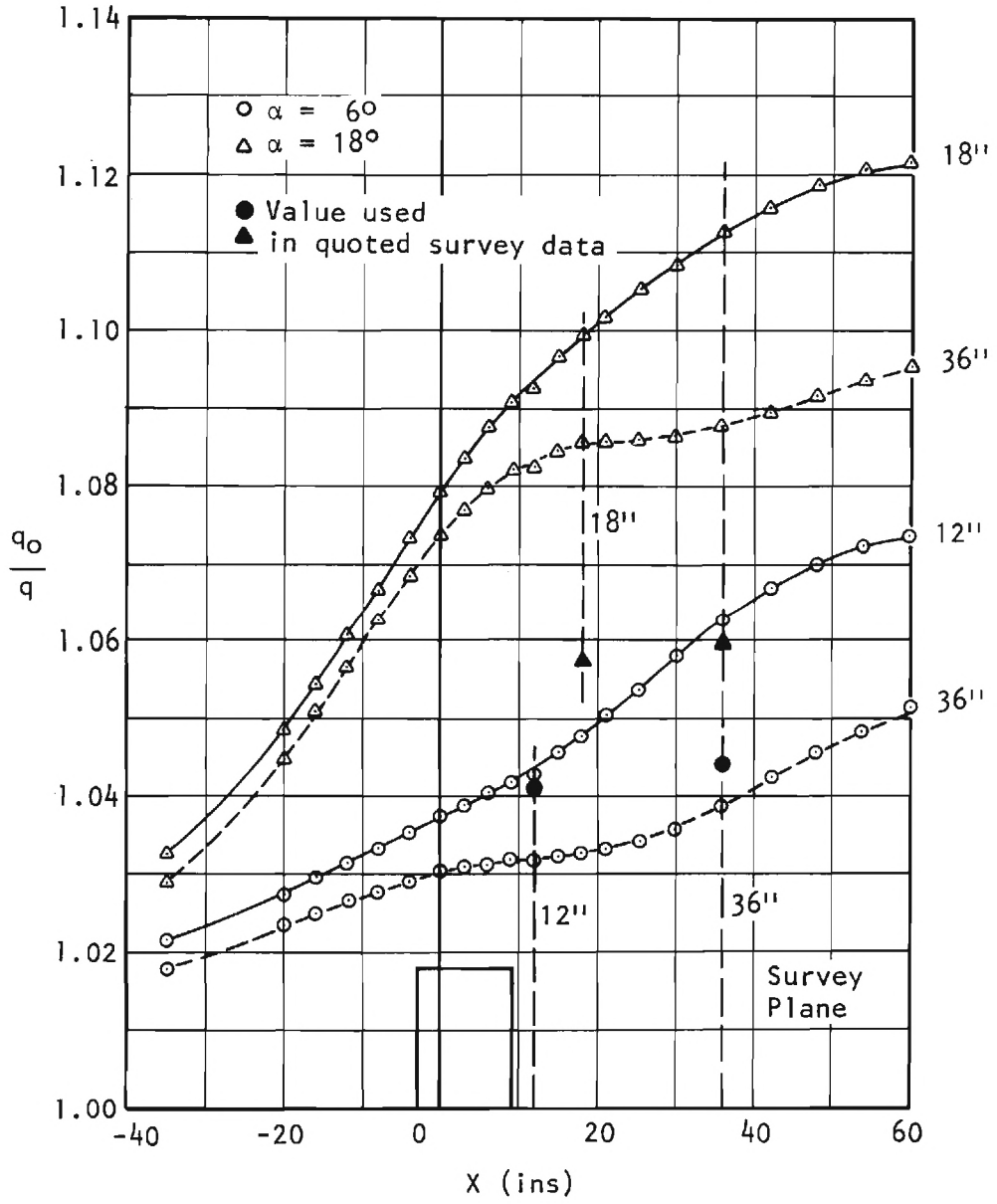

Figure 2.7 Blockage-corrected dyanmic pressure distribution along the x-axis for the wing model with traverse gear installed.

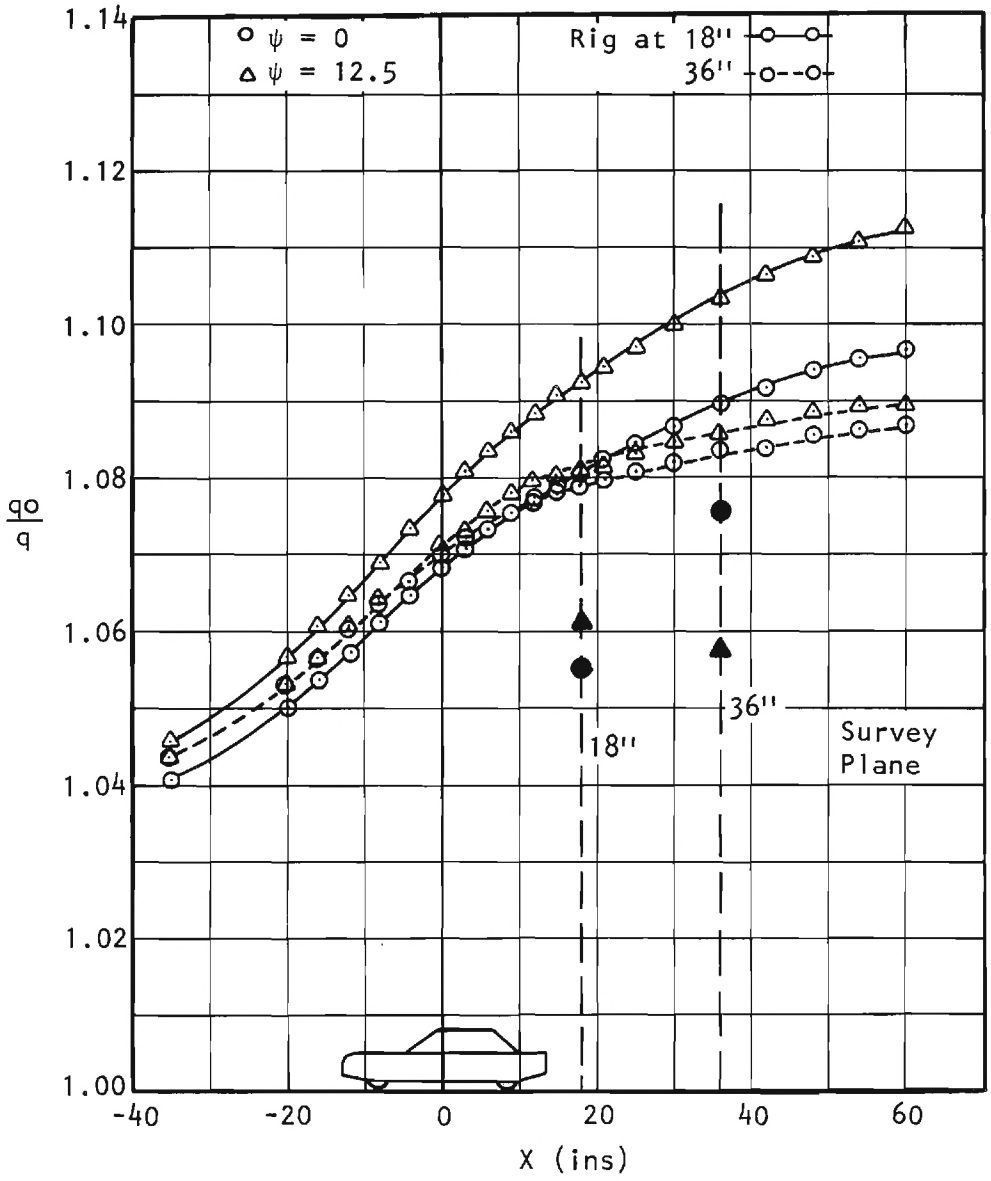

Figure 2.8 Blockage-corrected dynamic pressure distribution along the x-axis for the car model with traverse gear installed.

WING

α	TRAVERSE GEAR LOCATION	q_c/q_u			
		@ MODEL POSITION		@ TRAVERSE PLANE	
		ON-LINE	OFF-LINE	ON-LINE	OFF-LINE
6°	12"	1.041	1.037	1.041	1.044
	36"	1.044	1.030	1.044	1.039
18°	12"	1.057	1.080†	1.057	1.099†
	36"	1.060	1.074	1.060	1.087

†Data for 18" Traverse Plane, but With T. Gear at 12"

CAR

ψ	TRAVERSE GEAR LOCATION	q_c/q_u			
		@ MODEL POSITION		@ TRAVERSE PLANE	
		ON-LINE	OFF-LINE	ON-LINE	OFF-LINE
0°	18"	1.055	1.071	1.055	1.081
	36"	1.076	1.069	1.076	1.079
12½°	18"	1.061	1.077	1.061	1.093
	36"	1.057	1.071	1.057	1.085

Figure 2.9 Summary of On-Line and Off-Line Dynamic Pressure Corrections

WING DATA: ON-LINE BLOCKAGE CORRECTION ONLY

α	C_L	C_D	C_M	C_R
0	0.0202	0.0099	0.0023	0.014
2.0	0.1297	0.0110	0.0064	0.091
4.0	0.2375	0.0151	0.0116	0.167
6.0	0.3672	0.0234	0.0123	0.259
8.0	0.5153	0.0367	0.0085	0.365
10.0	0.7574	0.0713	0.0135	0.540
14.0	0.8559	0.0913	0.0143	0.618
15.9	0.9320	0.1182	0.0057	0.688
17.0	0.6106	0.2402	-0.0843	0.537

CAR DATA: ON-LINE BLOCKAGE CORRECTION ONLY

ψ	C_Y	C_D	C_N
0	0.0050	0.4080	-0.0311
2	0.1058	0.4135	-0.0004
4	0.1846	0.4310	+0.0485
6	0.2783	0.4551	0.0930
8	0.3637	0.4902	0.1394
10	0.4530	0.5361	0.1791
12	0.5477	0.5910	0.2182
12	0.5475	0.5902	0.2173
13	0.5914	0.6158	0.2441
13	0.5926	0.6168	0.2387
14	0.6528	0.6404	0.2597
16	0.7516	0.7078	0.3064

Figure 3.1 Tabulation of force measurements.

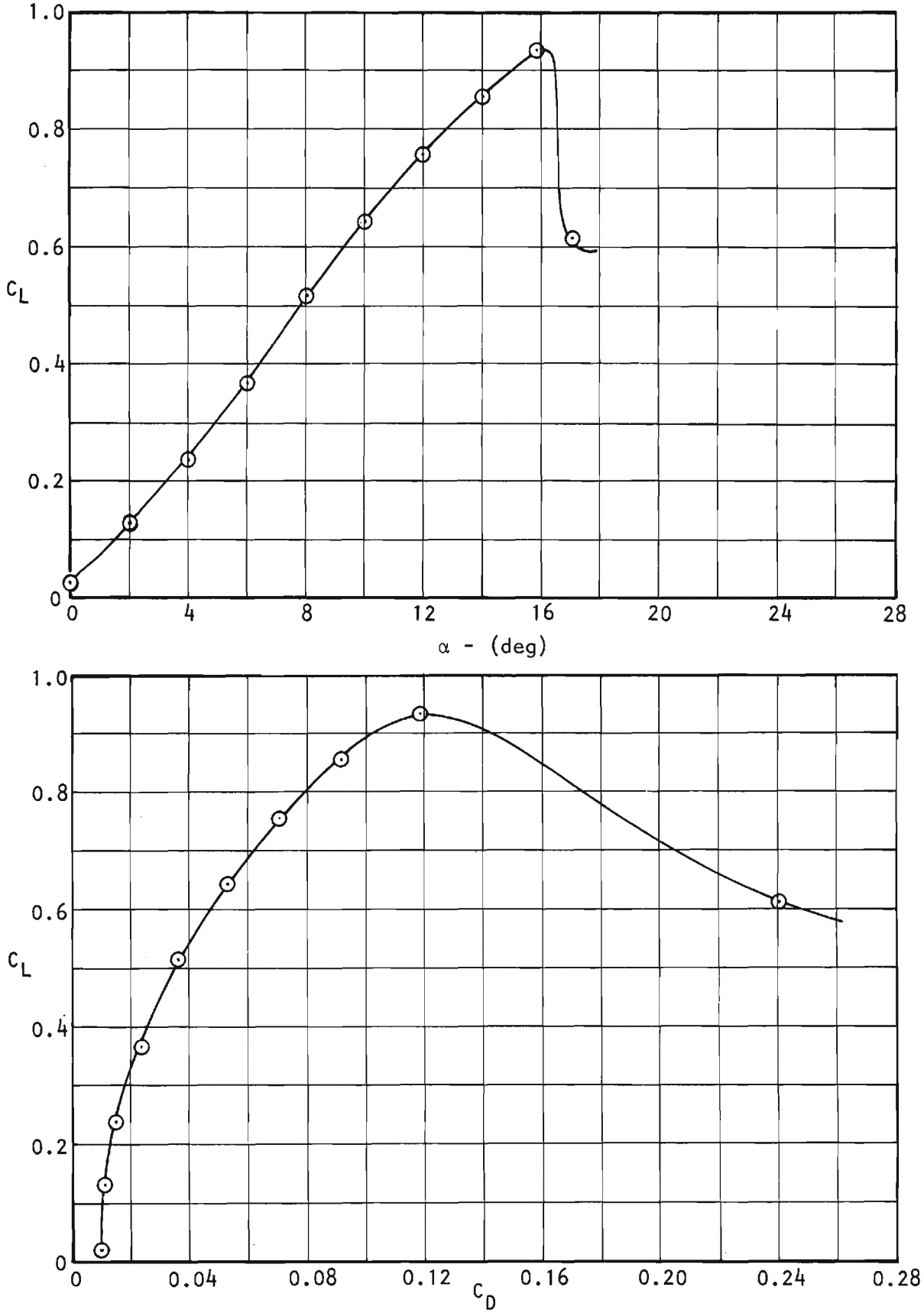

Figure 3.2 Lift and Drag Coefficients for Wing

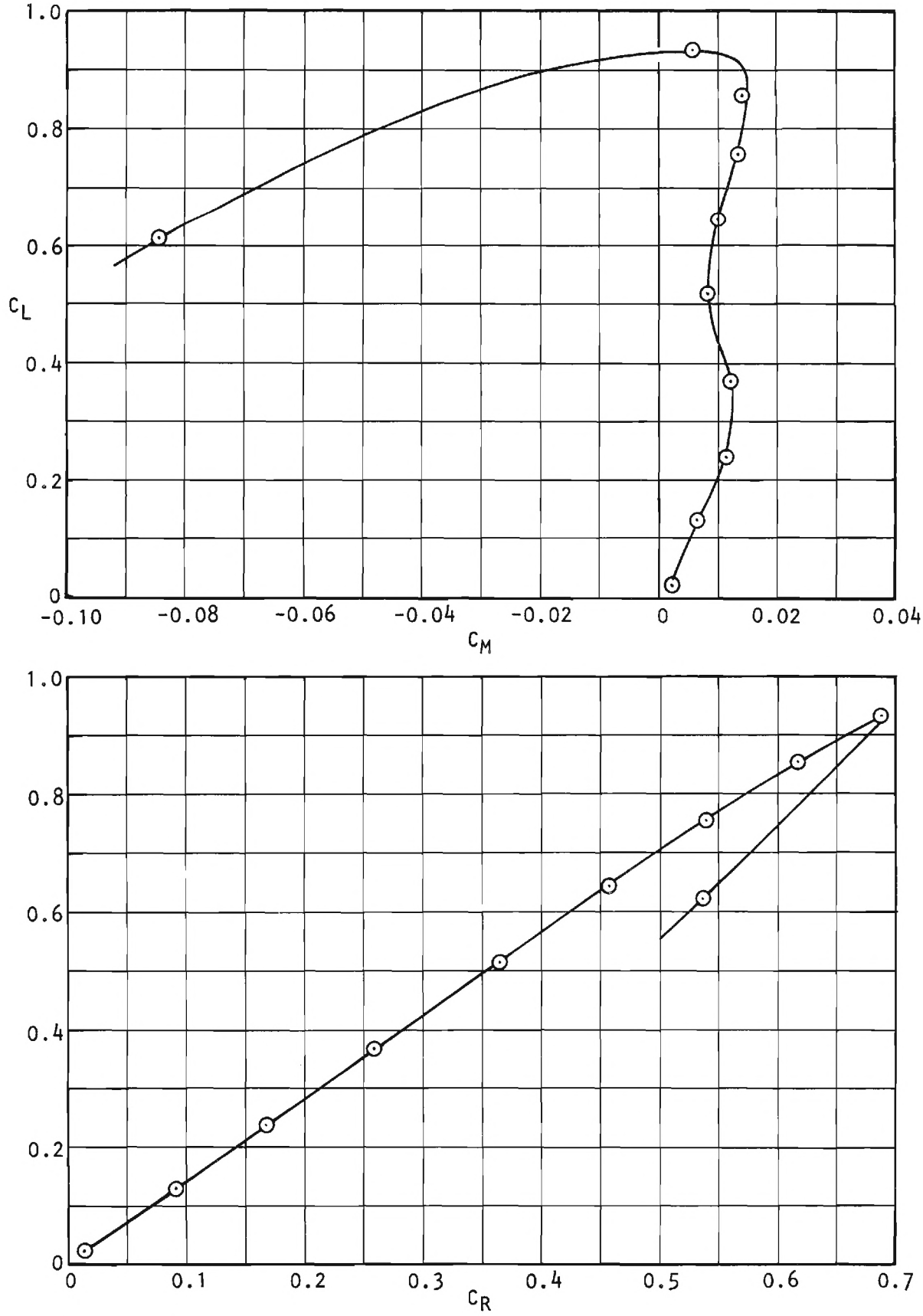

Figure 3.3 Pitching and Root Bending Moment Coefficients for Wing

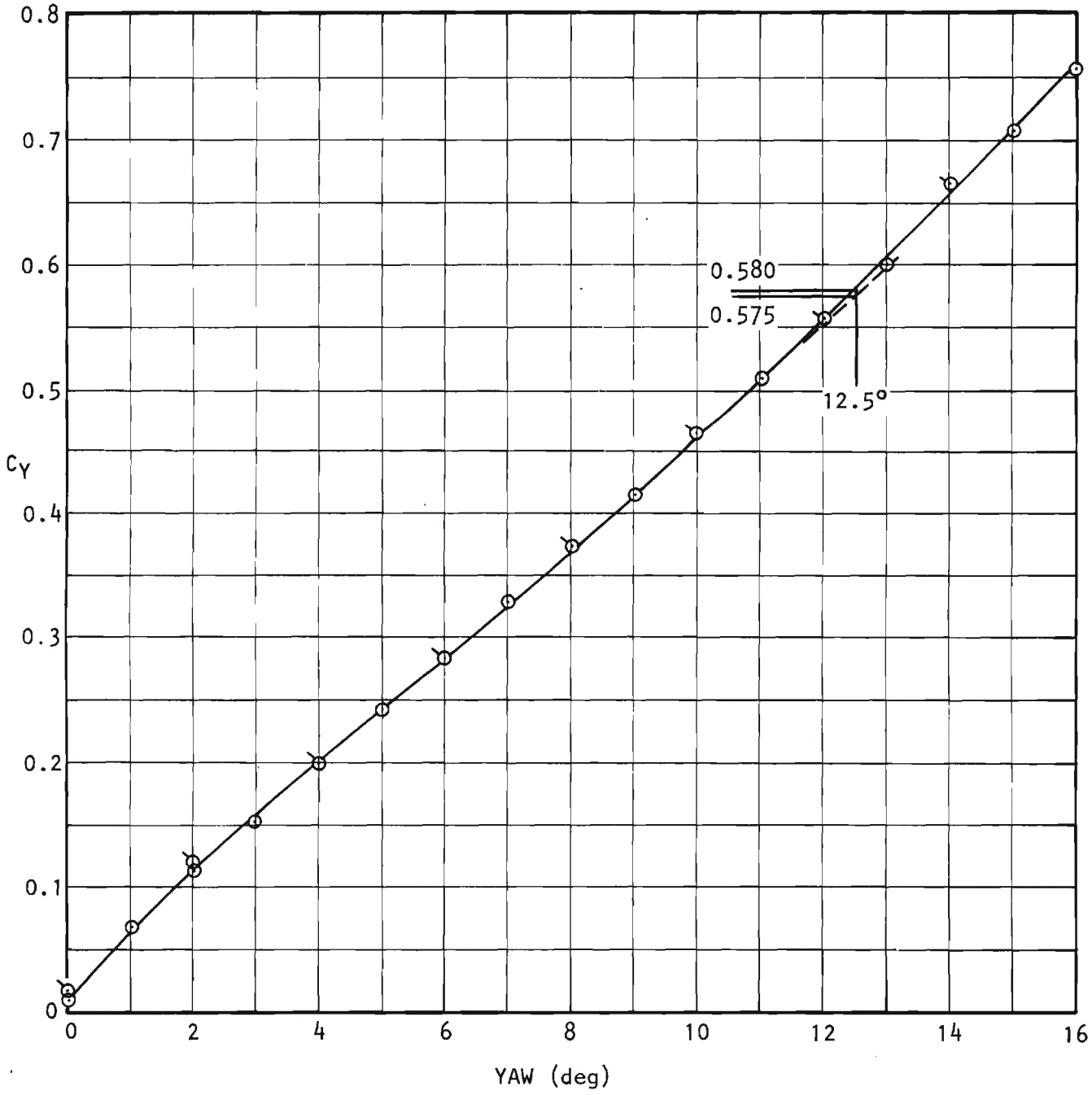

Figure 3.4 Sideforce coefficients for car

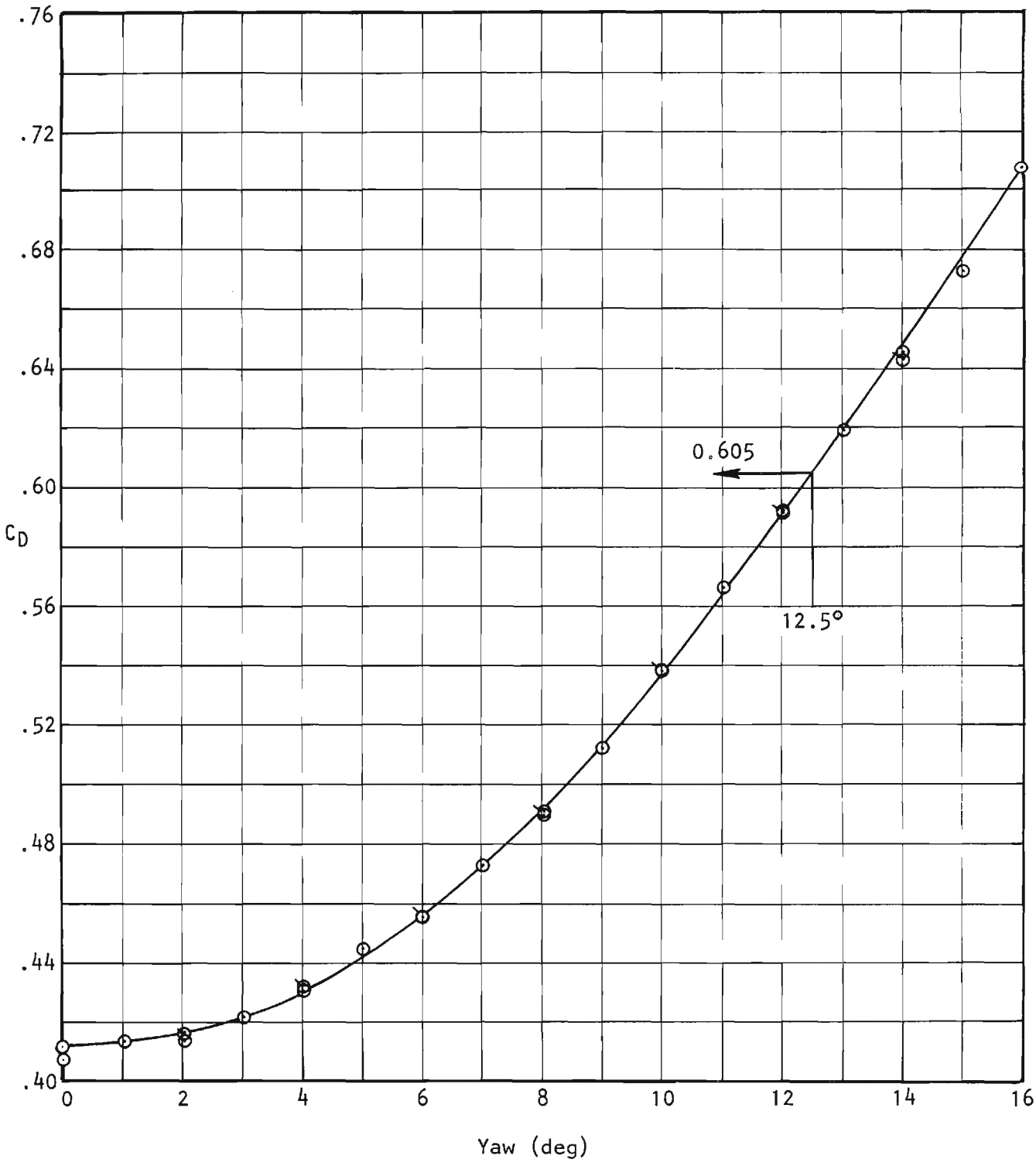

Figure 3.5 Drag coefficients for car

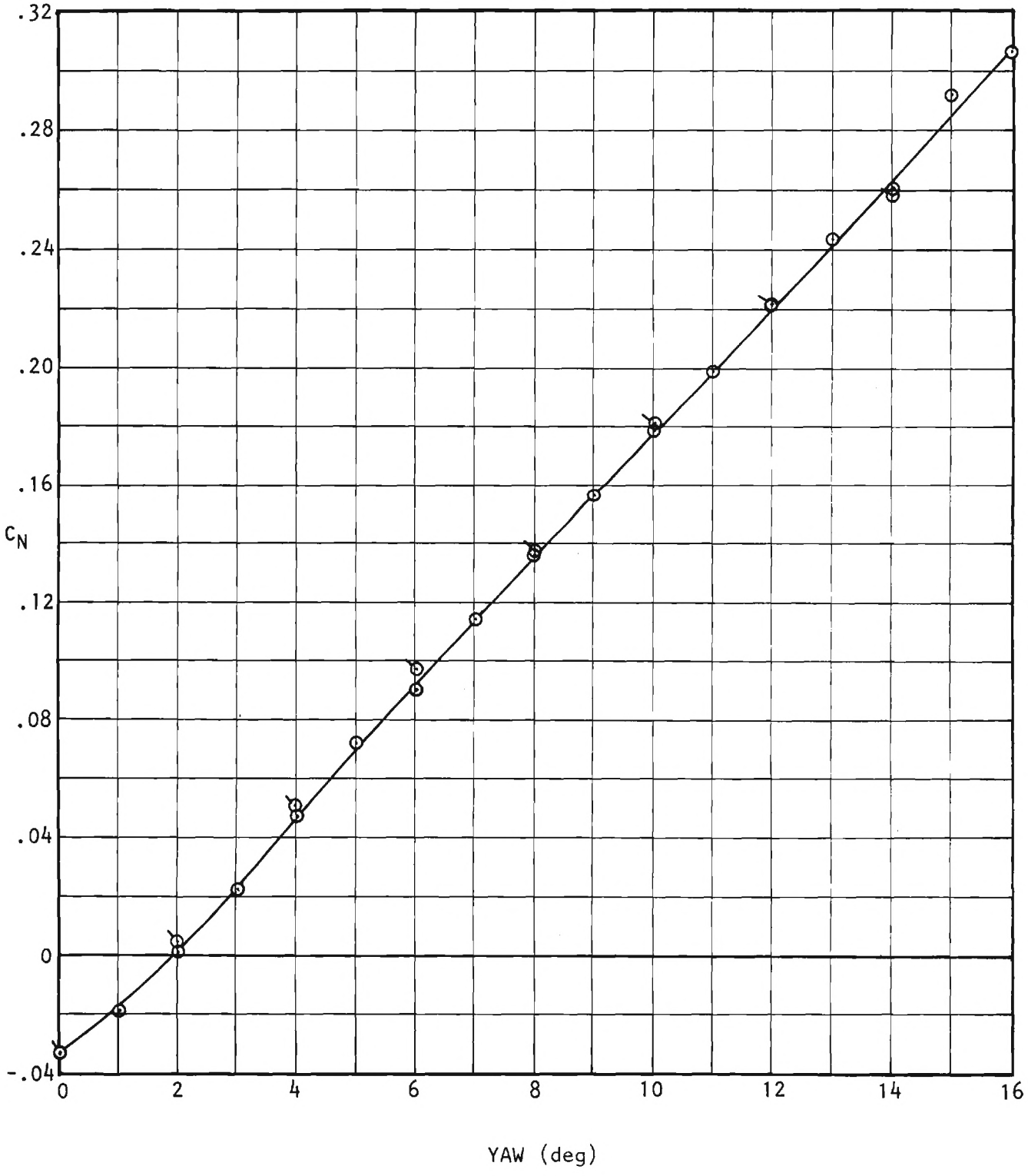

Figure 3.6 Yawing moment coefficients for car

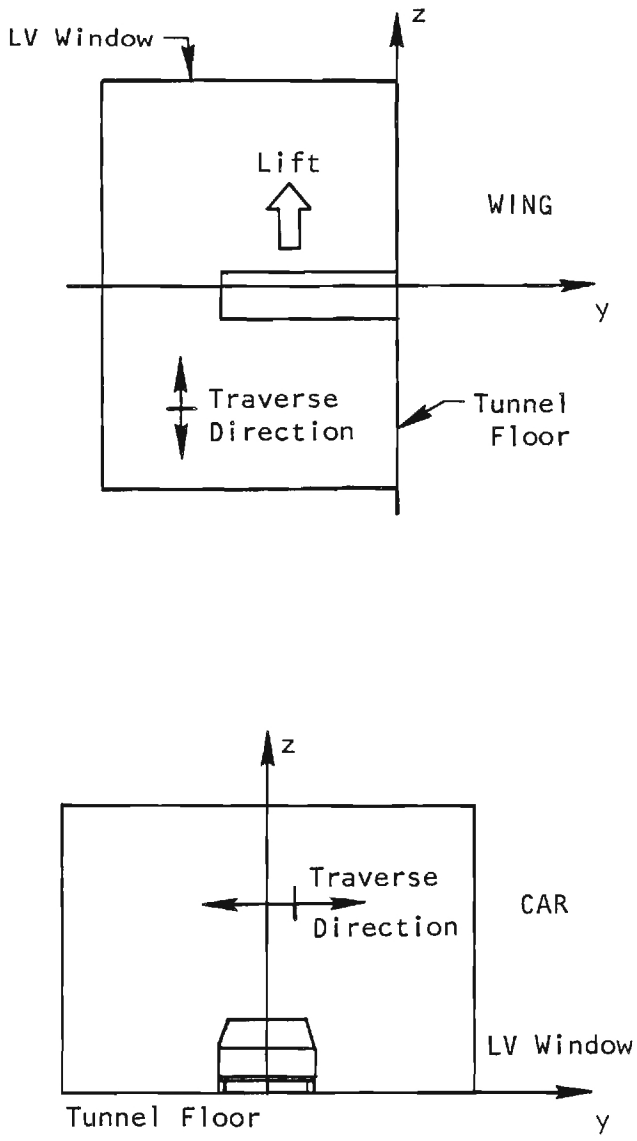

Figure 4.1 Aerodynamic axes for wing and car models.

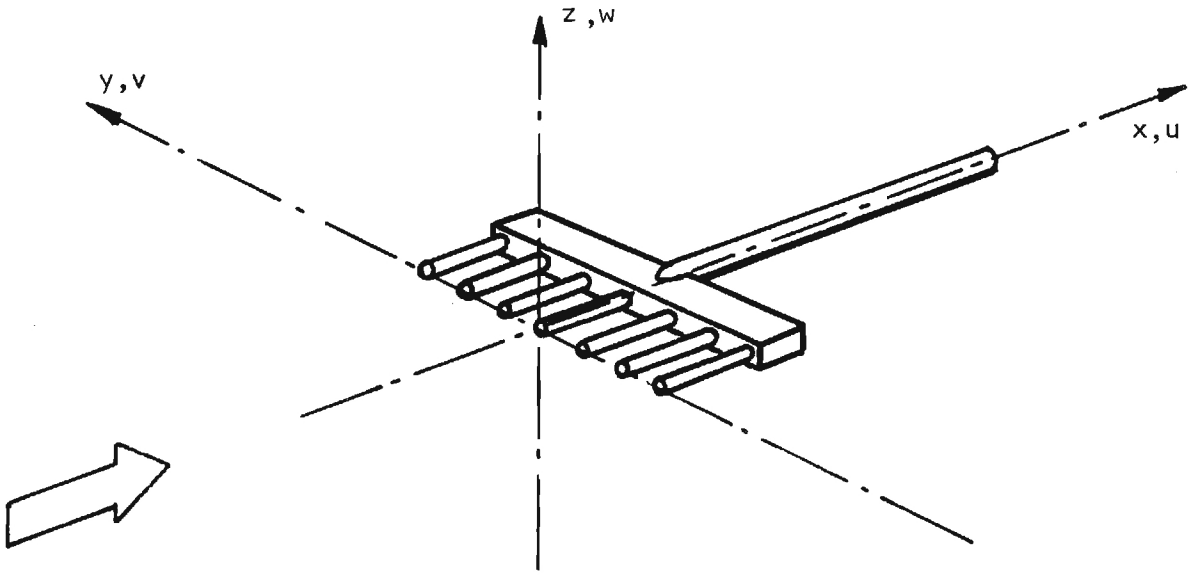

5-Hole Probe Axis System

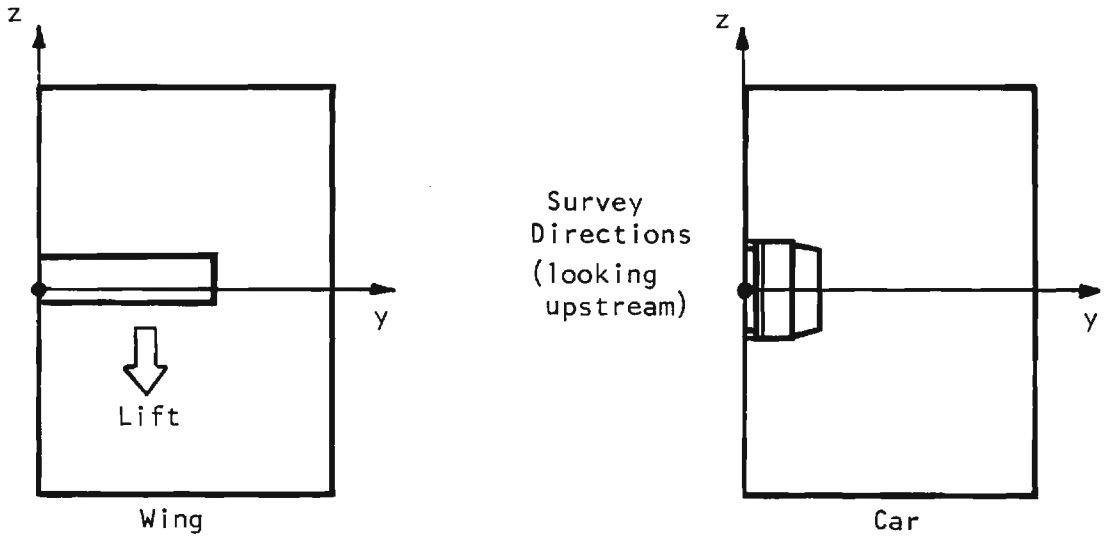

Figure 4.2 5-Holed Probe Data Transmittal Axis System

WING - X=-6 - ALPHA=6 TOTAL PRESSURE (HO-P)/QO

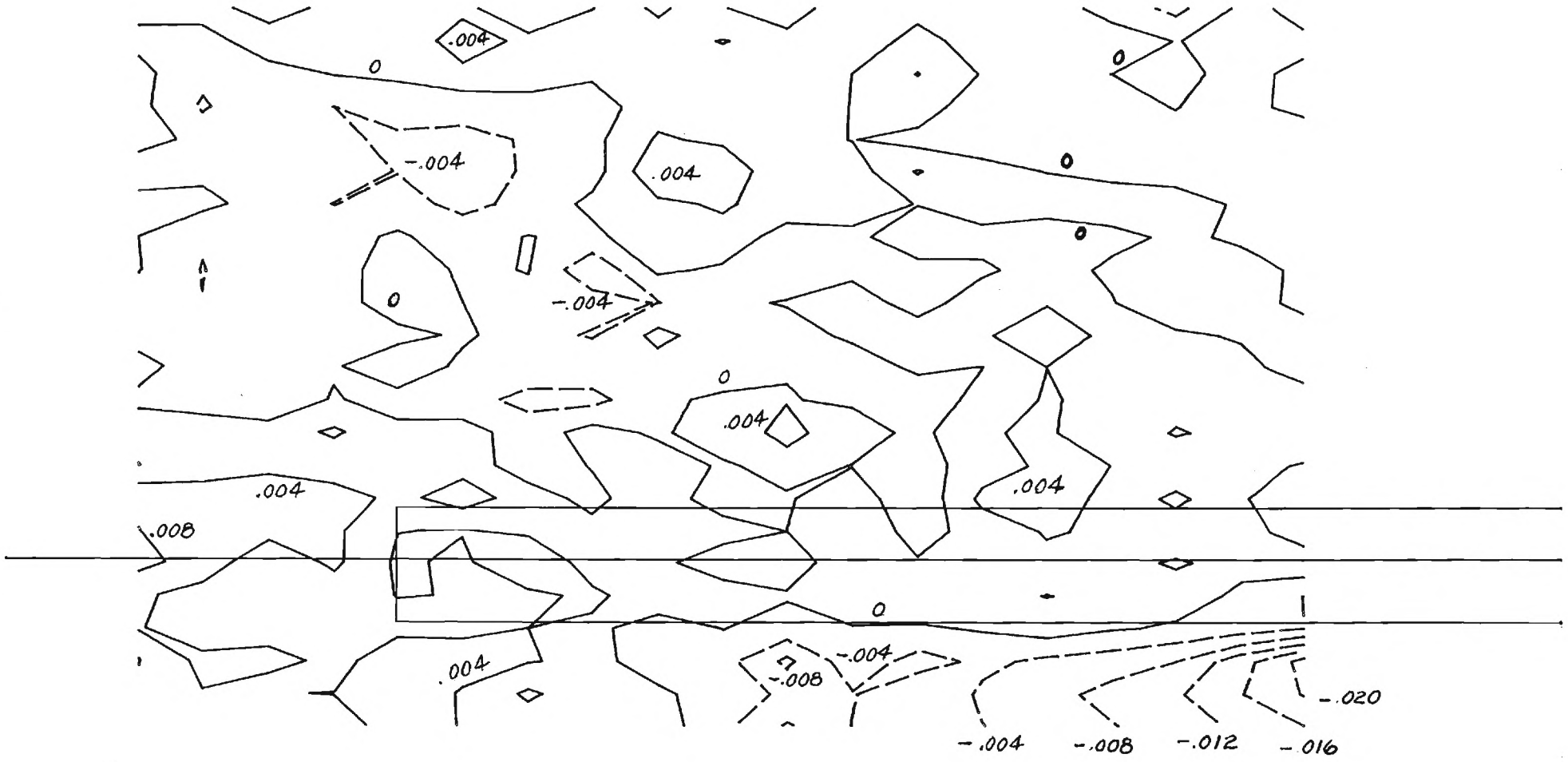

5.1 Total pressure deficit ahead of wing, $\alpha = 6^{\circ}$

. WING - X=-6 - ALPHA=18 TOTAL PRESSURE (HO-P)/QO

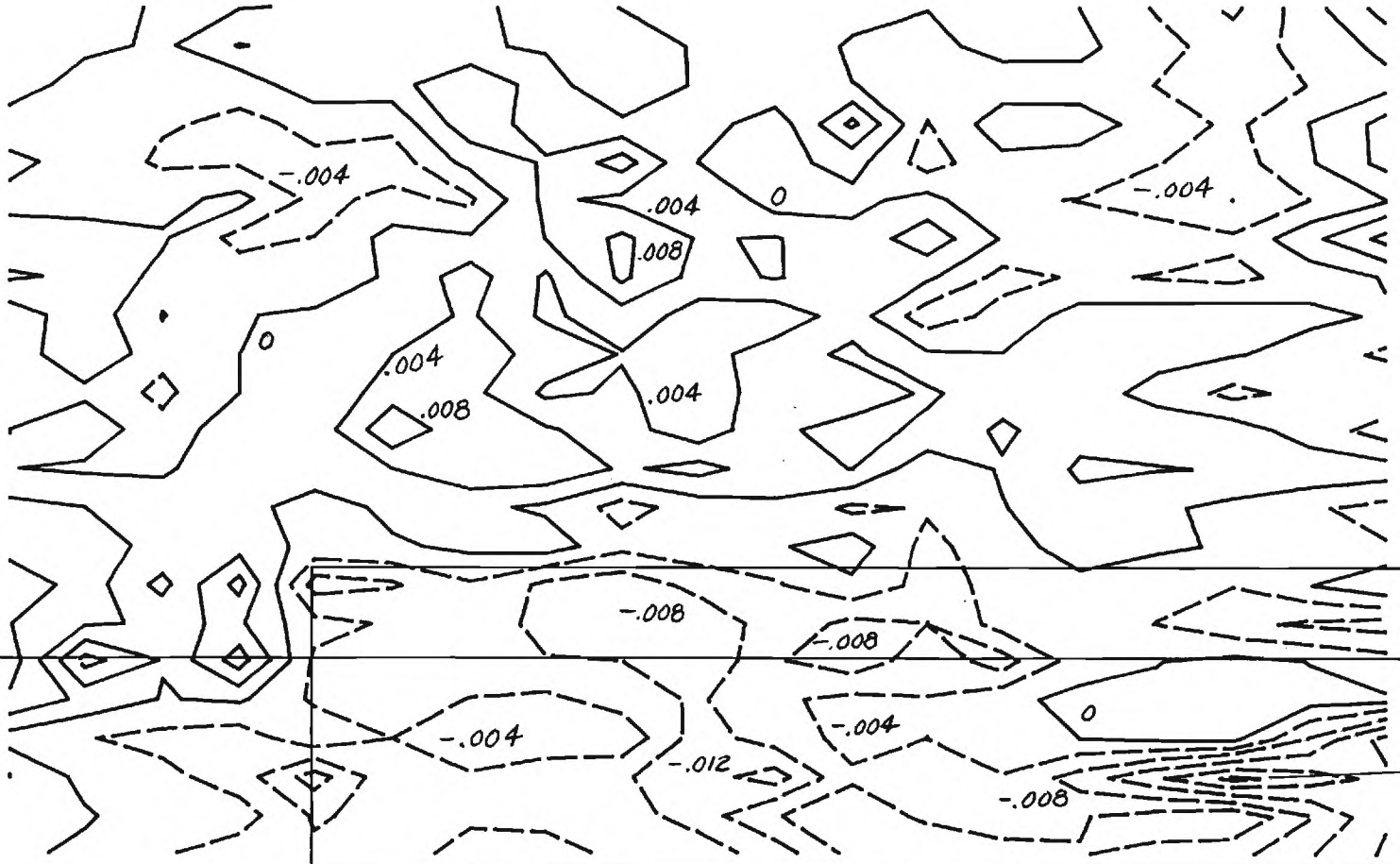

5.2 Total pressure deficit ahead of wing, α = 18°

WING - X=-6 - ALPHA=6 VORTICITY

NOTE

$$\left(\frac{\xi c}{U_o}\right) = \text{(CONTOUR VALUE)} \times 1152$$

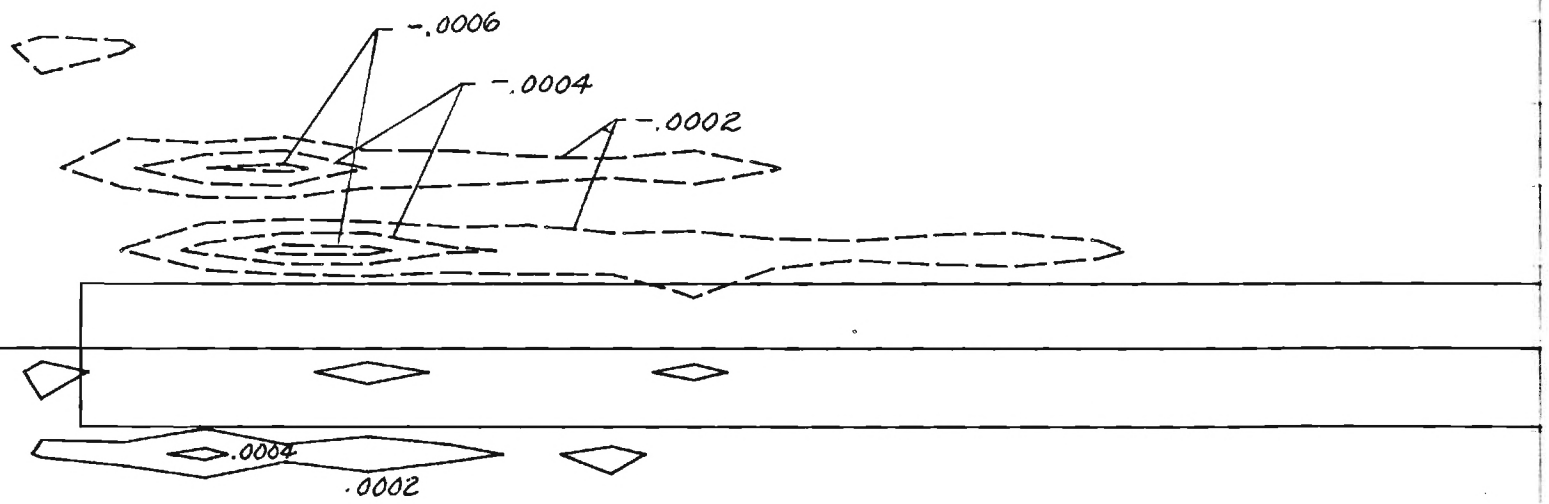

5.3 Apparent vorticity ahead of wing, $\alpha = 6°$

WING - X=-6 - ALPHA=18 VORTICITY

NOTE

$(\frac{\xi c}{U_o})$ = (CONTOUR VALUE) x 576

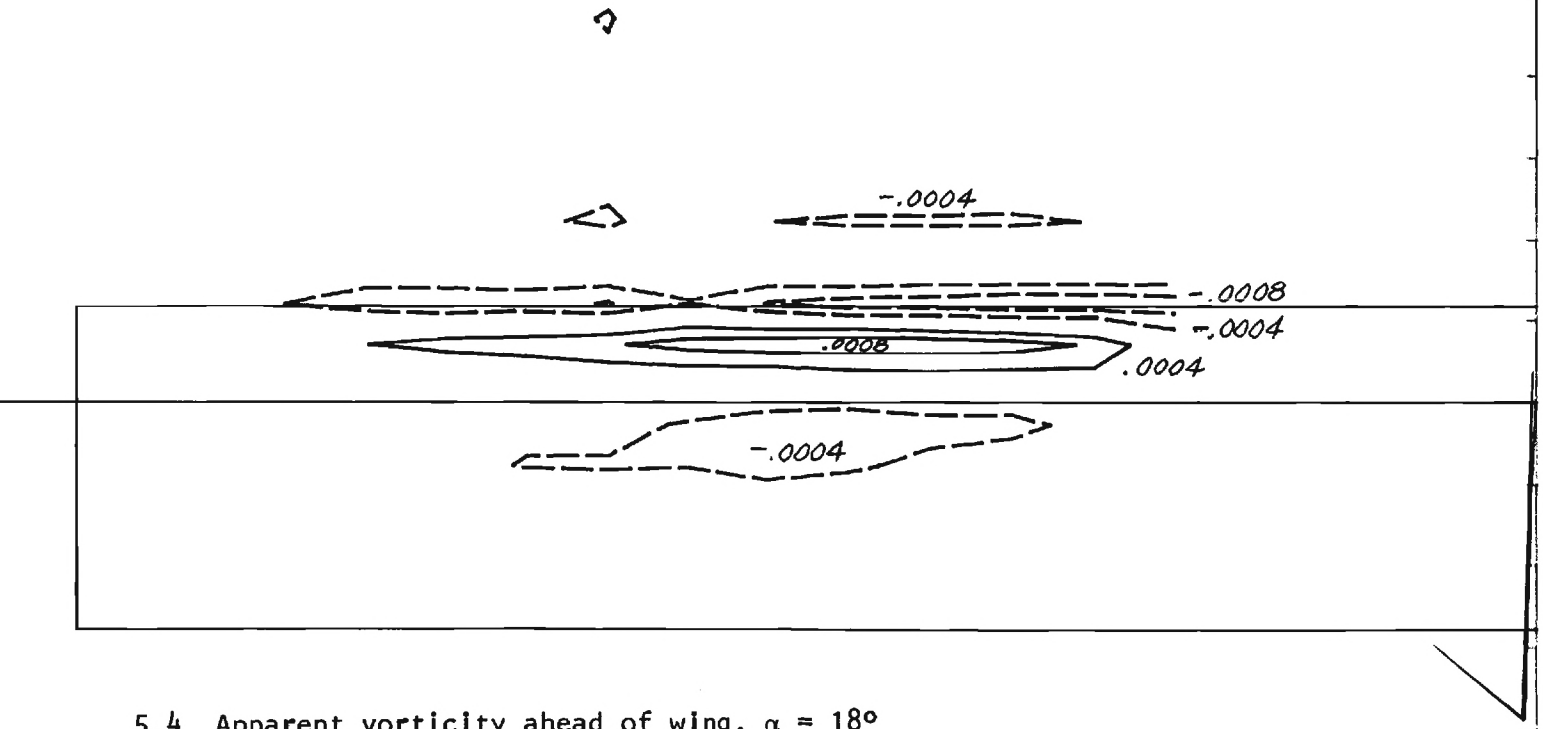

5.4 Apparent vorticity ahead of wing, α = 18°

WING - X=-6 - ALPHA=18 AXIAL VELOCITY RATIO U/UO

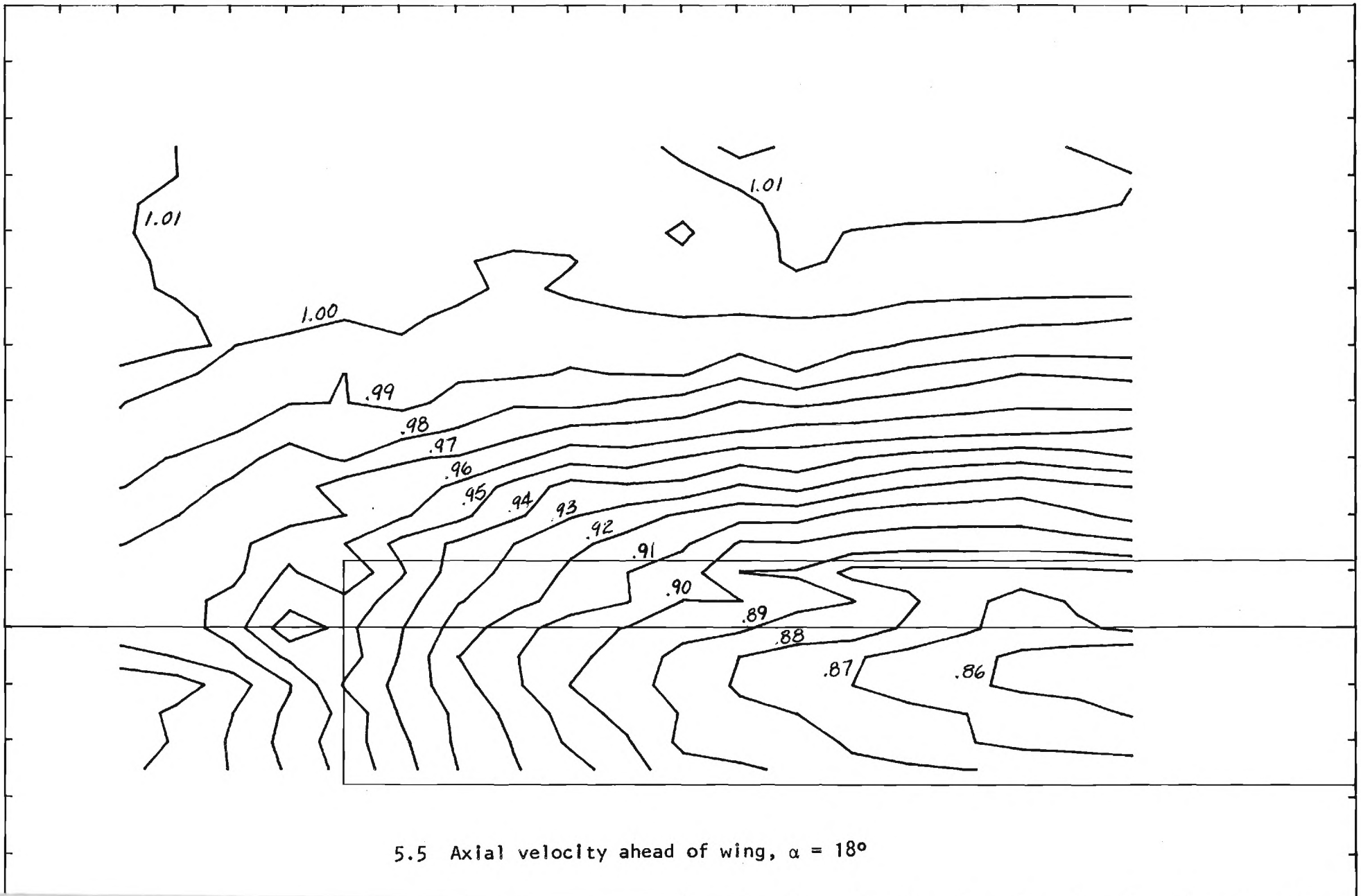

5.5 Axial velocity ahead of wing, α = 18°

WING - X=-6 - ALPHA=18 CROSSFLOW VELOCITY VC/UO

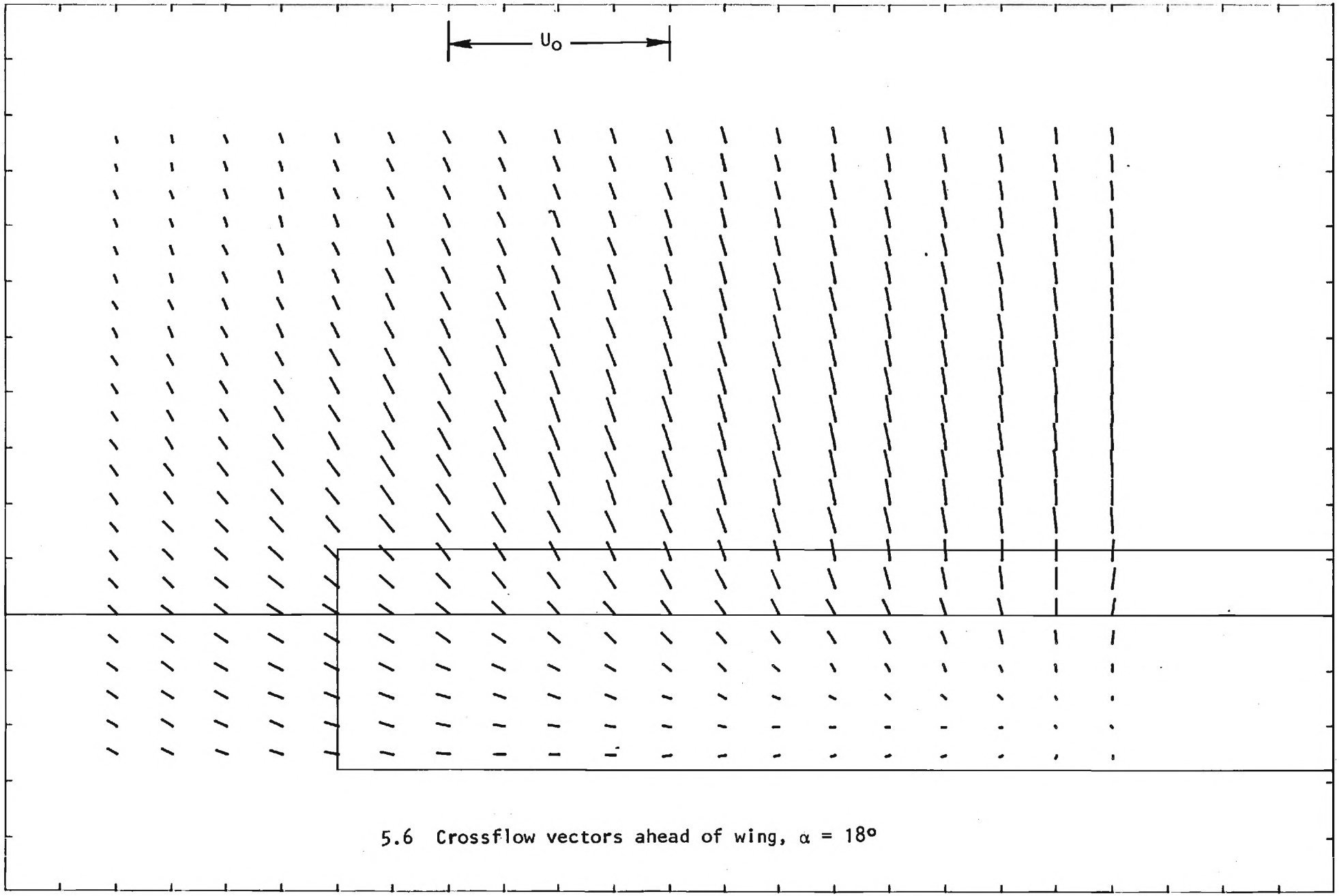

5.6 Crossflow vectors ahead of wing, $\alpha = 18^o$

WING - X=-6 - ALPHA=18 VERT. VELOCITY RATIO W/UO

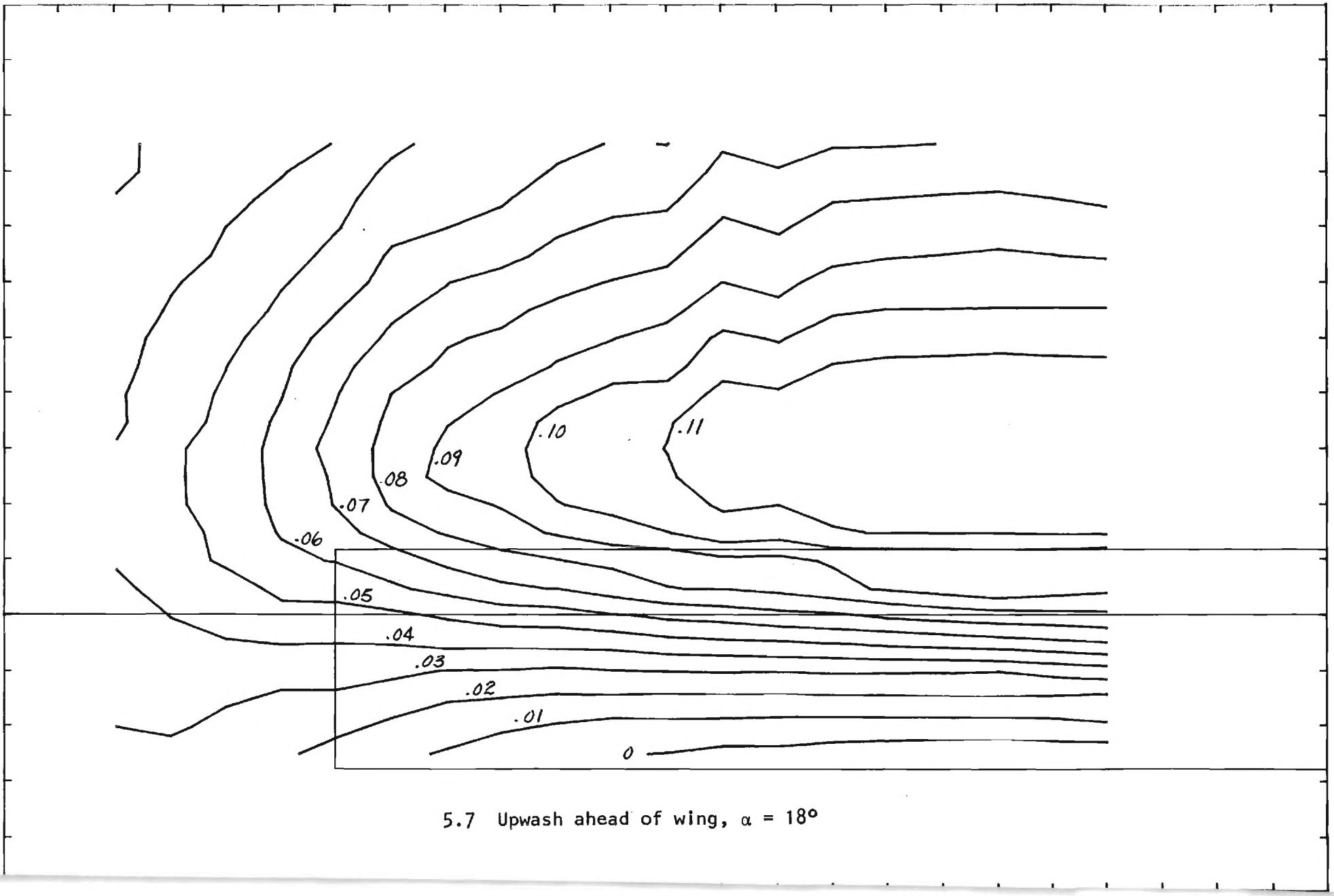

5.7 Upwash ahead of wing, α = 18°

WING - X=-6 - ALPHA=18 LAT. VELOCITY RATIO V/UO

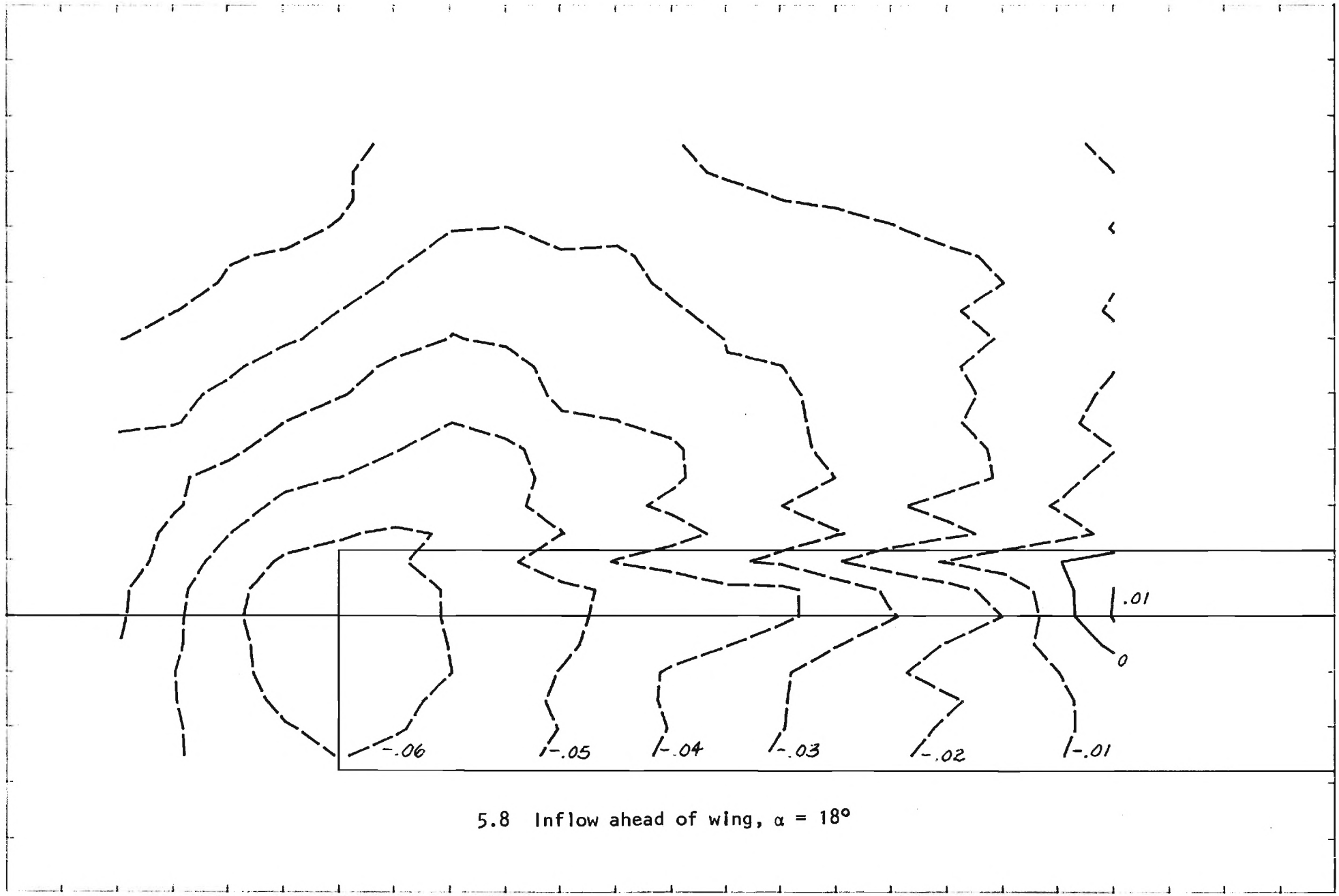

5.8 Inflow ahead of wing, $\alpha = 18°$

WING - X=-6 - ALPHA=18 SOURCE/SINK

NOTE

$(\frac{\sigma c}{U_o})$ = (CONTOUR VALUE) x 1152

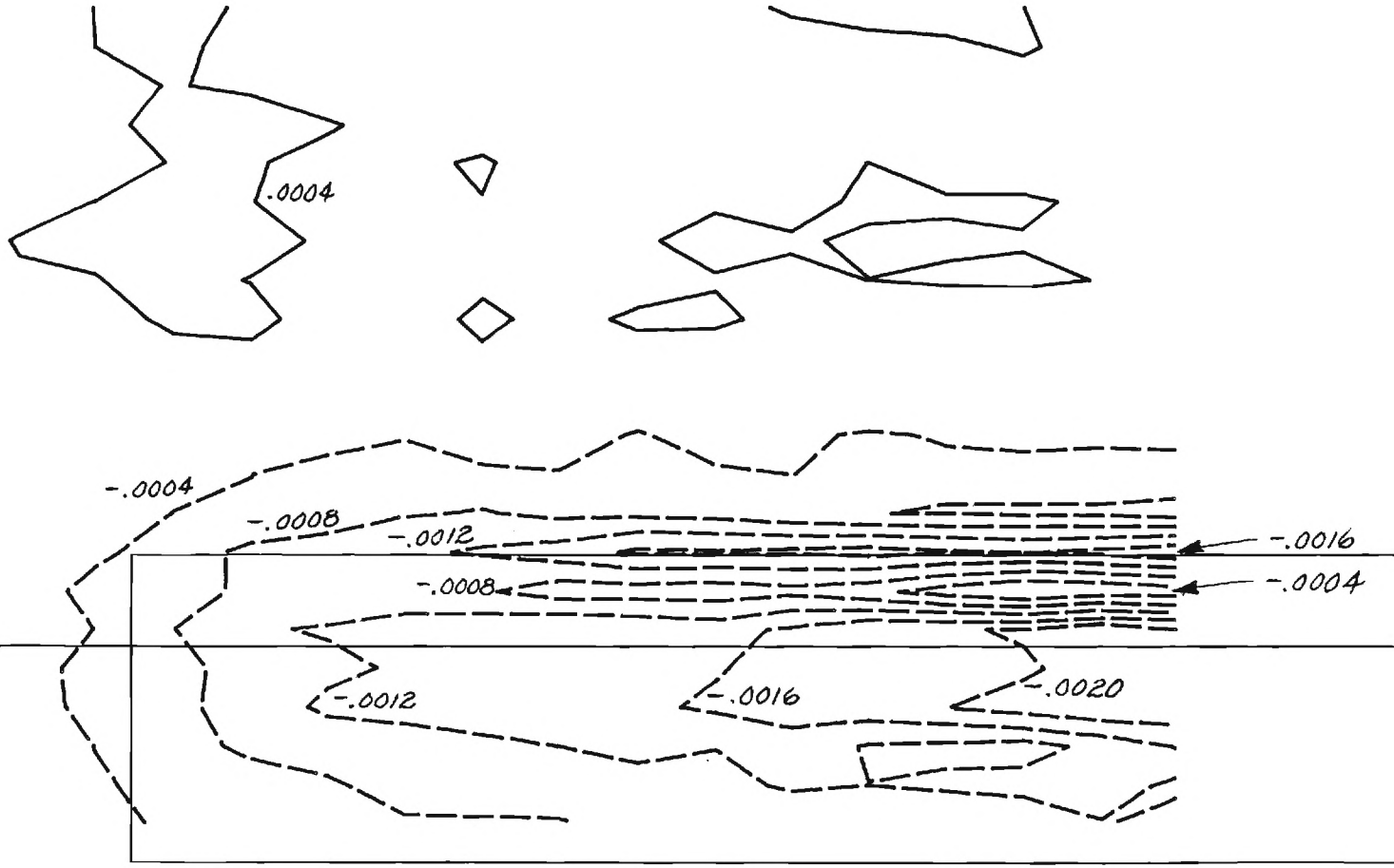

5.9 Apparent source strength ahead of wing, α = 18°

WING - X=-6 - ALPHA=6 AXIAL VELOCITY RATIO U/UO

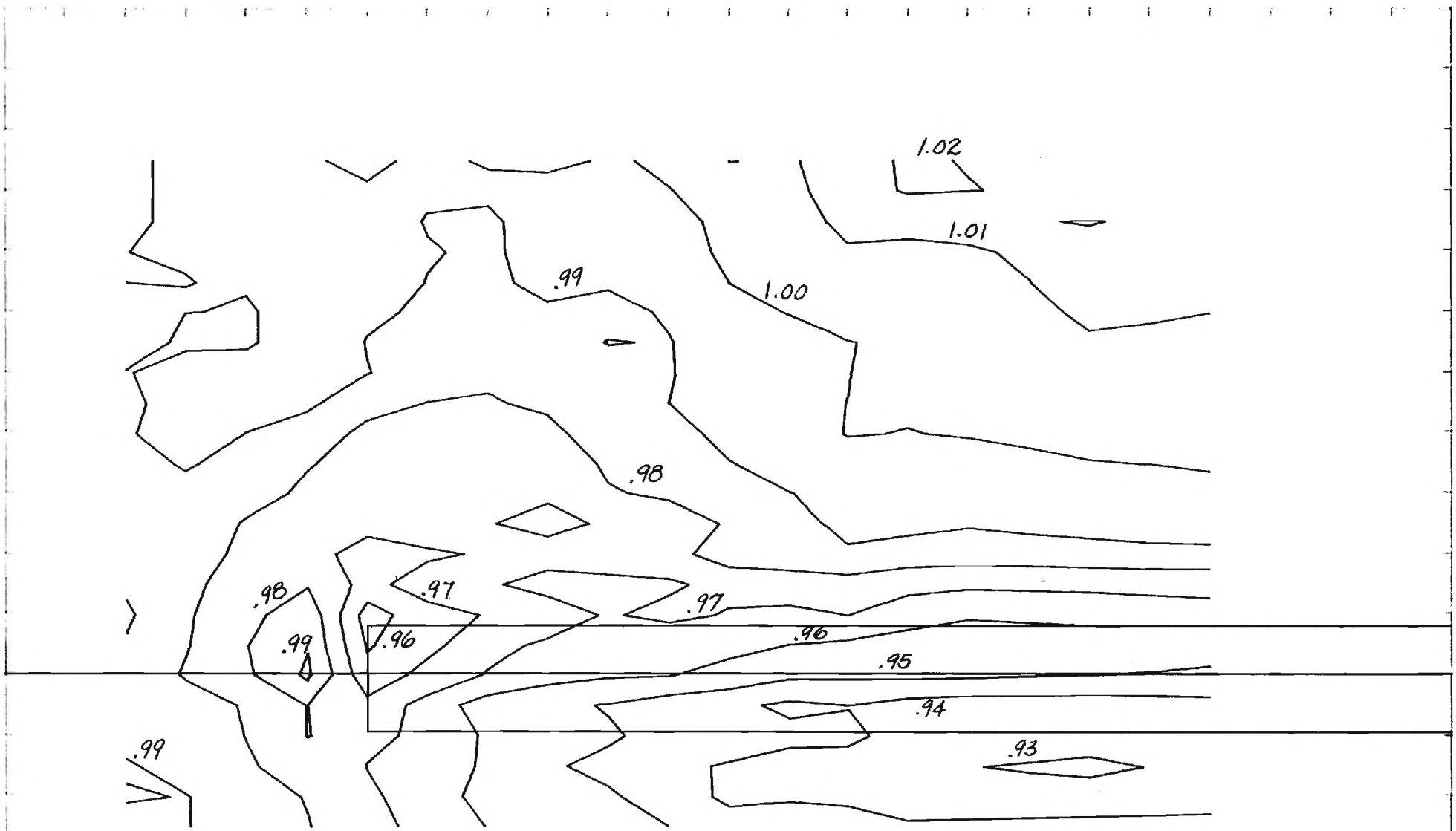

5.10 Axial velocity ahead of wing, $\alpha = 6°$

WING - X=-6 - ALPHA=6 CROSSFLOW VELOCITY VC/UO

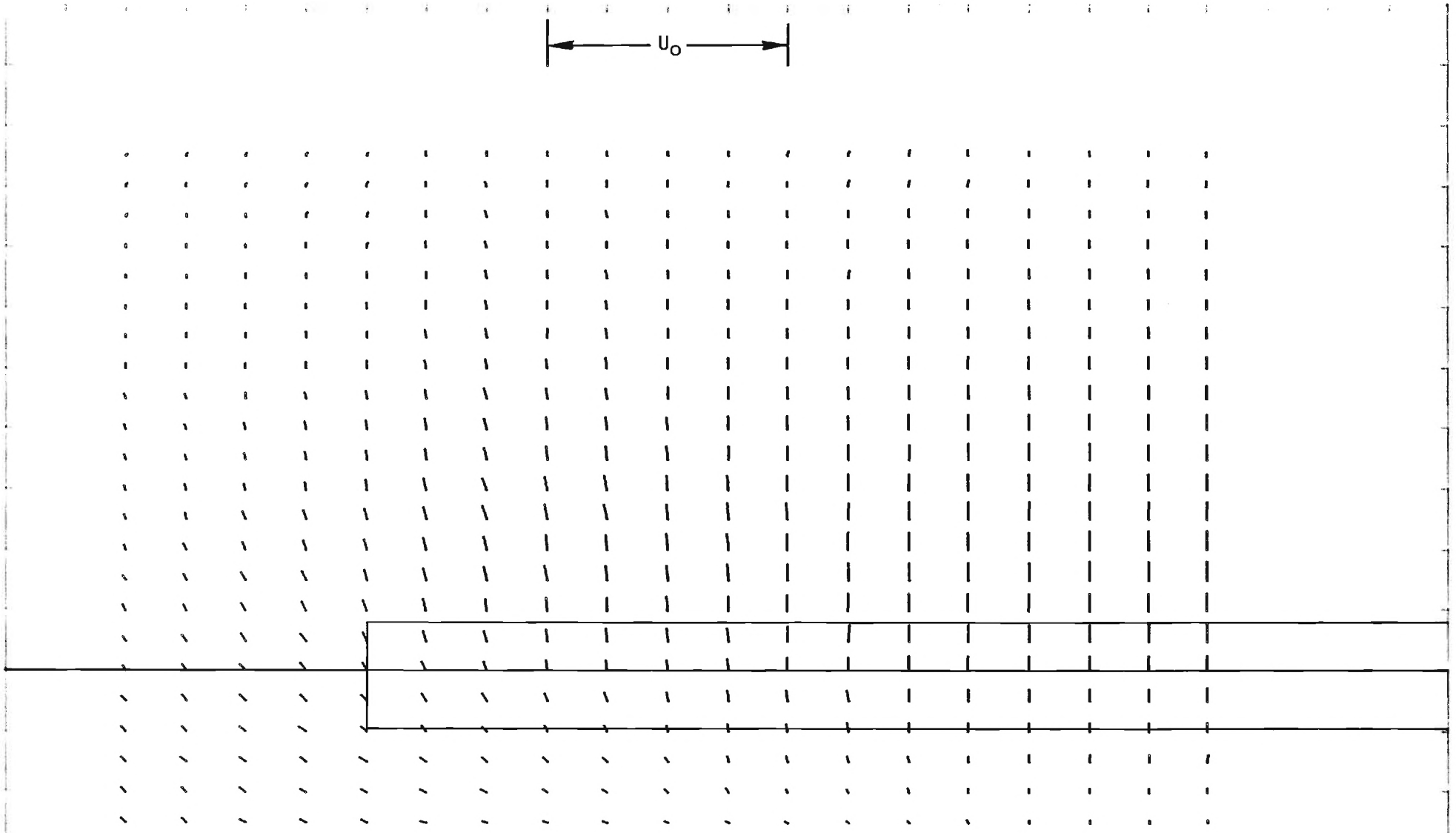

5.11 Crossflow vectors ahead of wing, $\alpha = 6°$

WING - X=-6 - ALPHA=6 VERT. VELOCITY RATIO W/UO

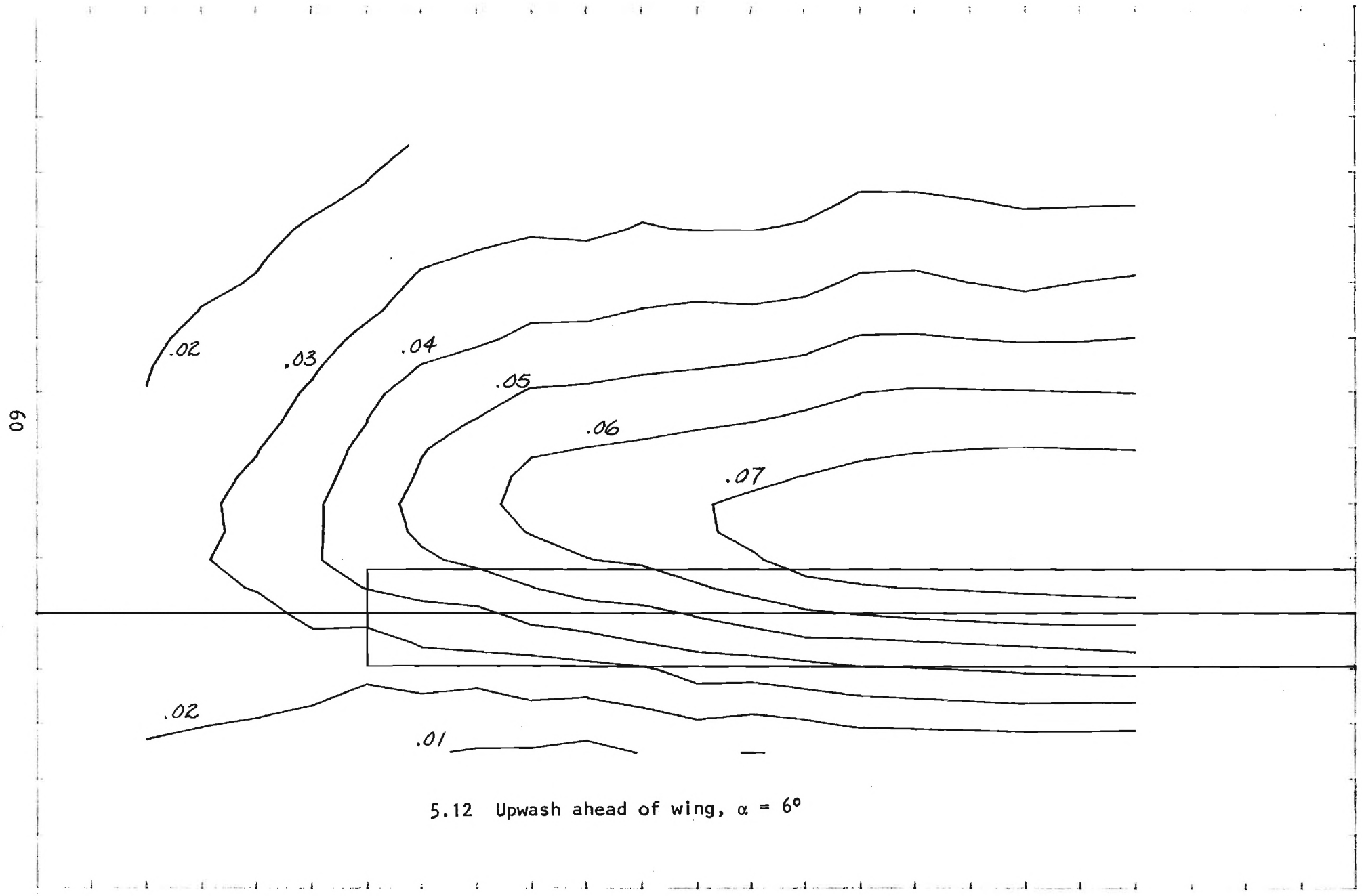

5.12 Upwash ahead of wing, $\alpha = 6°$

WING - X=-6 - ALPHA=6 LAT. VELOCITY RATIO V/UO

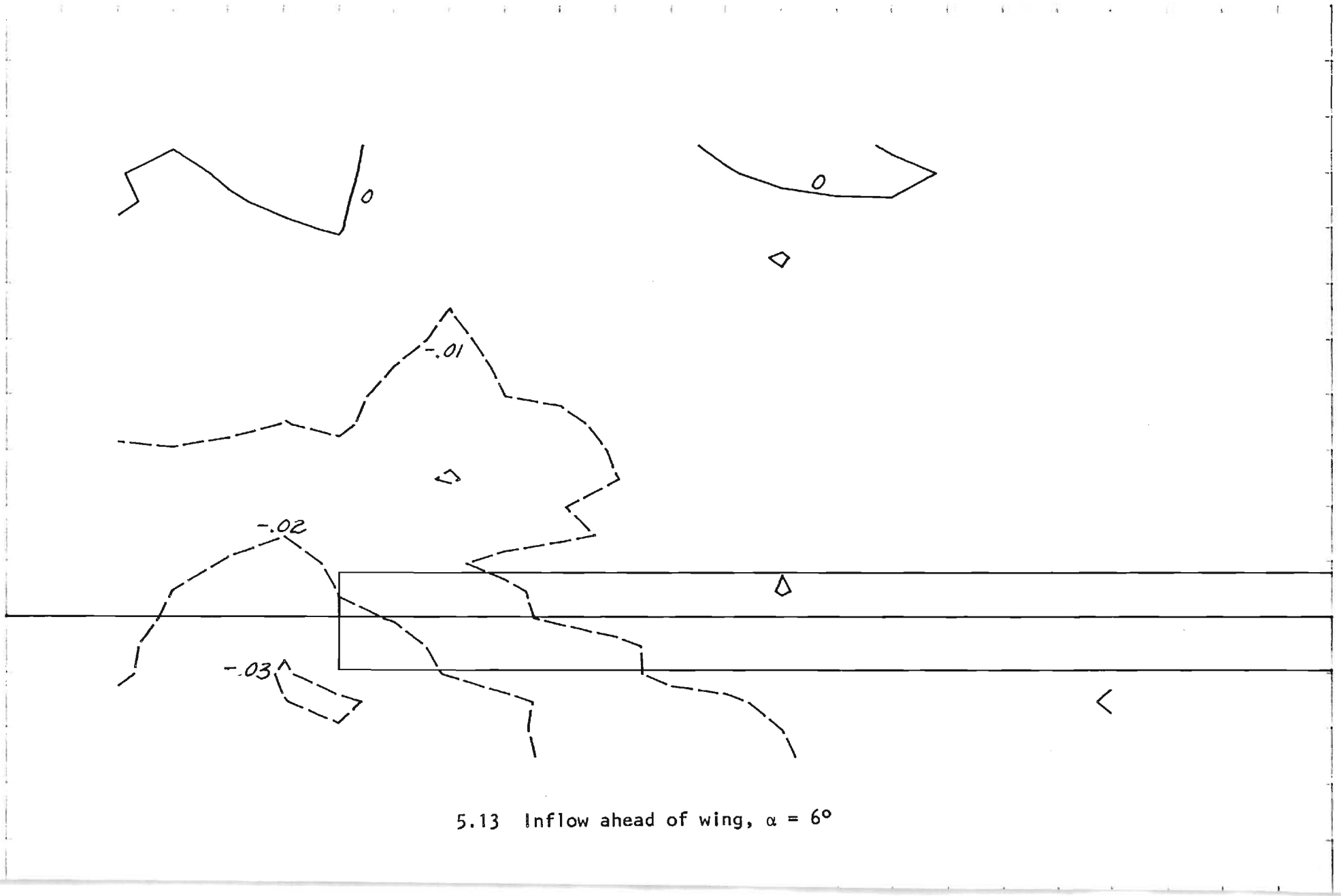

5.13 Inflow ahead of wing, $\alpha = 6^{\circ}$

WING - X=-6 - ALPHA=6 SOURCE/SINK

NOTE

$(\frac{\sigma c}{U_o})$ = (CONTOUR VALUE) x 576

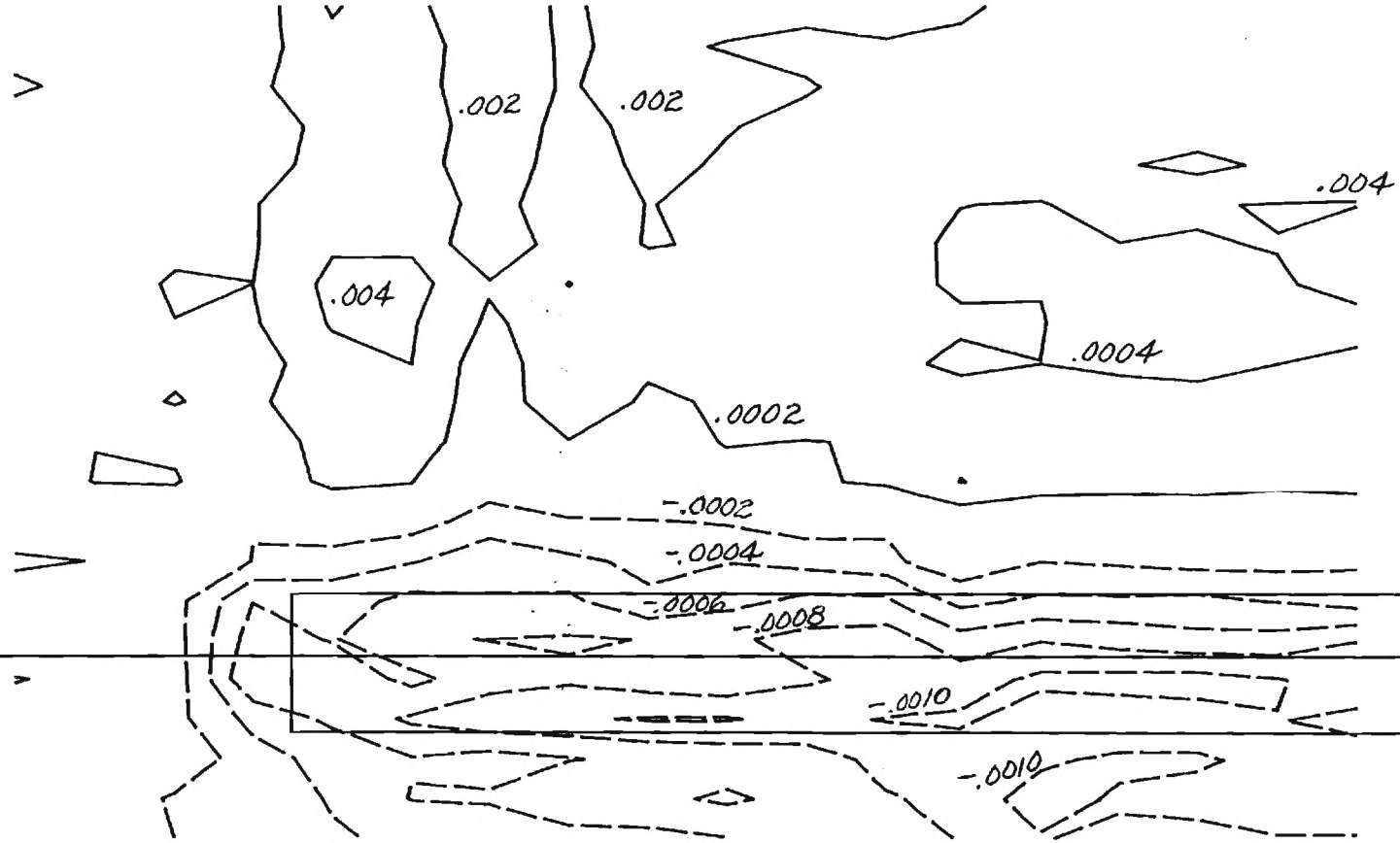

5.14 Apparent source strength ahead of wing, $\alpha = 6°$

MODEL	WING				CAR			
ANGLE (ALPHA OR PSI) - DEG	6		18		0		12.5	
TRAVERSE PLANE - X - INS	12	36	18	36	18	36	18	36
TRAVERSE NUMBER - TEST 64-	01	02	06	07	04	03	05	08
MEASURED QUANTITIES								
CROSSFLOW VECTORS	1	11	21	31	41	51	61	71
LATERAL VELOCITIES	2	12	22	32	42	52	62	72
VERTICAL VELOCITIES	3	13	23	33	43	53	63	73
AXIAL VELOCITIES	4	14	24	34	44	54	64	74
TOTAL PRESSURE	5	15	25	35	45	55	65	75
DERIVED QUANTITIES								
CROSSFLOW KINETIC ENERGY	6	16	26	36	46	56	66	76
AXIAL VORTICITY	7	17	27	37	47	57	67	77
* CORRECTED LATERAL VEL.	8	18	28	38	48	58	68	78
* CORRECTED VERTICAL VEL.	9	19	29	39	49	59	69	79
STREAM FUNCTION	10	20	30	40	50	60	70	80

* IE. DERIVED FROM AXIAL VORTICITY AND INCLUDING TUNNEL BOUNDARY CONSTRAINTS

NOTE:
Machine Plots, MP1 to MP80 indexed above are situated at the end of this report.

Figure 6.1 Index for machine plots

APPENDIX I

IMPLEMENTATION AND CALIBRATION OF "BLOCKAGE CORRECTED q" SCHEME

(This appendix is taken from NASA CR 137857 (Ref 8), with slight modifications)

The accepted correction to the dynamic pressure due to model blockage is:

$$q_c = q_{uc} + 2\varepsilon_s q_{uc} + 2\varepsilon_w q_{uc} \tag{A1}$$

where q_c = corrected dynamic pressure at model station

q_{uc} = uncorrected dynamic pressure at model station

ε_s = solid blockage coefficient

ε_w = wake blockage coefficient.

Reference 9 gives the blockage due to the wake in the form

$$\frac{\Delta q}{q_{uc}} = 2\varepsilon_w = \frac{1}{2}\left\{\frac{p_{cm} - p_{co}}{q_{uc}}\right\} \tag{A2}$$

where p_{cm} = static pressure at end of contraction section with model present

p_{co} = static pressure at end of contraction section with tunnel empty.

The tunnel conditions are obtained from static pressure tapping at the start of the contraction section (assumed to be approximately total pressure) and a static pressure tapping at the end of the contraction section (p_c). The total pressure line is connected to two differential pressure transducers, one open to atmosphere to give H_c, and the other connected to the static pressure line to give ΔP.

The static pressure at the end of the contraction section will then be

$$p_c = H_c - \Delta P \tag{A3}$$

Thus,

$$q_c = q_{uc} \{1 + 2\varepsilon_s + \frac{1}{2}\frac{(H_c - \Delta P - P_{co})}{q_{uc}} \}$$

$$= \frac{1}{2} \{H_c + [2 + 4\varepsilon_s - (\frac{P_{co}}{q_{uc}})] q_{uc} - \Delta P\}$$

$$= \frac{1}{2} \{H_c + [2 + 4\varepsilon_s - (\frac{P_{co}}{q_{uc}}) (\frac{q_{uc}}{\Delta P}) - 1]\Delta P\}$$

$$\therefore q_c = \frac{1}{2} (H_c + K\Delta P) \qquad (A4)$$

where

$$K = [2 + 4\varepsilon_s - (\frac{P_{co}}{q_{uc}})] (\frac{q_{uc}}{\Delta P}) - 1 \ . \qquad (A5)$$

(P_{co}/q_{uc}) and $(q_{uc}/\Delta P)$ are empty tunnel calibration slopes and ε_s is the conventional solid blockage correction. Equation (A4) is evaluated on-line.

APPENDIX II

EQUATIONS FOR VELOCITIES WITHIN THE VORTICITY FIELD

Figure A1 (see next page) shows part of the traversed region and the cell arrangement used to calculate v and w at point 0. The three levels of calculation include near field (shaded), an intermediate field above and below it for certain non-square cell cases and the far field which extends to the traverse boundaries. The velocity equations will be summarized below:

Near Field

We shall deal first with the innermost region depicted by broken lines. Vorticity values around this boundary are ξ_1 through ξ_8, which are determined at the cell centers from experimental data. The vorticity at 0, the 'receiving' point, is ξ_0. For the purpose of determining v and w velocities at 0, it is assumed that vorticity is linearly graded from 0 to 1, 1 to 2, 2 to 0, etc. For the region bounded by the broken lines, the required velocities may be obtained from Reference 10 as:

$$v = (1+e)^2 \frac{\Delta z}{4\pi}\left[\left\{\left(\frac{\Delta z}{\Delta y}\right)F_{11} - \left(\frac{\Delta y}{\Delta z}\right)^2 F_{22}\right\}(\xi_2 + \xi_4 - \xi_6 - \xi_8) + 2\left\{\left(\frac{\Delta z}{\Delta y}\right)F_{11} + F_{02}\right\}(\xi_7 - \xi_3)\right] \quad \text{(A1)}$$

and

$$w = (1+e)^2 \frac{\Delta y}{4\pi}\left[\left\{F_{21}\left(\frac{\Delta z}{\Delta y}\right)^2 - F_{12}\left(\frac{\Delta y}{\Delta z}\right)\right\}(\xi_2 - \xi_4 - \xi_6 + \xi_8) + 2\left\{F_{01} + \left(\frac{\Delta y}{\Delta z}\right)F_{12}\right\}(\xi_1 - \xi_5)\right] \quad \text{(A2)}$$

where

$$F_{01} = \tan^{-1}\left(\frac{\Delta z}{\Delta y}\right)$$

$$F_{11} = \log_e \sin\left\{\frac{\pi}{z} - \tan^{-1}\left(\frac{\Delta z}{\Delta y}\right)\right\}$$

$$F_{02} = \frac{\pi}{z} - \tan^{-1}\left(\frac{\Delta z}{\Delta y}\right)$$

$$F_{12} = \log_e \left\{1/\sin\left\{\tan^{-1}\left(\frac{\Delta z}{\Delta y}\right)\right\}\right\}$$

$$F_{21} = \frac{\Delta y}{\Delta z} - \left\{\frac{\pi}{2} - \tan^{-1}\left(\frac{\Delta z}{\Delta y}\right)\right\}$$

$$F_{22} = \frac{\Delta z}{\Delta y} - \tan^{-1}\left(\frac{\Delta z}{\Delta y}\right)$$

and ξ_1, ξ_2, ξ_3, ξ_4, ξ_5, ξ_6, ξ_7 and ξ_8 are the vorticity values at the nodal points shown in Figure A1.

The factor $(1+e)$ is introduced in equations A1 and A2 for use later when enlarging the domain of integration to include the entire near field. The results for the region within $1 \to 8$ are obtained by putting $e = 0$.

It will be noticed that ξ_0 is absent in Equations (A1) and (A2). This occurs because ξ_0 represents a uniformly-spread vorticity, within the boundary $1 \to 8$, which induces no resultant velocity at 0. This means that the 'active' part of the field comprises ξ components proportional to radius from 0: 0 to $(\xi_1 - \xi_0)$ along 01, 0 to $(\xi_2 - \xi_0)$ along 02, and similarly elsewhere. This fact may be used to scale the result for innermost region $1 \to 8$ so as to include the complete, nine-cell, inner field.

We seek to enlarge the region ABCD (See sketch on next page) by a linear scale of $(1+e)$ to give the outline A´B´C´D´. The vorticity values at A, B, C and D are to be left unchanged. The transformations take the form

$$y_{A'} = (1+e)y_A$$

$$z_{a'} = (1+e)z_A$$

$$(\xi_A - \xi_0)' = (1+e)(\xi_A - \xi_0), \text{ etc.}$$

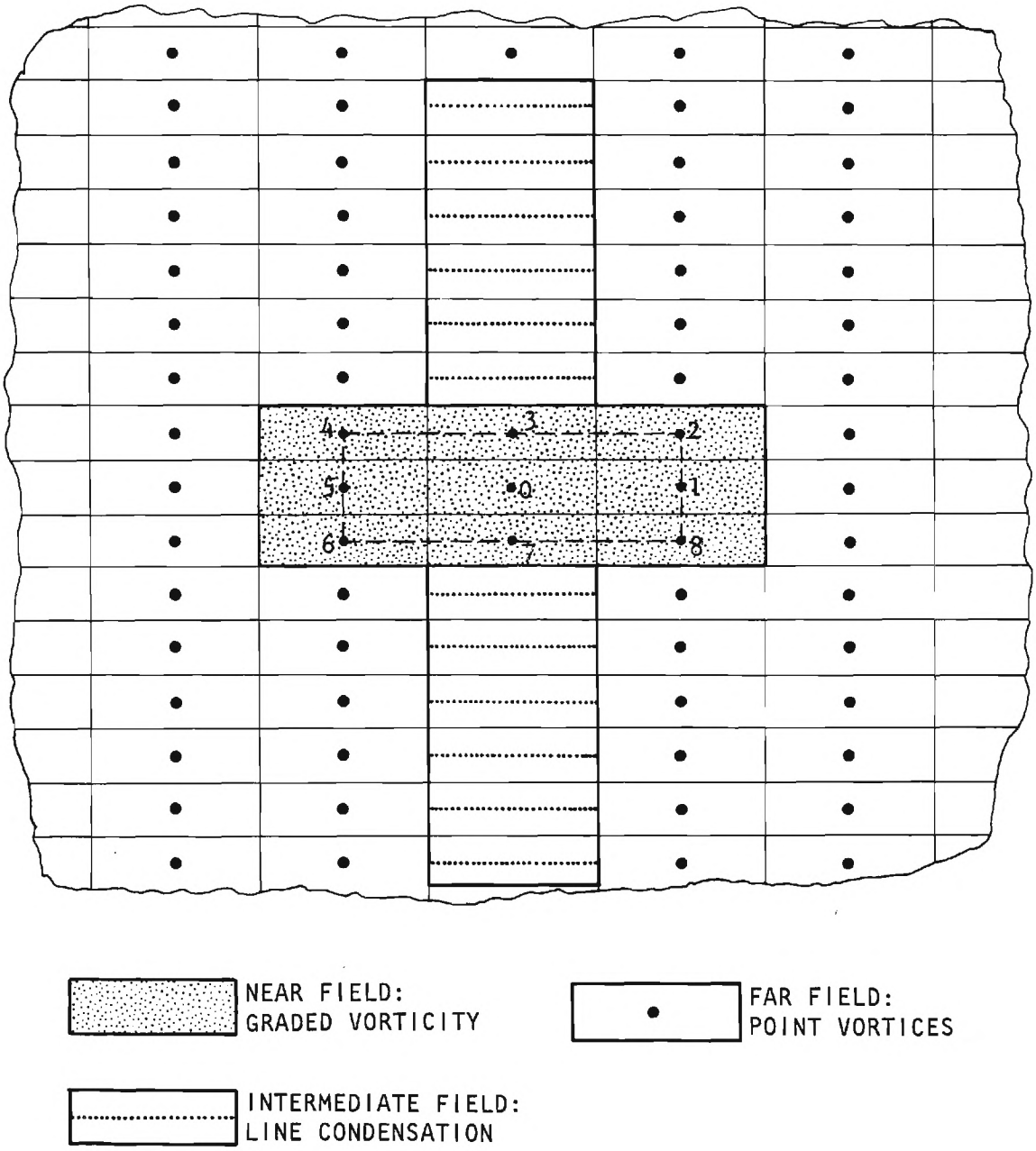

Figure A1 Calculation Field for Vorticity-Induced Velocities

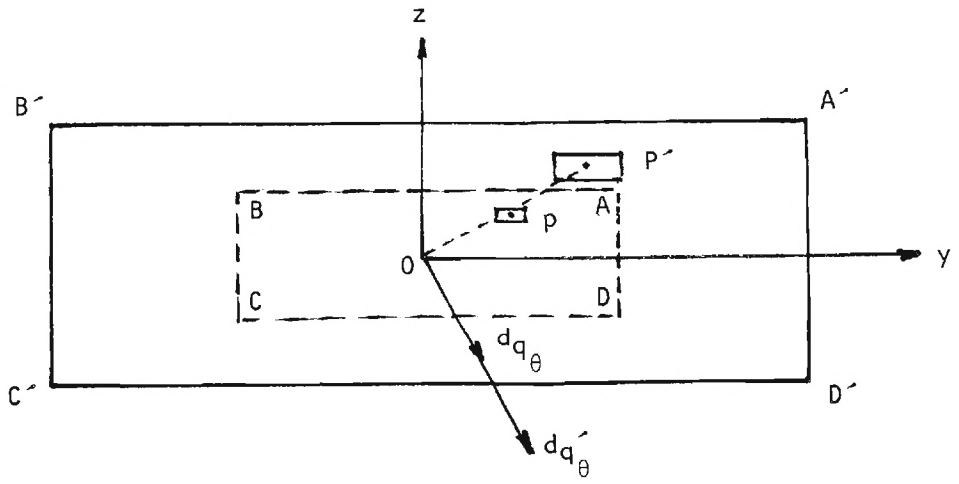

To determine the ratios of velocities, we may consider elementary velocities dq_θ and dq_θ' induced by typical elements P and P´, the radius of P´ being (1 + e) times that for P. We observe that the area of the element at P´ is (1 + e)-squared times that for P. We obtain:

$$dq_\theta = \frac{(\xi_p - \xi_0)dy\ dz}{2\pi\ r_p}$$

and

$$dq_\theta' = \frac{(\xi_p - \xi_0)'dy'dz'}{2\pi\ r_p'} = \frac{(1+e)(\xi_p - \xi_0)(1+e)dy\cancel{(1+e)}dz}{2\pi\cancel{(1+e)}r_p}$$

$$= (1+e)^2 dq_\theta \qquad \text{(A3)}$$

For e = 0, equations (A1) and (A2) give velocities for a 2-cell by 2-cell region. Since the desired result, for the complete near field, requires 3-cells by 3-cells it is evident from (A3) that a value $e \simeq 0.5$ should be employed in (A1) and (A2).

Far Field

If the vorticity in a far-field cell, sides Δy and Δz, is ξ then velocities at 0 are given by

$$v = -\frac{\xi \Delta y \Delta z}{2\pi} \cdot \frac{z}{(z^2 + y^2)} \qquad \text{(A4)}$$

and

$$w = \frac{\xi \Delta y \Delta z}{2\pi} \cdot \frac{y}{(z^2 + y^2)} \qquad \text{(A5)}$$

Intermediate field

A line of vorticity, strength γ ft/sec, is employed extending from $(-\Delta y/z, z)$ to $(+\Delta y/z, z)$, where

$$\gamma \Delta y \quad \xi \Delta y \Delta z$$

$$\text{giving } \gamma = \xi \Delta z$$

We obtain velocities by integrating from $-\Delta y/z$ to $+\Delta y/z$:

$$v = \int_{-\Delta y/z}^{\Delta y/z} \frac{-\gamma}{2\pi} \cdot \frac{z}{(z^2 + y^2)} \cdot dy$$

which results in

$$v = -\frac{\xi \Delta y}{2\pi} \frac{1}{2}\left[\text{Log}_e \frac{A^2 + 1}{B^2 + 1} + A \tan^{-1} \frac{1}{A} - B \tan^{-1} \frac{1}{B}\right] \qquad \text{(A6)}$$

where $A = (2z + \Delta z)/\Delta y$ and $B = (2z - \Delta z)/\Delta y$

Consideration of symmetry for cells in the intermediate field (Figure A1) reveals that

$$w = 0 \qquad \text{(A7)}$$

APPENDIX III

Introduction

The 5-holed probe data reduction programs reduce the pressures, measured by the 5-holed probe, to a plot file consisting of the survey ordinates, the three components of velocity and the total and static pressures. The machine plots included in this report, with the exception of the corrected velocity components and the stream functions, were generated from the plot file.

The rake analysis program, listed subsequently, takes the plot file (TAPE09) and in conjunction with some keyboard entries (TAPE05), described below, generates a new plot file (TAPE10) together with a tabulation of the integrations of the vorticity, vorticity/stream junction product and total pressure plots.

The input plot file (TAPE09) is the data that has been supplied to Georgia Tech on magnetic tape. The output file (TAPE10) was used to generate the additional machine plots, corrected velocities and stream junctions. The line printer tabulations are self-explanatory.

Keyboard Entries (TAPE05)

The keyboard entries are as follows:

Line (1):	NWING, LCDØ, NMS	(3I5)
Line (2):	WTY , WTZ , PGOMIN, PGTMIN	(4F8)
Line (3):	S , CBAR, SPAN	(3F8)
Line (4):	TITLE	(20A4)
Line (5):	NHOPT, NWOPT, NFOPT	(3I5)

The program will accept the following types of survey, designated 0 thru 3 (the value of NWING).

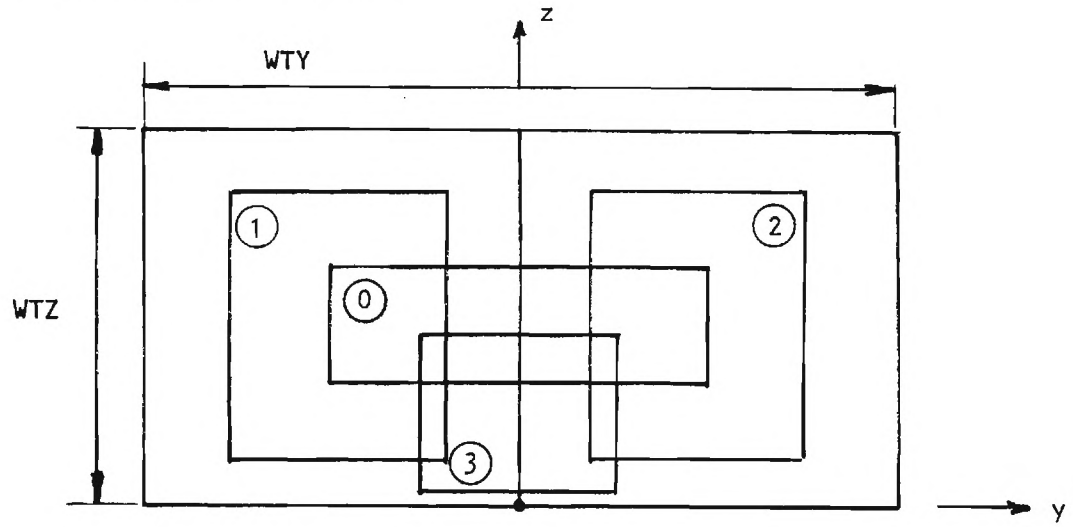

As these surveys are referenced to the probe, not tunnel, axes it can be seen from Figure 4.2 that a NWING = 2 value is required for these tests where the tunnel dimensions WTY and WTZ are 60.0 and 43.0 respectively.

The integration of the profile drag require an extrapolation of the total pressure data to the axis of symmetry. The extrapolation is based on the y-ordinate number LCDØ. This permits the exclusion of any data in the boundary layer if the axis of symmetry is a hard surface (which is the case in these tests - see machine plots MP5, MP15, etc.).

MNS is the number of data points to be omitted in the z direction. A value of '1' would result in every other data point being used, a value of '2' would result in every 3rd point being used. This permits the effect of grid aspect ratio to be determined. A value of zero was used in the supplied data.

The value PGØMIN and PGTMIN allow for filtering of the data in the induced drag integration. This option is no longer used and value of zero inserted.

Line (3) supplies the reference area, mean chord and semi-span (units of feet) and line (4) is an arbitrary title for the line printer output.

Line (5) controls the input of pressure data (NHOPT = 0), the elimination of tunnel induced velocities, described in Section 4.3 (NWOPT $\neq$ 0 to inhibit routine), and the filtering of the induced drag data (make NFOPT $\neq$ 1 to inhibit the routine).

```
C  ANALYSIS OF SURVEY WITH 5-HOLED MULTI-PROBED RAKE
C
C  READ SURVEY INPUT FROM DISC FILE (TAPE9)
C  WRITE SURVEY OUTPUT TO DISC FILE (TAPE10)
C-----------------------------------------------------------------------
C
      COMMON NWING,NWOPT,IEC,NEC,DELZ,DELY,ZG(50),YG(54),V(50,54),
     *       W(50,54),GAM(50,54),PSI(50,54),GPSI(50,54),HTOT(50,54)
      COMMON/COEFF/ S,CBAR,SPAN,WTZ2,CDI,CMI,CNI
      DIMENSION TITLE(20),Z(50),Y(54),T1(9),T2(9),T3(2),T4(3)
      DATA T1/4HI---,3*4H----,4H-I--,3*4H----,4H--I /
      DATA T2/4HI   ,3*4H    ,4H I  ,3*4H    ,4H  I /
      DATA T3/4HXX X,4HX   /
      DATA T4/3*4HXXXX/
C
C  CONTROL CARDS AND SURVEY INPUT
C-----------------------------------------------------------------------
      READ(5,220) NWING,LCDO,NMS
      READ(5,230) WTY,WTZ,PSOMIN,PGTMIN
      READ(5,230) S,CBAR,SPAN
      READ(5,240) TITLE
      READ(5,220) NHOPT,NWOPT,NFOPT
      WTY=WTY/2.
      WTZ2=WTZ/2.
      IF(NWING.EQ.3) WTZ2=0
      NM=NMS+1
C
      READ(9,220) NEND,IENN
      READ(9,230) (Z(I),I=1,IENN)
      READ(9,230) (Y(N),N=1,NEND)
      IEND=(IENN-1)/NM+1
      I=0
      DO 10 J=1,IENN,NM
      I=I+1
   10 Z(I)=Z(J)
      DO 20 K=1,2
      READ(9,230) (V(1,N),N=1,NEND)
      DO 20 I=2,IEND
      DO 20 J=1,NM
   20 READ(9,230) (V(I,N),N=1,NEND)
      READ(9,230) (W(1,N),N=1,NEND)
      DO 30 I=2,IEND
      DO 30 J=1,NM
   30 READ(9,230) (W(I,N),N=1,NEND)
C
C  REDEFINE GRID
C  SURVEY AREA REDUCED BY ONE HALF MESH ON ALL SIDES
C-----------------------------------------------------------------------
   35 YMIN=Y(1)
      YMAX=Y(NEND)
      ZMIN=Z(1)
      ZMAX=Z(IEND)
      IEC=IEND-1
      NEC=NEND-1
      DELZ=Z(2)-Z(1)
      DELY=Y(2)-Y(1)
      DO 40 I=1,IEC
   40 ZG(I)=Z(I)+DELZ/2.
      DO 50 N=1,NEC
   50 YG(N)=Y(N)+DELY/2.
      WRITE(10,220) NEC,IEC
      WRITE(10,230) (ZG(I),I=1,IEC)
      WRITE(10,230) (YG(N),N=1,NEC)
```

```
      IF(ZG(1).GT.Ø.) GO TO 6Ø
      DO 55 I=1,IEC
   55 ZG(I)=ZG(I)+WTZ2
      ZMIN=ZMIN+WTZ2
      ZMAX=ZMAX+WTZ2
C
C  CALCULATION OF CIRCULATION MATRIX
C-----------------------------------------------------------------------
   6Ø DO 65 N=1,NEC
      DO 65 I=1,IEC
      VT=DELY*((V(I+1,N)+V(I+1,N+1))-(V(I,N)+V(I,N+1)))*.5
      WT=DELZ*((W(I+1,N)+W(I,N))-(W(I+1,N+1)+W(I,N+1)))*.5
   65 GAM(I,N)=(VT+WT)/12.
C
C  CALCULATION OF NEW VELOCITIES AND (OPTIONAL) WALL EFFECTS
C-----------------------------------------------------------------------
      CALL WALL(Ø,WTY,WTZ)
      CALL VCAL
      CALL WALL(1,WTY,WTZ)
      DO 7Ø I=1,IEC
   7Ø WRITE(1Ø,25Ø) (V(I,N),N=1,NEC)
      DO 75 I=1,IEC
   75 WRITE(1Ø,25Ø) (W(I,N),N=1,NEC)
C
C  CALCULATION OF STREAM FUNCTIONS MATRICES
C-----------------------------------------------------------------------
      ICEN=IEC/2+1
      NCEN=NEC/2+1
      SUMNL=Ø.
      SUMNR=Ø.
      DO 1ØØ N=1,NCEN
      NL=NCEN-N+1
      NR=NCEN+N-1
      IF(N.EQ.1) GO TO 8Ø
      SUMNL=SUMNL-DELY*(W(ICEN,NL)+W(ICEN,NL+1))/2.
      IF(NR.GT.NEC) GO TO 8Ø
      SUMNR=SUMNR+DELY*(W(ICEN,NR-1)+W(ICEN,NR))/2.
   8Ø SUMIBL=Ø.
      SUMITL=Ø.
      SUMIBR=Ø.
      SUMITR=Ø.
      VBL=V(ICEN,NL)
      VTL=VBL
      VBR=V(ICEN,NR)
      VTR=VBR
      DO 1ØØ I=1,ICEN
      IB=ICEN-I+1
      IT=ICEN+I-1
      IF(I.EQ.1) GO TO 9Ø
      SUMIBL=SUMIBL+DELZ*(V(IB,NL)+VBL)/2.
      SUMIBR=SUMIBR+DELZ*(V(IB,NR)+VBR)/2.
      VBL=V(IB,NL)
      VBR=V(IB,NR)
      IF(IT.GT.IEC) GO TO 9Ø
      SUMITL=SUMITL-DELZ*(VTL+V(IT,NL))/2.
      SUMITR=SUMITR-DELZ*(VTR+V(IT,NR))/2.
      VTL=V(IT,NL)
      VTR=V(IT,NR)
   9Ø PSI(IB,NL)=(SUMNL+SUMIBL)
      IF(IT.GT.IEC) GO TO 95
      PSI(IT,NL)=(SUMNL+SUMITL)
   95 IF(NR.GT.NEC) GO TO 1ØØ
      PSI(IB,NR)=(SUMNR+SUMIBR)
      IF(IT.GT.IEC) GO TO 1ØØ
```

```
      PSI(IT,NR)=(SUMNR+SUM)TR)
  100 CONTINUE
C
      IF((NWING.EQ.1).OR.(NWING.EQ.2)) CALL PSIZC(ICEN,PSIO)
      IF((NWING.EQ.0).OR.(NWING.EQ.3)) CALL PSIZW(NCEN,PSIO,WTY)
      DO 110 I=1,IEC
      DO 110 N=1,NEC
  110 PSI(I,N)=(PSI(I,N)-PSIO)/12.
      DO 120 I=1,IEC
  120 WRITE(10,250) (PSI(I,N),N=1,NEC)
C
C  CALCULATION OF PSI*GAM AND FILTERING
C-----------------------------------------------------------------------
      PGMAX=0.
      DO 130 N=1,NEC
      DO 130 I=1,IEC
      GPSI(I,N)=GAM(I,N)*PSI(I,N)
      IF(GPSI(I,N).LT.PGMAX) GO TO 130
      PGMAX=GPSI(I,N)
      YF=YG(N)
      ZF=ZG(I)
  130 CONTINUE
      IF(NFOPT.NE.0) GO TO 160
C
      DO 150 N=1,NEC
      X=(YF-YG(N))**2
      DO 150 I=1,IEC
      IF(NWING.NE.3) X=(ZF-ZG(N))**2
      IF(GPSI(I,N).LT.PGOMIN) GO TO 140
      IF(ABS(X).LT.0.01) GO TO 150
      PGOM=GPSI(I,N)/X
      IF(PGOM.GT.PGTMIN) GO TO 150
  140 GAM(I,N)=0.
      GPSI(I,N)=0.
  150 CONTINUE
C
  160 DO 170 I=1,IEC
  170 WRITE(10,250) (GPSI(I,N),N=1,NEC)
C
C  OUTPUT OF COEFFICIENTS
C-----------------------------------------------------------------------
      WRITE(6,260) TITLE
      WRITE(6,270)
      WRITE(6,280) T1
      DO 175 I=1,13
      WRITE(6,280) T2
      IF(I.LT.6) GO TO 175
      IF(NWING.EQ.3) WRITE(6,290) T3
      IF((NWING.EQ.3).OR.(I.GT.8)) GO TO 175
      IF(NWING.LT.2) WRITE(6,300) T4
      IF((NWING.EQ.0).OR.(NWING.EQ.2)) WRITE(6,310) T4
  175 CONTINUE
      WRITE(6,280) T1
      IF(NWOPT.EQ.0) WRITE(6,320)
      IF(NFOPT.EQ.0) WRITE(6,330)
      IF(NMS  .NE.0) WRITE(6,340)
      WRITE(6,350)
      WRITE(6,360) YMIN,YMAX,ZMIN,ZMAX,S
      YMIN=-WTY
      ZMIN=0.
      WRITE(6,370) YMIN,WTY,ZMIN,WTZ
      CALL LIFT
      CALL DRAGI
      IF(NHOPT.NE.0) STOP
```

```
C
C   PROFILE DRAG
C   ARRAYS V AND W ARE USED FOR TOTAL AND STATIC PRESSURES
C-----------------------------------------------------------------------
      READ(9,230) (V(I,N),N=1,NEND)
      DO 180 I=2,IEND
      DO 180 J=1,NM
  180 READ(9,230) (V(I,N),N=1,NEND)
      READ(9,230) (W(I,N),N=1,NEND)
      DO 190 I=2,IEND
      DO 190 J=1,NM
  190 READ(9,230) (W(I,N),N=1,NEND)
C
      DO 200 I=1,IEC
      DO 200 N=1,NEC
      HT=(V(I,N)+V(I+1,N)+V(I,N+1)+V(I+1,N+1))/4.
      HS=(W(I,N)+W(I+1,N)+W(I,N+1)+W(I+1,N+1))/4.
  200 HTOT(I,N)=HT+HS
      DO 210 I=1,IEC
  210 WRITE(10,250) (HTOT(I,N),N=1,NEC)
      CALL DRAGO(LCDO)
      STOP
C
C-----------------------------------------------------------------------
  220 FORMAT(4I5)
  230 FORMAT(10F8.2)
  240 FORMAT(20A4)
  250 FORMAT(6E12.4)
  260 FORMAT(1H1//4X,'5-HOLED MULTI-PROBE RAKE SURVEY ANALYSIS'
     1       /4X,20A4)
  270 FORMAT(/)
  280 FORMAT(4X,9A4)
  290 FORMAT(1H+,18X,2A4)
  300 FORMAT(1H+,  8X,3A4)
  310 FORMAT(1H+,21X,3A4)
  320 FORMAT(/4X,'WALL CORRECTIONS APPLIED')
  330 FORMAT(4X,'CIRCULATION FILTERING APPLIED')
  340 FORMAT(4X,'REDUCED GRID POINTS IN Z DIRECTION')
  350 FORMAT(//5X,'SURVEY AND TUNNEL GEOMETRY'//8X,'PARAMETER      ',
     1       'YMIN     YMAX     ZMIN     ZMAX     SREF')
  360 FORMAT(8X,'SURVEY     ',4F8.2,F8.4)
  370 FORMAT(8X,'TUNNEL     ',4F8.2,F8.4)
      END
```

```
C  RE-CALCULATION OF THE VELOCITIES
C-----------------------------------------------------------------------
C
      SUBROUTINE VCAL
      COMMON NWING,NWOPT,IEC,NEC,DELZ,DELY,ZG(5Ø),YG(54),V(5Ø,54),
     *       W(5Ø,54),GAM(5Ø,54),PSI(5Ø,54),GPSI(5Ø,54),HTOT(5Ø,54)
      DIMENSION T1(15),T2(15),GB(9)
C
C  SET UP OF WABBAH AND UNIFORM VORTEX CONSTANTS
C-----------------------------------------------------------------------
      TERM1=(2.*3.14159)/12.
      TERM2=TERM1*DELY*DELZ
      ZOY=DELZ/DELY
      YOZ=DELY/DELZ
      IC=1.5/ZOY
      TS=ATAN(ZOY)
      FØ1=TS
      FØ2=1.57Ø796-TS
      F11=ALOG(SIN(FØ1))
      F12=ALOG(SIN(FØ2))
      F21=YOZ-FØ2
      F22=YOZ-FØ1
      DO 2 I=1,IC
      ZT=I*DELZ
      T1(I)=TERM1*(DELY*DELY+ZT*ZT)
      A=(2*I+1)*ZOY
      B=(2*I-1)*ZOY
    2 T2(I)=DELY*(Ø.5*ALOG((A*A+1.)/(B*B+1.))+A*ATAN(1./A)
     *       -B*ATAN(1./B))/TERM2
C
C  MAIN LOOP FOR TOTAL SURVEY
C-----------------------------------------------------------------------
      DO 14Ø N=1,NEC
      NL=N-1
      NH=N+1
      DO 14Ø I=1,IEC
      IL=I-IC
      IH=I+IC
C
C  VELOCITY SUMMATION BEYOND THE LOCAL AREA
C-----------------------------------------------------------------------
      VNL=Ø.
      WNL=Ø.
      DO 15 NN=1,NEC
      IF(NWING.EQ.1.AND.YG(NN).GT.Ø.Ø5) GO TO 14Ø
      IF(NWING.EQ.2.AND.YG(NN).LT.-Ø.Ø5) GO TO 14Ø
      K=Ø
      IF(NN.GE.NL.AND.NN.LE.NH) K=1
      YN1=YG(NN)-YG(N)
      YN2=-(YG(NN)+YG(N))
      IF(NWING.EQ.3) YN2=YN1
      DO 1Ø II=1,IEC
      ZN1=ZG(II)-ZG(I)
      ZN2=-(ZG(II)+ZG(I))
      IF(NWING.NE.3) ZN2=ZN1
      IF(NWING.EQ.Ø) GO TO 5
      RNLS=YN2**2+ZN2**2
      TERM3=GAM(II,NN)/(TERM1*RNLS)
      VNL=VNL+TERM3*ZN2
      WNL=WNL-TERM3*YN2
    5 IF(II.GE.IL.AND.II.LE.IH.AND.K.EQ.1) GO TO 1Ø
      RNLS=YN1**2+ZN1**2
```

```
      TERM3=GAM(II,NN)/(TERM1*RNLS)
      VNL=VNL-TERM3*ZN1
      WNL=WNL+TERM3*YN1
   1Ø  CONTINUE
   15  CONTINUE
C
C  VELOCITY SUMMATION WITHIN LOCAL AREA
C-----------------------------------------------------------------------
      DO 11Ø J=1,8
      GO TO (2Ø,3Ø,4Ø,5Ø,6Ø,7Ø,8Ø,9Ø),J
   2Ø  IF(N.EQ.NEC) GO TO 1ØØ
      GB(J)=GAM(I  ,N+1)
      GO TO 11Ø
   3Ø  IF(I.EQ.IEC.OR.N.EQ.NEC) GO TO 1ØØ
      GB(J)=GAM(I+1,N+1)
      GO TO 11Ø
   4Ø  IF(I.EQ.IEC) GO TO 1ØØ
      GB(J)=GAM(I+1,N  )
      GO TO 11Ø
   5Ø  IF(I.EQ.IEC.OR.N.EQ.1) GO TO 1ØØ
      GB(J)=GAM(I+1,N-1)
      GO TO 11Ø
   6Ø  IF(N.EQ.1) GO TO 1ØØ
      GB(J)=GAM(I  ,N-1)
      GO TO 11Ø
   7Ø  IF(I.EQ.1.OR.N.EQ.1) GO TO 1ØØ
      GB(J)=GAM(I-1,N-1)
      GO TO 11Ø
   8Ø  IF(I.EQ.1) GO TO 1ØØ
      GB(J)=GAM(I-1,N  )
      GO TO 11Ø
   9Ø  IF(I.EQ.1.OR.N.EQ.NEC) GO TO 1ØØ
      GB(J)=GAM(I-1,N+1)
      GO TO 11Ø
  1ØØ  GB(J)=Ø.
  11Ø  CONTINUE
      TERM3=2.*TERM2
      DV=-DELZ*((F22*YOZ*YOZ-F11*ZOY)*(GB(2)+GB(4)-GB(6)-GB(8))
     *          +2.*(F11*ZOY+FØ2)*(GB(3)-GB(7)))/TERM3
      DW= DELY*((F21*ZOY*ZOY-F12*YOZ)*(GB(2)-GB(4)-GB(6)+GB(8))
     *          +2.*(F12*YOZ+FØ1)*(GB(1)-GB(5)))/TERM3
      V(I,N)=VNL+2.25*DV
      W(I,N)=WNL+2.25*DW
C
C  VELOCITY SUMMATION IN INTERMEDIATE AREA (NON-SQUARE GRIDS)
C-----------------------------------------------------------------------
      IF(IC.EQ.1) GO TO 14Ø
      VNL=Ø.
      WNL=Ø.
      DO 13Ø J=2,IC
      IL=I-J
      IH=I+J
      ZT=J*DELZ
      IF(IL.LT.1) GO TO 12Ø
      IF(N.EQ.1) GO TO 115
      TERM3=GAM(IL,N-1)/T1(J)
      VNL=VNL+TERM3*ZT
      WNL=WNL-TERM3*DELY
  115 VNL=VNL+GAM(IL,N)*T2(J)
      IF(N.EQ.NEC) GO TO 12Ø
      TERM3=GAM(IL,N+1)/T1(J)
      VNL=VNL-TERM3*ZT
      WNL=WNL-TERM3*DELY
  12Ø  IF(IH.GT.IEC) GO TO 13Ø
```

```
      IF(N.EQ.1) GO TO 125
      TERM3=GAM(IH,N-1)/T1(J)
      VNL=VNL-TERM3*ZT
      WNL=WNL-TERM3*DELY
125   VNL=VNL-GAM(IH,N)*T2(J)
      IF(N.EQ.NEC) GO TO 130
      TERM3=GAM(IH,N+1)/T1(J)
      VNL=VNL-TERM3*ZT
      WNL=WNL+TERM3*DELY
130   CONTINUE
      V(I,N)=V(I,N)+VNL
      W(I,N)=W(I,N)+WNL
140   CONTINUE
      RETURN
      END
```

```
C  RECTANGULAR TUNNEL - WALL CORRECTION
C-----------------------------------------------------------------------
C
      SUBROUTINE WALL(K,WTY,WTZ)
      COMMON NWING,NWOPT,IEC,NEC,DELZ,DELY,ZG(50),YG(54),V(50,54),
     *       W(50,54),GAM(50,54),PSI(50,54),GP I(50,54),HTOT(50,54)
      DIMENSION YV(56),YC(56),ZV(56),ZC(56),VW(56),GAMW(56),
     *     CONST(56,56)
C
      IF(K.EQ.2) GO TO 300
      IF(NWOPT.NE.0) RETURN
      IF(K.EQ.1) GO TO 200
      TERM=12./(2.*3.14159)
C
C  VORTICITY INTEGERS
C-----------------------------------------------------------------------
      IF(NWING.EQ.3) GO TO 10
      N1=7
      N2=14
      N3=41
      N7=15
      N8=35
      WTZO=0.
      GO TO 20
   10 N1=21
      N2=36
      N3=29
      N7=9
      N8=37
      WTZO=-WTZ
   20 N4=N2+1
      N5=N2+12
      N6=N1+N2
      N9=N2+13
      DWTY=WTY/6.
      DWTZ=WTZ/8.
C
C  CALCULATION OF ORDINATES AND VELOCITIES
C-----------------------------------------------------------------------
      DO 50 I=N1,N2
      YC(I)=WTY
      YV(I)=WTY
      ZC(I)=WTZ-DWTZ*(I-N1)
      ZV(I)=ZC(I)-DWTZ/2.
      IF(I.GT.28) GO TO 30
      CALL SURV(YV(I),ZV(I),VW(I),WNL)
   30 IS=N3-I
      IF(IS.LE.0) IS=85-I
      YC(IS)=-WTY
      YV(IS)=-WTY
      ZC(IS)=ZC(I)-DWTZ
      ZV(IS)=ZV(I)
      VW(IS)=-VW(I)
      IF(NWING.EQ.1.OR.NWING.EQ.2) GO TO 50
      IF(I.GT.28) GO TO 40
      CALL SURV(YV(IS),ZV(IS),VW(IS),WNL)
      GO TO 50
   40 II=57-I
      VW(I)=VW(II)
      II=57-IS
      VW(IS)=VW(II)
   50 CONTINUE
```

```
      DO 100 I=N4,N5
      YC(I)=WTY-DWTY*(I-N4)
      YV(I)=YC(I)-DWTY/2.
      ZC(I)=WTZO
      ZV(I)=WTZO
      IF(I.LT.21) GO TO 60
      IF(NWING.EQ.0.OR.NWING.EQ.3) GO TO 60
      II=41-I
      VW(I)=VW(II)
      GO TO 70
   60 CALL SURV(YV(I),ZV(I),VNL,VW(I))
   70 IS=N6-I
      IF(IS.LE.0) IS=61-I
      YC(IS)=YC(I)-DWTY
      YV(IS)=YV(I)
      ZC(IS)=WTZ
      ZV(IS)=WTZ
      IF(NWING.EQ.3) GO TO 90
      IF(NWING.EQ.0.OR.I.LT.21) GO TO 80
      II=41-IS
      VW(IS)=VW(II)
      GO TO 100
   80 CALL SURV(YV(IS),ZV(IS),VNL,VW(IS))
      GO TO 100
   90 VW(IS)=-VW(I)
  100 CONTINUE
C
C  GENERATION OF THE CIRCULATIONS
C-------------------------------------------------------------------------
      NW=NWING/3
      J=1-NW
      NM=40+16*NW
      DO 110 N=1,NM
      IF(N.EQ.N7.OR.N.EQ.N8) J=1
      IF(N.EQ.N1.OR.N.EQ.N9) J=0
      DO 110 M=1,NM
      RS=(YC(M)-YV(N))**2+(ZC(M)-ZV(N))**2
      DEL=ZV(N)-ZC(M)
      IF(J.EQ.1) DEL=YC(M)-YV(N)
  110 CONST(N,M)=DEL*TERM/RS
      NS=1
      IF(NWING.EQ.0) GO TO 130
      NS=2
      KKO=NM+2
      NM=NM/2
      GAMW(1)=0.
      DO 120 N=1,NM
      DO 120 M=2,NM
      KK=KKO-M
  120 CONST(N,M)=CONST(N,M)-CONST(N,KK)
  130 CALL GJRV(CONST,NM,56,.1E-10,IERR)
      GAMW(NM+1)=0.
      DO 150 N=NS,NM
      GAMW(N)=0.
      DO 140 M=1,NM
  140 GAMW(N)=GAMW(N)-VW(M)*CONST(N,M)
      IF(NWING.EQ.0) GO TO 150
      KKN=KKO-N
      GAMW(KKN)=-GAMW(N)
  150 CONTINUE
      IF(NWING.NE.0) NM=NM*2
      RETURN
C
C  CALCULATION OF WALL INDUCED VELOCITIES
```

```
C-----------------------------------------------------------------------
 200   DO 210 I=1,IEC
       DO 210 N=1,NEC
       DO 210 M=1,NM
       RS=(YC(M)-YG(N))**2+(ZC(M)-ZG(I))**2
       TERMB=GAMW(M)*TERM/RS
       V(I,N)=V(I,N)+(ZG(I)-ZC(M))*TERMB
 210   W(I,N)=W(I,N)-(YG(N)-YC(M))*TERMB
       RETURN
C
C   INCREMENTS BEYOND SURVEY AREA
C-----------------------------------------------------------------------
 300   VNL=0.
       WNL=0.
       IF(NWOPT.NE.0) GO TO 320
       DO 310 M=1,NM
       RS=(YC(M)-WTY)**2+(ZC(M)-WTZ)**2
       TERMB=GAMW(M)*TERM/RS
       VNL=VNL+(WTZ-ZC(M))*TERMB
 310   WNL=WNL-(WTY-YC(M))*TERMB
 320   WTY=VNL
       WTZ=WNL
       RETURN
       END
```

```
C  VELOCITIES DUE TO DISTRIBUTION OF CIRCULATION
C-----------------------------------------------------------------------
C
      SUBROUTINE SURV(YWW,ZWW,VNL,WNL)
      COMMON NWING,NWOPT,IEC,NEC,DELZ,DELY,ZG(50),YG(54),V(50,54),
     *       W(50,54),GAM(50,54),PSI(50,54),GPSI(50,54),HTOT(50,54)
C
      TERMA=12./(2.*3.14159)
      IF(NWING.EQ.0) TERMC=0.
      VNL=0.
      WNL=0.
      DO 20 NN=1,NEC
      IF(NWING.EQ.1.AND.YG(NN).GT.0.05) RETURN
      IF(NWING.EQ.2.AND.YG(NN).LT.-0.05) GO TO 20
      DY1=YG(NN)-YWW
      DY2=-(YG(NN)+YWW)
      IF(NWING.EQ.3) DY2=DY1
      DO 10 II=1,IEC
      DZ1=ZG(II)-ZWW
      DZ2=-(ZG(II)+ZWW)
      IF(NWING.NE.3) DZ2=DZ1
      TERMB=GAM(II,NN)*TERMA/(DY1**2+DZ1**2)
      IF(NWING.NE.0) TERMC=GAM(II,NN)*TERMA/(DY2**2+DZ2**2)
      VNL=VNL-TERMB*DZ1+TERMC*DZ2
   10 WNL=WNL+TERMB*DY1-TERMC*DY2
   20 CONTINUE
      RETURN
      END
```

```
C  MATRIX INVERSION ROUTINE
C
C  A IS THE INPUT ARRAY WHICH WILL BE DESTROYED, N IS THE RANK
C  OF A, NL IS THE ROW DIMENSION OF A, EPSIL IS THE TEST
C  VALUE FOR THE PIVOT POINT SINGULARITY CHECK,
C  IERR IS NONZERO IF THE MATRIX IS SINGULAR
C  IF THE MATRIX IS NONSINGULAR, A CONTAINS A-INVERSE
C-----------------------------------------------------------------------
      SUBROUTINE GJRV(A,N,NL,EPSIL,IERR)
      DIMENSION A(1),B(96),C(96),IP(96),IQ(96)
      IERR=0
      DO 160 K=1,N
      PIVOT=0.
C
C  GET LARGEST ELEMENT IN MATRIX  PLACE IN PIVOT
C-----------------------------------------------------------------------
      DO 30 I=K,N
      DO 20 J=K,N
      IDEX=(J-1)*NL+I
      IF (ABS(A(IDEX))-ABS(PIVOT)) 20,20,10
   10 CONTINUE
      PIVOT=A(IDEX)
      IP(K)=I
      IQ(K)=J
   20 CONTINUE
   30 CONTINUE
      IF (ABS(PIVOT)-EPSIL) 230,230,40
   40 CONTINUE
      IF (IP(K)-K) 50,70,50
   50 CONTINUE
C
C  SWAP ROWS
C-----------------------------------------------------------------------
      DO 60 J=1,N
      IPX=IP(K)
      IDEX=(J-1)*NL+IPX
      KDEX=(J-1)*NL+K
      Z=A(IDEX)
      A(IDEX)=A(KDEX)
      A(KDEX)=Z
   60 CONTINUE
   70 CONTINUE
      IF (IQ(K)-K) 80,100,80
   80 CONTINUE
C
C  SWAP COLUMNS
C-----------------------------------------------------------------------
      DO 90 I=1,N
      IPX=IQ(K)
      IDEX=(IPX-1)*NL+I
      KDEX=(K-1)*NL+I
      Z=A(IDEX)
      A(IDEX)=A(KDEX)
      A(KDEX)=Z
   90 CONTINUE
  100 CONTINUE
      DO 140 J=1,N
      KDEX=(J-1)*NL+K
      JDEX=(K-1)*NL+J
      IF (J-K) 120,110,120
  110 CONTINUE
      B(J)=1./PIVOT
```

```
      C(J)=1.
      GO TO 130
  120 CONTINUE
      B(J)=-A(KDEX)/PIVOT
      C(J)=A(JDEX)
  130 CONTINUE
      A(KDEX)=0.
      A(JDEX)=0.
  140 CONTINUE
      DO 150 I=1,N
      DO 150 J=1,N
      IDEX=(J-1)*NL+I
      A(IDEX)=A(IDEX)+C(I)*B(J)
  150 CONTINUE
  160 CONTINUE
      DO 220 KP=1,N
      K=N+1-KP
      IF (IP(K)-K) 170,190,170
  170 CONTINUE
      DO 180 I=1,N
      IPX=IP(K)
      IDEX=(IPX-1)*NL+I
      KDEX=(K-1)*NL+I
      Z=A(IDEX)
      A(IDEX)=A(KDEX)
      A(KDEX)=Z
  180 CONTINUE
  190 CONTINUE
      IF (IQ(K)-K) 200,220,200
  200 CONTINUE
      DO 210 J=1,N
      IPX=IQ(K)
      IDEX=(J-1)*NL+IPX
      KDEX=(J-1)*NL+K
      Z=A(IDEX)
      A(IDEX)=A(KDEX)
      A(KDEX)=Z
  210 CONTINUE
  220 CONTINUE
      GO TO 240
  230 CONTINUE
      IERR=-1
  240 CONTINUE
      RETURN
      END
```

```
C  STREAM FUNCTION ORIGIN TO CENTERLINE
C-----------------------------------------------------------------------
C
      SUBROUTINE PSIZC(ICEN,PSIO)
      COMMON NWING,NWOPT,IEC,NEC,DELZ,DELY,ZG(50),YG(54),V(50,54),
     *       W(50,54),GAM(50,54),PSI(50,54),GPSI(50,54),HTOT(50,54)
      TERM=(2.*3.14159)/12.
      ZN=ZG(ICEN)
      IF(NWING.EQ.2) GO TO 10
      YN=YG(NEC)
      DY=-DELY
      WNL=W(ICEN,NEC)
      PSIO=PSI(ICEN,NEC)
      IF(YN.LT.0.) GO TO 50
      GO TO 20
   10 YN=YG(1)
      DY=DELY
      WNL=W(ICEN,1)
      PSIO=PSI(ICEN,1)
      IF(YN.GT.0.) GO TO 50
   20 DO 30 N=2,NEC
      IF(YG(N).GT.0.) GO TO 40
   30 CONTINUE
   40 PSIO=PSI(ICEN,N)+(PSI(ICEN,N)-PSI(ICEN,N-1))*YG(N)/DELY
      RETURN
C
   50 KK=ABS(YN/DELY)+1
      DO 70 K=1,KK
      AYN=ABS(YN/DELY)
      IF(AYN.LT.0.01) RETURN
      YN=YN-DY
      WN=WNL
      WNL=0.
      DO 60 N=1,NEC
      YN1=YN-YG(N)
      YN2=YN+YG(N)
      DO 60 I=1,IEC
      ZN1=ZN-ZG(I)
      ZN2=ZN1
      RNS1=YN1*YN1+ZN1*ZN1
      RNS2=YN2*YN2+ZN2*ZN2
      RNT=YN2/RNS2-YN1/RNS1
   60 WNL=WNL+GAM(I,N)*RNT/TERM
      YNT=YN
      ZNT=ZN
      CALL WALL(2,YNT,ZNT)
      WNL=WNL+ZNT
      DPSI=-DY*(WNL+WN)/2.
   70 PSIO=PSIO+DPSI
C
      PSIO=PSIO-DPSI*AYN
      RETURN
      END
```

```
C  STREAM FUNCTION ORIGIN TO WALL
C-----------------------------------------------------------------------
C
      SUBROUTINE PSIZW(NCEN,PSIO,WTY)
      COMMON NWING,NWOPT,IEC,NEC,DELZ,DELY,ZG(50),YG(54),V(50,54),
     *       W(50,54),GAM(50,54),PSI(50,54),GPSI(50,54),HTOT(50,54)
C
      TERM=(2.*3.14159)/12.
      YN=YG(NCEN)
      IF(NWING.EQ.3) GO TO 20
      DW=WTY/6.
      YW=WTY+DW/2.
   10 YW=YW-DW
      IF(YW.GT.YN) GO TO 10
      NY=(YN-YW)/DELY
      NCEN=NCEN-NY
      YN=YG(NCEN)
   20 ZN=ZG(1)
      VNL=V(1,NCEN)
      PSIO=PSI(1,NCEN)
C
   30 ZN=ZN-DELZ
      VN=VNL
      VNL=0.
      DO 40 N=1,NEC
      YN1=YN-YG(N)
      YN2=YN1
      DO 40 I=1,IEC
      ZN1=ZN-ZG(I)
      ZN2=ZN+ZG(I)
      RNS1=YN1*YN1+ZN1*ZN1
      RNS2=YN2*YN2+ZN2*ZN2
      RNT=ZN1/RNS1
      IF(NWING.EQ.0) GO TO 40
      RNT=RNT-ZN2/RNS2
   40 VNL=VNL+GAM(I,N)*RNT/TERM
      YNT=YN
      ZNT=ZN
      CALL WALL(2,YNT,ZNT)
      VNL=VNL+YNT
      DPSI=DELZ*(VNL+VN)/2.
      PSIO=PSIO+DPSI
      AZN=ZN/DELZ
      IF(AZN.GT.0.01) GO TO 30
C
      PSIO=PSIO+DPSI*AZN
      RETURN
      END
```

```
C  LIFT INTEGRATION
C-----------------------------------------------------------------------
C
      SUBROUTINE LIFT
      COMMON NWING,NWOPT,IEC,NEC,DELZ,DELY,ZG(50),YG(54),V(50,54),
     *       W(50,54),GAM(50,54),PSI(50,54),GPSI(50,54),HTOT(50,54)
      COMMON/COEFF/ S,CBAR,SPAN,WTZ2,CDI,CMI,CNI
C
C  CIRCULATION SUMMATION AND CENTER OF GRAVITY
C-----------------------------------------------------------------------
      CIR1=0.
      CIR2=0.
      CIRY1=0.
      CIRY2=0.
      CIRZ1=0.
      CIRZ2=0.
      CIYZ1=0.
      CIYZ2=0.
      DO 20 N=1,NEC
      IF(YG(N).GT.0.0) GO TO 30
      IF(NWING.EQ.2) GO TO 20
      DO 10 I=1,IEC
      CIR1=CIR1+GAM(I,N)
      CIRY1=CIRY1+GAM(I,N)*YG(N)
      CIRZ1=CIRZ1+GAM(I,N)*(ZG(I)-WTZ2)
   10 CIYZ1=CIYZ1+GAM(I,N)*(YG(N)**2+(ZG(I)-WTZ2)**2)
   20 CONTINUE
      GO TO 50
   30 NS=N
      IF(NWING.EQ.1) GO TO 50
      DO 40 N=NS,NEC
      DO 40 I=1,IEC
      CIR2=CIR2+GAM(I,N)
      CIRY2=CIRY2+GAM(I,N)*YG(N)
      CIRZ2=CIRZ2+GAM(I,N)*(ZG(I)-WTZ2)
   40 CIYZ2=CIYZ2+GAM(I,N)*(YG(N)**2+(ZG(I)-WTZ2)**2)
C
C  LIFT COMPUTATIONS
C-----------------------------------------------------------------------
   50 CL1=0.
      CL2=0.
      CY1=0.
      CY2=0.
      CR1=0.
      CR2=0.
      YV1=0.
      YV2=0.
      ZV1=0.
      ZV2=0.
      IF(NWING.EQ.3) GO TO 70
      IF(NWING.EQ.2) GO TO 60
      YV1=CIRY1/CIR1
      ZV1=CIRZ1/CIR1+WTZ2
      CL1=-2.*CIRY1/(S*12.)
      CY1= 2.*CIRZ1/(S*12.)
      CR1=    CIYZ1/(S*SPAN*144.)
      IF(NWING.EQ.1) GO TO 80
   60 YV2=CIRY2/CIR2
      ZV2=CIRZ2/CIR2+WTZ2
      CL2=-2.*CIRY2/(S*12.)
      CY2= 2.*CIRZ2/(S*12.)
      CR2=    CIYZ2/(S*SPAN*144.)
```

```
      GO TO 80
   70 ZV1=(CIRZ1+CIRZ2)/(CIR1+CIR2)
      YV1=(CIRY1+CIRY2)/(CIR1+CIR2)
      CL1=-2.*(CIRZ1+CIRZ2)/(S*12.)
      CY1= 2.*(CIRY1+CIRY2)/(S*12.)
      CR1=    (CIYZ1+CIYZ2)/(S*SPAN*144.)
   80 CL=CL1+CL2
      CY=CY1+CY2
      CR=CR1+CR2
      YV=YV1+YV2
      ZV=ZV1+ZV2
      IF(NWING.NE.0) GO TO 90
      YV=(CIRY1-CIRY2)/(CIR1-CIR2)
      ZV=(CIRZ1-CIRZ2)/(CIR1-CIR2)
C
   90 WRITE(6,100)
      WRITE(6,110) YV1,YV2,YV
      WRITE(6,120) ZV1,ZV2,ZV
      WRITE(6,130) CL1,CL2,CL
      WRITE(6,140) CY1,CY2,CY
      WRITE(6,150) CR1,CR2,CR
      RETURN
C
C-----------------------------------------------------------------------
  100 FORMAT(//4X,'GAMMA DERIVATIVES'//8X,'WING',18X,
     1       'LEFT    RIGHT    TOTAL')
  110 FORMAT(8X,'VORTEX Y POSITION ',3F8.3)
  120 FORMAT(8X,'VORTEX Z POSITION ',3F8.3)
  130 FORMAT(8X,'LIFT COEFFICIENT  ',3F8.4)
  140 FORMAT(8X,'SF   COEFFICIENT  ',3F8.4)
  150 FORMAT(8X,'ROLL COEFFICIENT  ',3F8.4)
      END
```

```
C  VORTEX DRAG INTEGRATION
C-----------------------------------------------------------------------
C
      SUBROUTINE DRAGI
      COMMON NWING,NWOPT,IEC,NEC,DELZ,DELY,ZG(5Ø),YG(54),V(5Ø,54),
     *       W(5Ø,54),GAM(5Ø,54),PSI(5Ø,54),GPSI(5Ø,54),HTOT(5Ø,54)
      COMMON/COEFF/ S,CBAR,SPAN,WTZ2,CDI,CMI,CNI
C
C  DRAG SUMMATION
C-----------------------------------------------------------------------
      CDI=Ø.
      CMI=Ø.
      CNI=Ø.
      DO 2Ø N=1,NEC
      IF(NWING.EQ.1.AND.YG(N).GT.Ø.Ø5) GO TO 2Ø
      IF(NWING.EQ.2.AND.YG(N).LT.-Ø.Ø5) GO TO 2Ø
      DO 1Ø I=1,IEC
      CDI=CDI+GPSI(I,N)
      CMI=CMI+GPSI(I,N)*(ZG(I)-WTZ2)
  1Ø  CNI=CNI+GPSI(I,N)*YG(N)
  2Ø  CONTINUE
      CDI=CDI/S
      CMI=CMI/(S*CBAR*12.)
      CNI=CNI/(S*SPAN*12.)
      IF(NWING.EQ.Ø) GO TO 3Ø
      CCC=CMI
      CMI=CNI
      CNI=CCC
C
  3Ø  WRITE(6,4Ø)
      RETURN
C
C-----------------------------------------------------------------------
  4Ø  FORMAT(//4X,'GAMMA*PSI DERIVATIVES'//8X,'COMPONENT',11X,
     *       'VORTEX   PRESS   TOTAL')
      END
```

```
C  INTEGRATION OF PRESSURE DRAG
C-----------------------------------------------------------------------
C
      SUBROUTINE DRAGO(LCDO)
      COMMON NWING,NWOPT,IEC,NEC,DELZ,DELY,ZG(50),YG(54),V(50,54),
     *       W(50,54),GAM(50,54),PSI(50,54),GPSI(50,54),HTOT(50,54)
      COMMON/COEFF/ S,CBAR,SPAN,WTZ2,CDI,CMI,CNI
C
C  REMOVAL OF -VE PROFILE DRAG
C-----------------------------------------------------------------------
      HT=0.
      HM=0.
      HN=0.
      NWG=NWING+1
      DO 10 I=1,IEC
      DO 10 N=1,NEC
      IF(HTOT(I,N).LT.0.) HTOT(I,N)=0.
  10  CONTINUE
      NS=1
      NE=NEC
      IS=1
      IF(NWG/2-1) 60,20,40
C
C  CENTER TUNNEL HALF SURVEY
C-----------------------------------------------------------------------
  20  AREA=((NWING*2-3)*YG(LCDO)-DELY/2.)*DELZ/144.
      DO 30 I=1,IEC
      HTT=HTOT(I,LCDO)*AREA
      HT=HT+HTT
      HM=HM+HTT*(ZG(I)-WTZ2)
  30  HN=HN+HTT*YG(LCDO)/2.
      NS=NS+(NWING-1)*(LCDO-NS)
      NE=NE+(2-NWING)*(LCDO-NE)
      GO TO 60
C
C  FLOOR MOUNTED SEMI-SPAN SURVEY
C-----------------------------------------------------------------------
  40  IS=LCDO
      AREA=DELY*(ZG(LCDO)-DELZ/2.)/144.
      DO 50 N=1,NEC
      HTT=HTOT(LCDO,N)*AREA
      HT=HT+HTT
      HM=HM+HTT*ZG(LCDO)/2.
  50  HN=HN+HTT*YG(N)
C
C  MEASURED SURVEY AREA
C-----------------------------------------------------------------------
  60  AREA=DELY*DELZ/144.
      DO 110 N=NS,NE
      GO TO (90,70,80,90),NWG
  70  IF(YG(N).GT.0.05) GO TO 110
      GO TO 90
  80  IF(YG(N).LT.-.05) GO TO 110
  90  DO 100 I=IS,IEC
      HTT=HTOT(I,N)*AREA
      HT=HT+HTT
      HM=HM+HTT*(ZG(I)-WTZ2)
 100  HN=HN+HTT*YG(N)
 110  CONTINUE
C
      CDO=HT/S
      CMO=HM/(S*CBAR*12.)
```

```
      CNO=HN/(S*SPAN*12.)
      IF(NWING.NE.3) GO TO 120
      CCC=CMO
      CMO=CNO
      CNO=CCC
  120 CD=CDI+CDO
      CM=CMI+CMO
      CN=CNI+CNO
      WRITE(6,130) CDO,CDI,CD,LCDO
      WRITE(6,140) CMI,CMO,CM
      WRITE(6,150) CNI,CNO,CN
      RETURN
C
C-----------------------------------------------------------------------
  130 FORMAT(8X,'DRAG COEFFICIENT  ',3F8.4,110)
  140 FORMAT(8X,'PM   COEFFICIENT  ',3F8.4)
  150 FORMAT(8X,'YAW  COEFFICIENT  ',3F8.4)
      END
```

APPENDIX IV

MACHINE PLOTS OF TRAVERSE DATA

(For cross reference table see Figure 6.1)

(For data reduction details see Section 4)

(For discussion of aerodynamics see Section 6)

LOCKHEED-GEORGIA COMPANY - RESEARCH CENTER - TEST 64-Ø1

WING - 6 DEG - 12 INS CROSSFLOW VELOCITY VC/UO

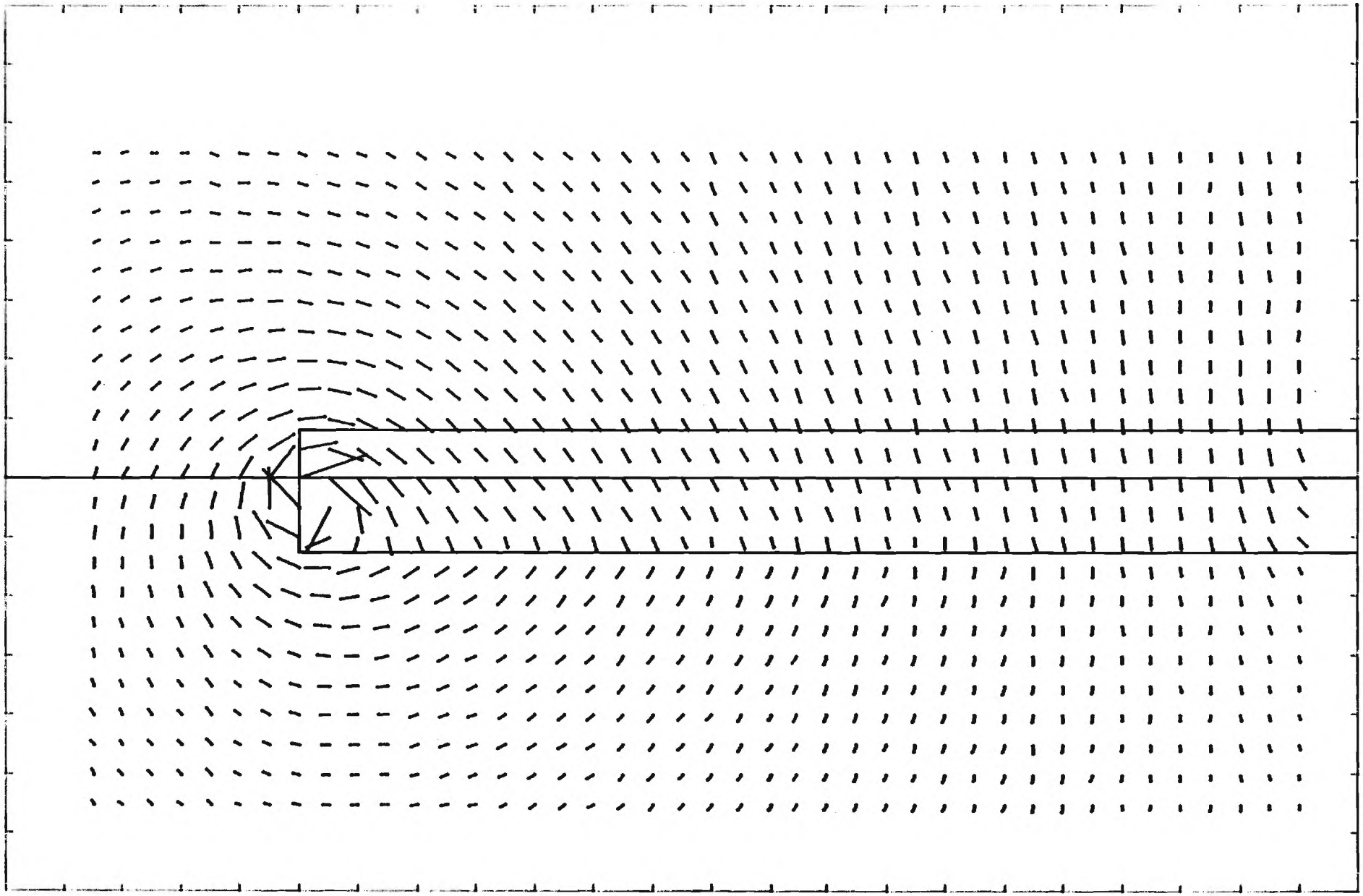

MP1

LOCKHEED-GEORGIA COMPANY - RESEARCH CENTER - TEST 64-01

WING - 6 DEG - 12 INS LAT. VELOCITY RATIO V/UO

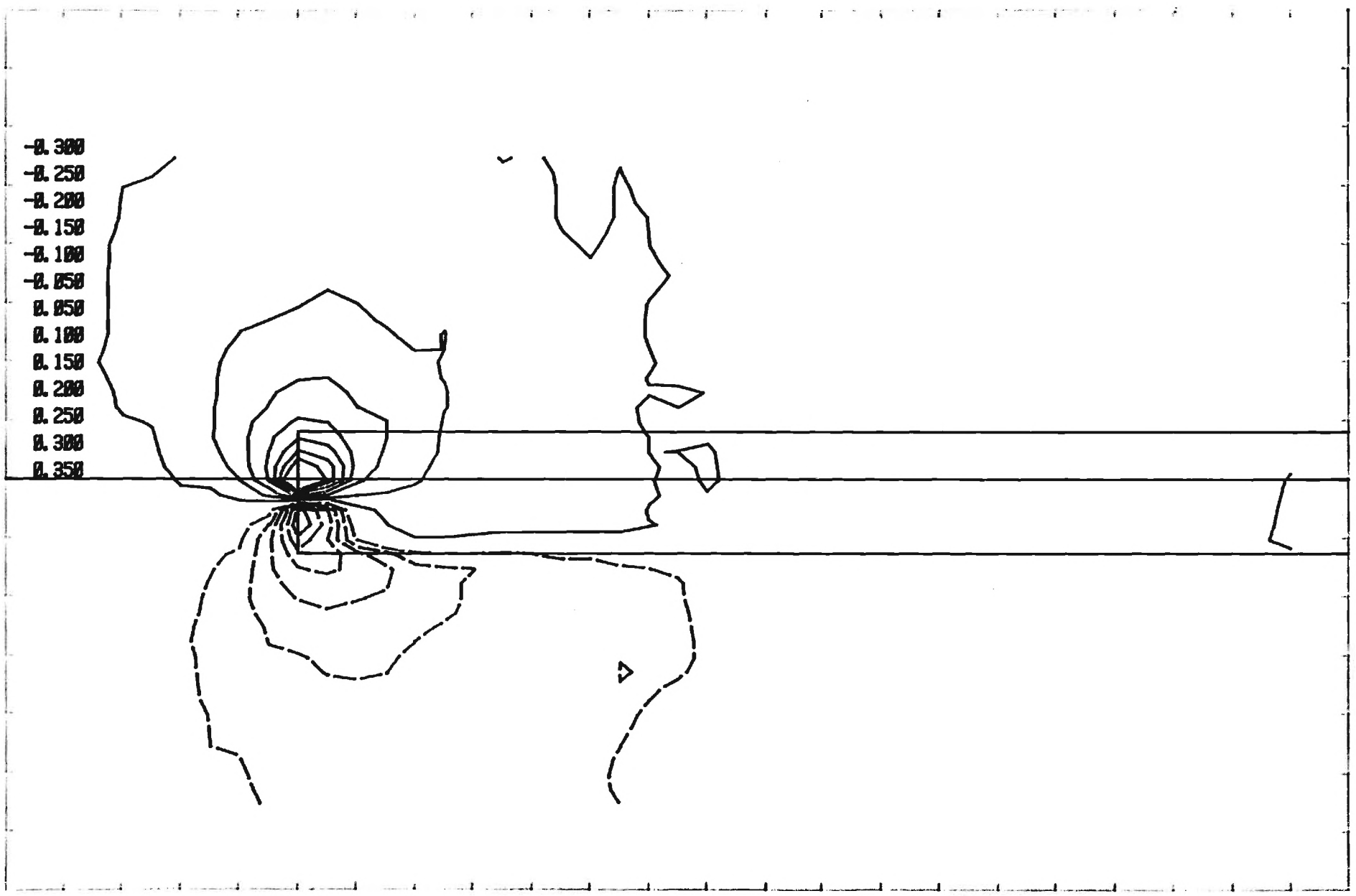

MP2

LOCKHEED-GEORGIA COMPANY - RESEARCH CENTER - TEST 64-Ø1

WING - 6 DEG - 12 INS

VERT. VELOCITY RATIO W/UO

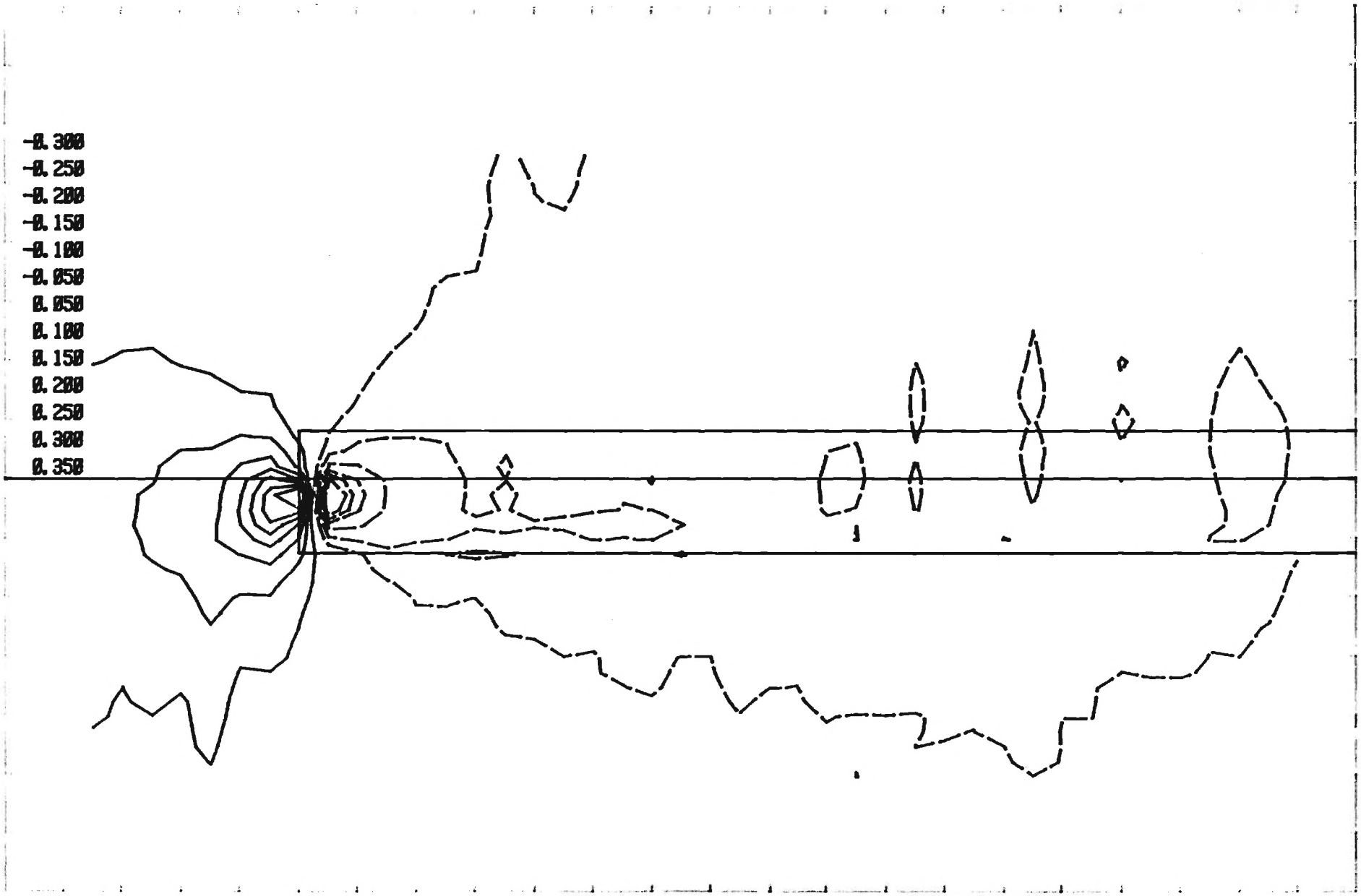

MP3

LOCKHEED-GEORGIA COMPANY - RESEARCH CENTER - TEST 64-01

WING - 6 DEG - 12 INS

AXIAL VELOCITY RATIO U/UO

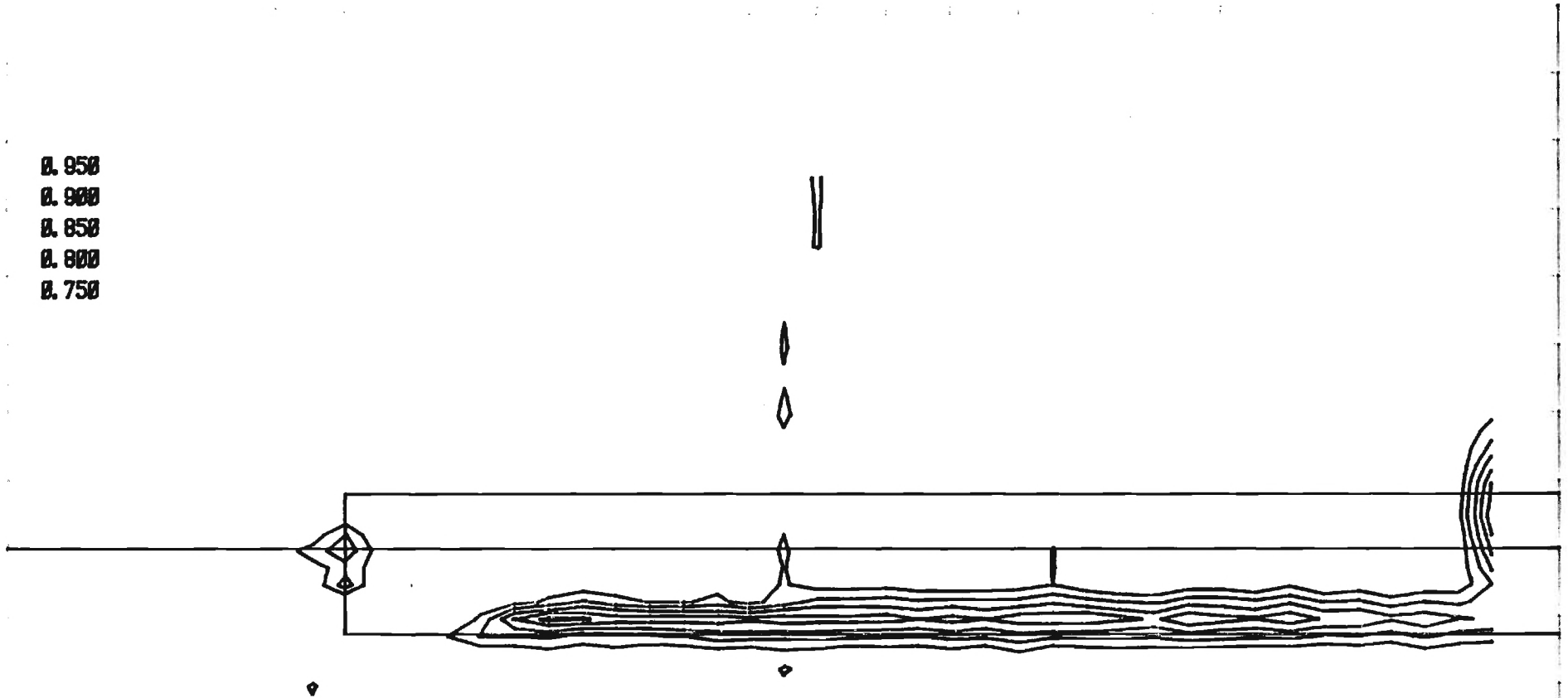

MP4

LOCKHEED-GEORGIA COMPANY - RESEARCH CENTER - TEST 64-01

WING - 6 DEG - 12 INS

TOTAL PRESSURE DEFICIT (HO-P)/QO

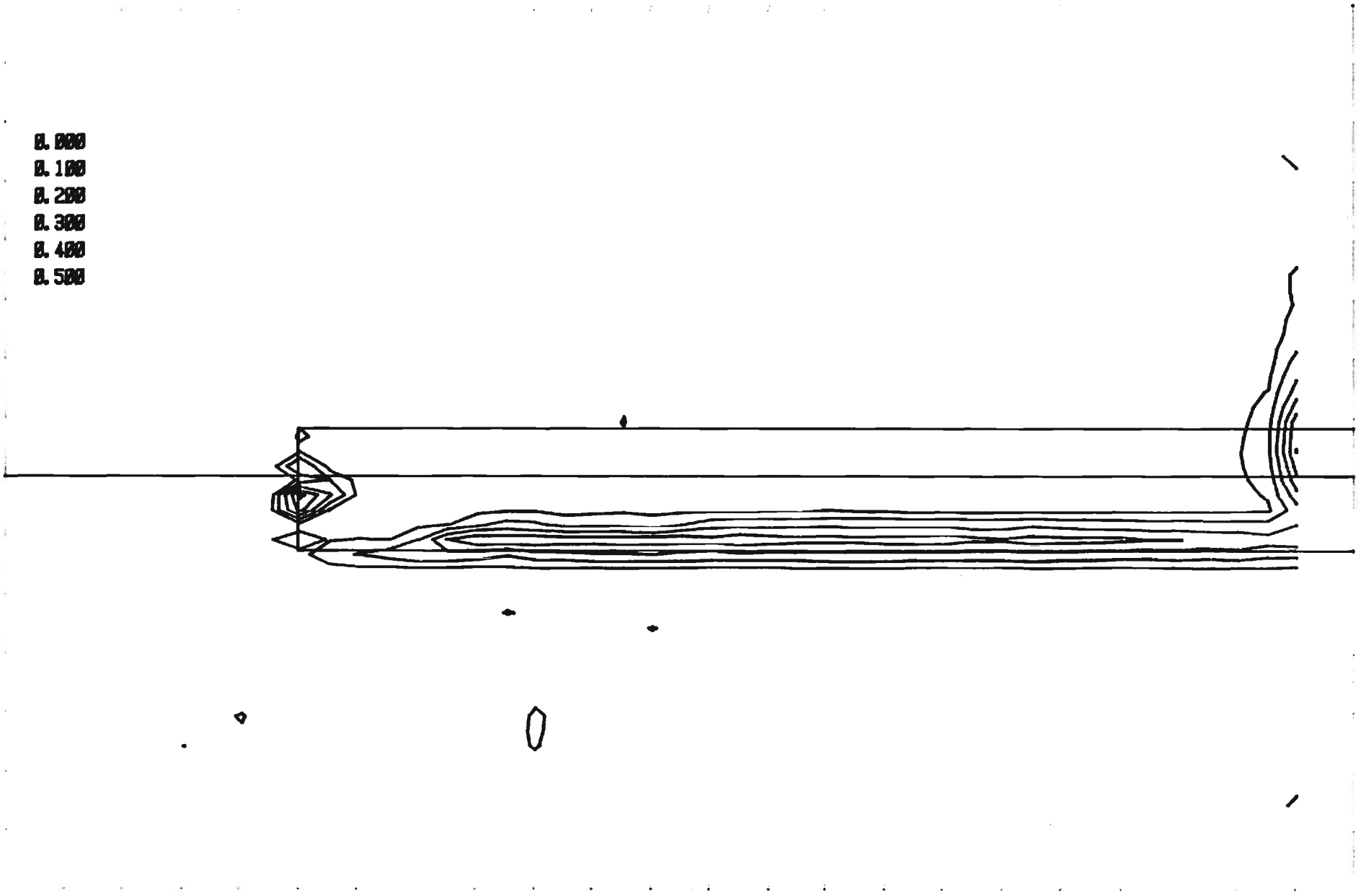

MP5

LOCKHEED-GEORGIA COMPANY - RESEARCH CENTER - TEST 64-01

WING - 6 DEG - 12 INS CROSS-FLOW KINETIC ENERGY (VC*VC)/(UO*UO)

0.000
0.040
0.080
0.120
0.160
0.200
0.240

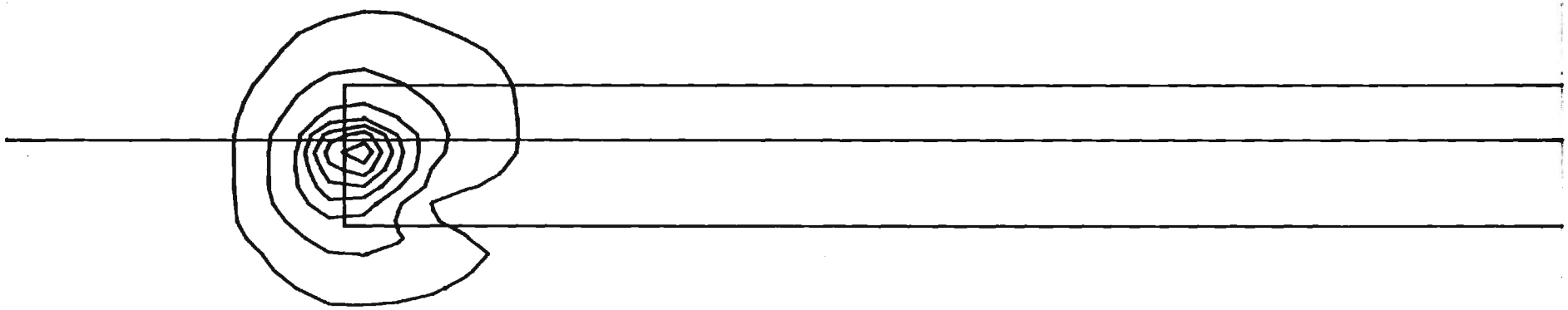

MP6

WING - 6 DEG - 12 INS VORTICITY

NOTE

$$\left(\frac{\xi c}{U_o}\right) = \text{(CONTOUR VALUE)} \times 1152$$

0.002
0.004
0.008
0.016
0.024
0.032

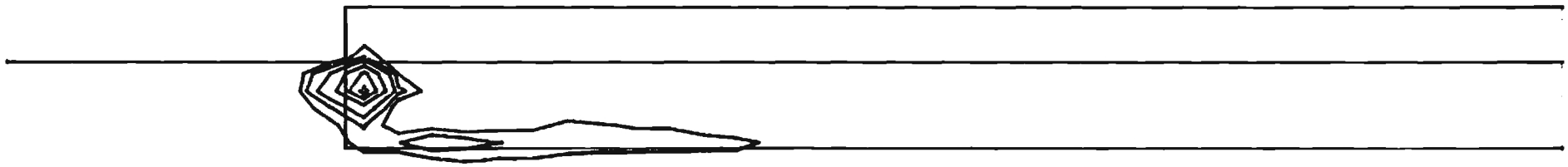

LOCKHEED-GEORGIA COMPANY - RESEARCH CENTER - TEST 64-Ø1

WING - 6 DEG - 12 INS CORR LAT VELOCITY V/UO

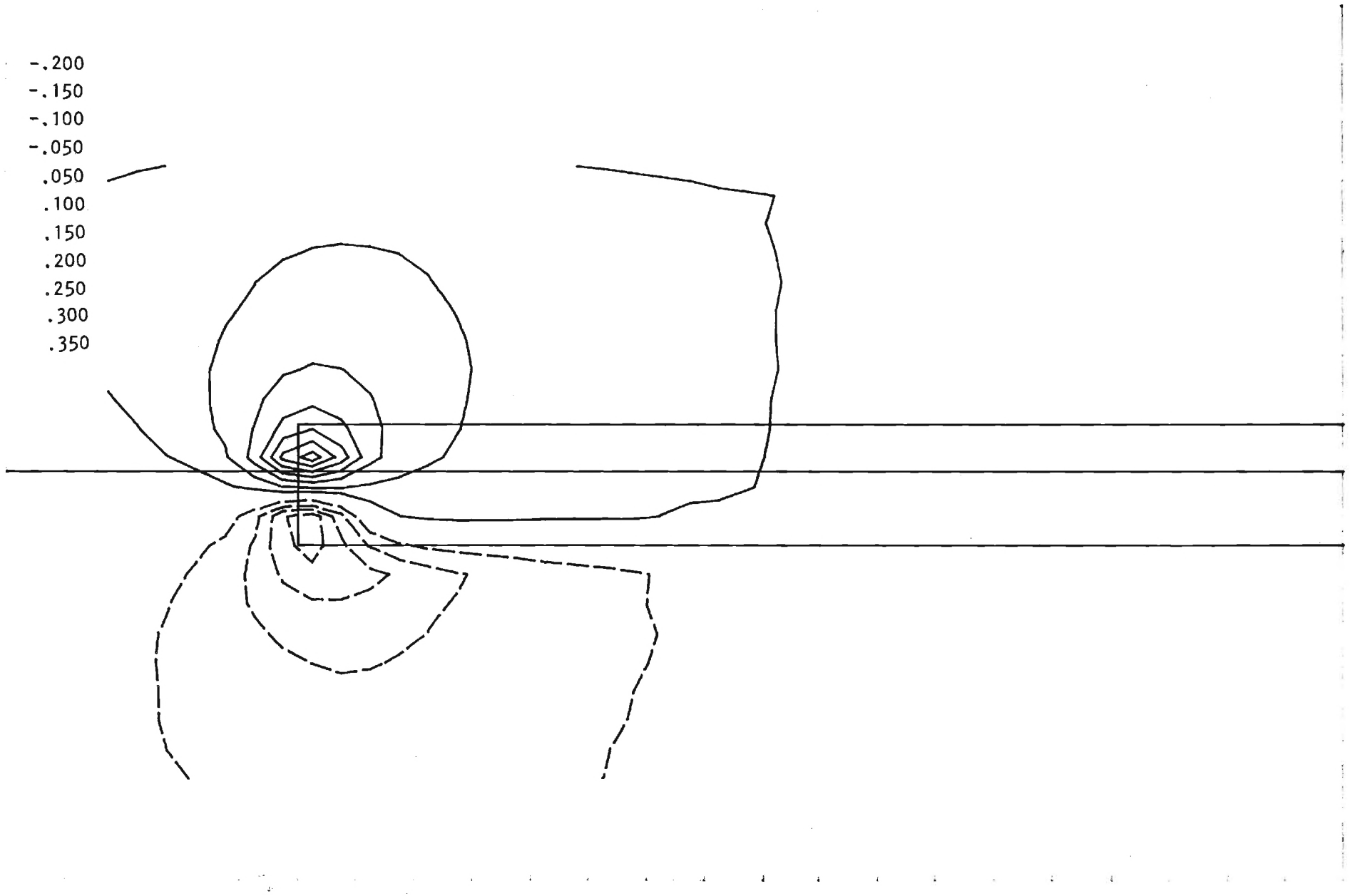

MP8

LOCKHEED-GEORGIA COMPANY - RESEARCH CENTER - TEST 64-Ø1

WING - 6 DEG - 12 INS CORR VERT VELOCITY W/UO

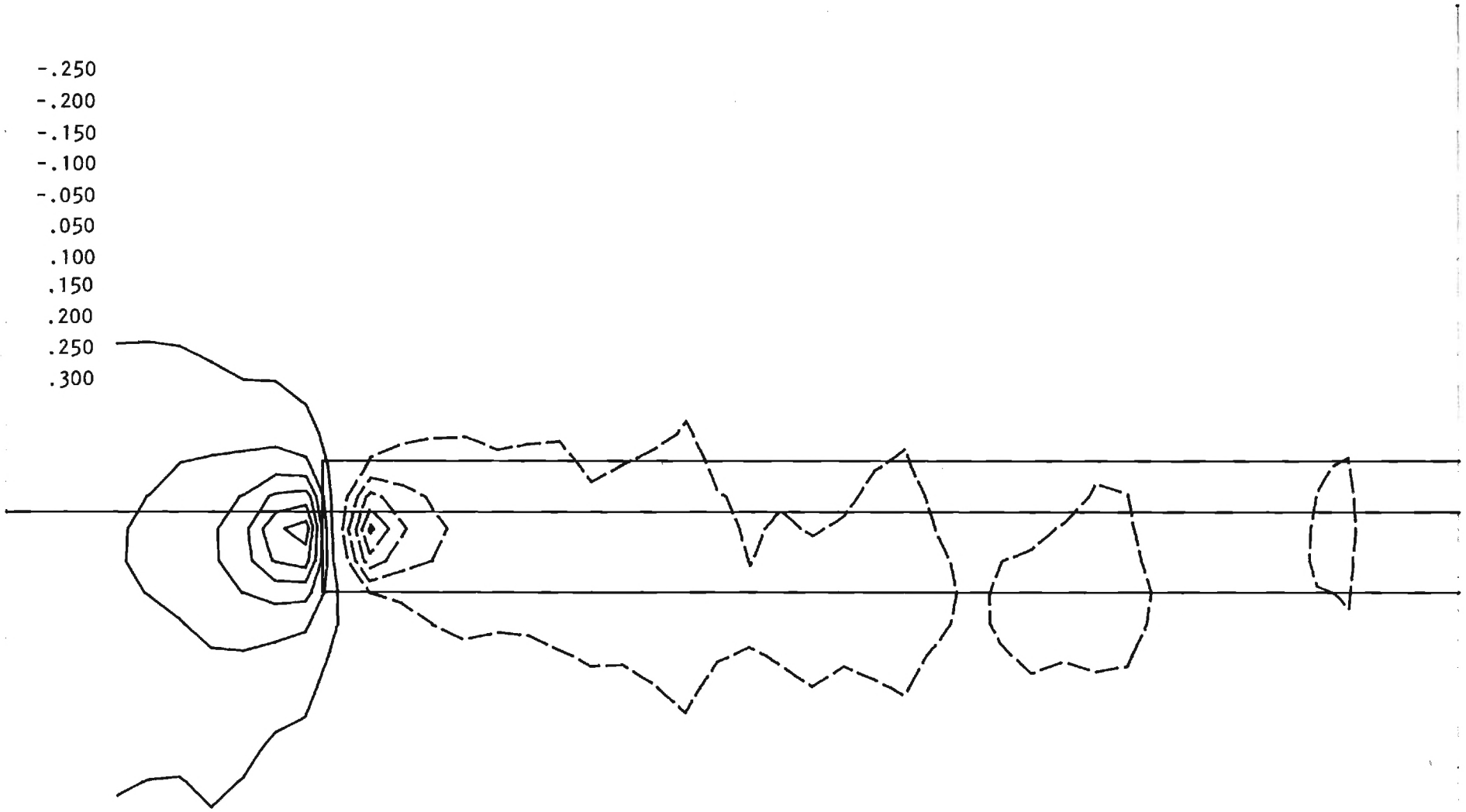

MP9

WING - 6 DEG - 12 INS

STREAM FUNCTIONS

NOTE

$(\frac{\psi}{U_o c})$ = (CONTOUR VALUE) x 1.0

0.010
0.020
0.030
0.040
0.050
0.060
0.070
0.080
0.090

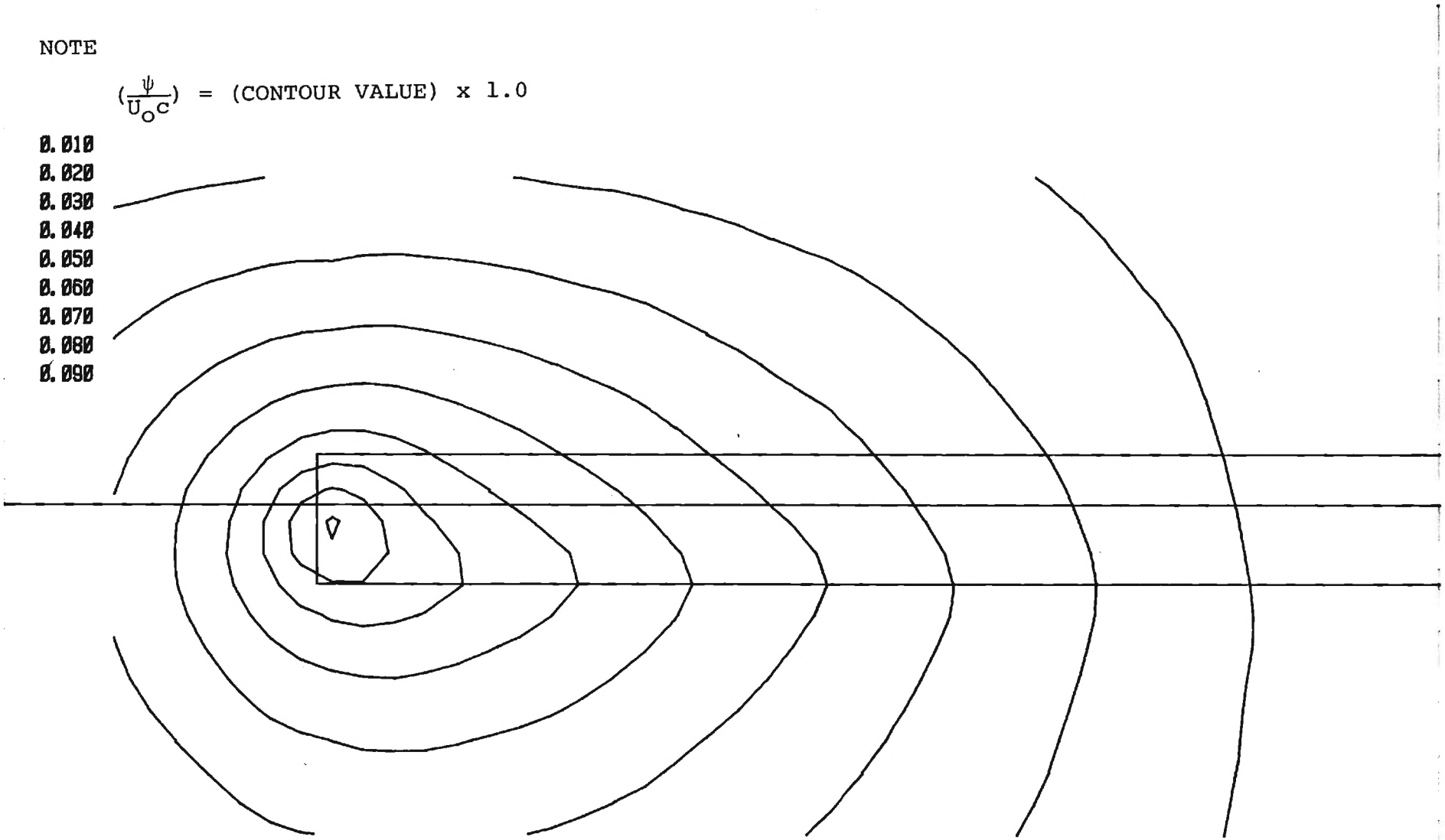

LOCKHEED-GEORGIA COMPANY - RESEARCH CENTER - TEST 64-Ø2

WING - 6 DEG - 36 INS CROSSFLOW VELOCITY VC/UO

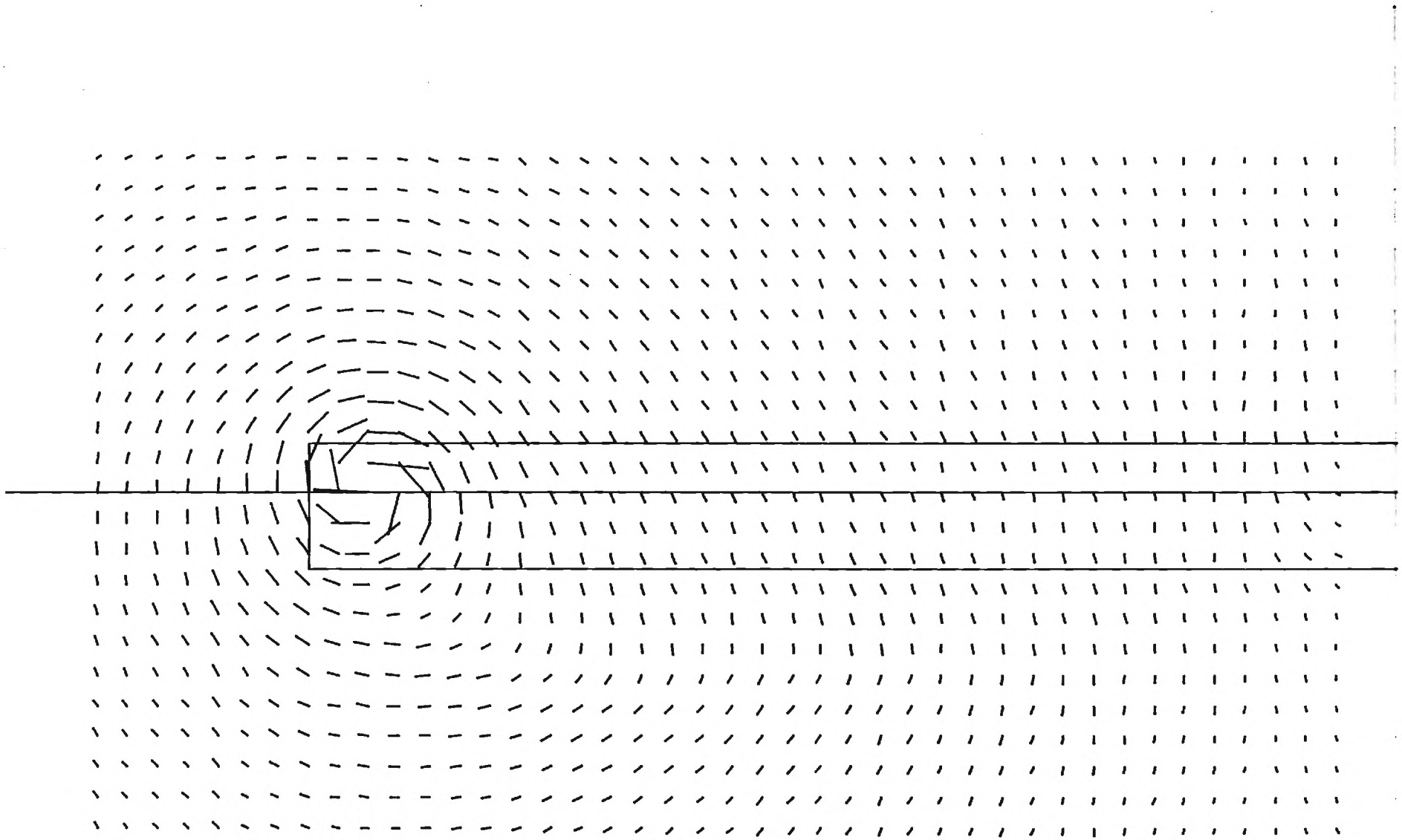

MP11

LOCKHEED-GEORGIA COMPANY - RESEARCH CENTER - TEST 64-02

WING - 6 DEG - 36 INS LAT. VELOCITY RATIO V/UO

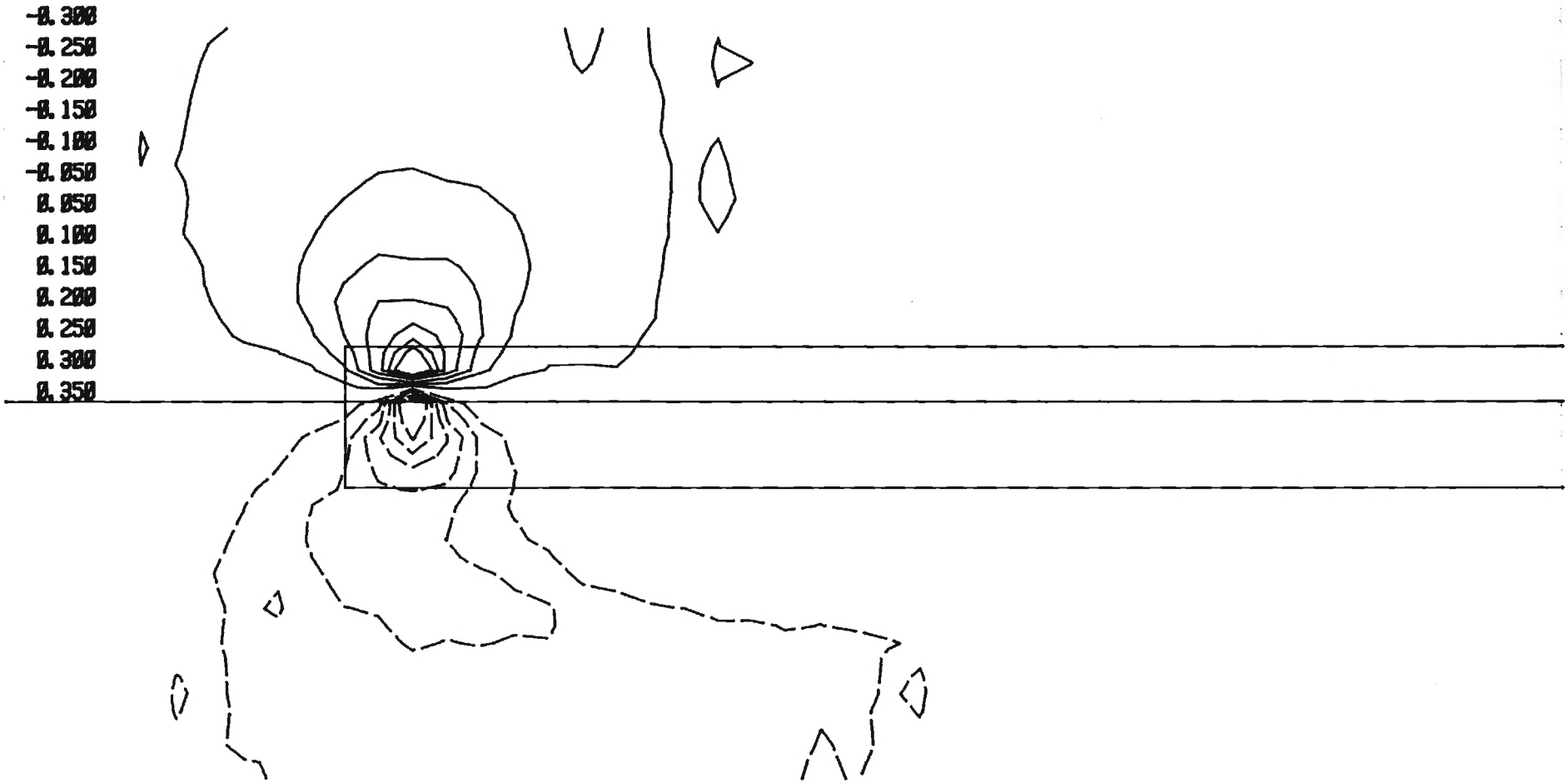

MP12

LOCKHEED-GEORGIA COMPANY - RESEARCH CENTER - TEST 64-02

WING - 6 DEG - 36 INS

VERT. VELOCITY RATIO W/UO

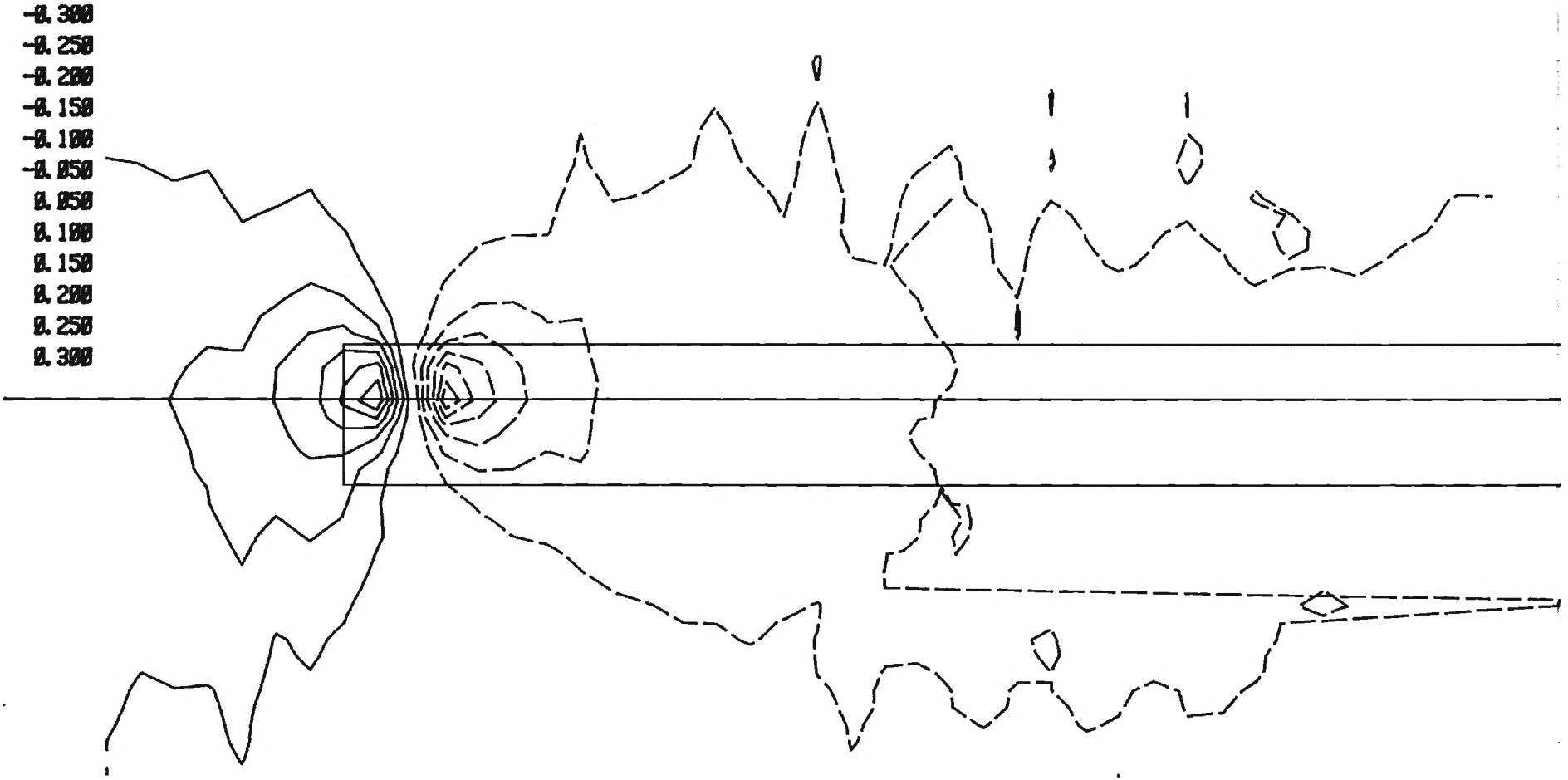

MP13

LOCKHEED-GEORGIA COMPANY - RESEARCH CENTER - TEST 64-02

WING - 6 DEG - 36 INS

AXIAL VELOCITY RATIO U/UO

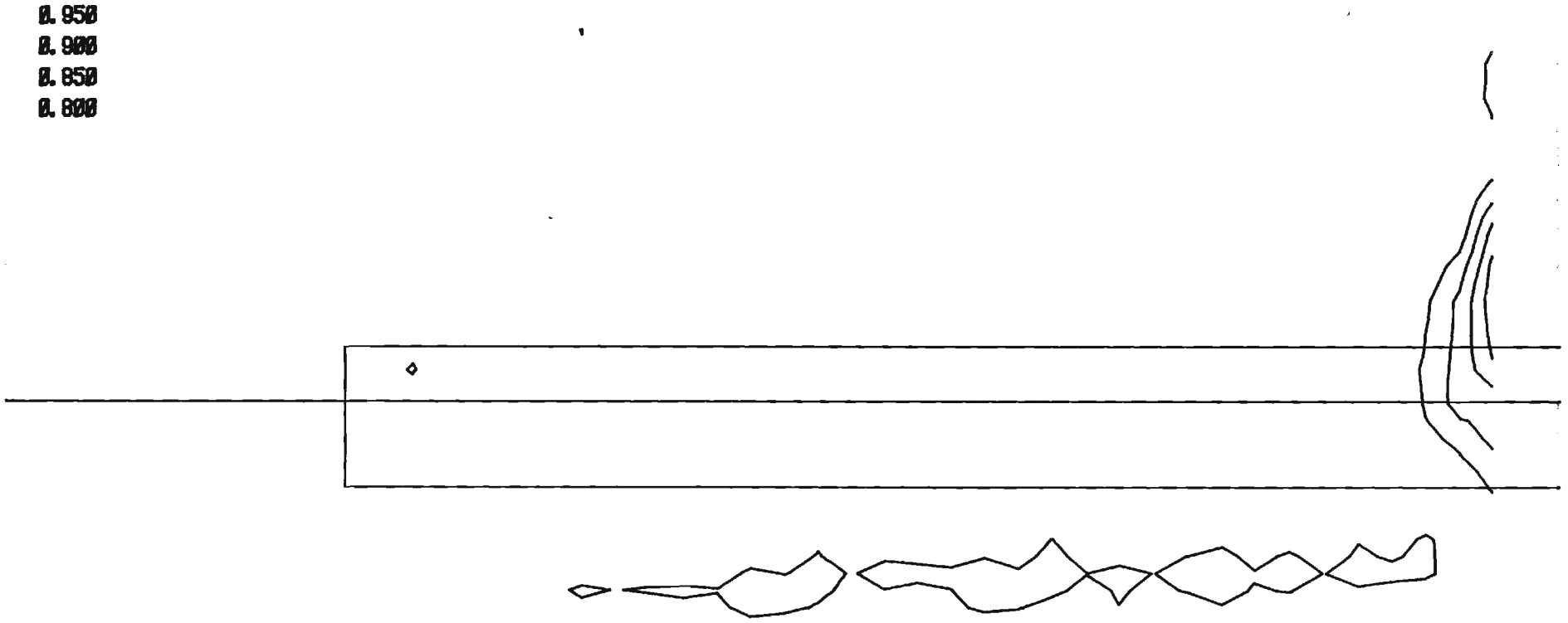

LOCKHEED-GEORGIA COMPANY - RESEARCH CENTER - TEST 64-02

WING - 6 DEG - 36 INS

TOTAL PRESSURE DEFICIT (HO-P)/QO

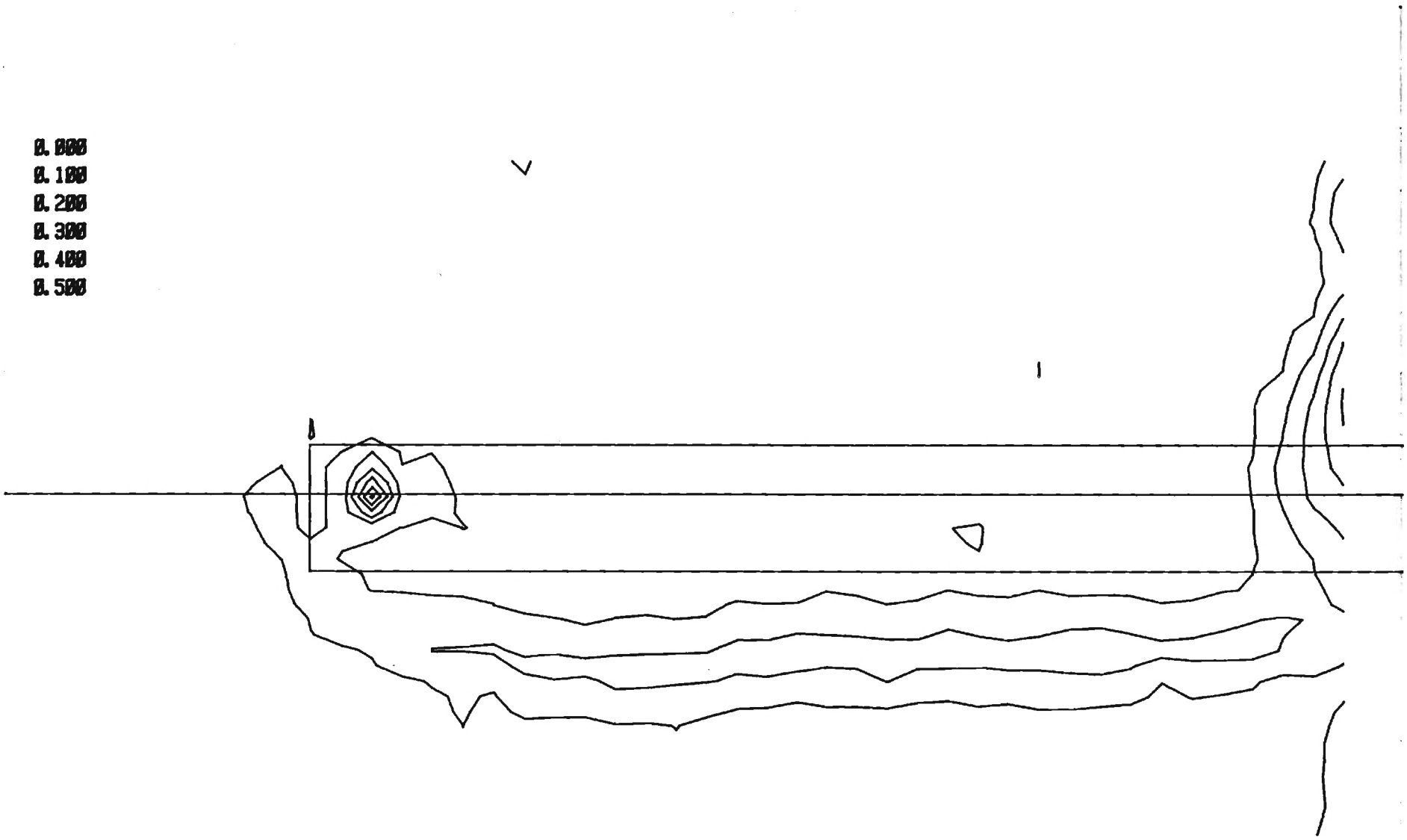

MP15

LOCKHEED-GEORGIA COMPANY - RESEARCH CENTER - TEST 64-02

WING - 6 DEG - 36 INS CROSS-FLOW KINETIC ENERGY (VC*VC)/(UO*UO)

0.000
0.040
0.080
0.120

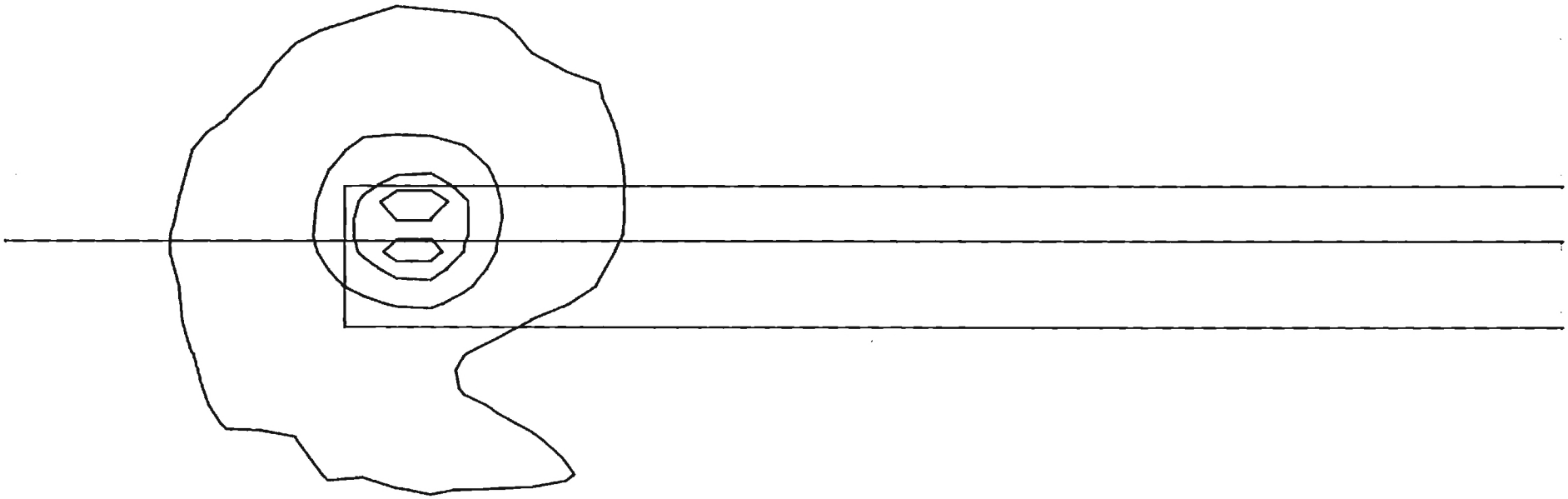

MP16

WING - 6 DEG - 36 INS VORTICITY

NOTE

$$\left(\frac{\xi c}{U_o}\right) = (\text{CONTOUR VALUE}) \times 1152$$

0.002
0.004
0.008
0.016

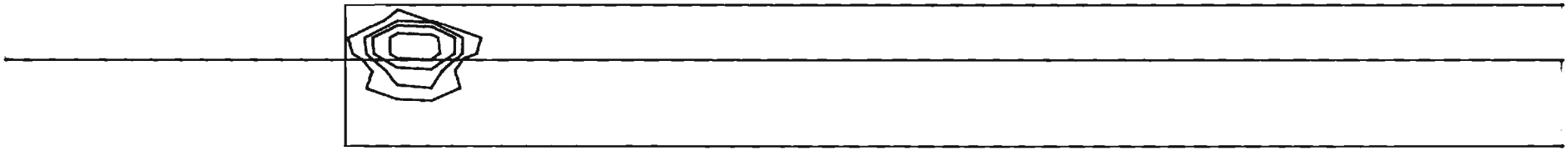

LOCKHEED-GEORGIA COMPANY - RESEARCH CENTER - TEST 64-Ø2

WING - 6 DEG - 36 INS CORR LAT VELOCITY V/UO

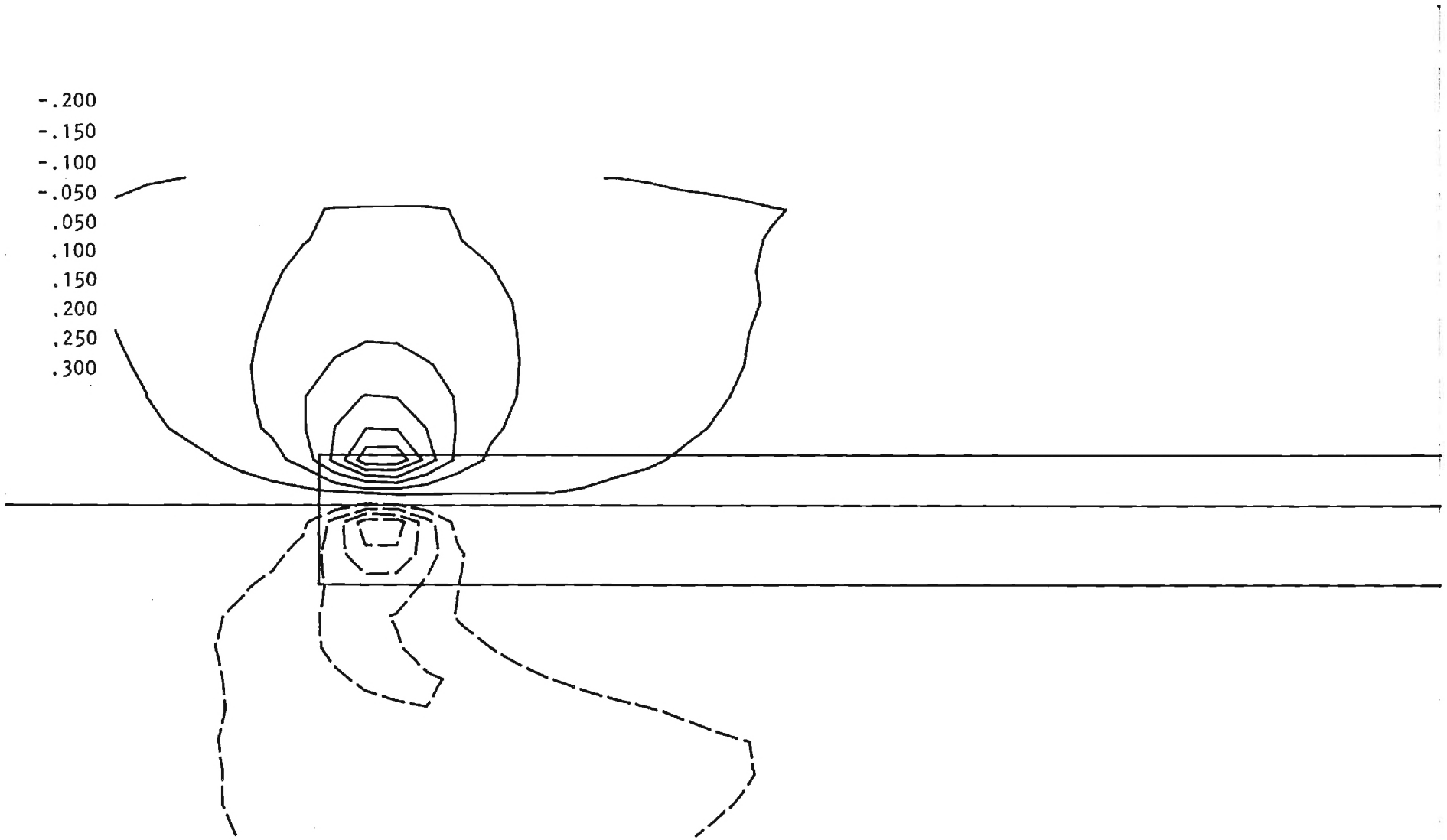

LOCKHEED-GEORGIA COMPANY - RESEARCH CENTER - TEST 64-02

WING - 6 DEG - 36 INS CORR VERT VELOCITY W/UO

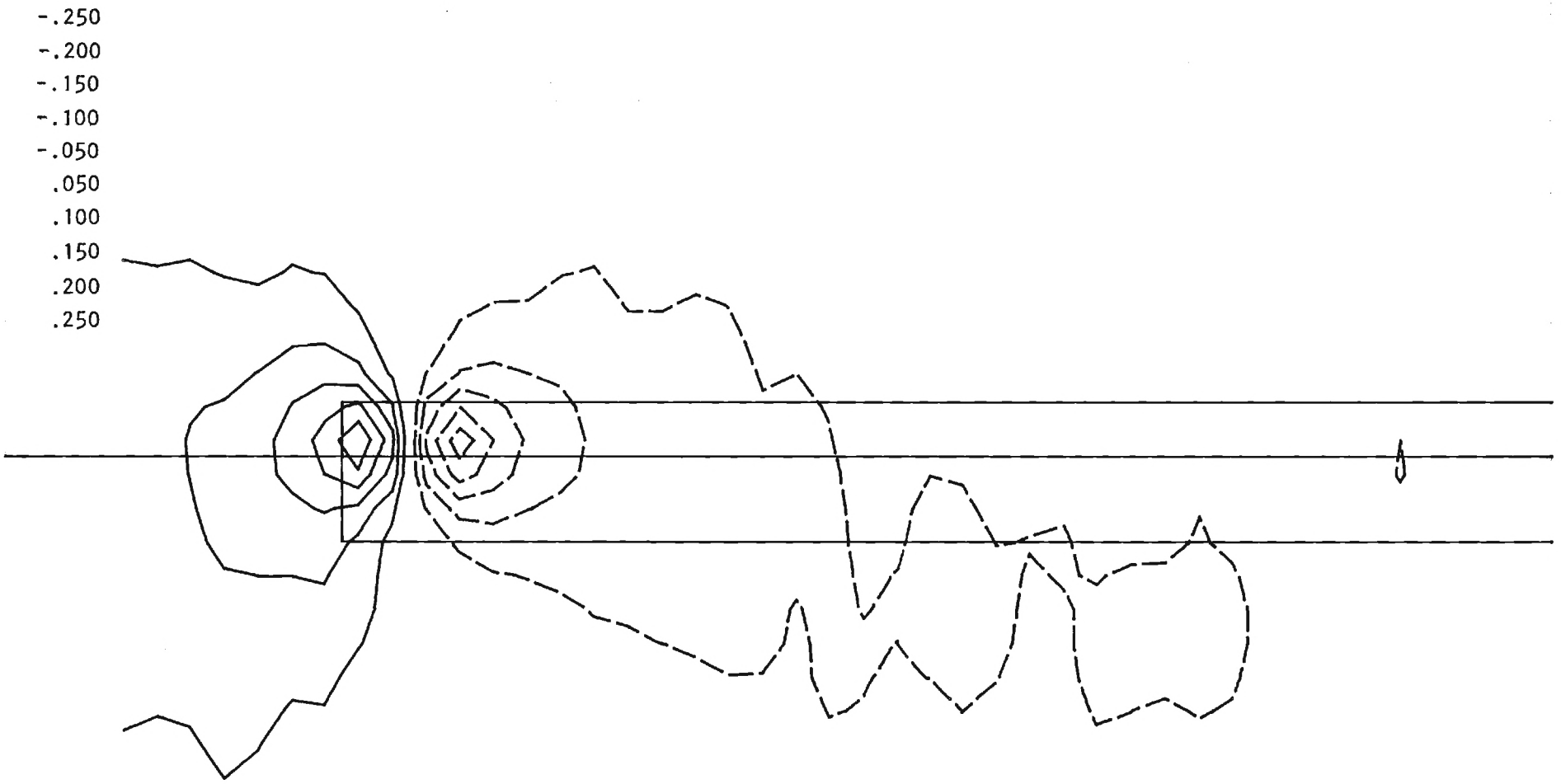

MP19

LOCKHEED-GEORGIA COMPANY - RESEARCH CENTER - TEST 64-02

WING - 6 DEG - 36 INS

STREAM FUNCTIONS

NOTE

$(\frac{\psi}{U_o c})$ = (CONTOUR VALUE) x 1.0

0.010
0.020
0.030
0.040
0.050
0.060
0.070
0.080

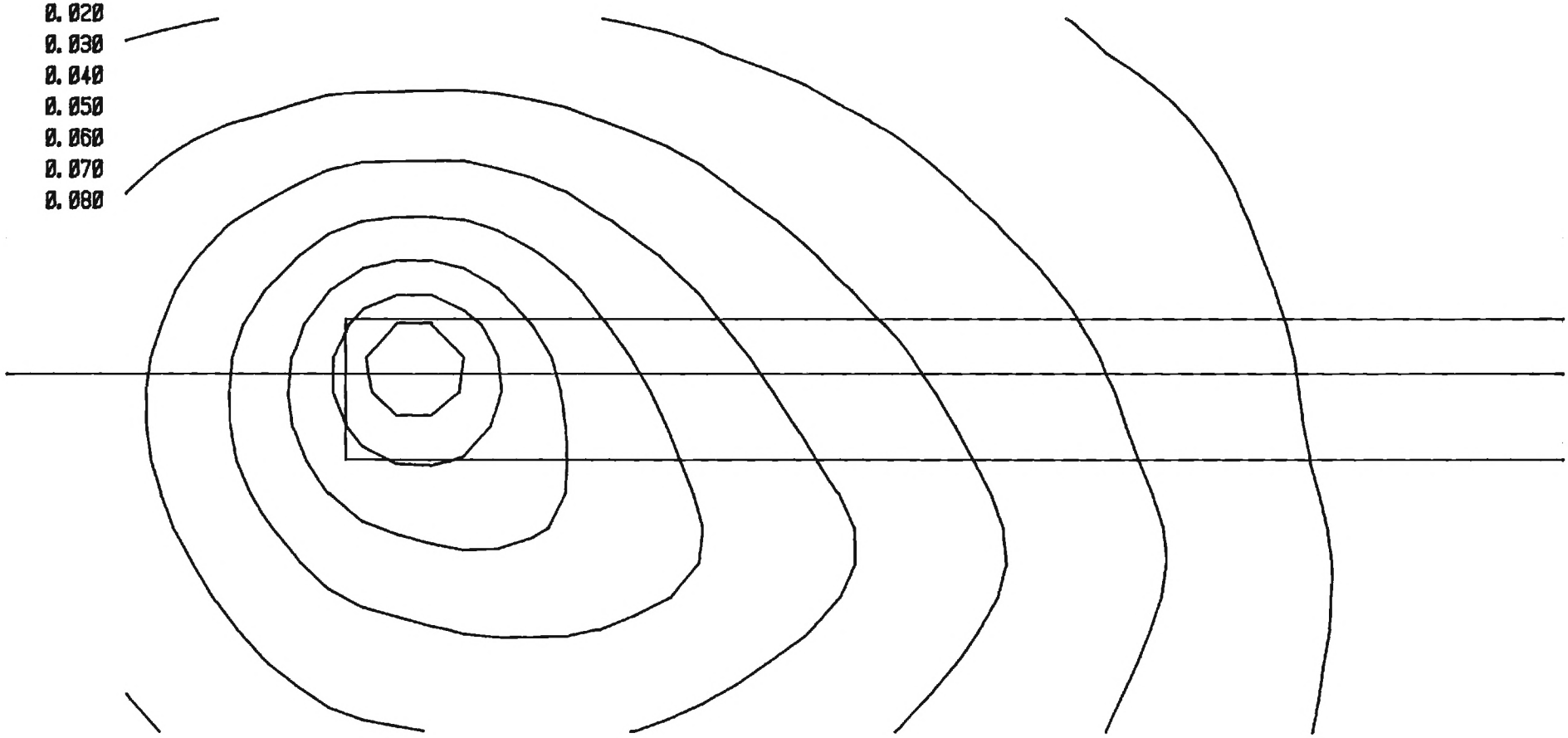

LOCKHEED-GEORGIA COMPANY - RESEARCH CENTER - TEST 64-06

WING - 18 DEG - 18 INS

CROSSFLOW VELOCITY VC/UO

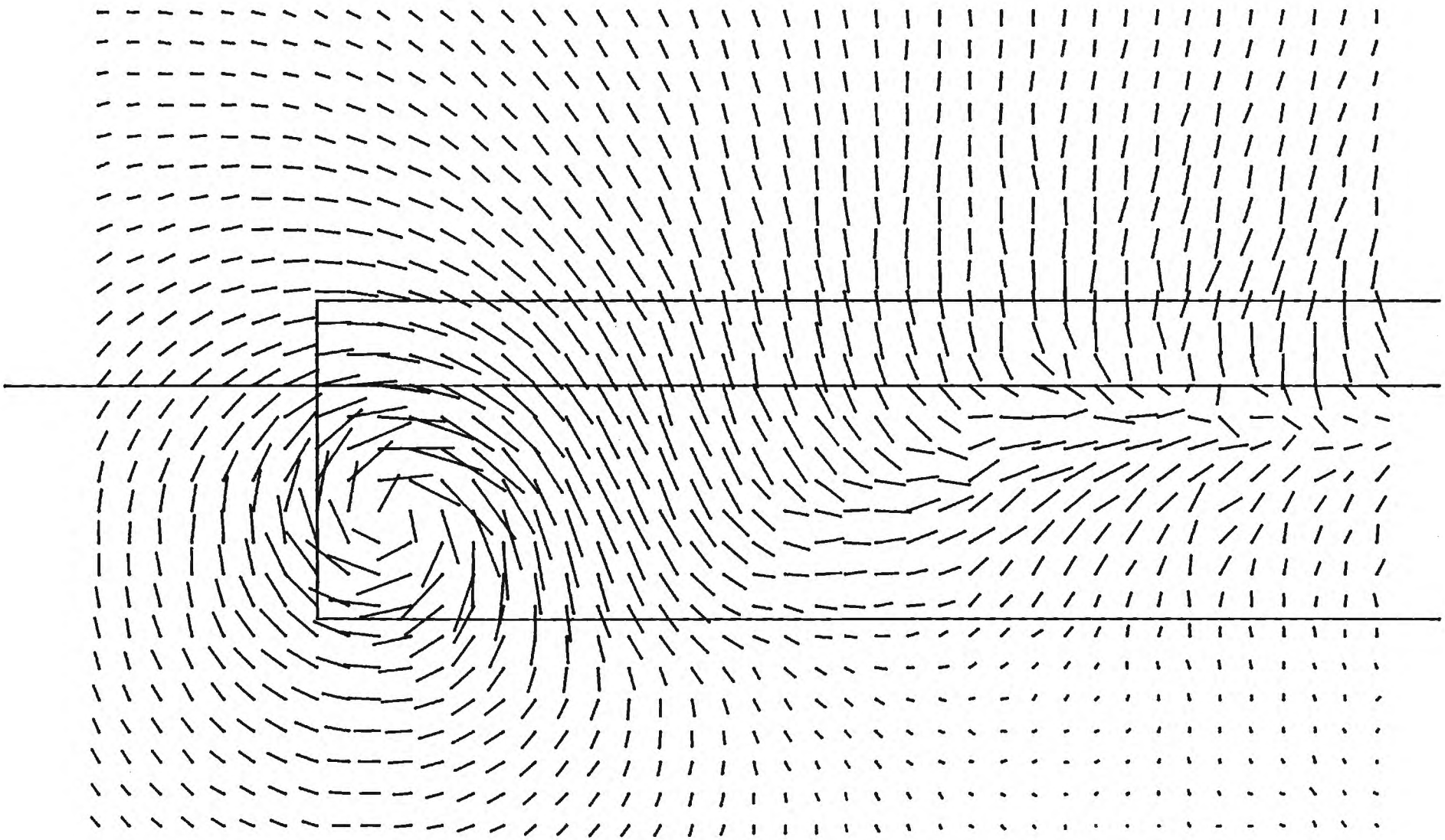

MP21

LOCKHEED-GEORGIA COMPANY - RESEARCH CENTER - TEST 64-06

WING - 18 DEG - 18 INS

LAT. VELOCITY RATIO V/U0

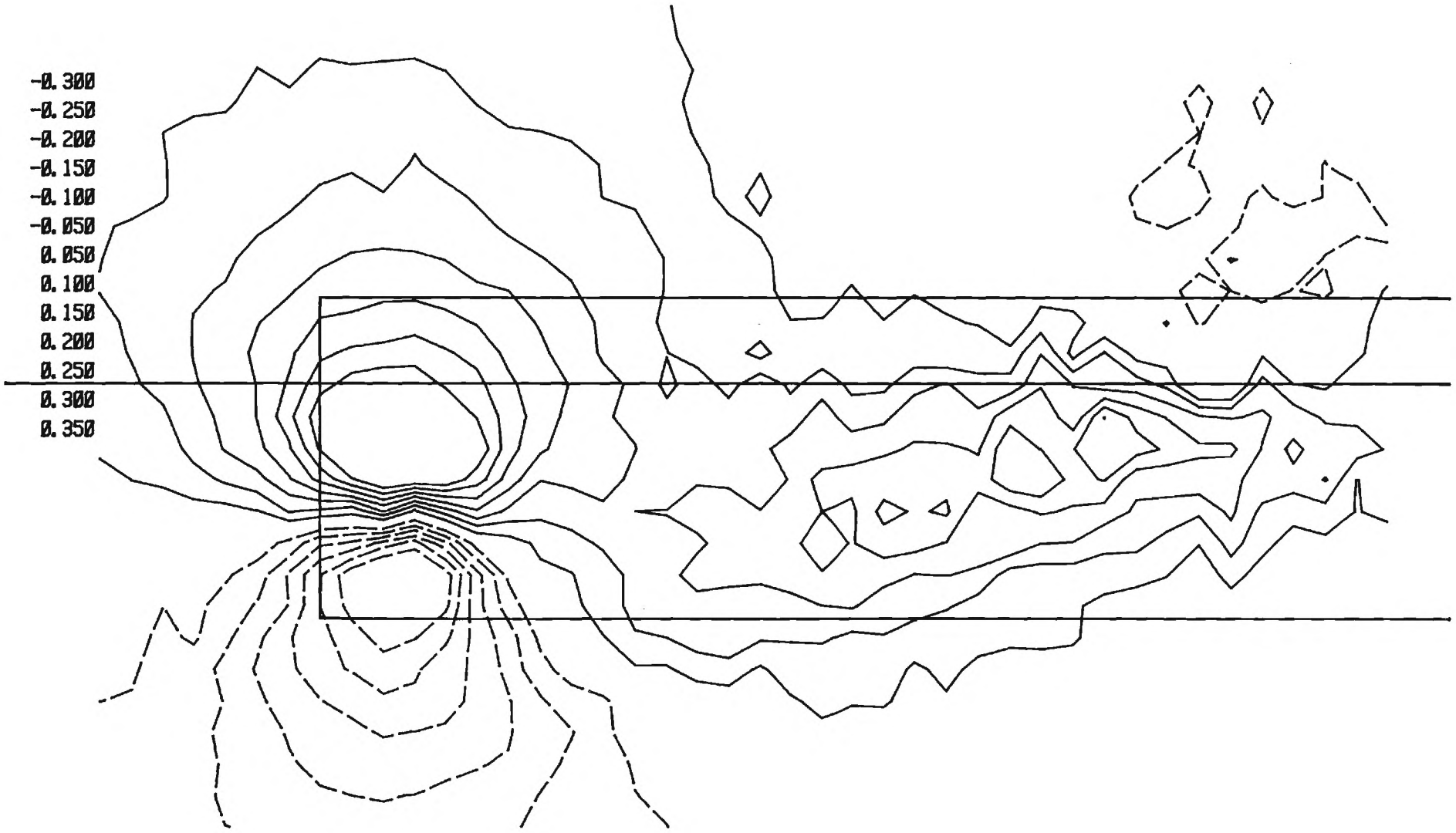

LOCKHEED-GEORGIA COMPANY - RESEARCH CENTER - TEST 64-06

- 18 DEG - 18 INS

VERT. VELOCITY RATIO W/UO

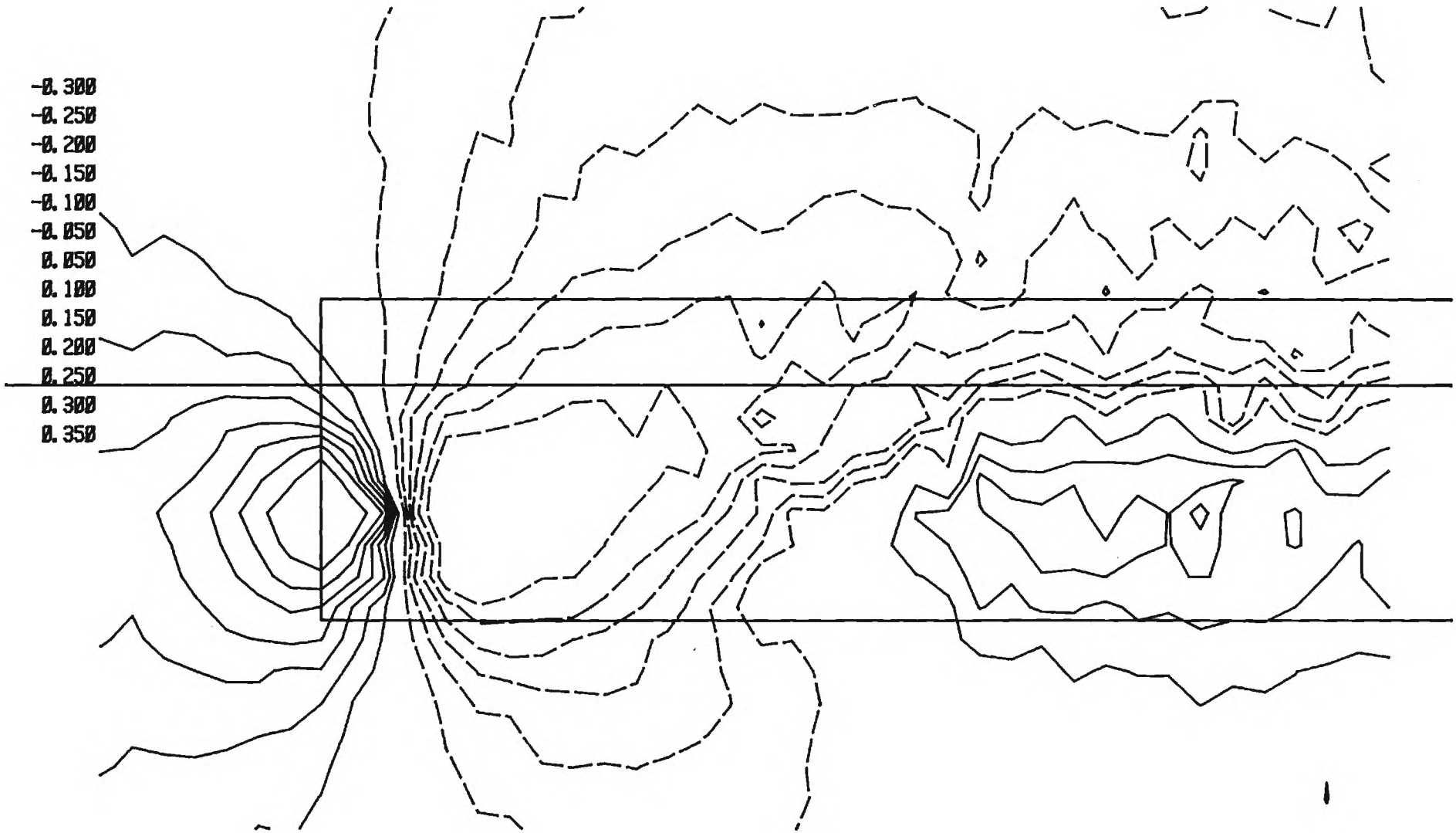

MP23

LOCKHEED-GEORGIA COMPANY - RESEARCH CENTER - TEST 64-06

WING - 18 DEG - 18 INS

AXIAL VELOCITY RATIO U/U0

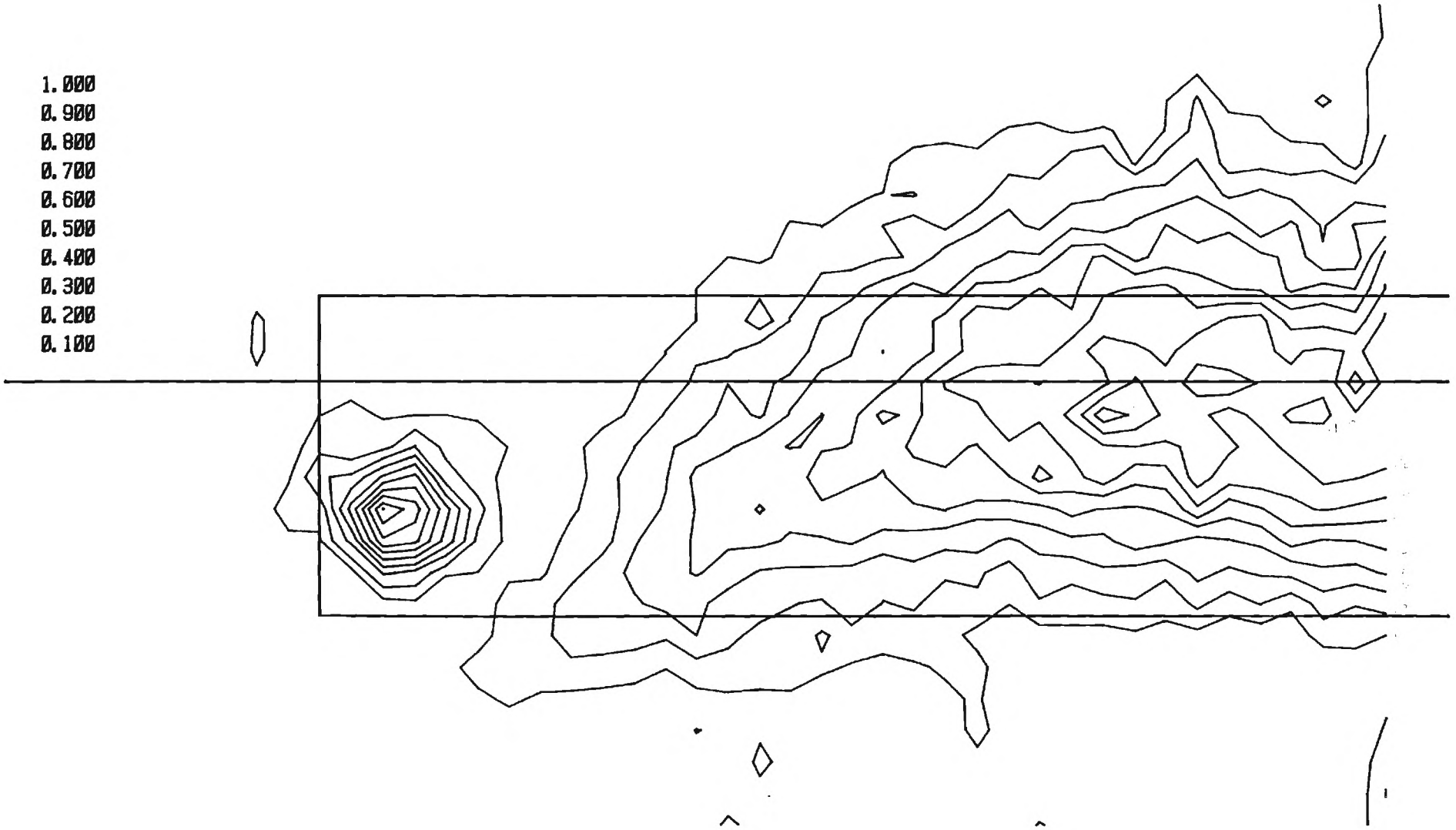

MP24

LOCKHEED-GEORGIA COMPANY - RESEARCH CENTER - TEST 64-06

WING - 18 DEG - 18 INS

TOTAL PRESSURE DEFICIT (HO-P)/QO

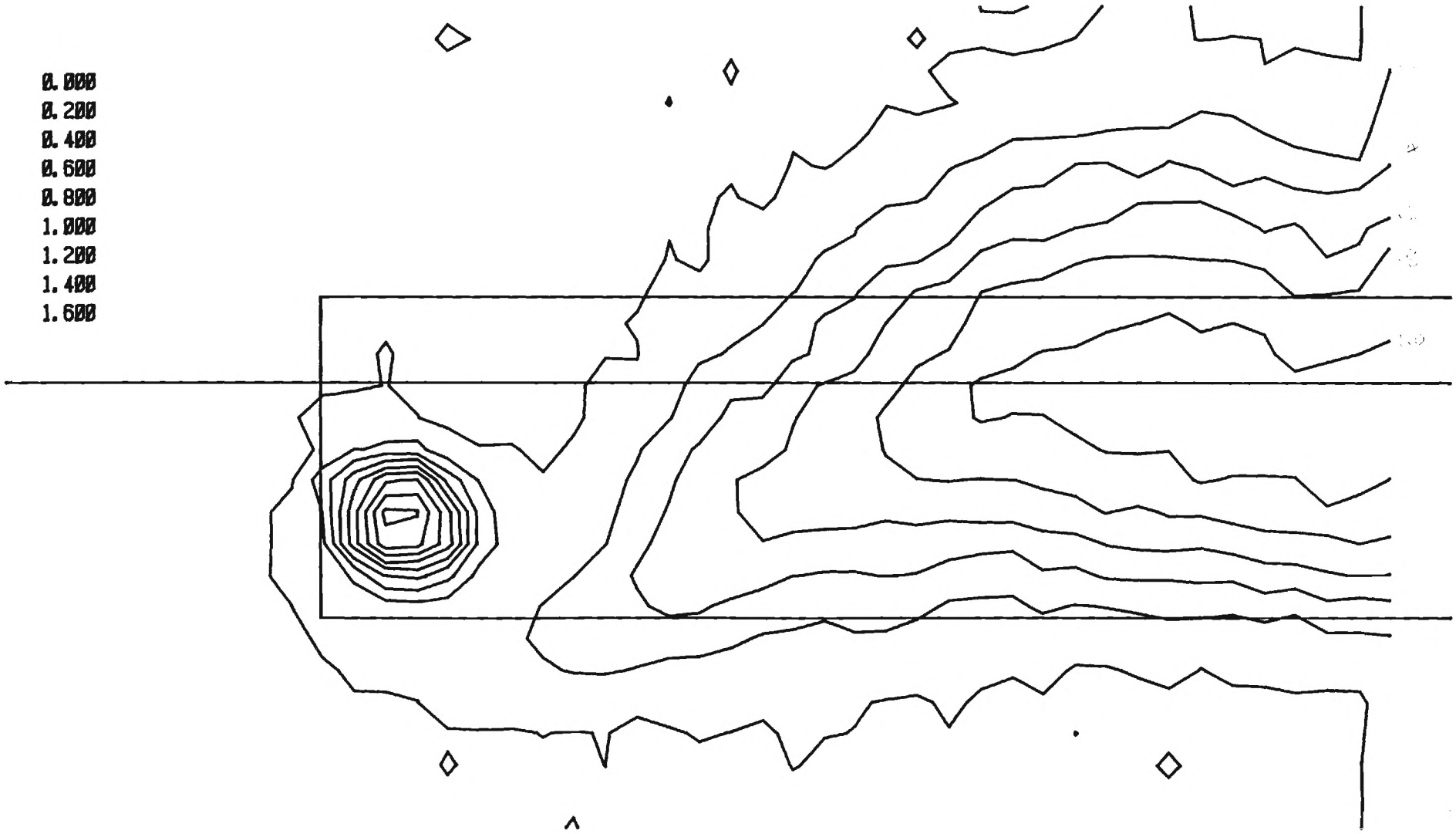

MP25

LOCKHEED-GEORGIA COMPANY - RESEARCH CENTER - TEST 64-06

WING - 18 DEG - 18 INS CROSS-FLOW KINETIC ENERGY (VC*VC)/(UO*UO)

MP26

LOCKHEED-GEORGIA COMPANY - RESEARCH CENTER - TEST 64-Ø6

WING - 18 DEG - 18 INS VORTICITY

NOTE

$(\frac{\xi c}{U_o})$ = (CONTOUR VALUE) x 576

-Ø.ØØ8
-Ø.ØØ4
-Ø.ØØ2
Ø.ØØ2
Ø.ØØ4
Ø.ØØ8
Ø.Ø12
Ø.Ø16
Ø.Ø20
Ø.Ø24
Ø.Ø28

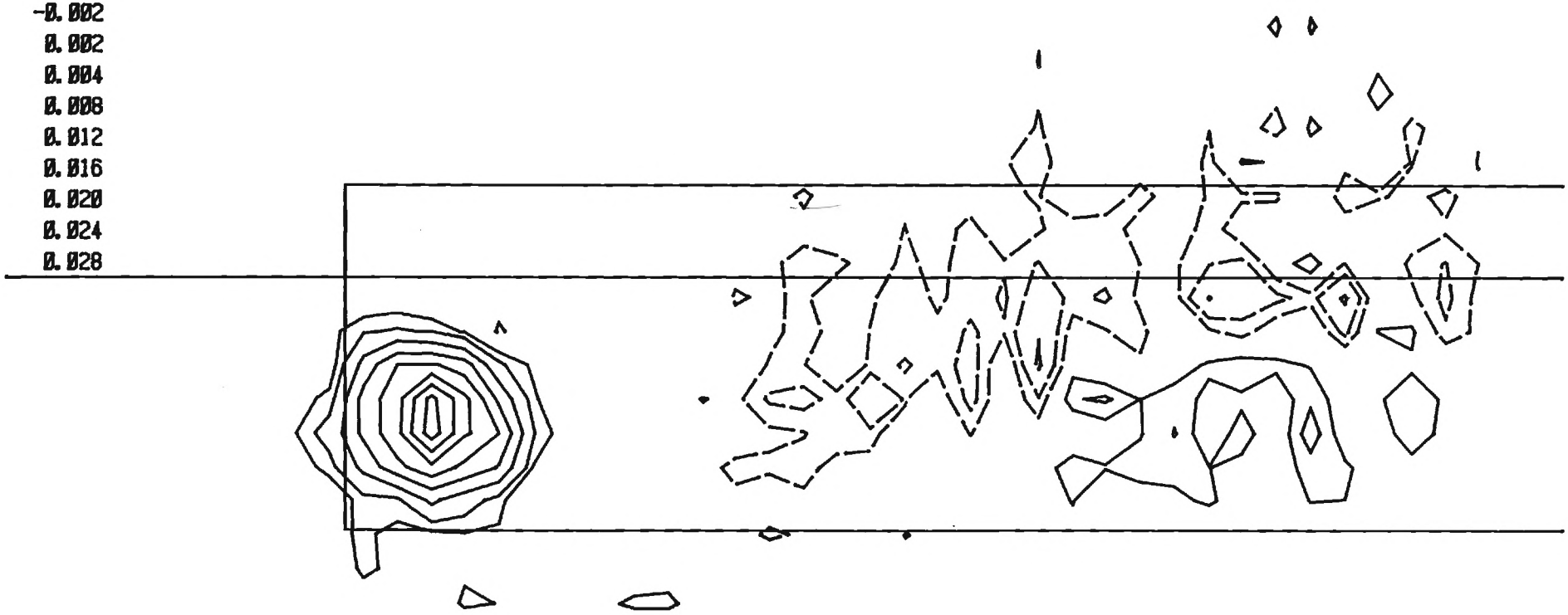

LOCKHEED-GEORGIA COMPANY - RESEARCH CENTER - TEST 64-06

WING - 18 DEG - 18 INS CORR LAT VELOCITY V/UO

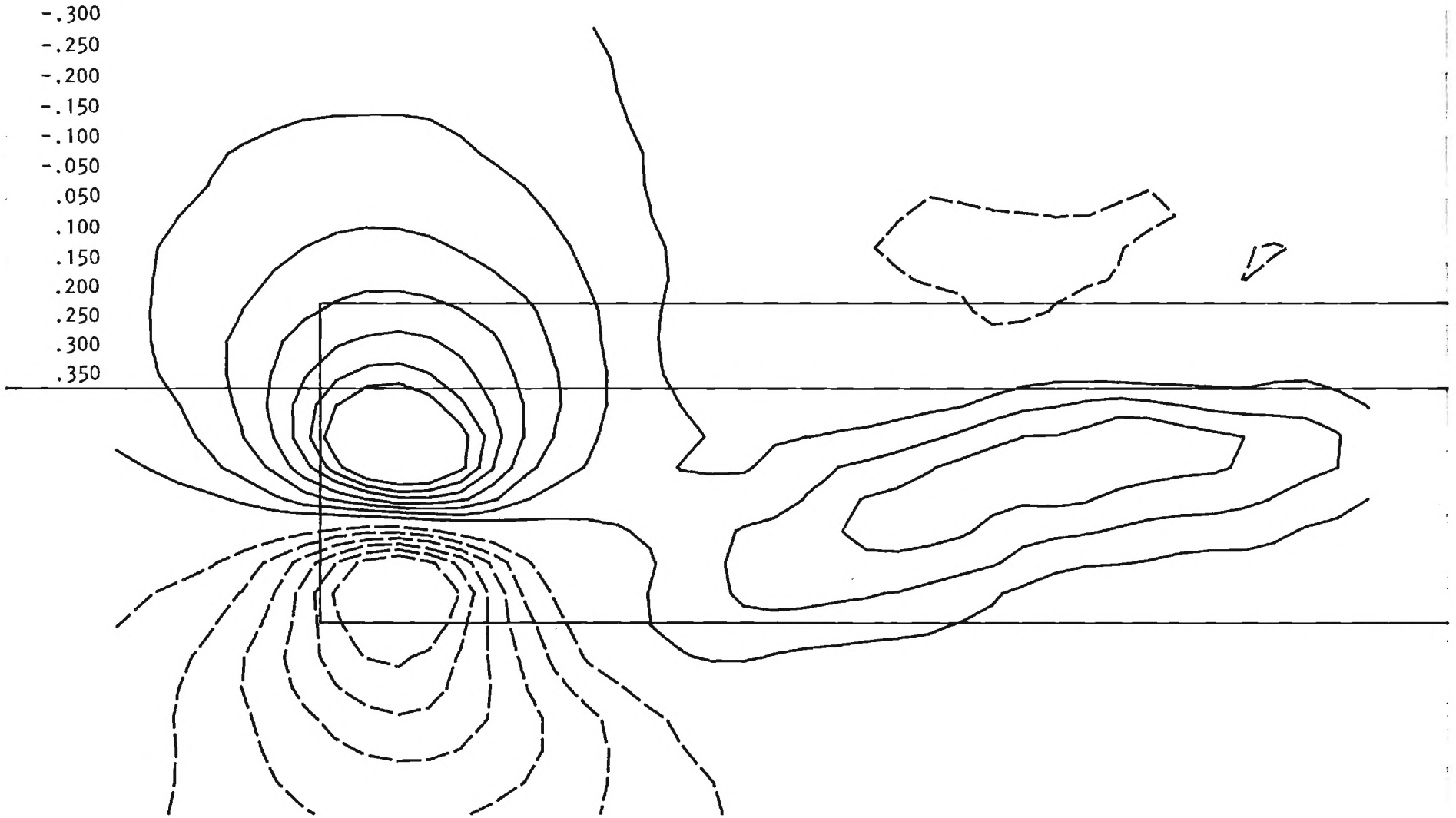

MP28

LOCKHEED-GEORGIA COMPANY - RESEARCH CENTER - TEST 64-Ø6

WING - 18 DEG - 18 INS CORR VERT VELOCITY W/UO

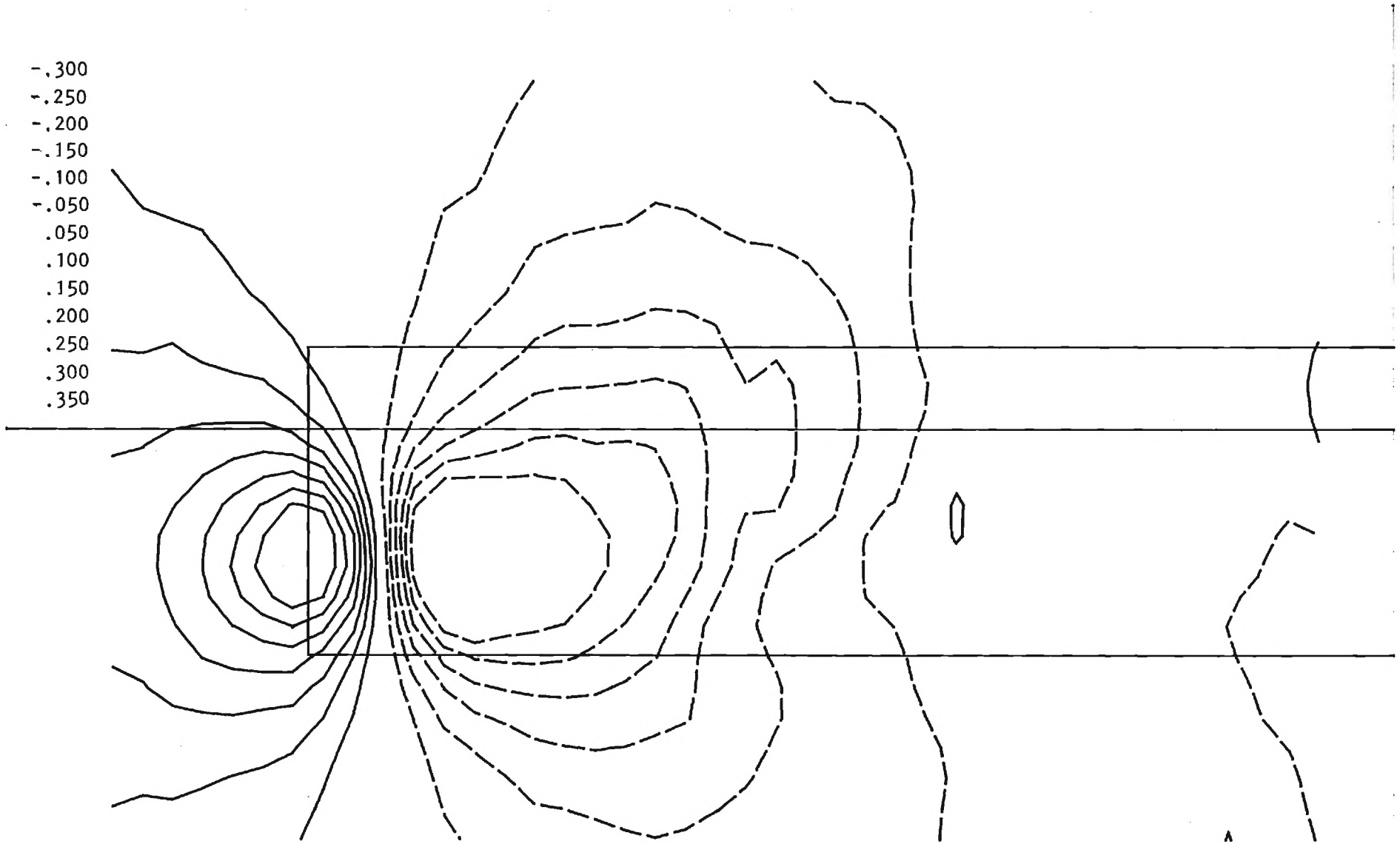

MP29

LOCKHEED-GEORGIA COMPANY - RESEARCH CENTER - TEST 64-06

WING - 18 DEG - 18 INS

STREAM FUNCTIONS

NOTE

$(\frac{\psi}{U_O c})$ = (CONTOUR VALUE) x 1.0

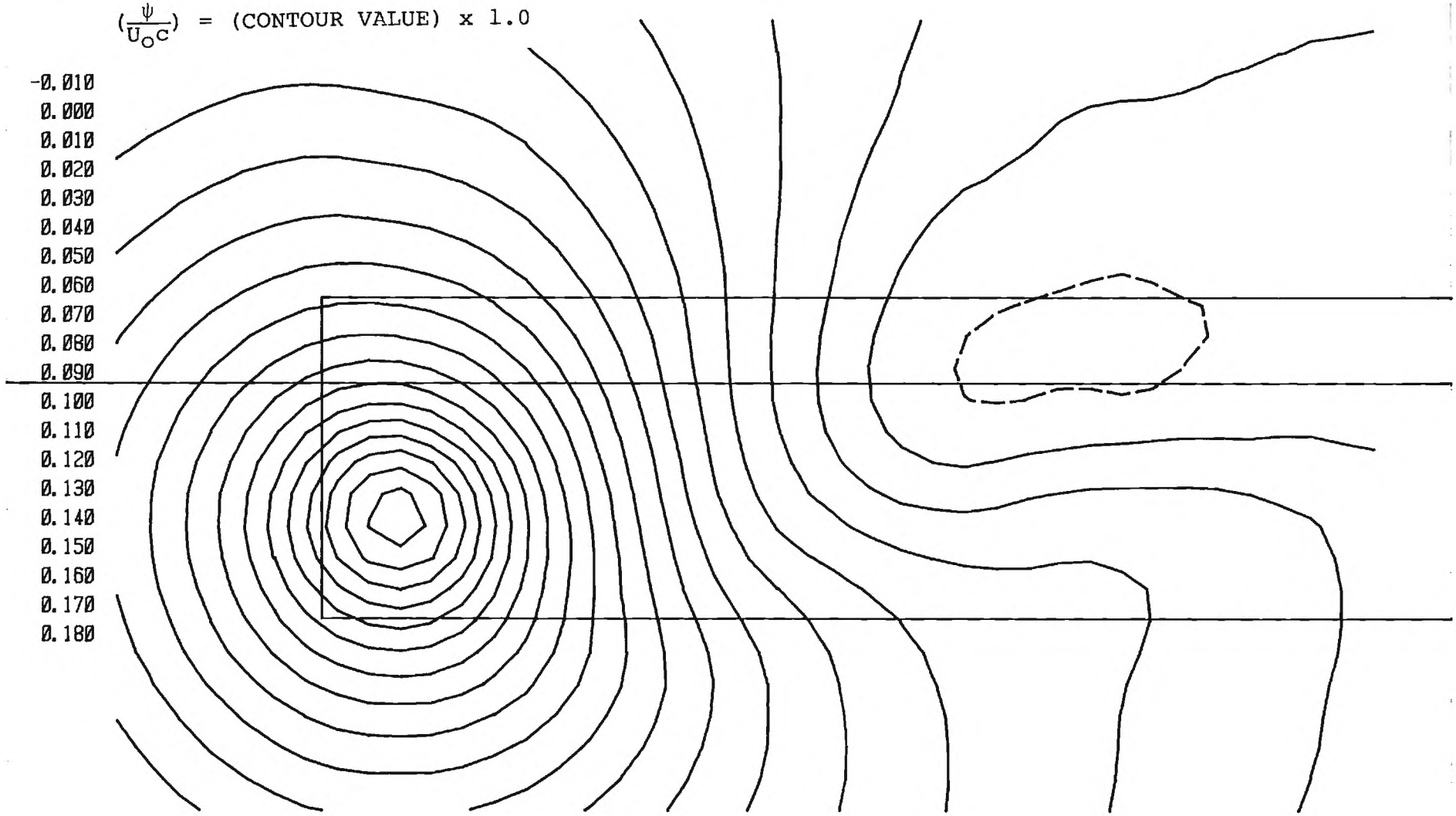

MP30

LOCKHEED-GEORGIA COMPANY - RESEARCH CENTER - TEST 64-07

WING - 18 DEG - 36 INS

CROSSFLOW VELOCITY VC/UO

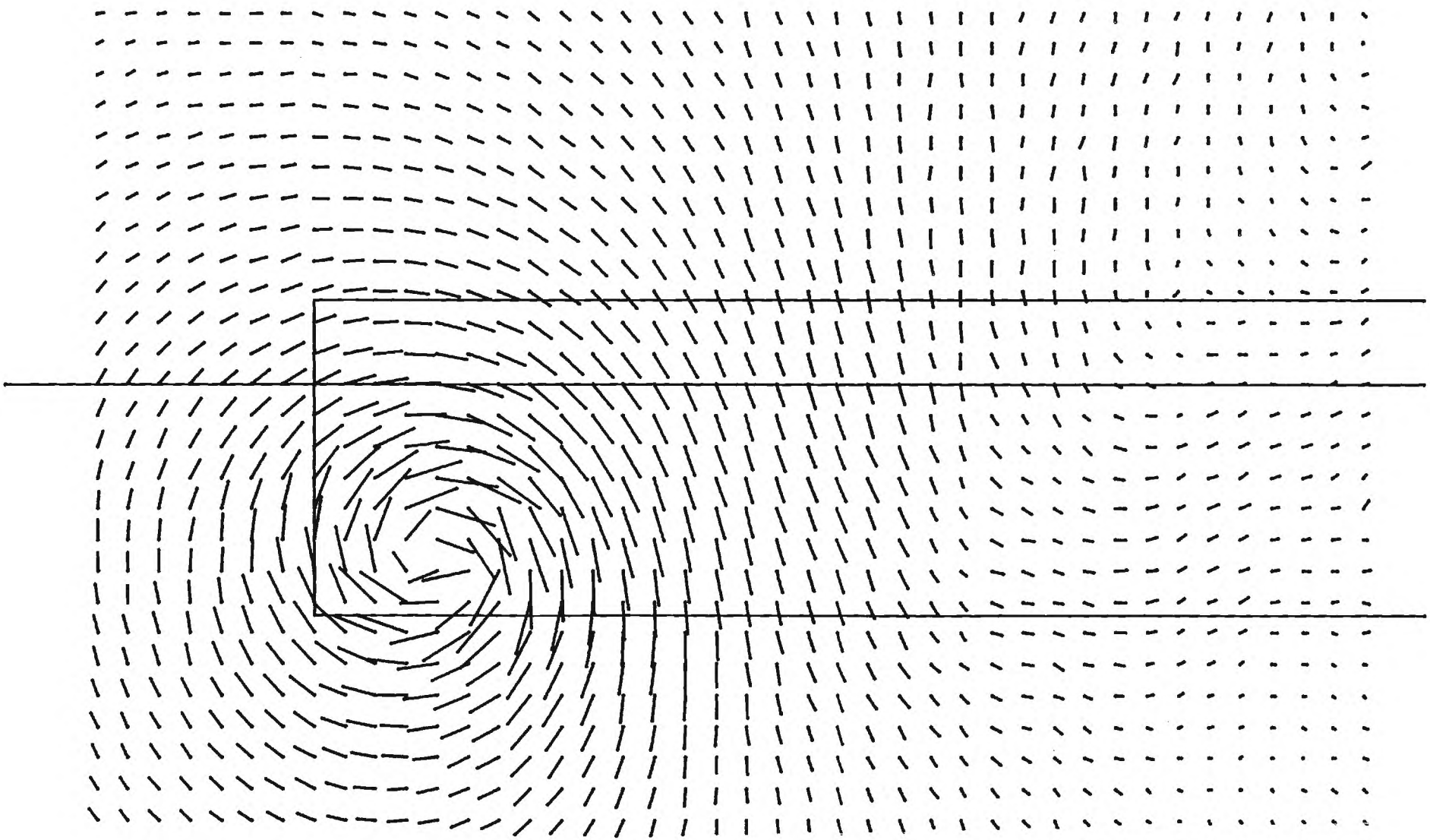

MP31

LOCKHEED-GEORGIA COMPANY - RESEARCH CENTER - TEST 64-07

WING - 18 DEG - 36 INS

LAT. VELOCITY RATIO V/U0

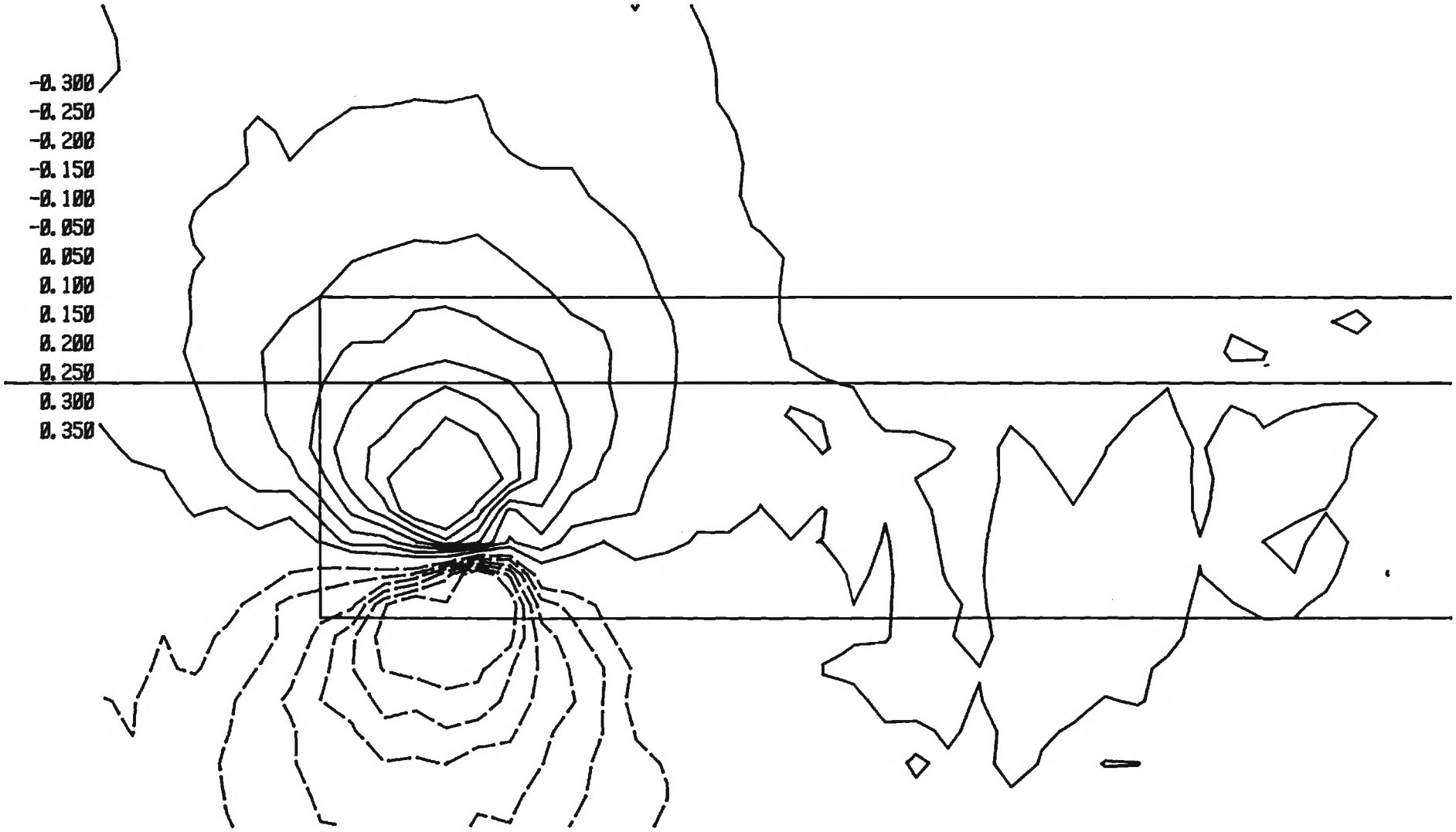

MP32

LOCKHEED-GEORGIA COMPANY - RESEARCH CENTER - TEST 64-07

WING - 18 DEG - 36 INS

VERT. VELOCITY RATIO W/U0

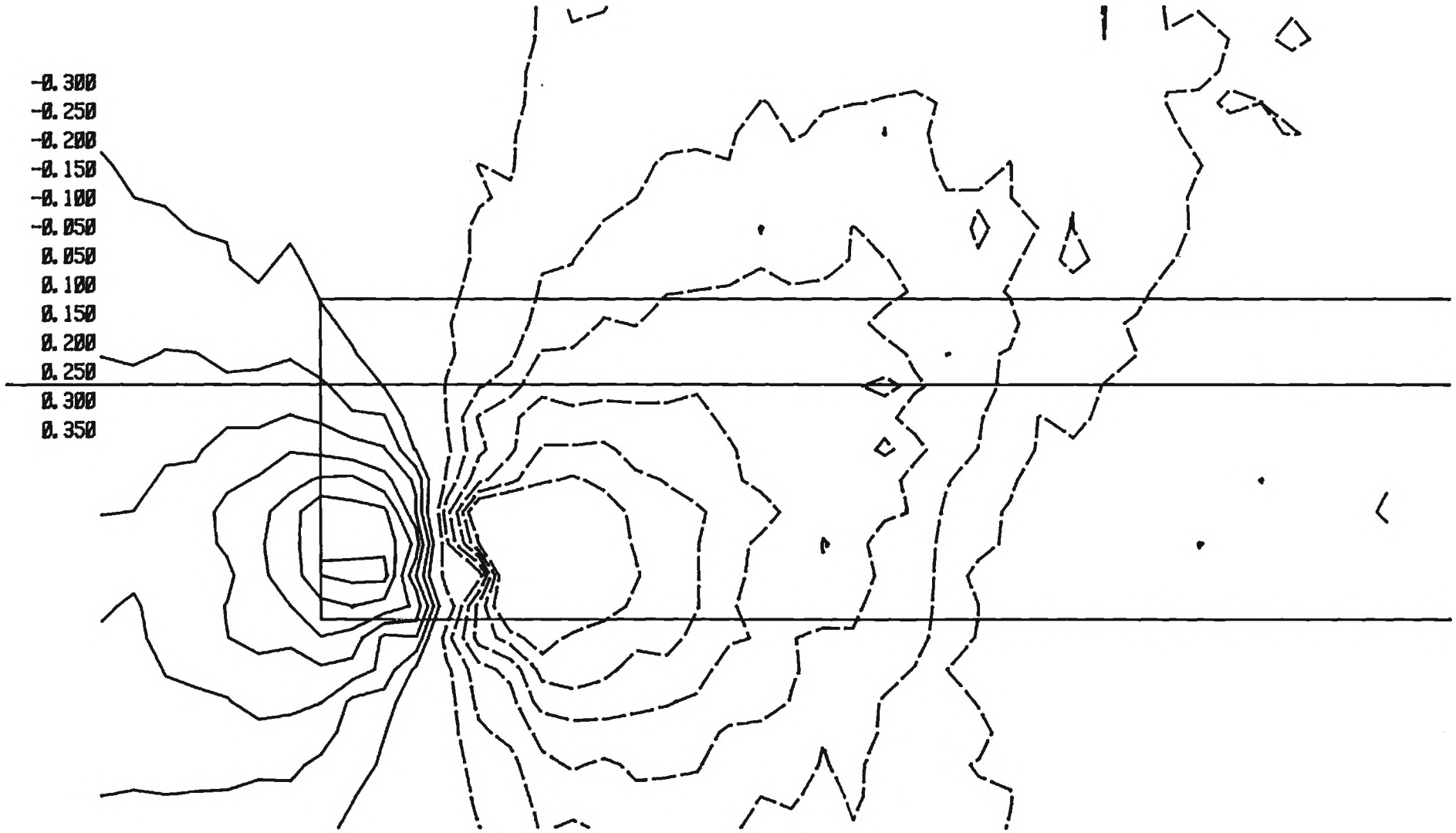

MP33

LOCKHEED-GEORGIA COMPANY - RESEARCH CENTER - TEST 64-07

WING - 18 DEG - 36 INS

AXIAL VELOCITY RATIO U/UO

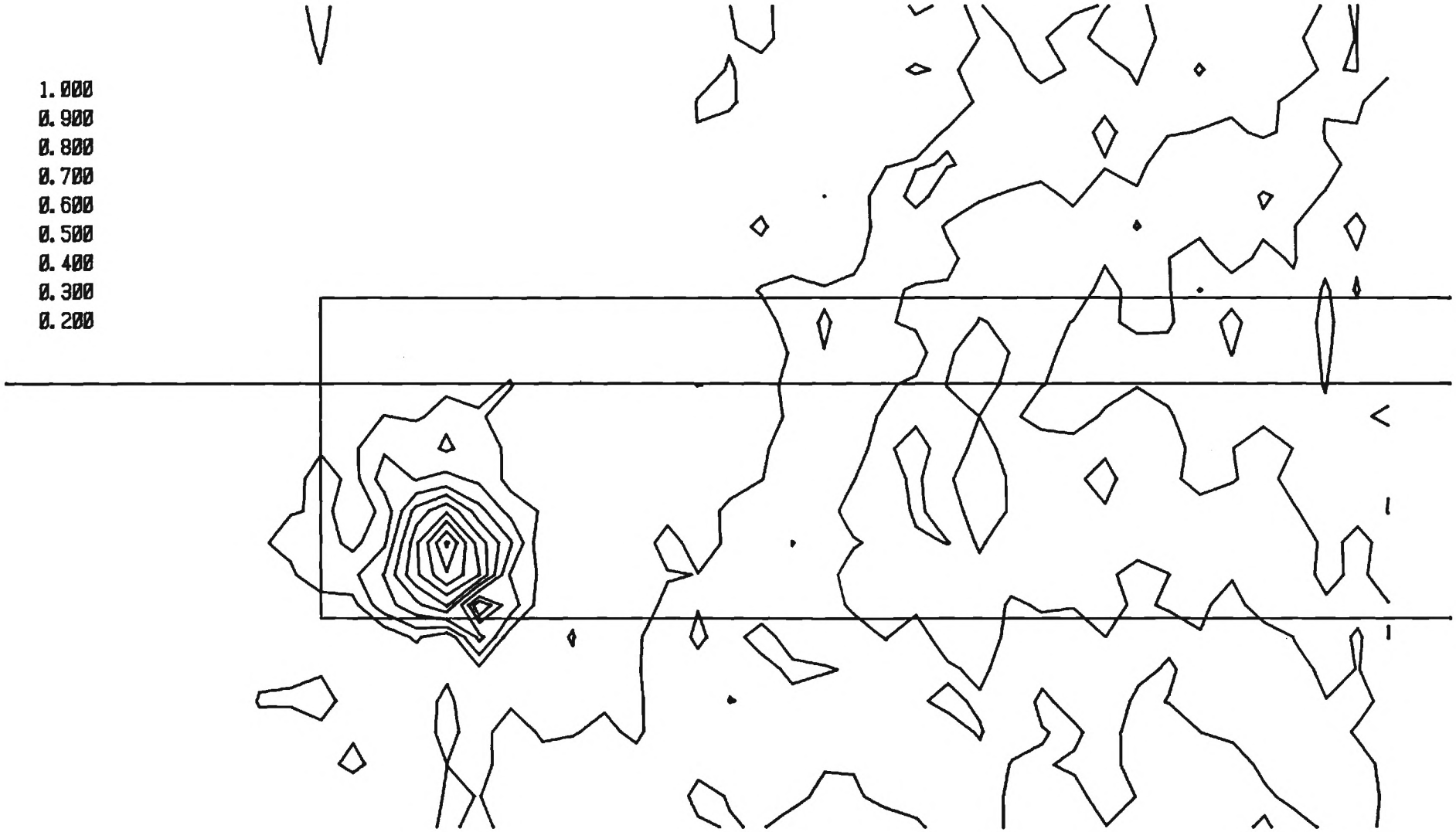

MP34

LOCKHEED-GEORGIA COMPANY - RESEARCH CENTER - TEST 64-07

WING - 18 DEG - 36 INS

TOTAL PRESSURE DEFICIT (HO-P)/QO

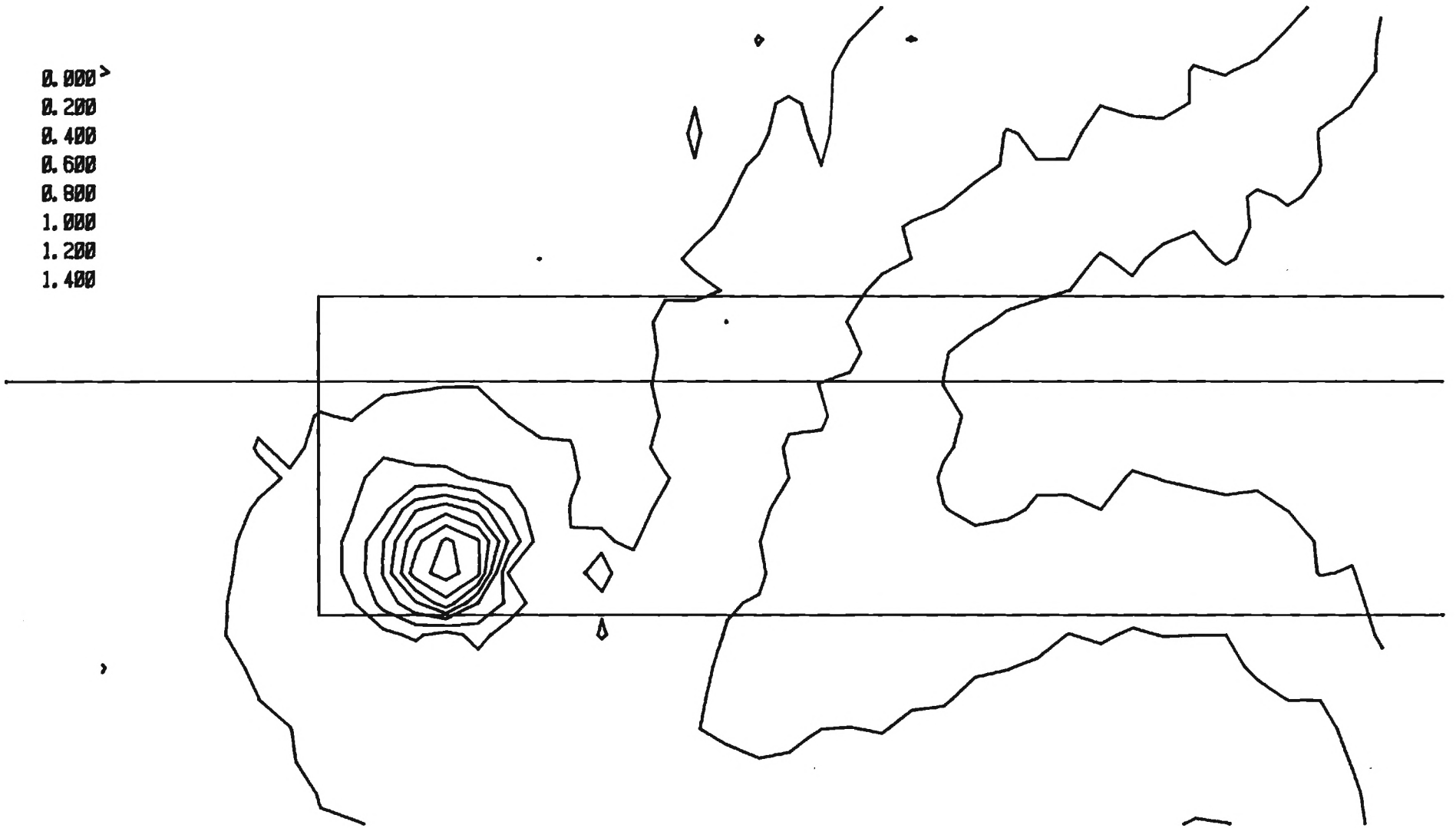

MP35

LOCKHEED-GEORGIA COMPANY - RESEARCH CENTER - TEST 64-07

WING - 18 DEG - 36 INS CROSS-FLOW KINETIC ENERGY (VC*VC)/(UO*UO)

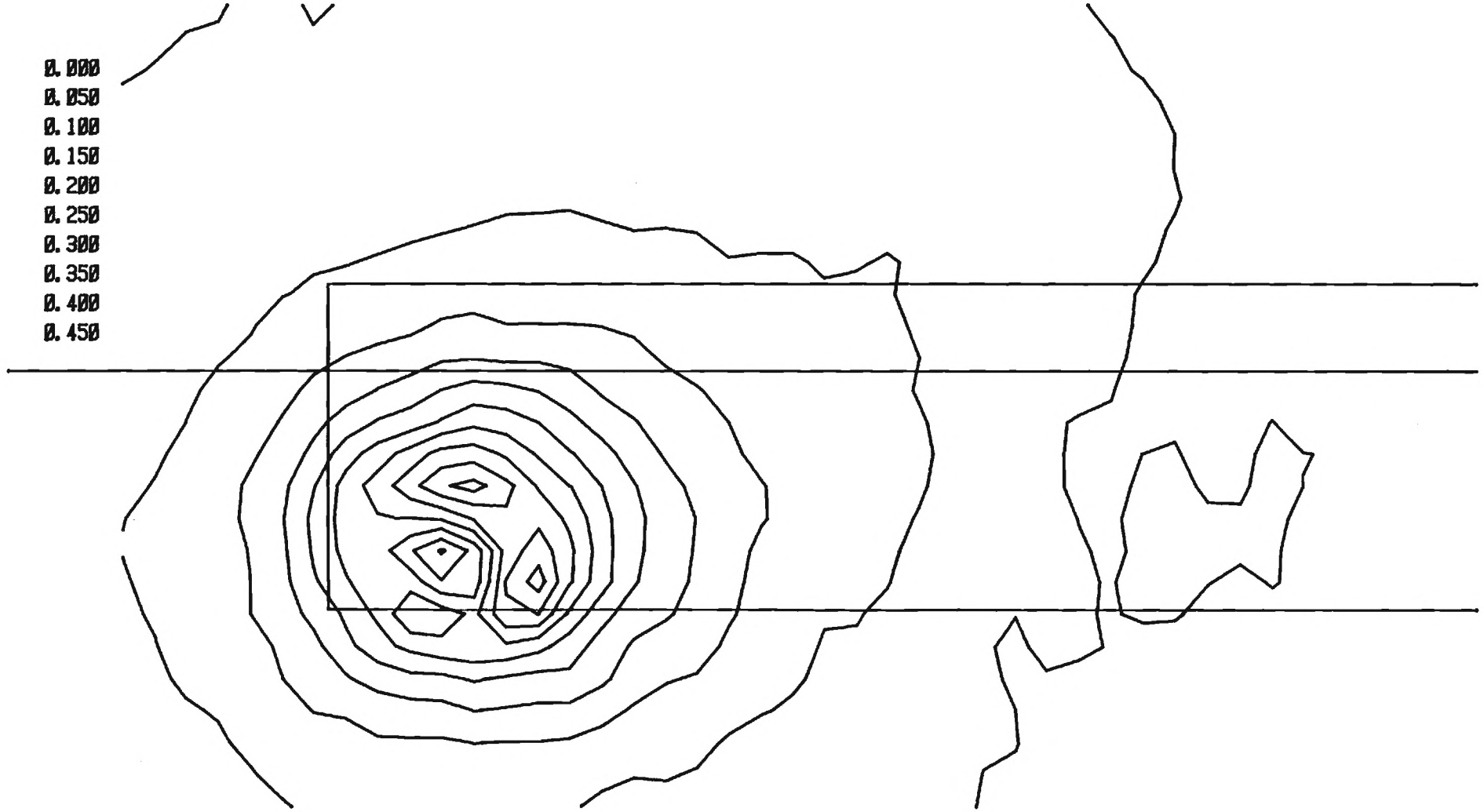

MP36

LOCKHEED-GEORGIA COMPANY - RESEARCH CENTER - TEST 64-07

WING - 18 DEG - 36 INS VORTICITY

NOTE

$(\frac{\xi c}{U_o})$ = (CONTOUR VALUE) x 576

-0.002
0.002
0.004
0.008
0.012
0.016
0.020
0.024
0.028

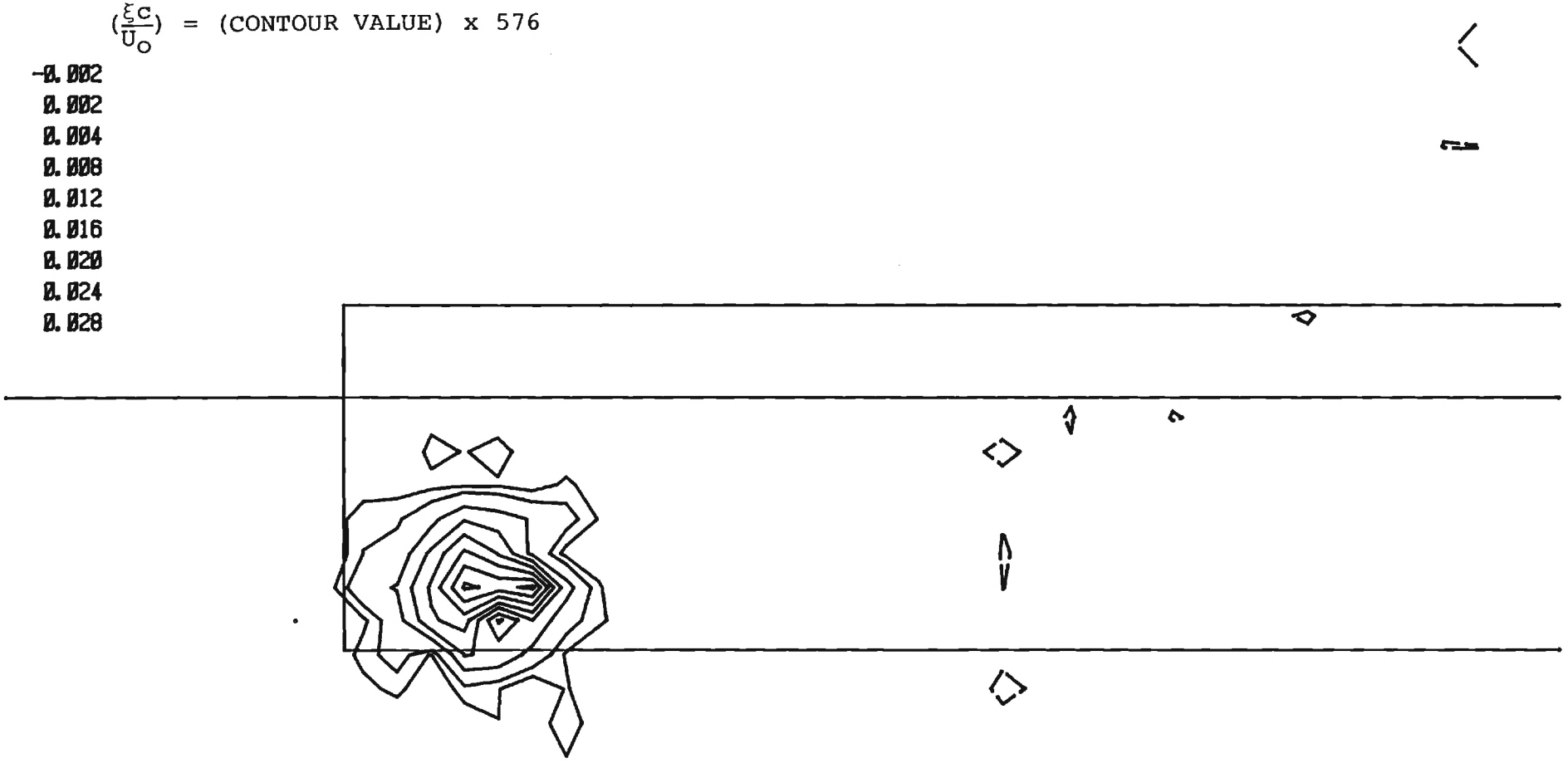

LOCKHEED-GEORGIA COMPANY - RESEARCH CENTER - TEST 64-Ø7

WING - 18 DEG - 36 INS CORR LAT VELOCITY V/UO

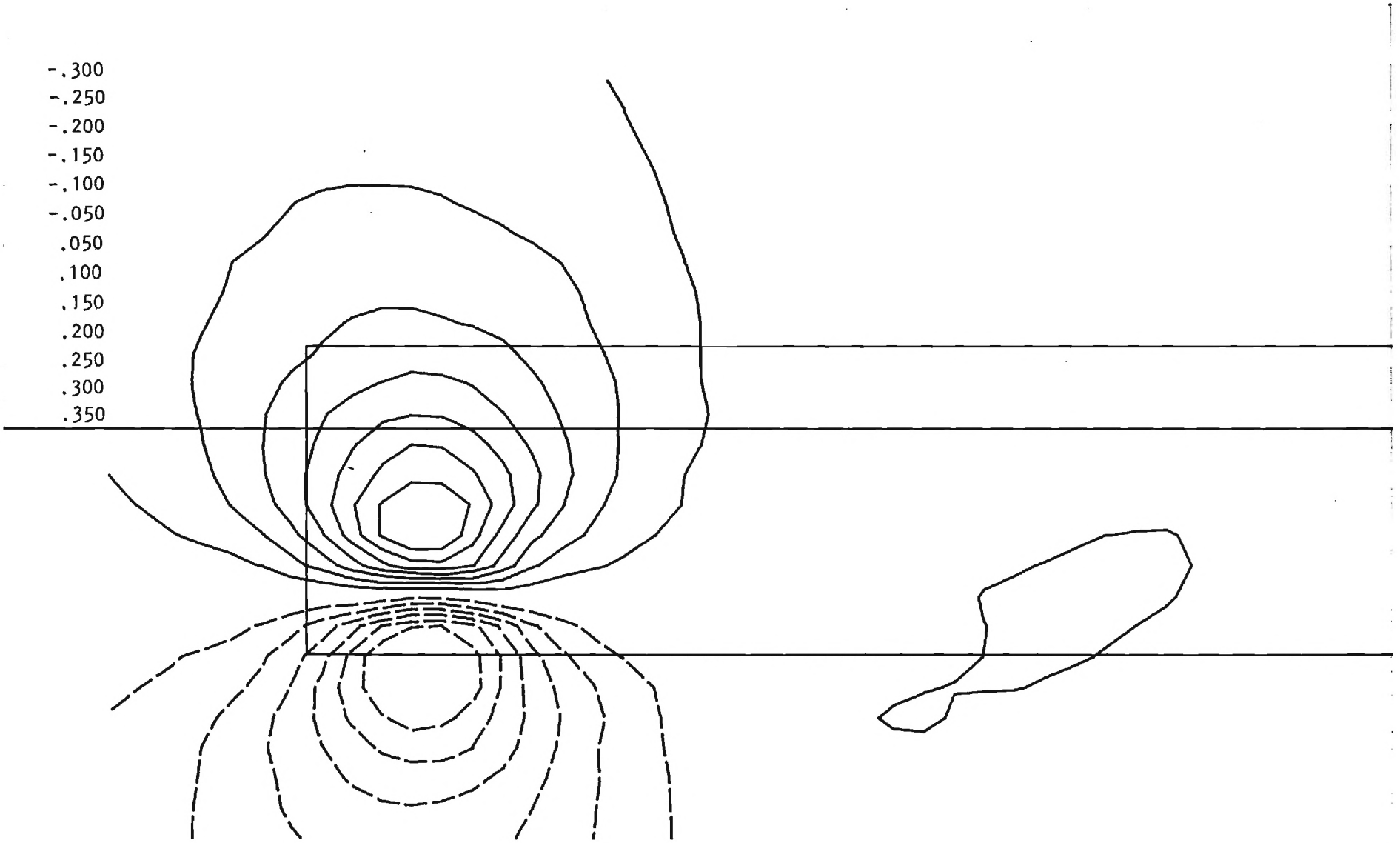

MP38

LOCKHEED-GEORGIA COMPANY - RESEARCH CENTER - TEST 64-07

WING - 18 DEG - 36 INS CORR VERT VELOCITY W/UO

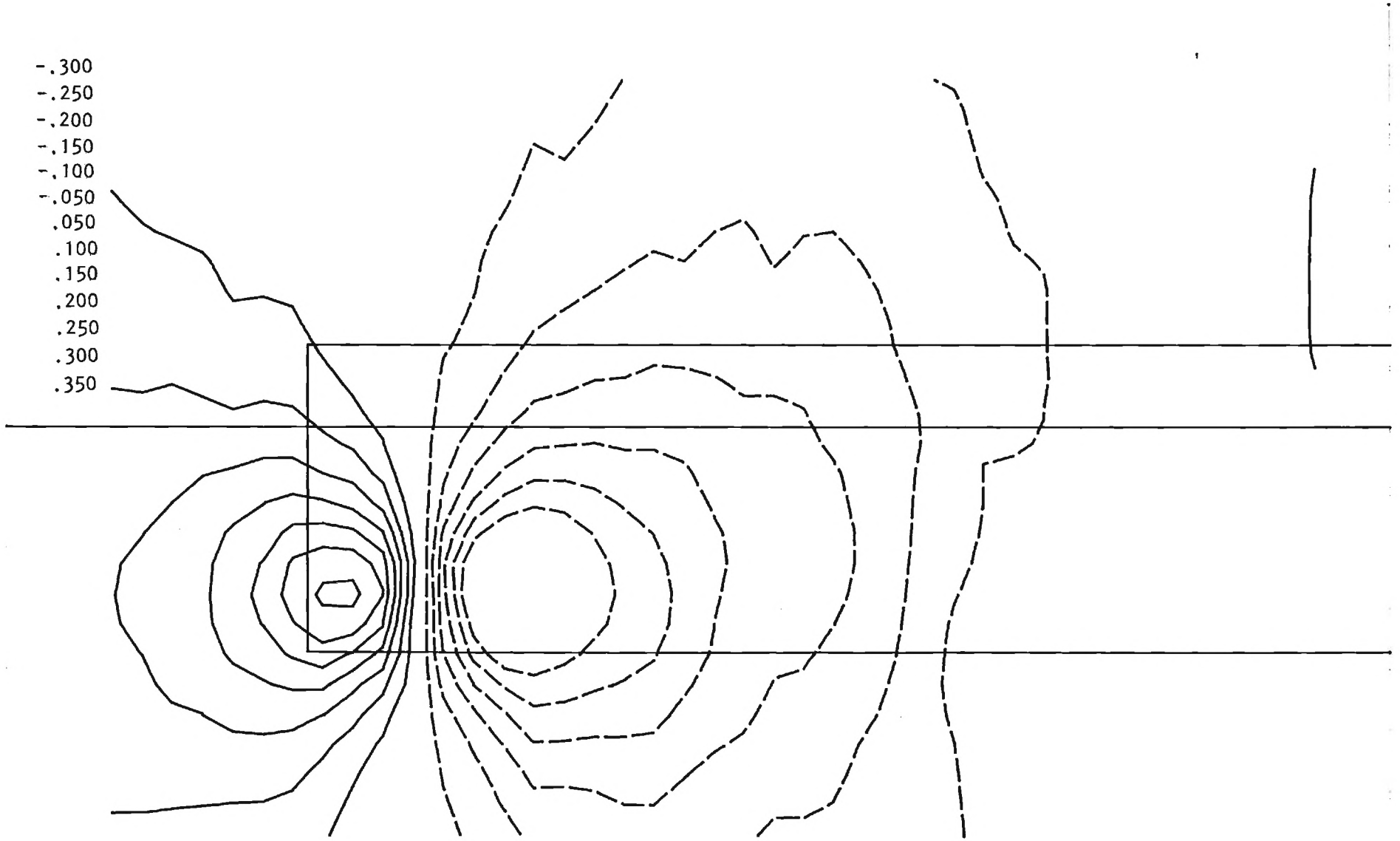

MP39

LOCKHEED-GEORGIA COMPANY - RESEARCH CENTER - TEST 64-07

WING - 18 DEG - 36 INS

STREAM FUNCTIONS

NOTE

$(\frac{\psi}{U_o c})$ = (CONTOUR VALUE) x 1.0

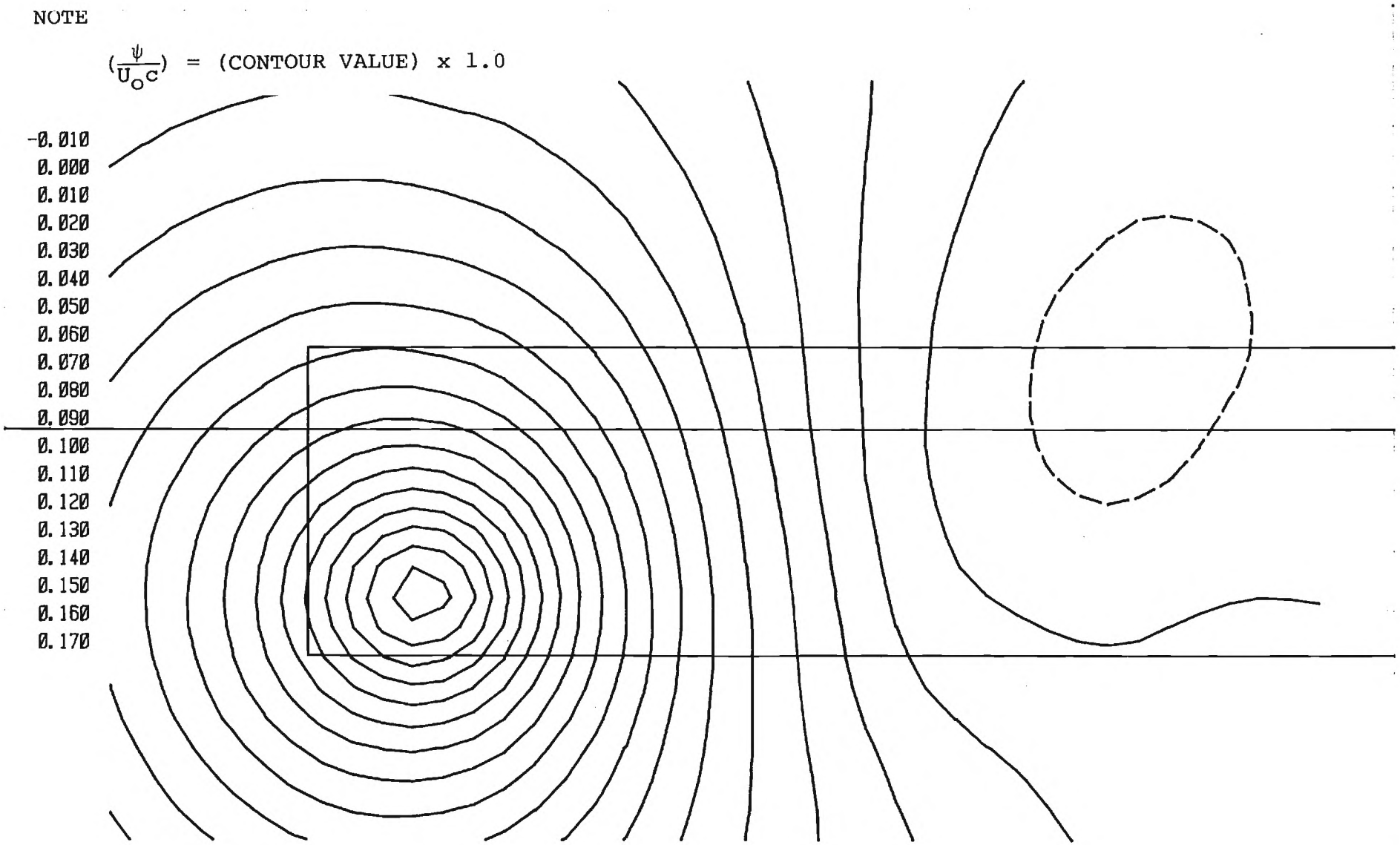

MP40

LOCKHEED-GEORGIA COMPANY - RESEARCH CENTER - TEST 64-04

S. A. S. - 0.0 DEG - 18 INS

CROSSFLOW VELOCITY VC/UO

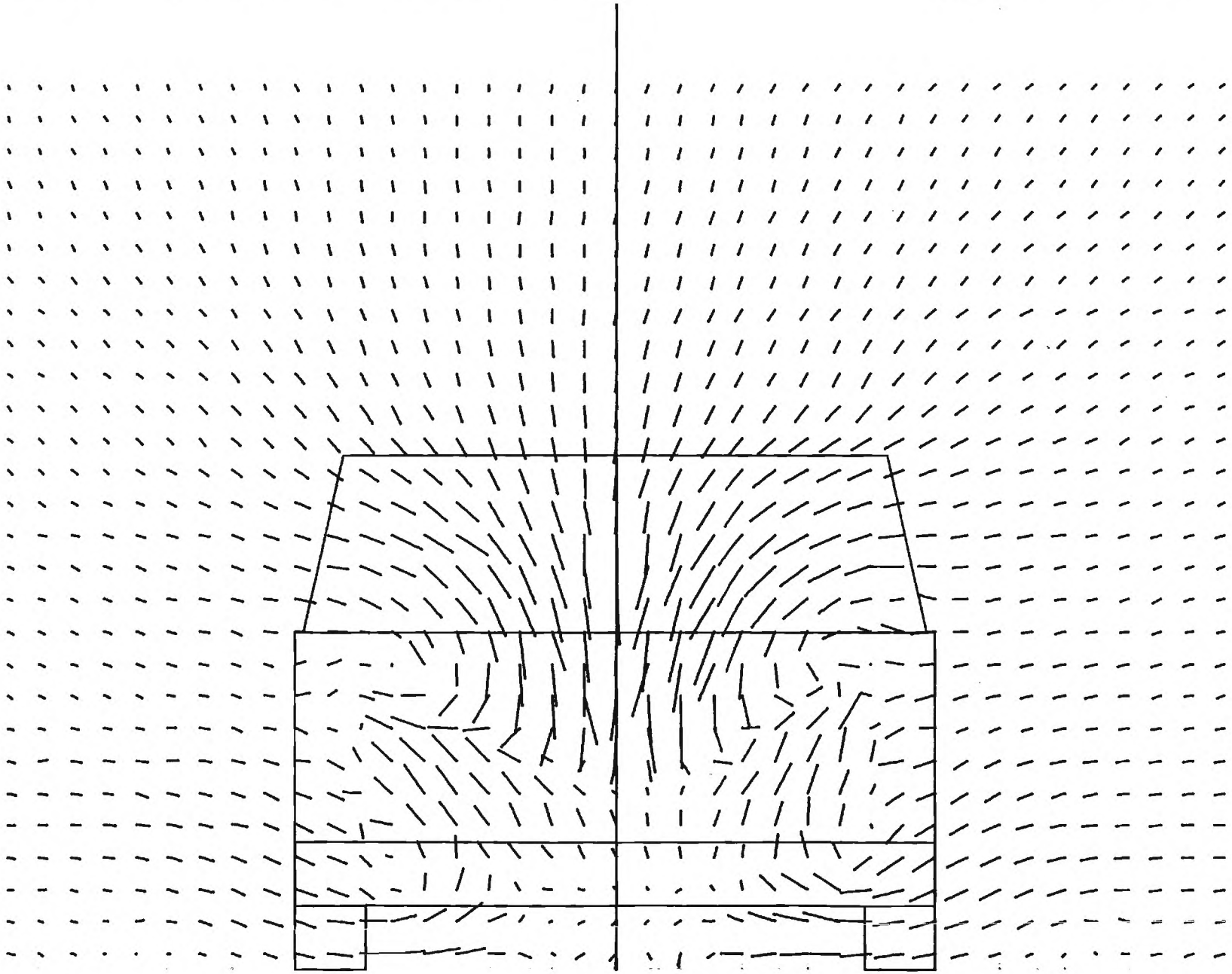

MP41

LOCKHEED-GEORGIA COMPANY - RESEARCH CENTER - TEST 64-04

S. A. S. - 0.0 DEG - 18 INS

LAT. VELOCITY RATIO V/UO

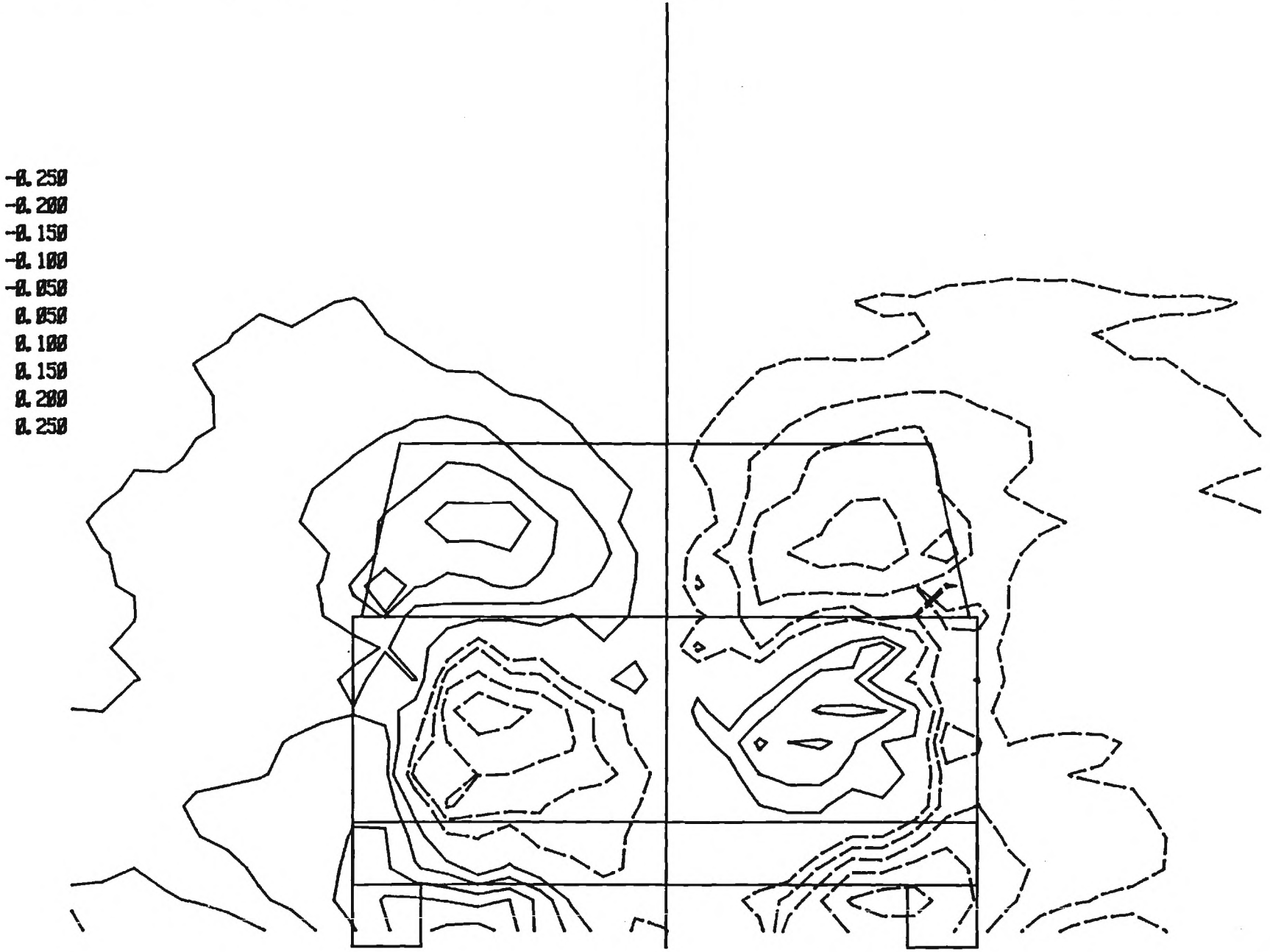

MP42

LOCKHEED-GEORGIA COMPANY - RESEARCH CENTER - TEST 64-04

S. A. S. - 0.0 DEG - 18 INS

VERT. VELOCITY RATIO W/U0

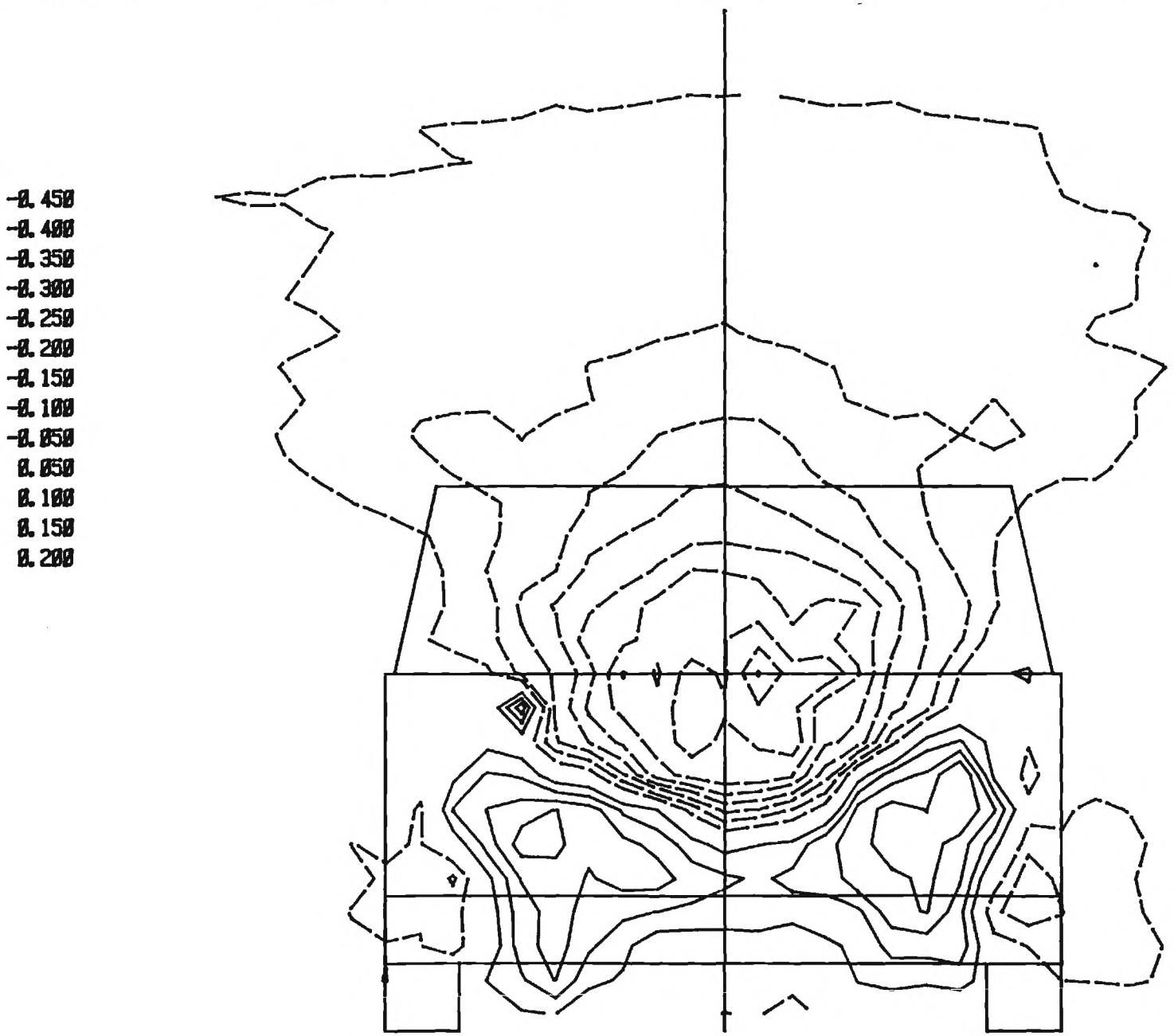

MP43

LOCKHEED-GEORGIA COMPANY - RESEARCH CENTER - TEST 64-Ø4

S. A. S. - Ø.Ø DEG - 18 INS

AXIAL VELOCITY RATIO U/UO

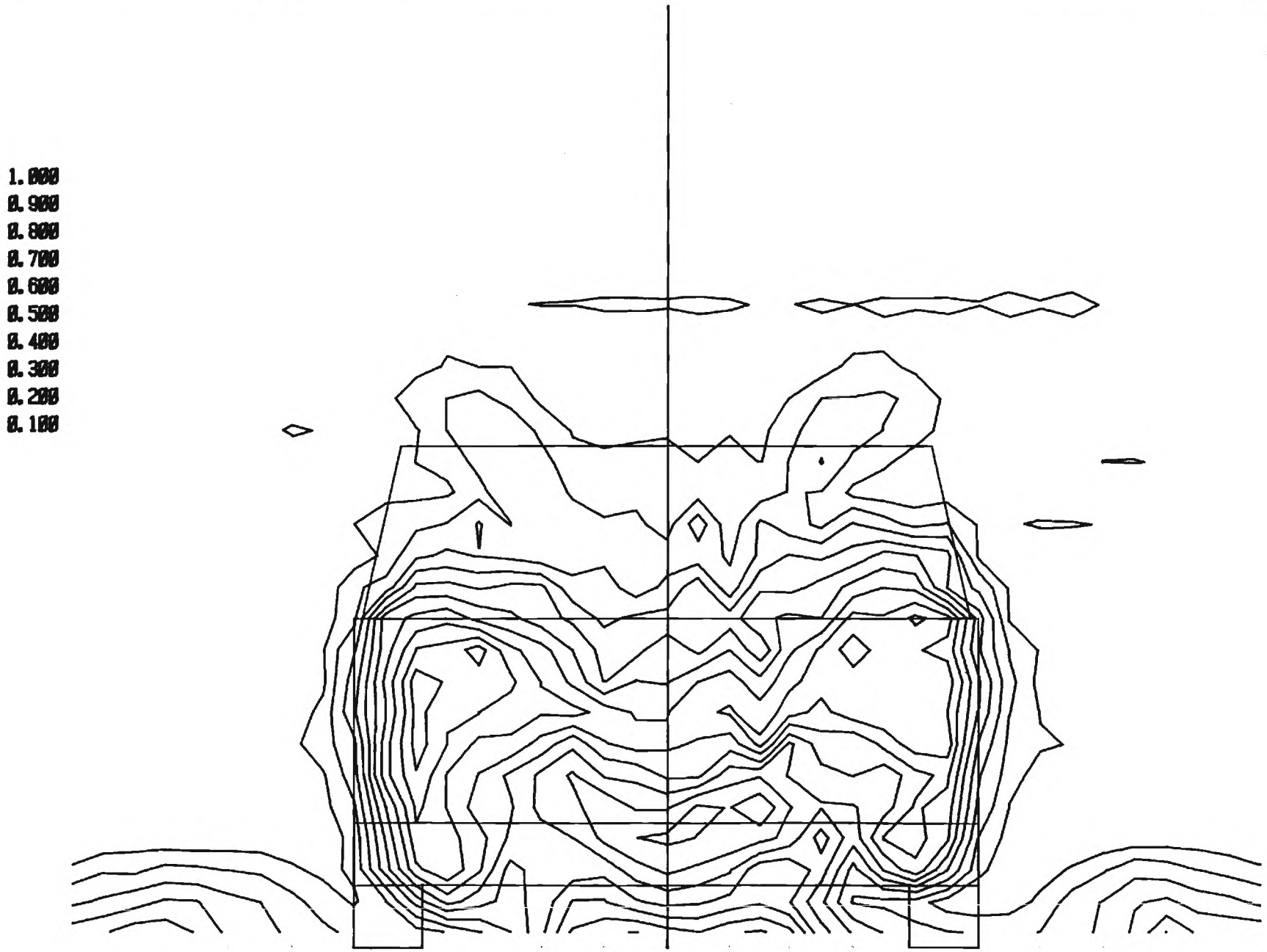

MP44

LOCKHEED-GEORGIA COMPANY - RESEARCH CENTER - TEST 64-04

S. A. S. - 0.0 DEG - 18 INS

TOTAL PRESSURE DEFICIT (HO-P)/QO

0.000
0.100
0.200
0.300
0.400
0.500
0.600
0.700
0.800
0.900
1.000

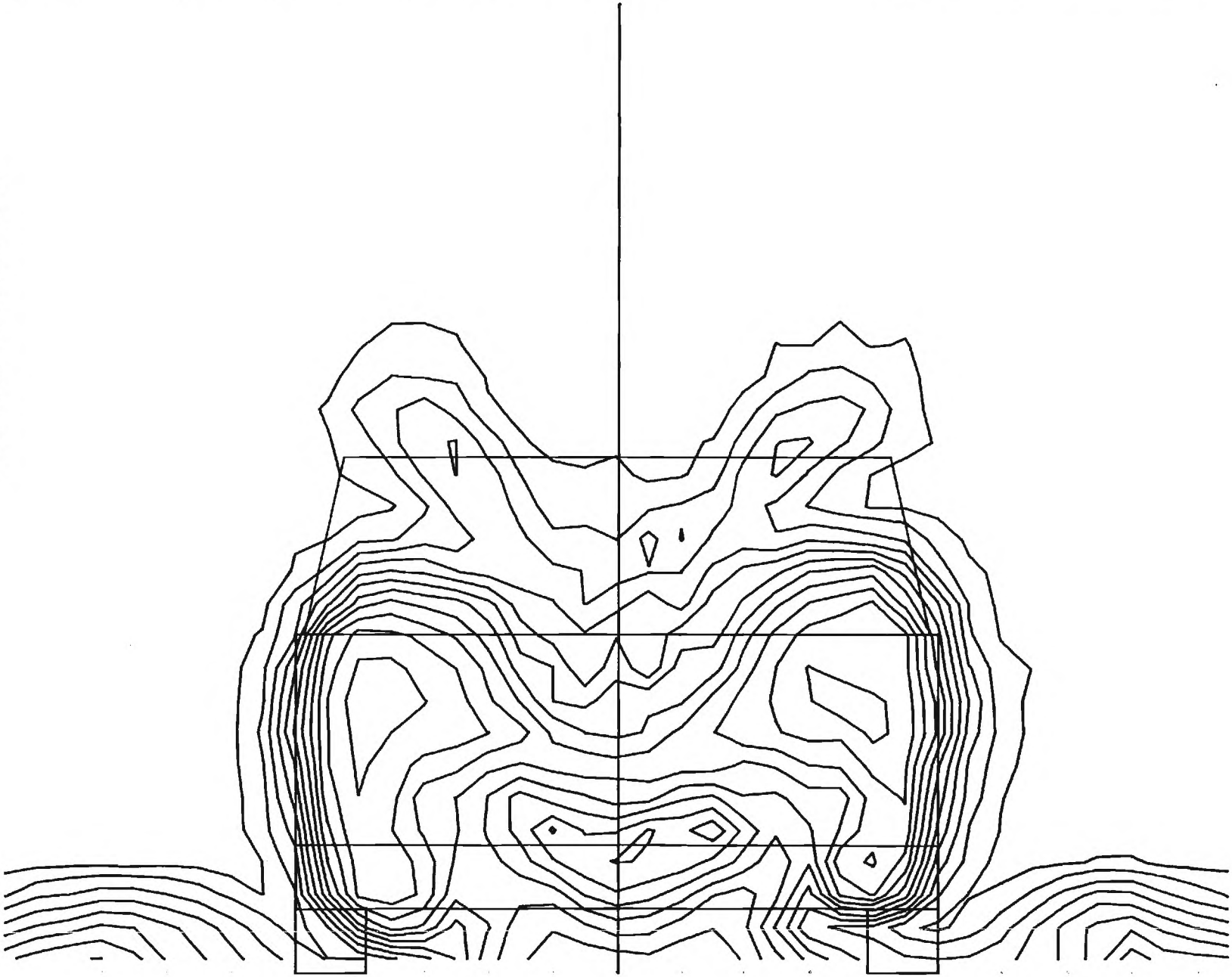

MP45

LOCKHEED-GEORGIA COMPANY - RESEARCH CENTER - TEST 64-04

S. A. S. - 0.0 DEG - 18 INS

CROSS-FLOW KINETIC ENERGY (VC*VC)/(UO*UO)

0.040
0.080
0.120
0.160
0.200
0.240
0.280
0.320

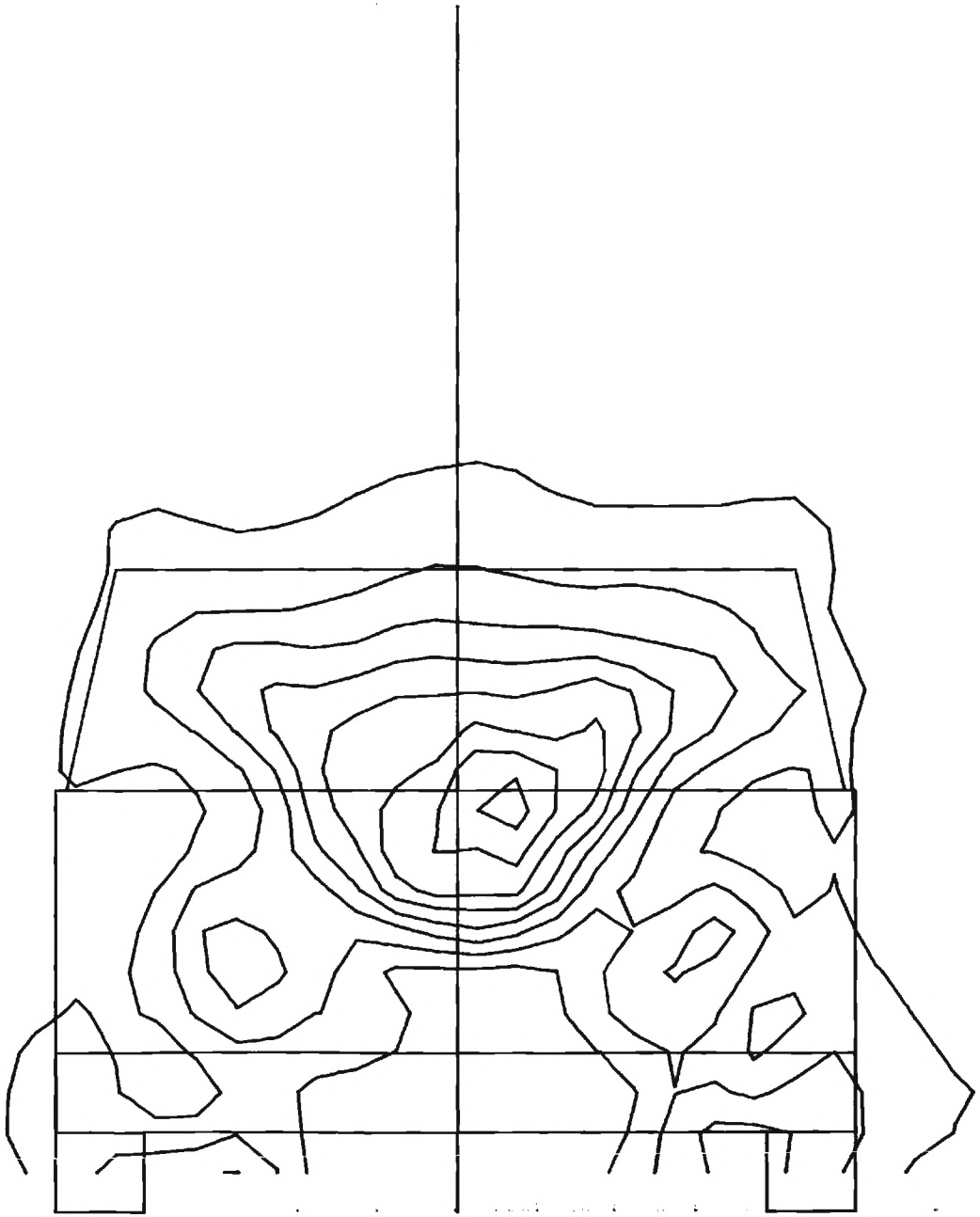

MP46

LOCKHEED-GEORGIA COMPANY - RESEARCH CENTER - TEST 64-Ø4

S. A. S. - Ø.Ø DEG - 18 INS VORTICITY

NOTE

$$\left(\frac{\xi \ell}{U_o}\right) = \text{(CONTOUR VALUE)} \times 739.2$$

where ℓ = wheelbase

-Ø.Ø12Ø
-Ø.Ø1ØØ
-Ø.ØØ8Ø
-Ø.ØØ6Ø
-Ø.ØØ4Ø
-Ø.ØØ2Ø
Ø.ØØ2Ø
Ø.ØØ4Ø
Ø.ØØ6Ø
Ø.ØØ8Ø
Ø.Ø1ØØ
Ø.Ø12Ø
Ø.Ø14Ø

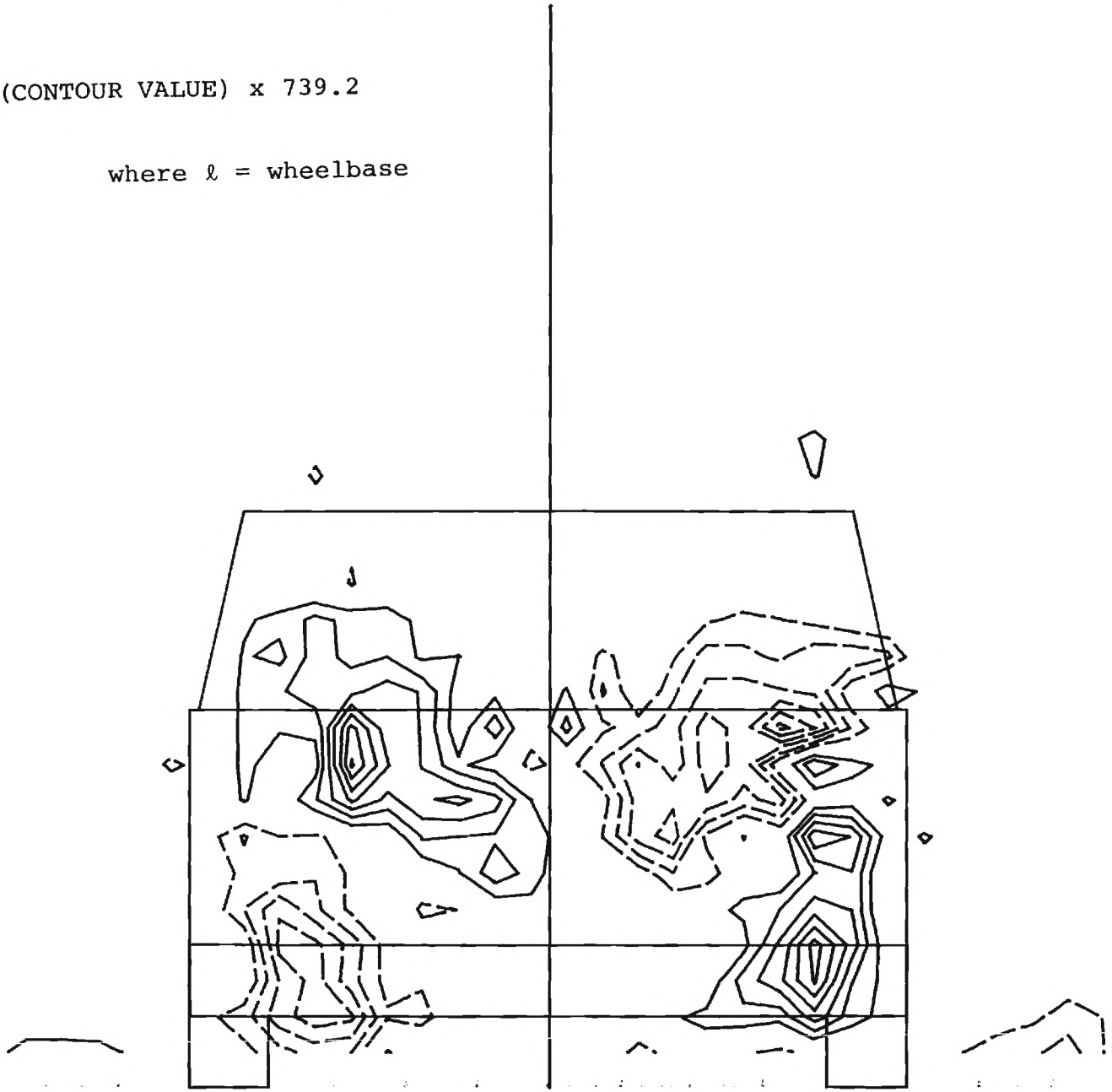

MP47

LOCKHEED-GEORGIA COMPANY - RESEARCH CENTER - TEST 64-Ø4

S. A. S. - Ø.Ø DEG - 18 INS CORR LAT VELOCITY V/UO

-.250
-.200
-.150
-.100
-.050
.050
.100
.150
.200

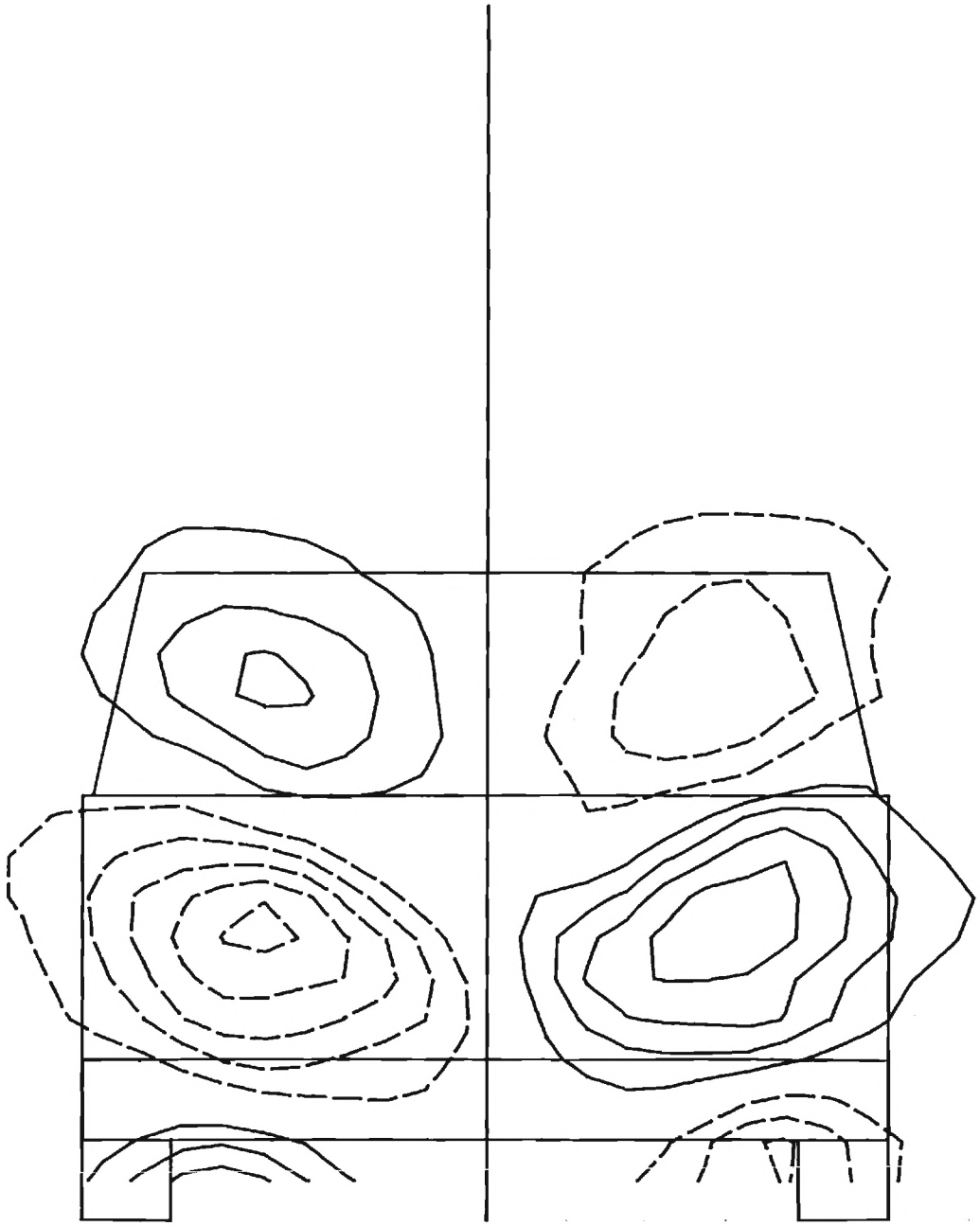

MP48

LOCKHEED-GEORGIA COMPANY - RESEARCH CENTER - TEST 64-Ø4

S. A. S. - Ø.Ø DEG - 18 INS

CORR VERT VELOCITY W/UO

-.250
-.200
-.150
-.100
-.050
.050
.100
.150

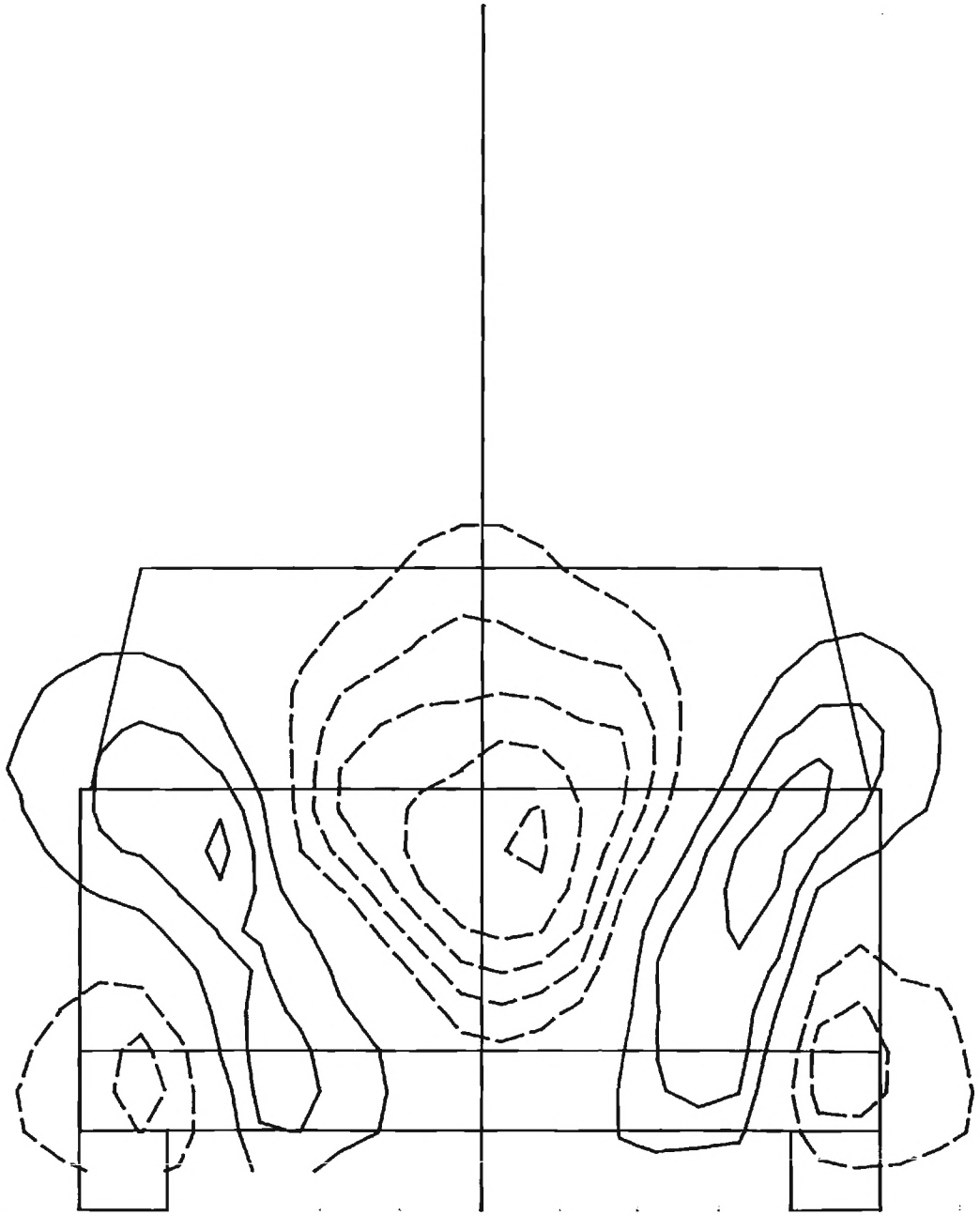

MP49

LOCKHEED-GEORGIA COMPANY - RESEARCH CENTER - TEST 64-04

S. A. S. - 0.0 DEG - 18 INS

STREAM FUNCTIONS

NOTE

$$\left(\frac{\psi}{U_o \ell}\right) = \text{(CONTOUR VALUE)} \times 0.7792$$

where ℓ = wheelbase

-0.030
-0.025
-0.020
-0.015
-0.010
-0.005
0.000
0.005
0.010
0.015
0.020
0.025
0.030

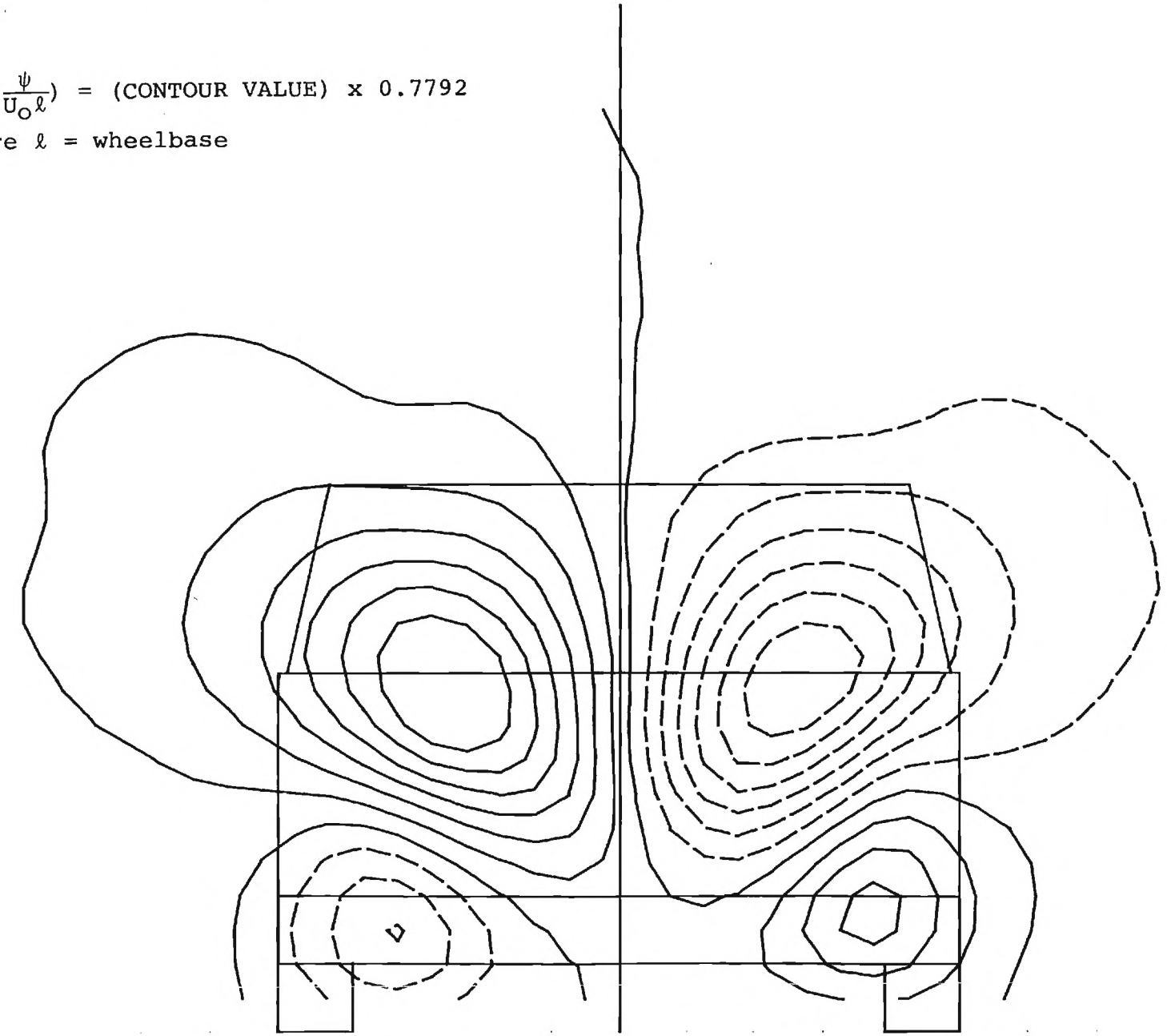

MP50

LOCKHEED-GEORGIA COMPANY - RESEARCH CENTER - TEST 64-03

S. A. S. - 0.0 DEG - 36 INS

CROSSFLOW VELOCITY VC/UO

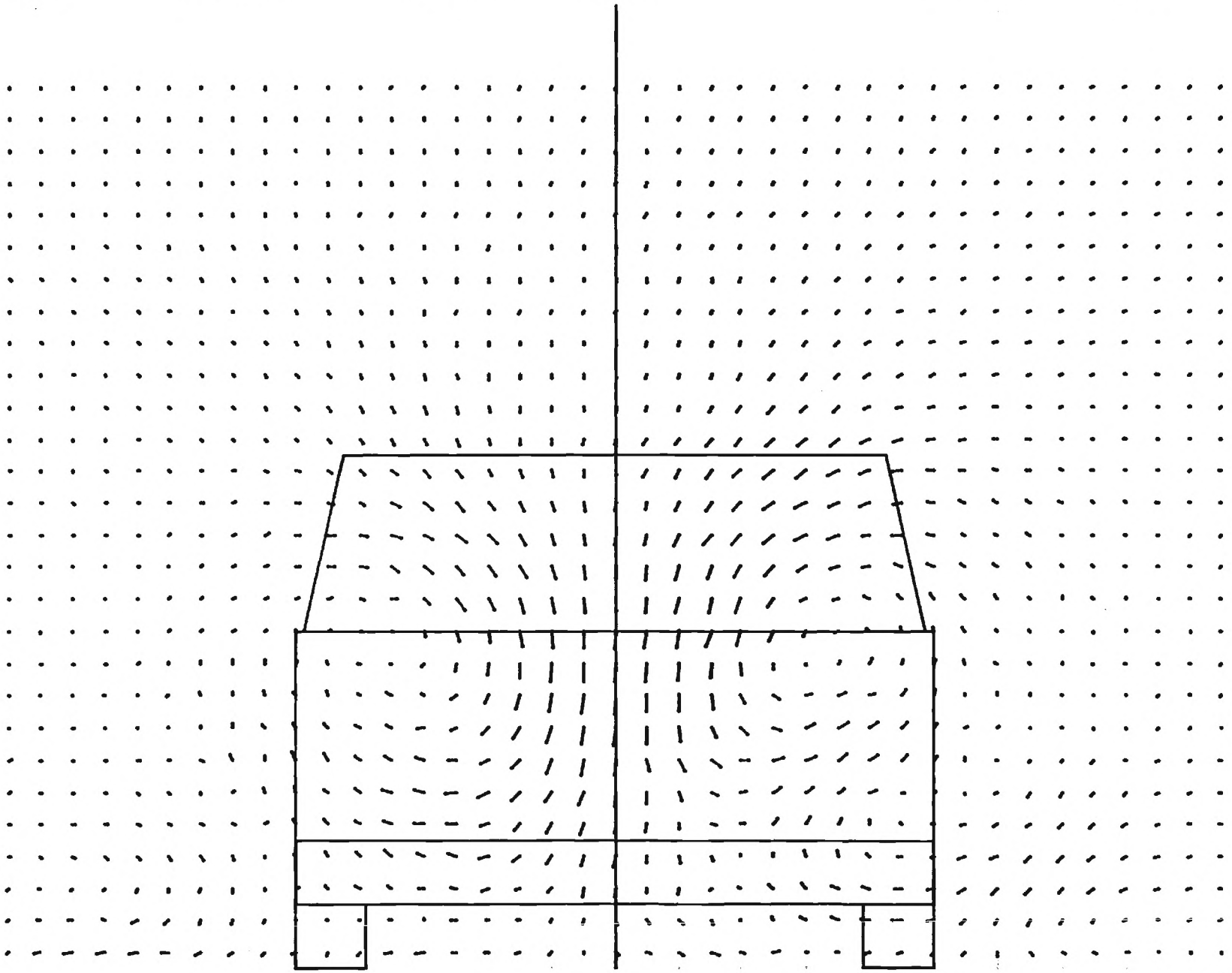

MP51

LOCKHEED-GEORGIA COMPANY - RESEARCH CENTER - TEST 64-Ø3

S. A. S. - Ø.Ø DEG - 36 INS LAT. VELOCITY RATIO V/UO

-Ø.Ø8Ø
-Ø.Ø6Ø
-Ø.Ø4Ø
-Ø.Ø2Ø
Ø.Ø2Ø
Ø.Ø4Ø
Ø.Ø6Ø
Ø.Ø8Ø

MP52

LOCKHEED-GEORGIA COMPANY - RESEARCH CENTER - TEST 64-03

S. A. S. - 0.0 DEG - 36 INS

VERT. VELOCITY RATIO W/UO

-0.140
-0.120
-0.100
-0.080
-0.060
-0.040
-0.020
0.020
0.040
0.060

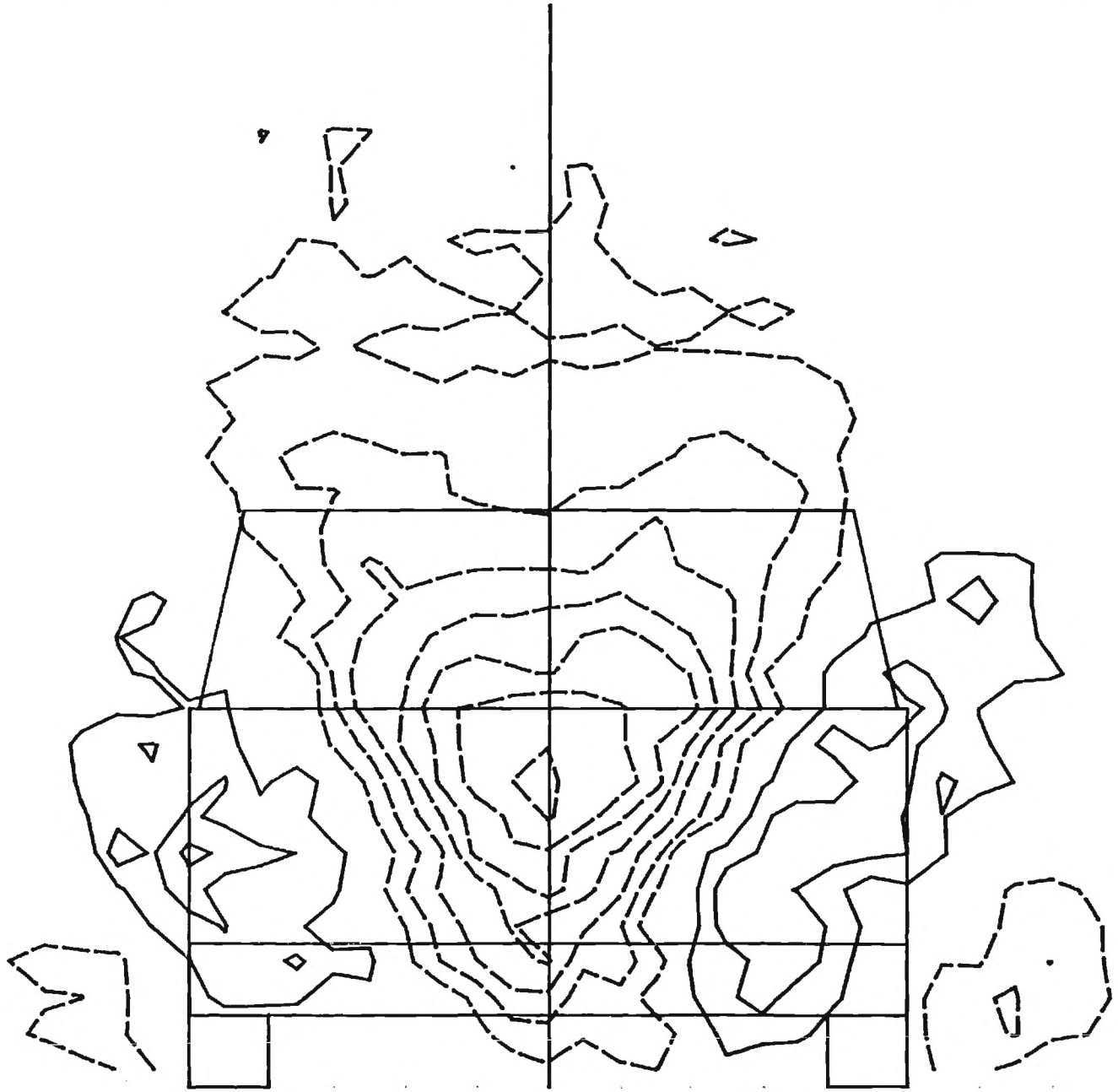

MP53

LOCKHEED-GEORGIA COMPANY - RESEARCH CENTER - TEST 64-03

S. A. S. - 0.0 DEG - 36 INS

AXIAL VELOCITY RATIO U/U0

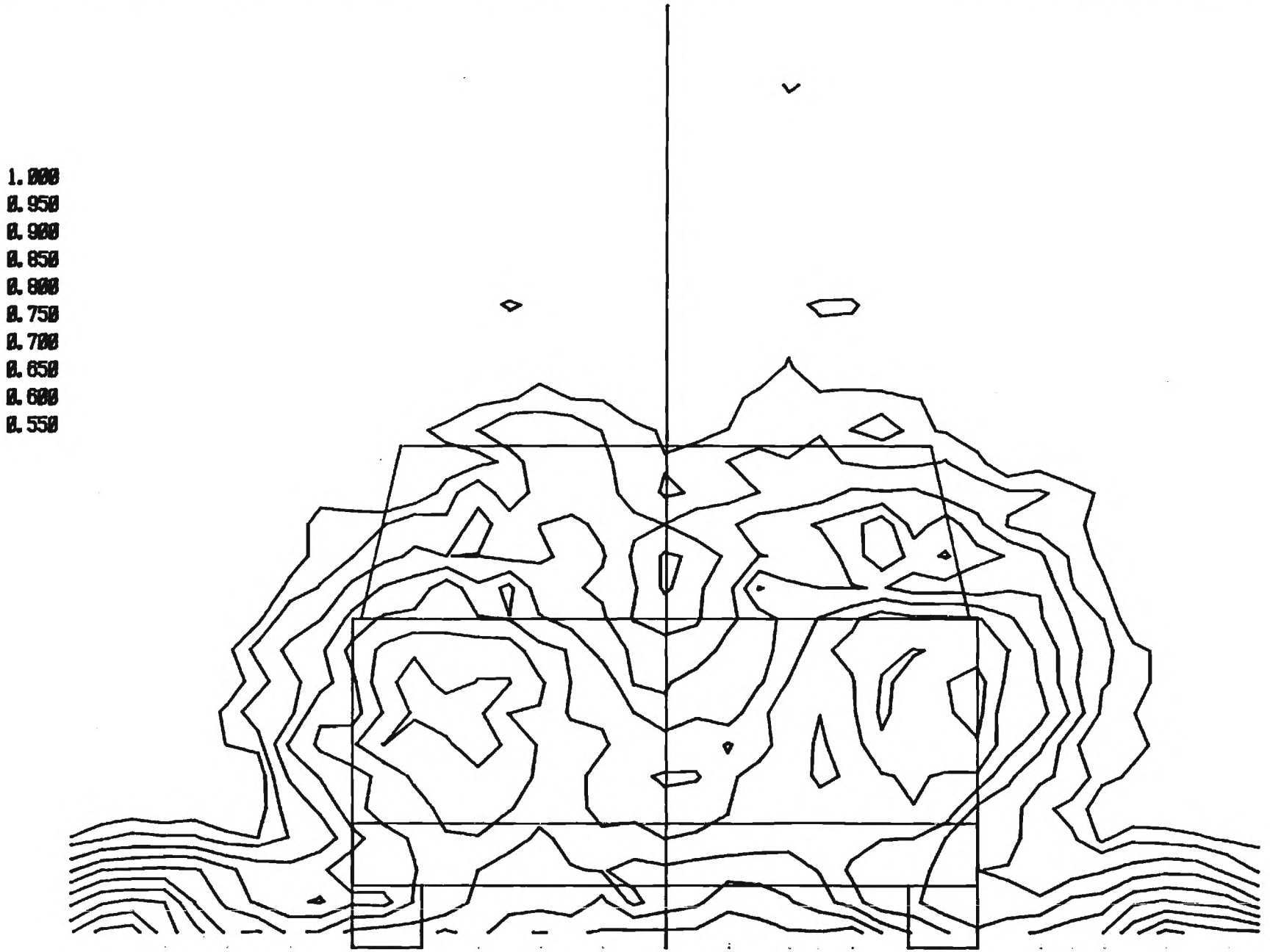

MP54

LOCKHEED-GEORGIA COMPANY - RESEARCH CENTER - TEST 64-03

S. A. S. - 0.0 DEG - 36 INS

TOTAL PRESSURE DEFICIT (HO-P)/QO

0.000
0.050
0.100
0.150
0.200
0.250
0.300
0.350
0.400
0.450
0.500
0.550
0.600

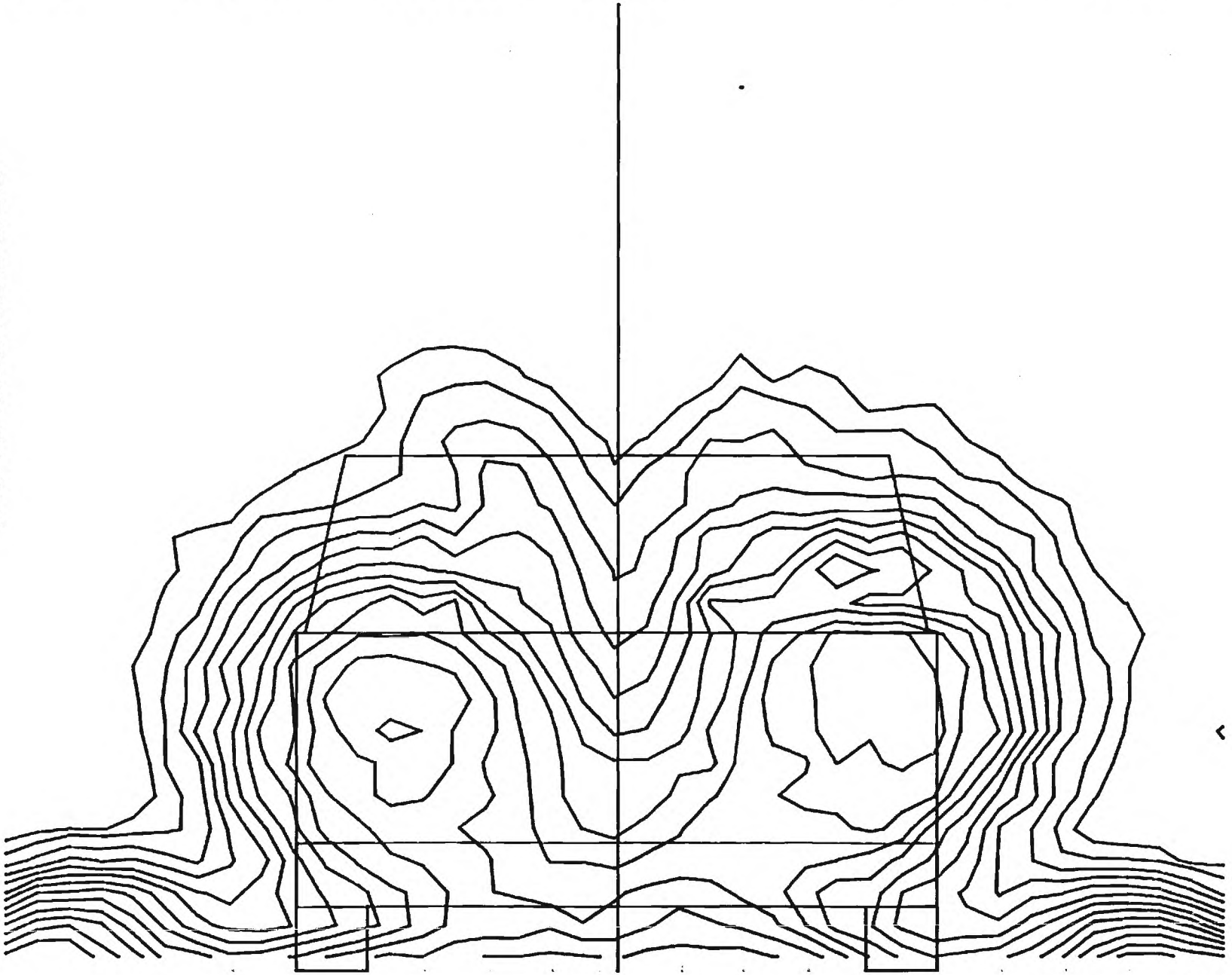

MP55

LOCKHEED-GEORGIA COMPANY - RESEARCH CENTER - TEST 64-03

S. A. S. - 0.0 DEG - 36 INS

CROSS-FLOW KINETIC ENERGY (VC*VC)/(UO*UO)

0.000
0.010
0.020
0.030
0.040

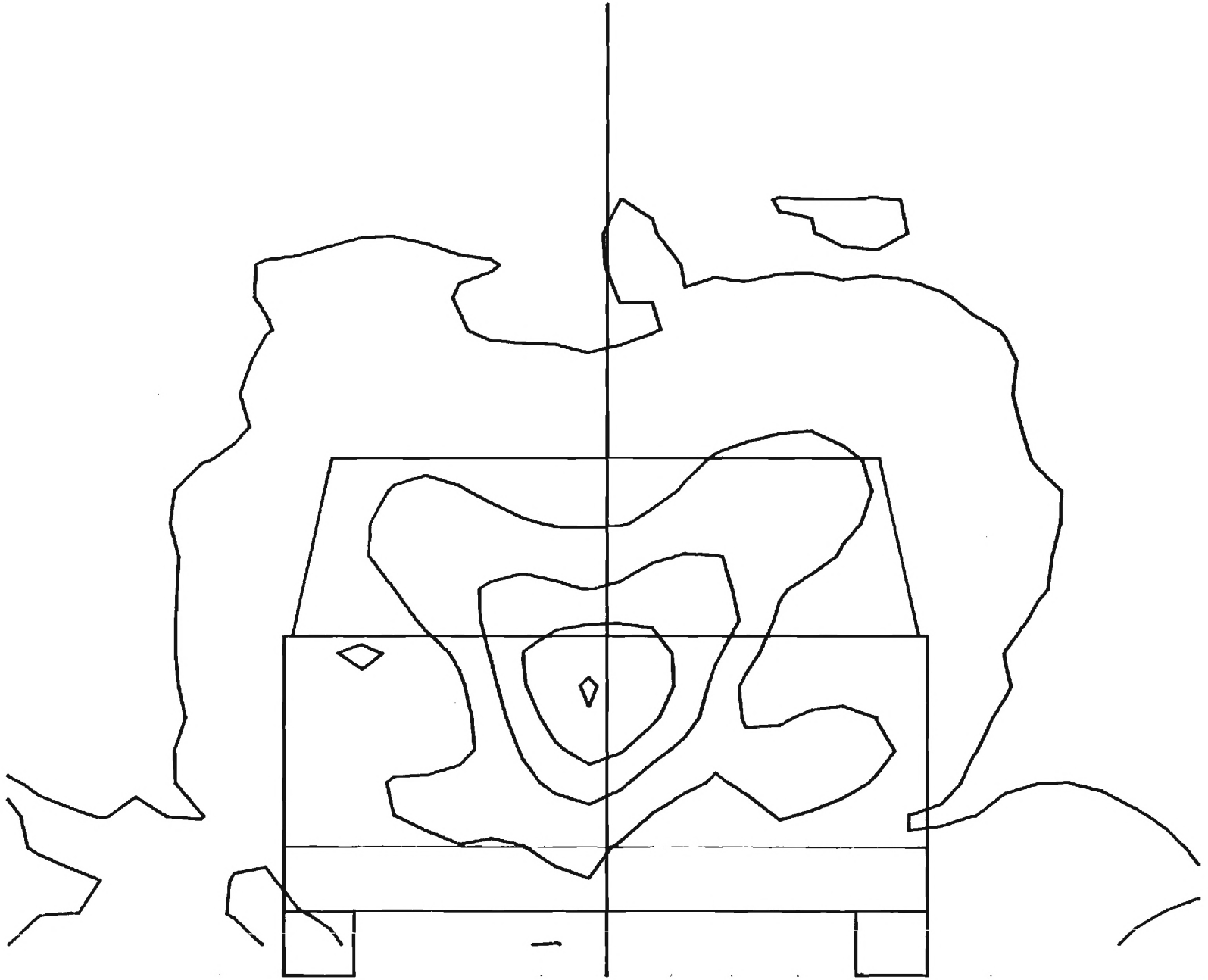

MP56

LOCKHEED-GEORGIA COMPANY - RESEARCH CENTER - TEST 64-03

S. A. S. - 0.0 DEG - 36 INS VORTICITY

NOTE

$$\left(\frac{\xi \ell}{U_o}\right) = \text{(CONTOUR VALUE)} \times 739.2$$

where ℓ = wheelbase

-0.0035
-0.0030
-0.0025
-0.0020
-0.0015
-0.0010
0.0010
0.0015
0.0020
0.0025
0.0030
0.0035

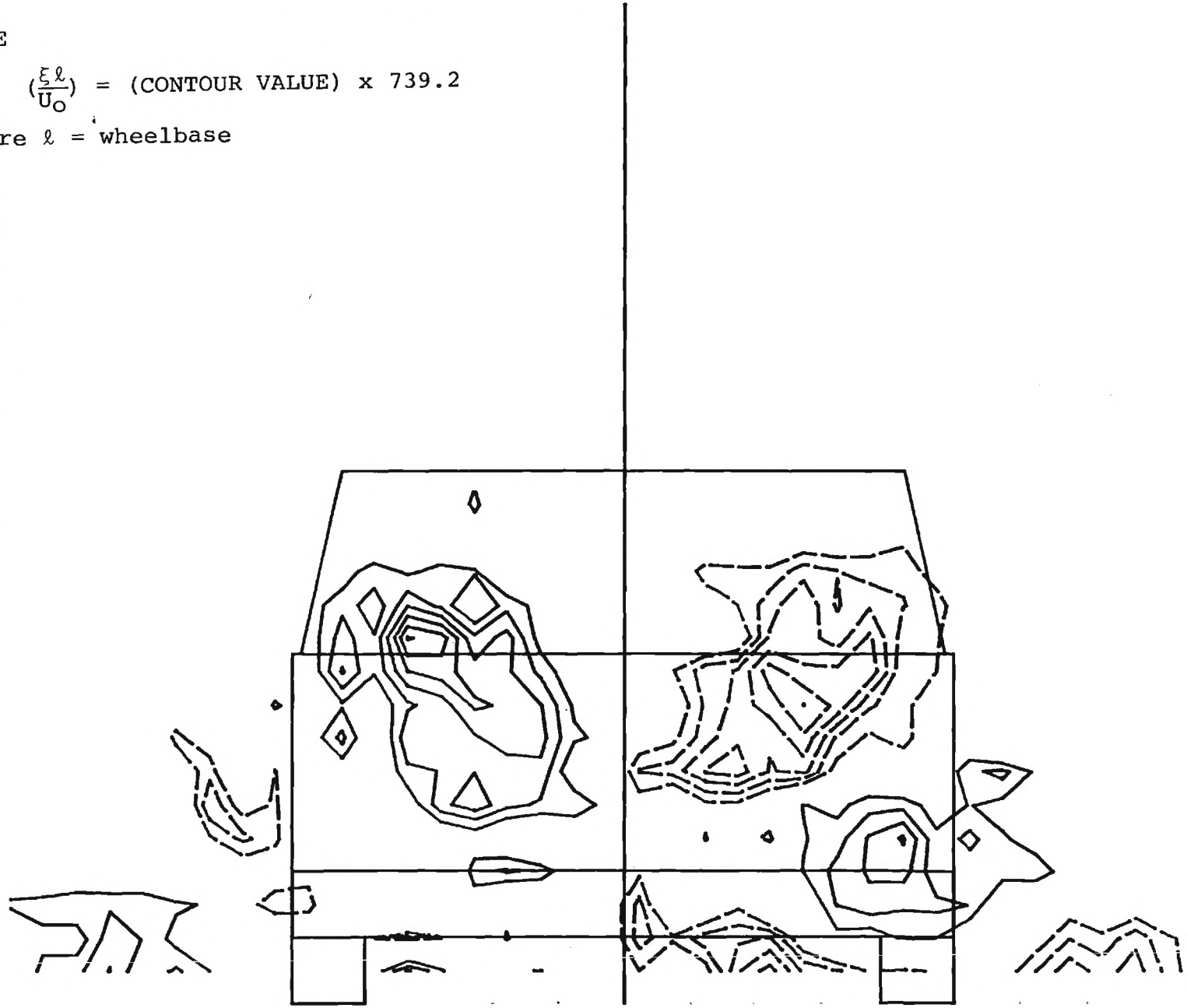

MP57

LOCKHEED-GEORGIA COMPANY - RESEARCH CENTER - TEST 64-03

S. A. S. - 0.0 DEG - 36 INS

CORR LAT VELOCITY V/U0

-.060
-.040
-.020
.020
.040
.060
.080
.100

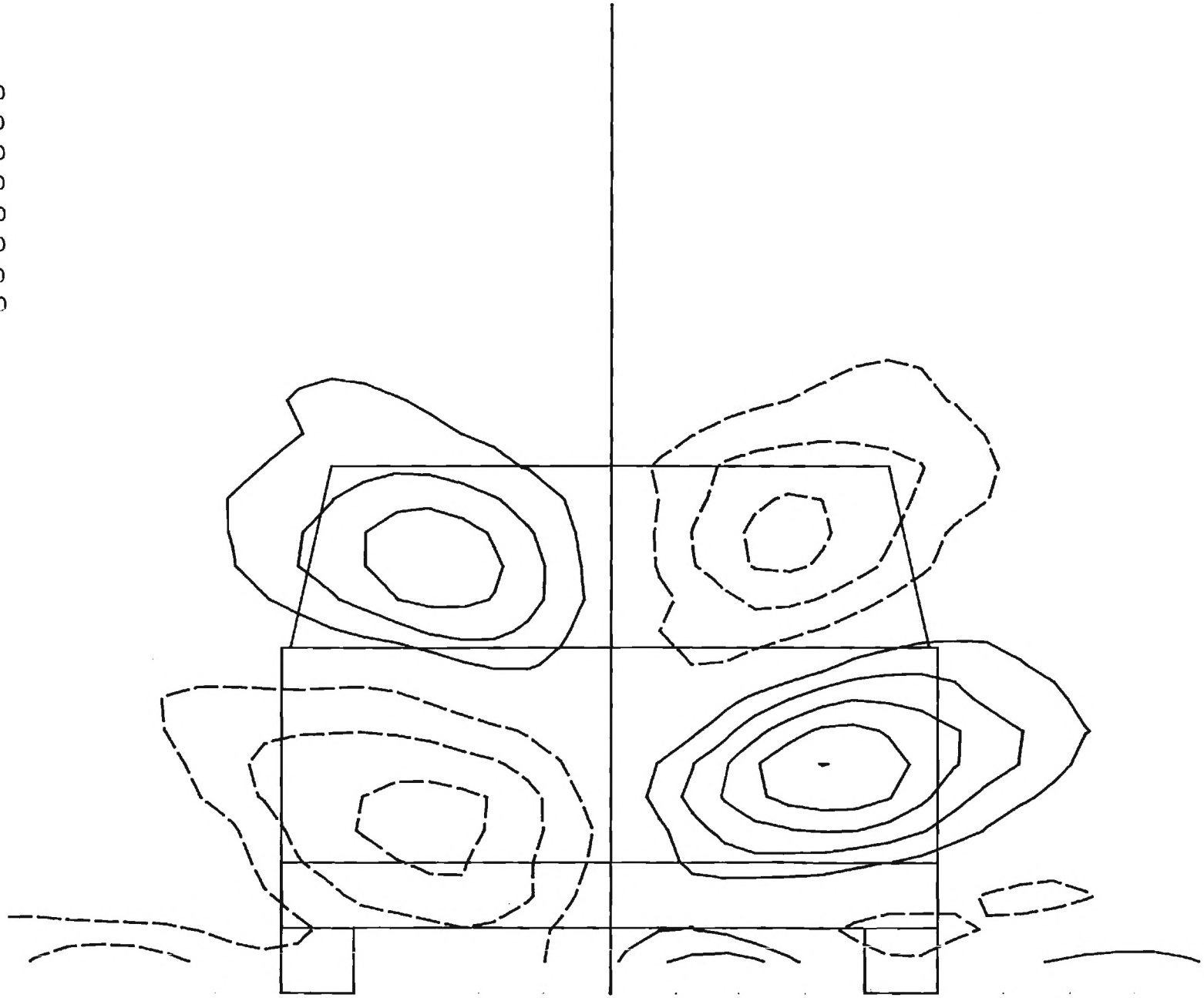

MP58

LOCKHEED-GEORGIA COMPANY - RESEARCH CENTER - TEST 64-Ø3

S. A. S. - Ø.Ø DEG - 36 INS

CORR VERT VELOCITY W/UO

-.120
-.100
-.080
-.060
-.040
-.020
.020
.040
.060

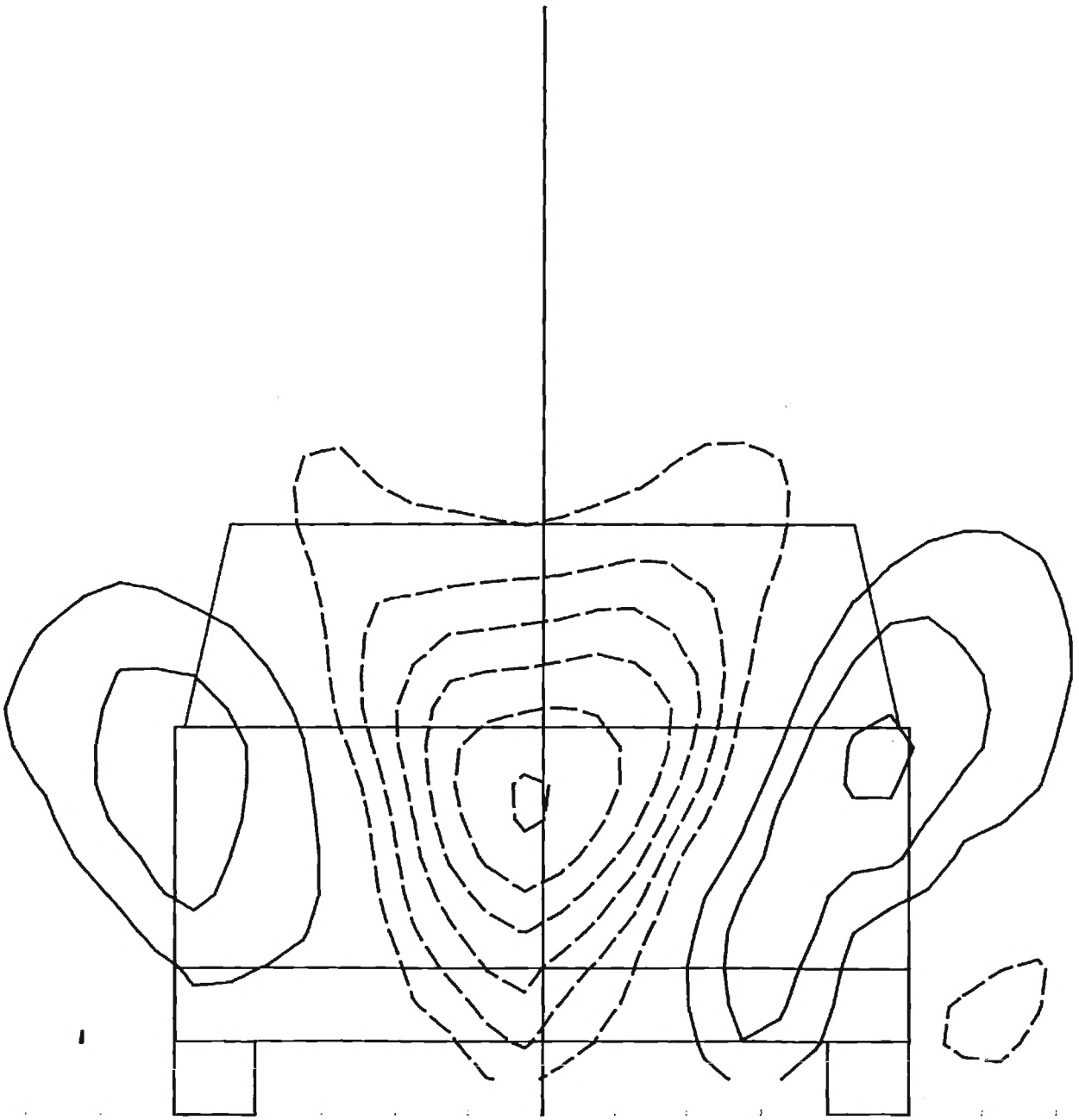

MP59

LOCKHEED-GEORGIA COMPANY - RESEARCH CENTER - TEST 64-03

S. A. S. - 0.0 DEG - 36 INS

STREAM FUNCTIONS

NOTE

$$\left(\frac{\psi}{U_o \ell}\right) = \text{(CONTOUR VALUE)} \times 0.7792$$

where ℓ = wheelbase

-0.016
-0.012
-0.008
-0.004
0.000
0.004
0.008
0.012
0.016

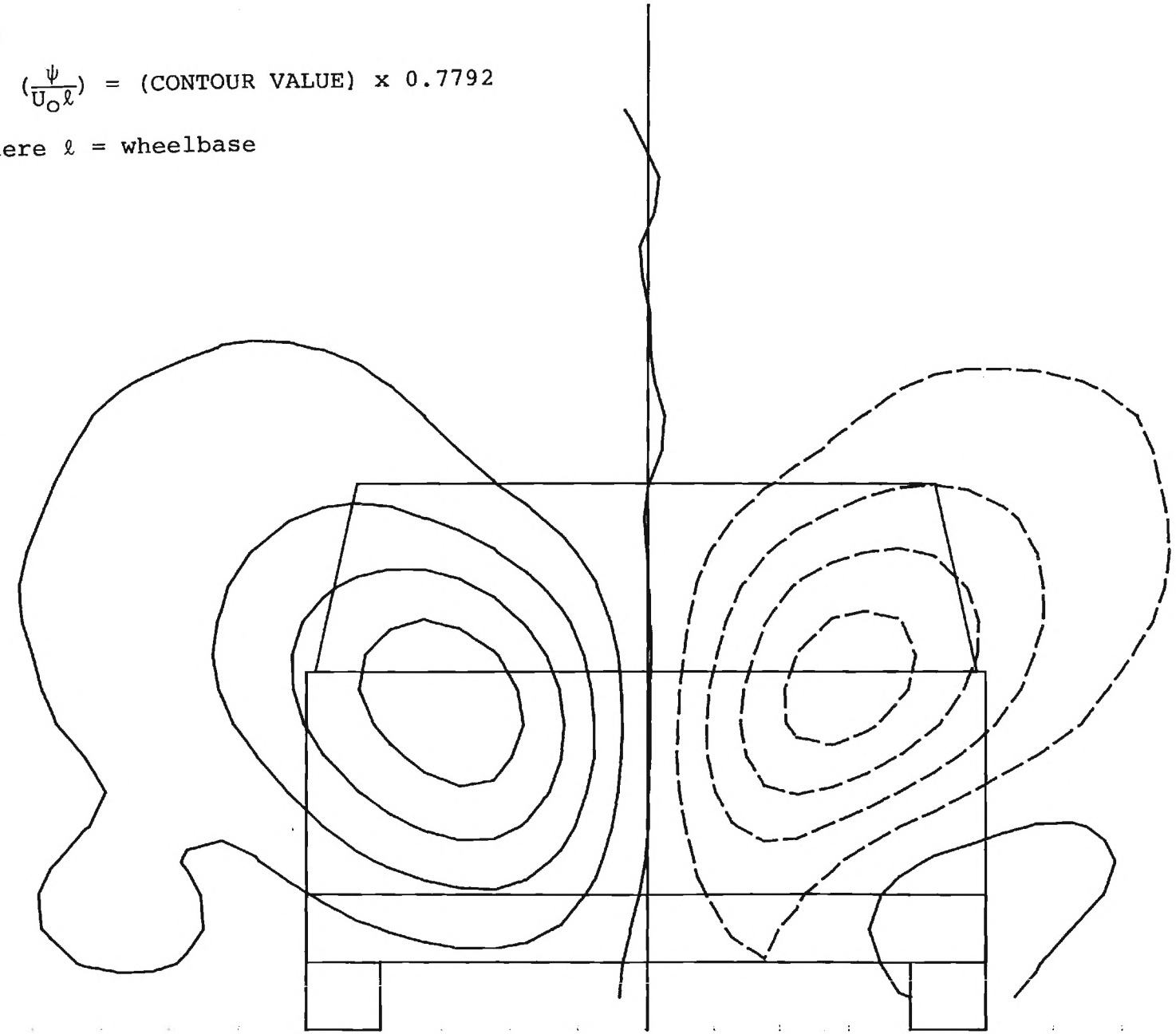

MP60

LOCKHEED-GEORGIA COMPANY -- RESEARCH CENTER -- TEST 64-05

S. A. S. -- 12.5 DEG -- 18 INS

CROSSFLOW VELOCITY VC/U0

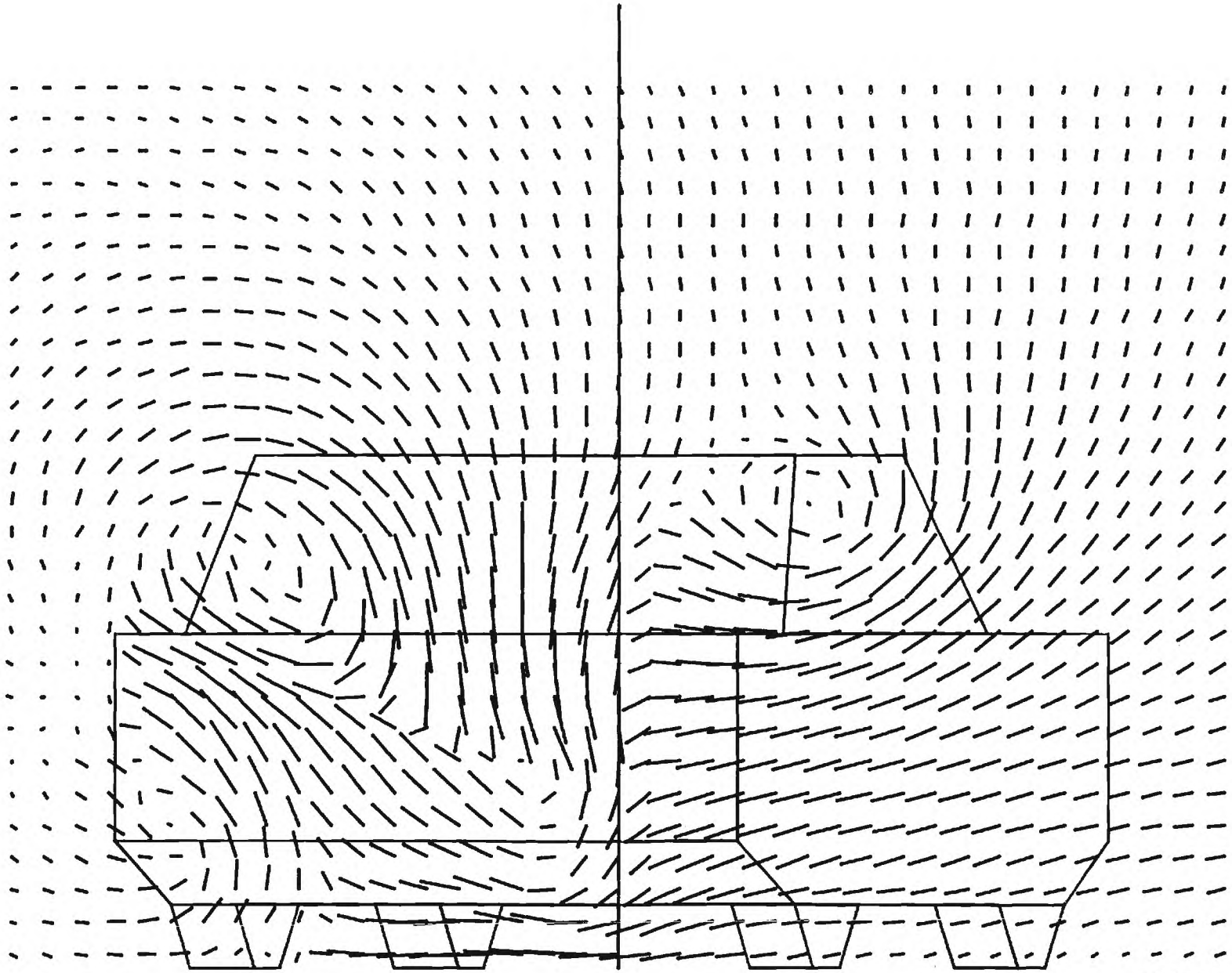

MP61

LOCKHEED-GEORGIA COMPANY - RESEARCH CENTER - TEST 64-05

S. A. S. - 12.5 DEG - 18 INS

LAT. VELOCITY RATIO V/U0

MP62

LOCKHEED-GEORGIA COMPANY - RESEARCH CENTER - TEST 64-Ø5

S. A. S. - 12.5 DEG - 18 INS

VERT. VELOCITY RATIO W/UO

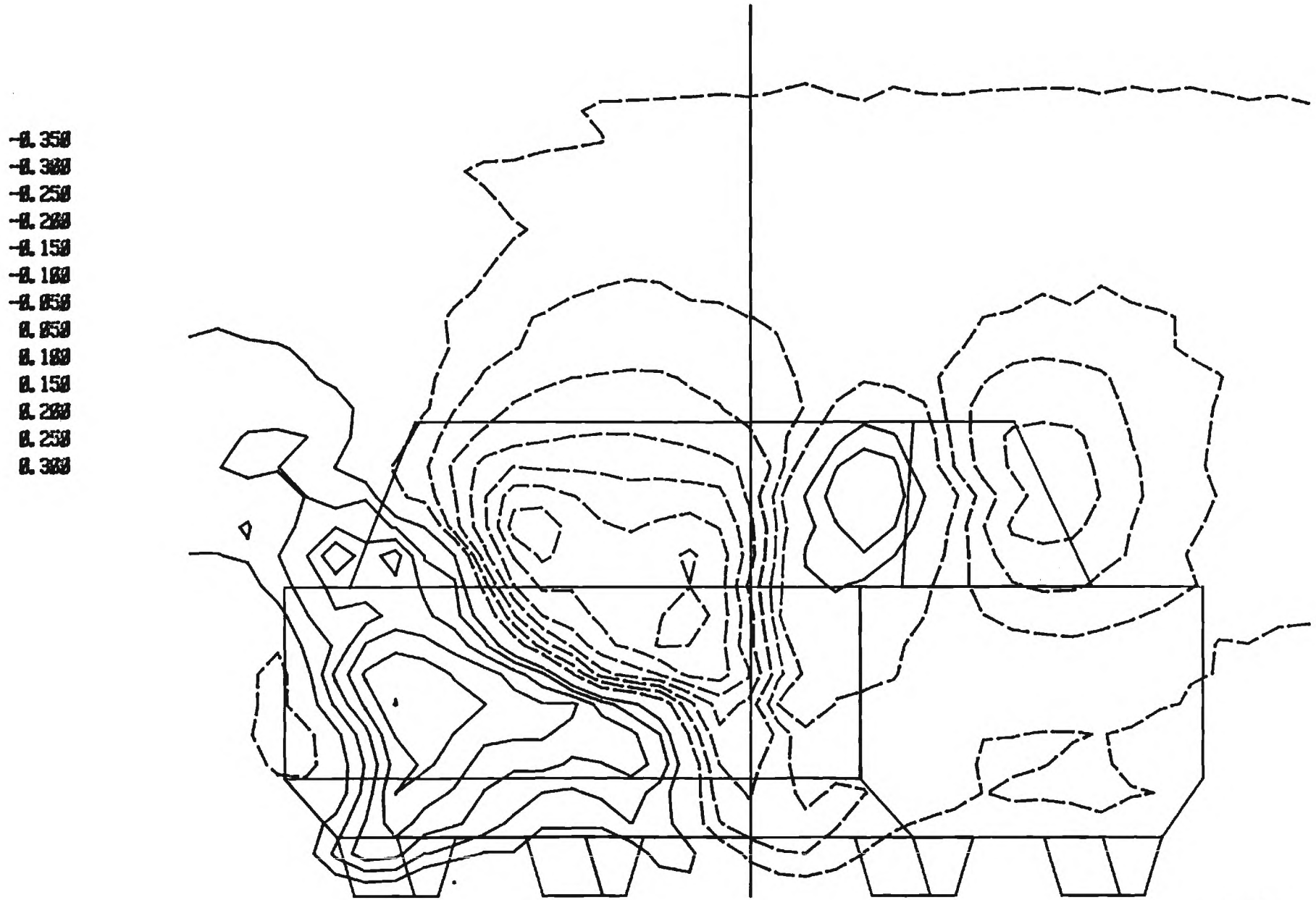

MP63

LOCKHEED-GEORGIA COMPANY - RESEARCH CENTER - TEST 64-05

S. A. S. - 12.5 DEG - 18 INS

AXIAL VELOCITY RATIO U/U0

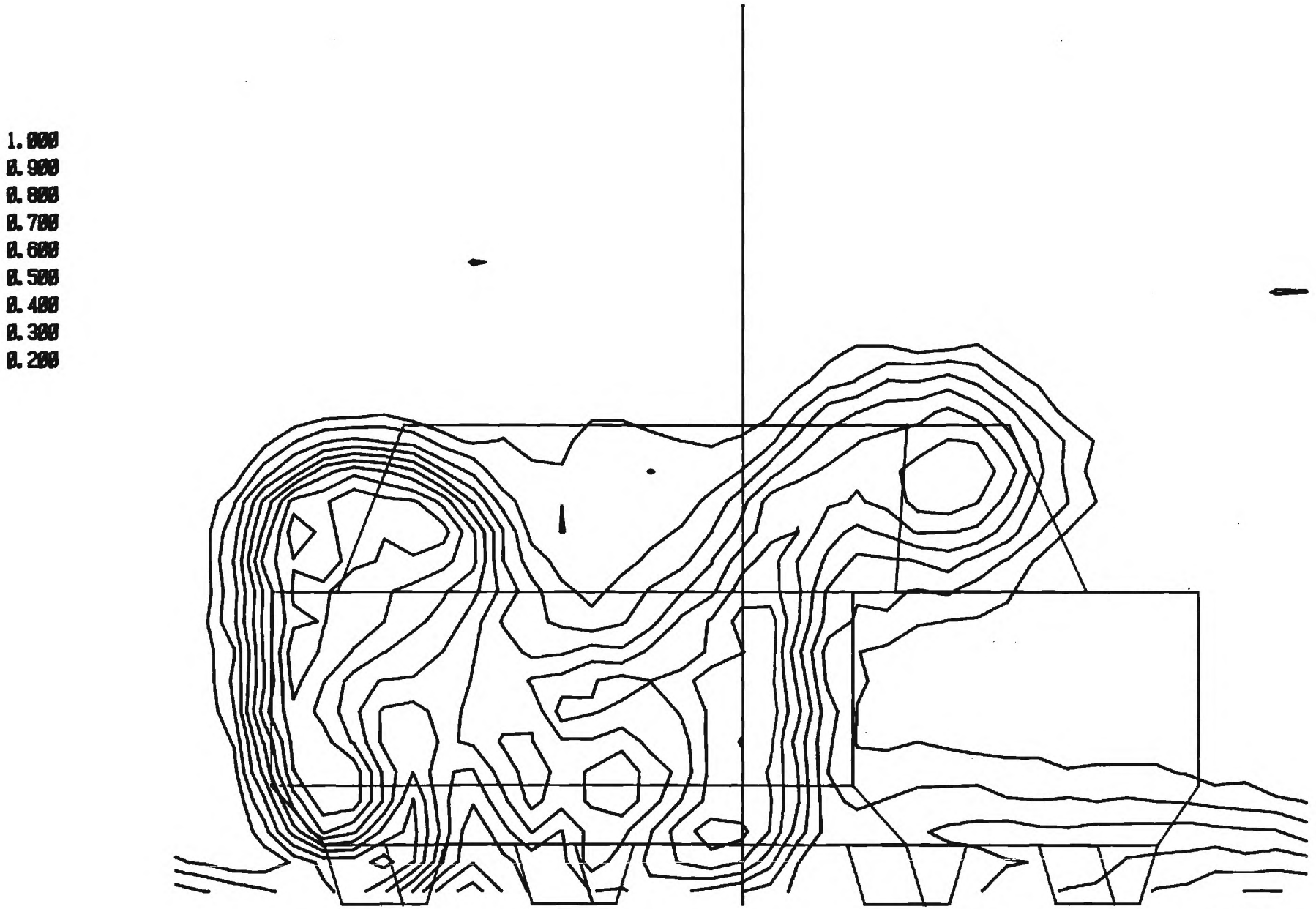

MP64

LOCKHEED-GEORGIA COMPANY - RESEARCH CENTER - TEST 64-05

S. A. S. - 12.5 DEG - 18 INS

TOTAL PRESSURE DEFICIT (HO-P)/QO

0.000
0.100
0.200
0.300
0.400
0.500
0.600
0.700
0.800
0.900
1.000
1.100

MP65

LOCKHEED-GEORGIA COMPANY - RESEARCH CENTER - TEST 64-05

S. A. S. - 12.5 DEG - 18 INS

CROSS-FLOW KINETIC ENERGY (VC*VC)/(UO*UO)

0.000
0.040
0.080
0.120
0.160
0.200
0.240
0.280
0.320

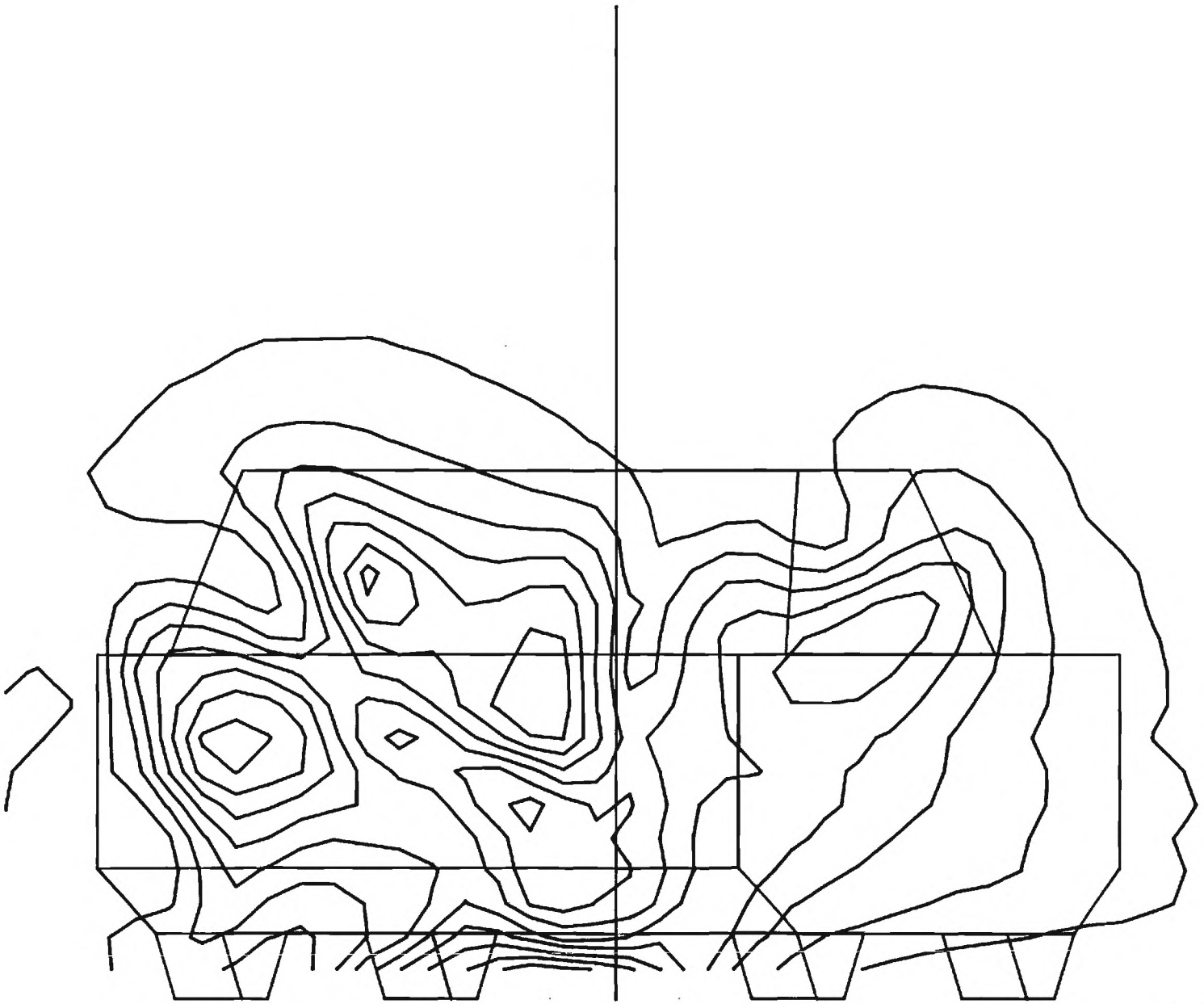

MP66

LOCKHEED-GEORGIA COMPANY - RESEARCH CENTER - TEST 64-05

S. A. S. - 12.5 DEG - 18 INS VORTICITY

NOTE

$(\frac{\xi \ell}{U_o})$ = (CONTOUR VALUE) x 739.2

-0.0080
-0.0060
-0.0040
-0.0020
0.0020
0.0040
0.0060
0.0080
0.0100
0.0120

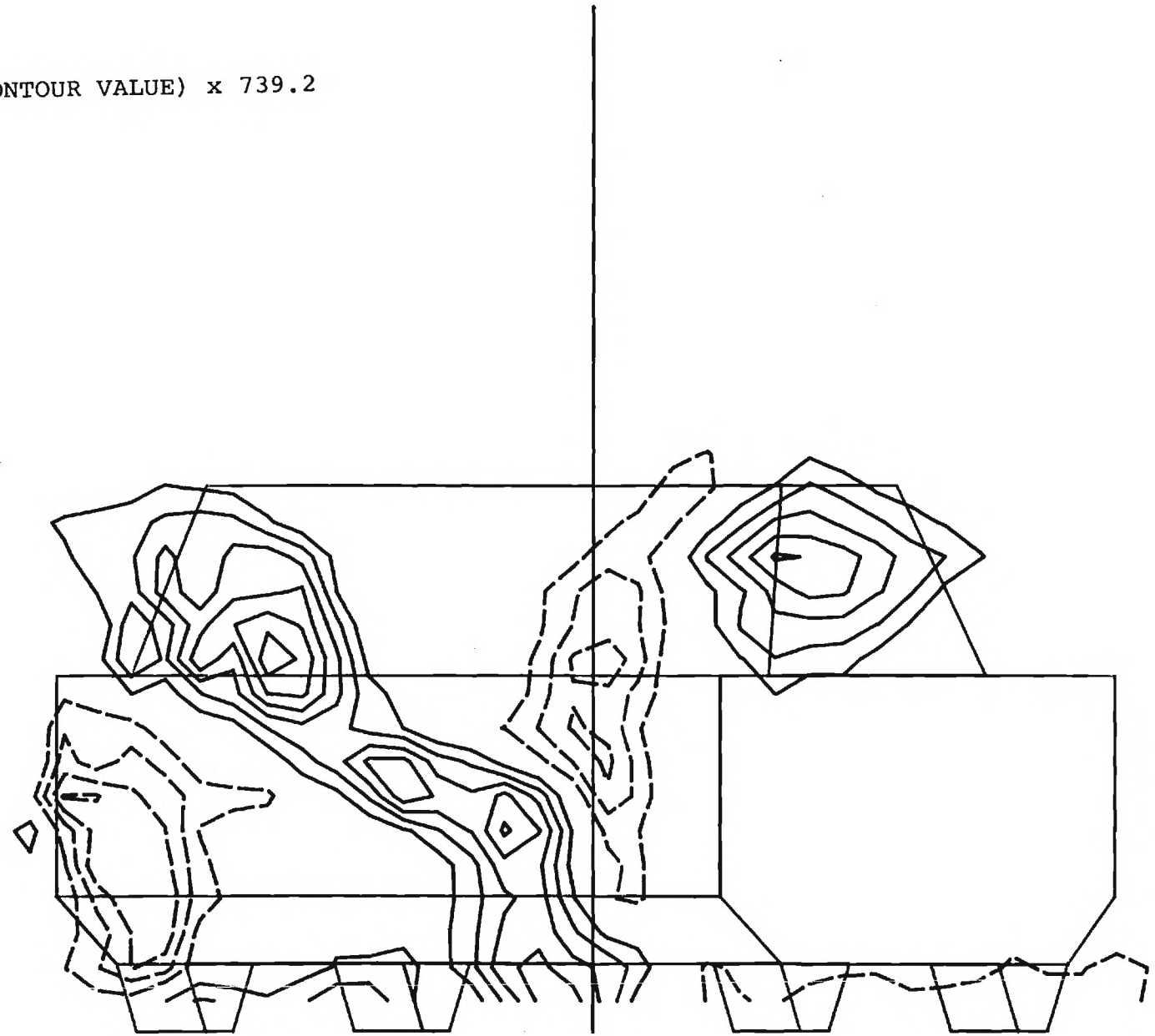

MP67

LOCKHEED-GEORGIA COMPANY - RESEARCH CENTER - TEST 64-05

S. A. S. - 12.5 DEG - 18 INS

CORR LAT VELOCITY V/UO

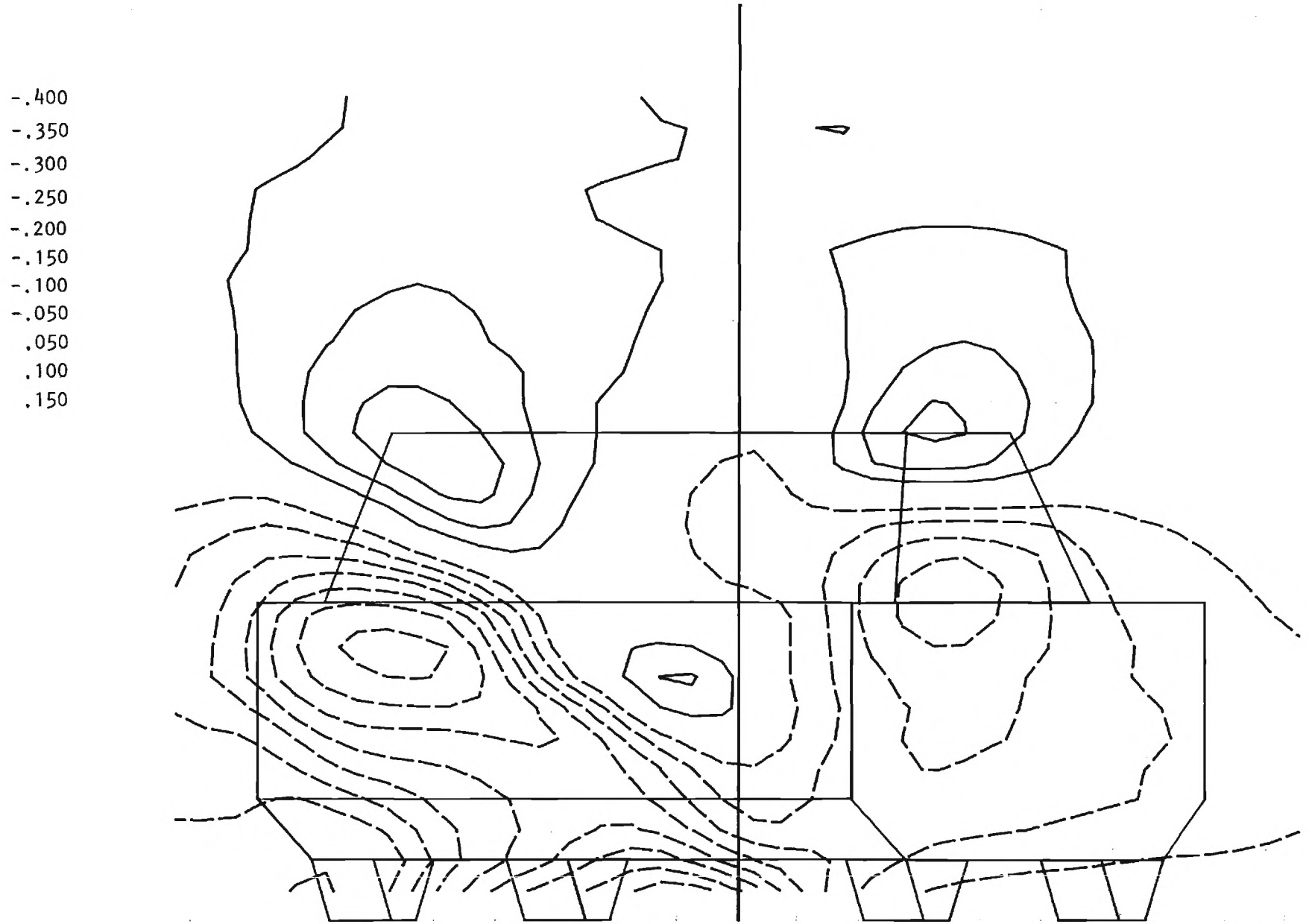

MP68

LOCKHEED-GEORGIA COMPANY - RESEARCH CENTER - TEST 64-05

S. A. S. - 12.5 DEG - 18 INS

CORR VERT VELOCITY W/UO

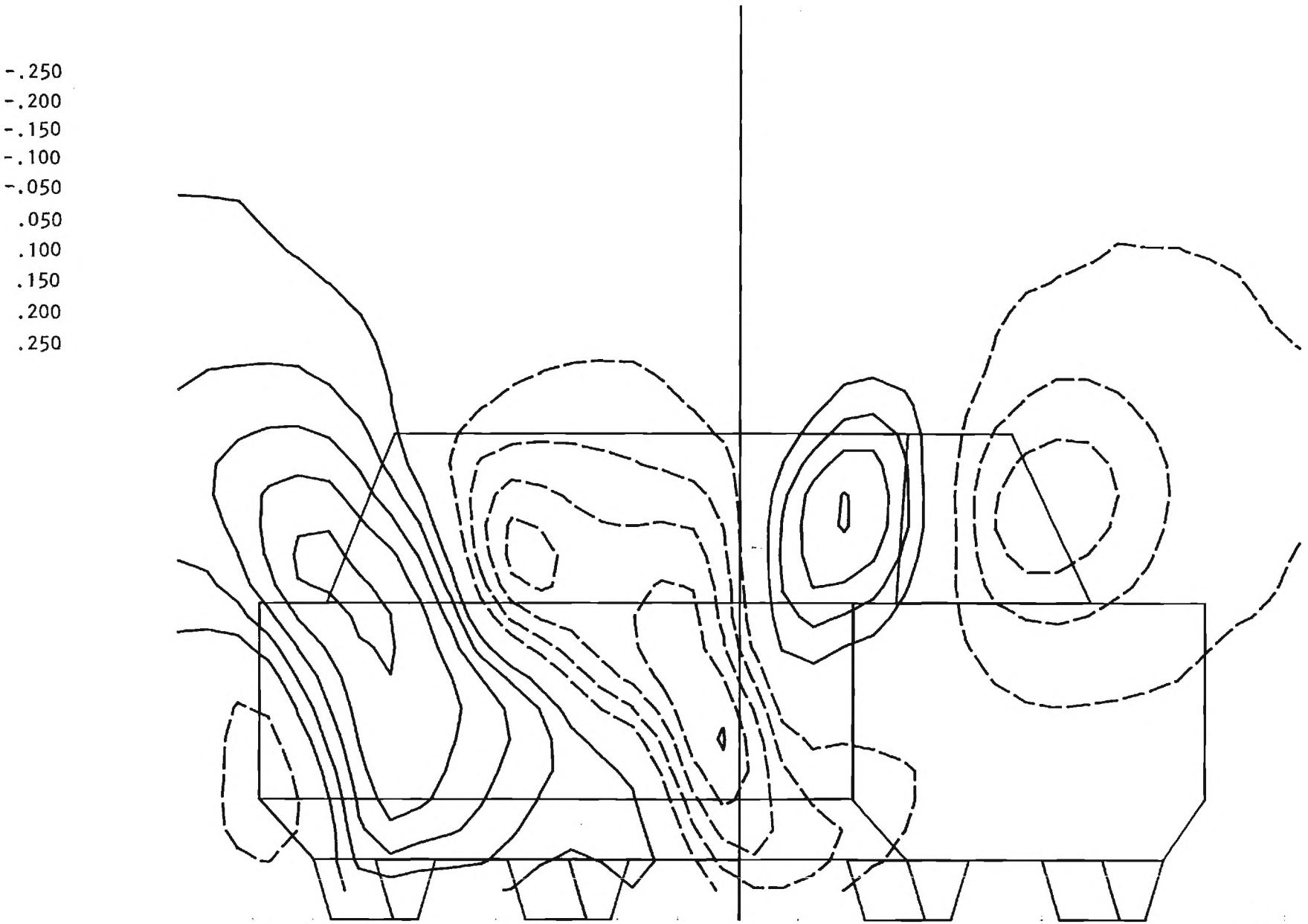

MP69

LOCKHEED-GEORGIA COMPANY - RESEARCH CENTER - TEST 64-05

S. A. S. - 12.5 DEG - 18 INS

STREAM FUNCTIONS

NOTE

$(\frac{\psi}{U_o \ell})$ = (CONTOUR VALUE x 0.7792

where ℓ = wheelbase

0.000
0.010
0.020
0.030
0.040
0.050
0.060
0.070
0.080
0.090
0.100

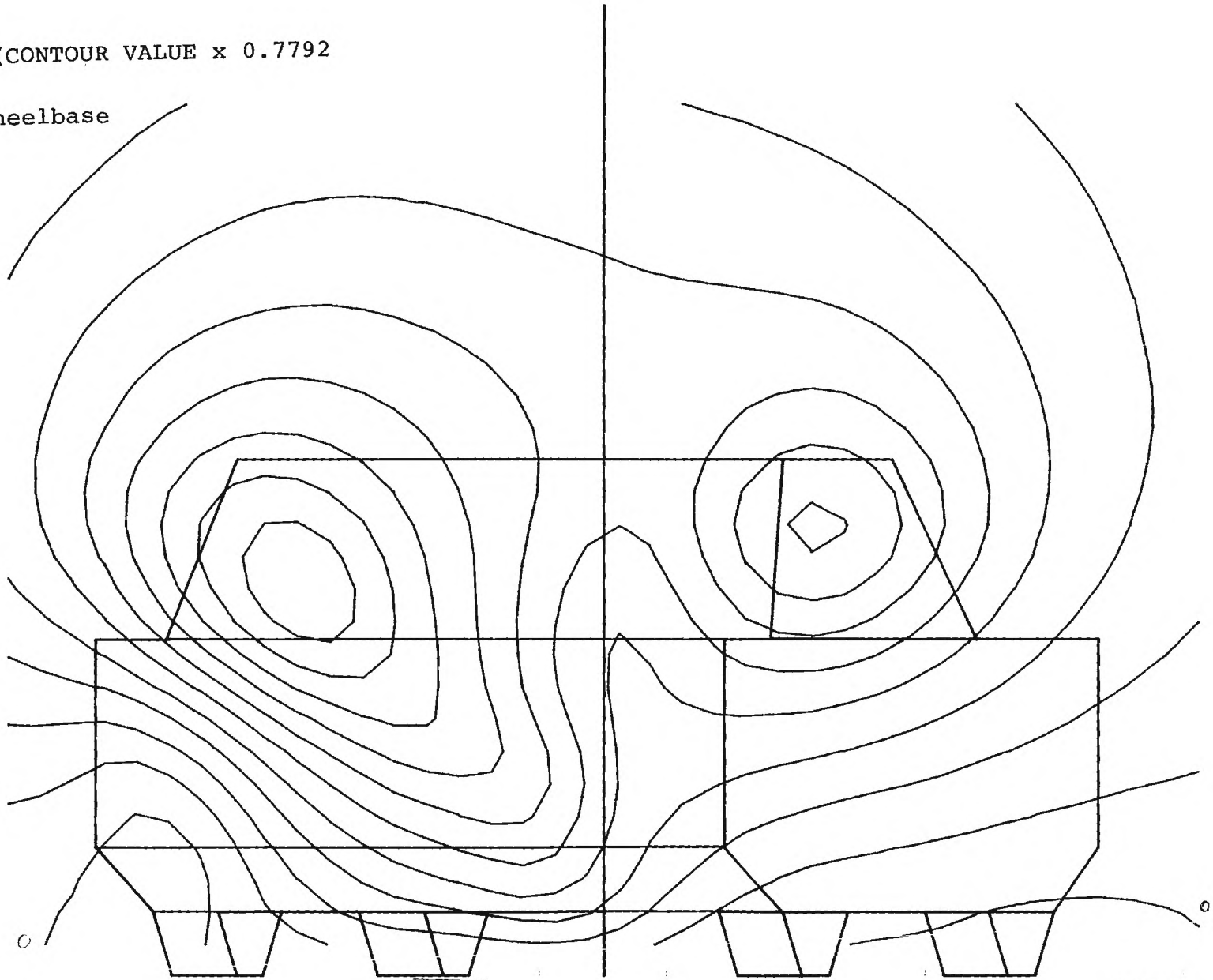

MP70

LOCKHEED-GEORGIA COMPANY - RESEARCH CENTER - TEST 64-08

S. A. S. - 12.5 DEG - 36 INS

CROSSFLOW VELOCITY VC/UO

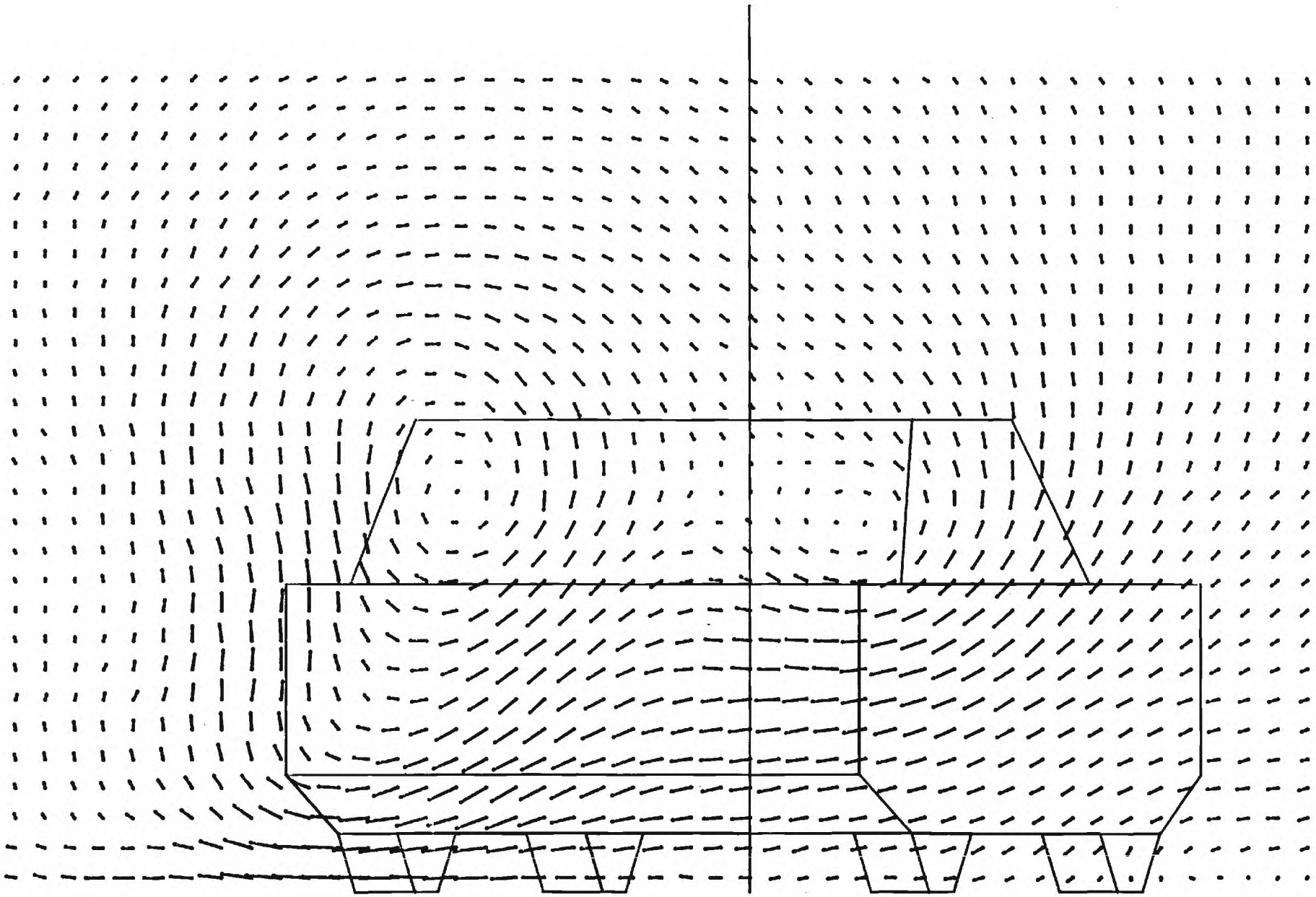

MP71

LOCKHEED-GEORGIA COMPANY - RESEARCH CENTER - TEST 64-Ø8

S. A. S. - 12.5 DEG - 36 INS

LAT. VELOCITY RATIO V/UO

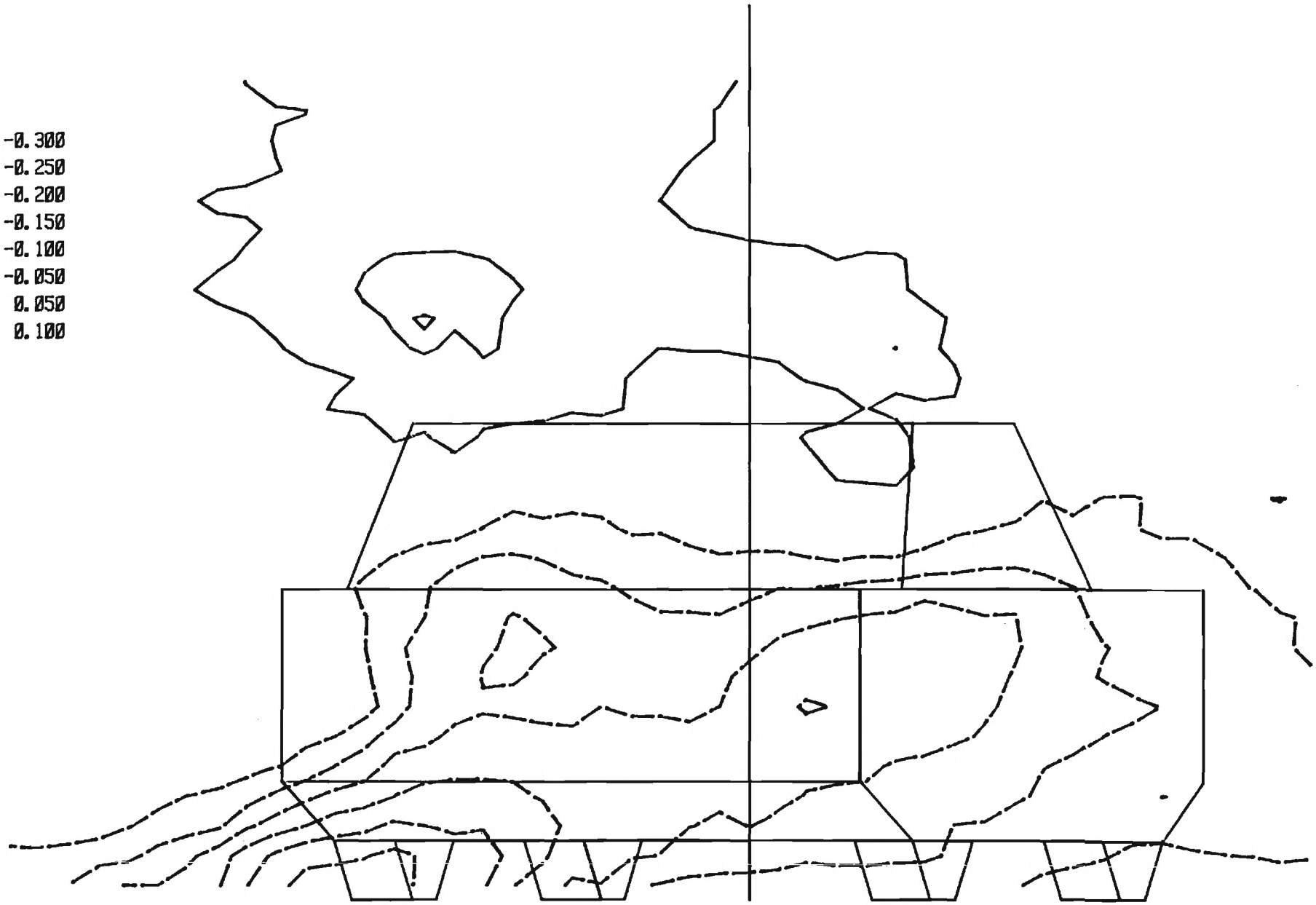

LOCKHEED-GEORGIA COMPANY - RESEARCH CENTER - TEST 64-Ø8

S. A. S. - 12.5 DEG - 36 INS

VERT. VELOCITY RATIO W/UO

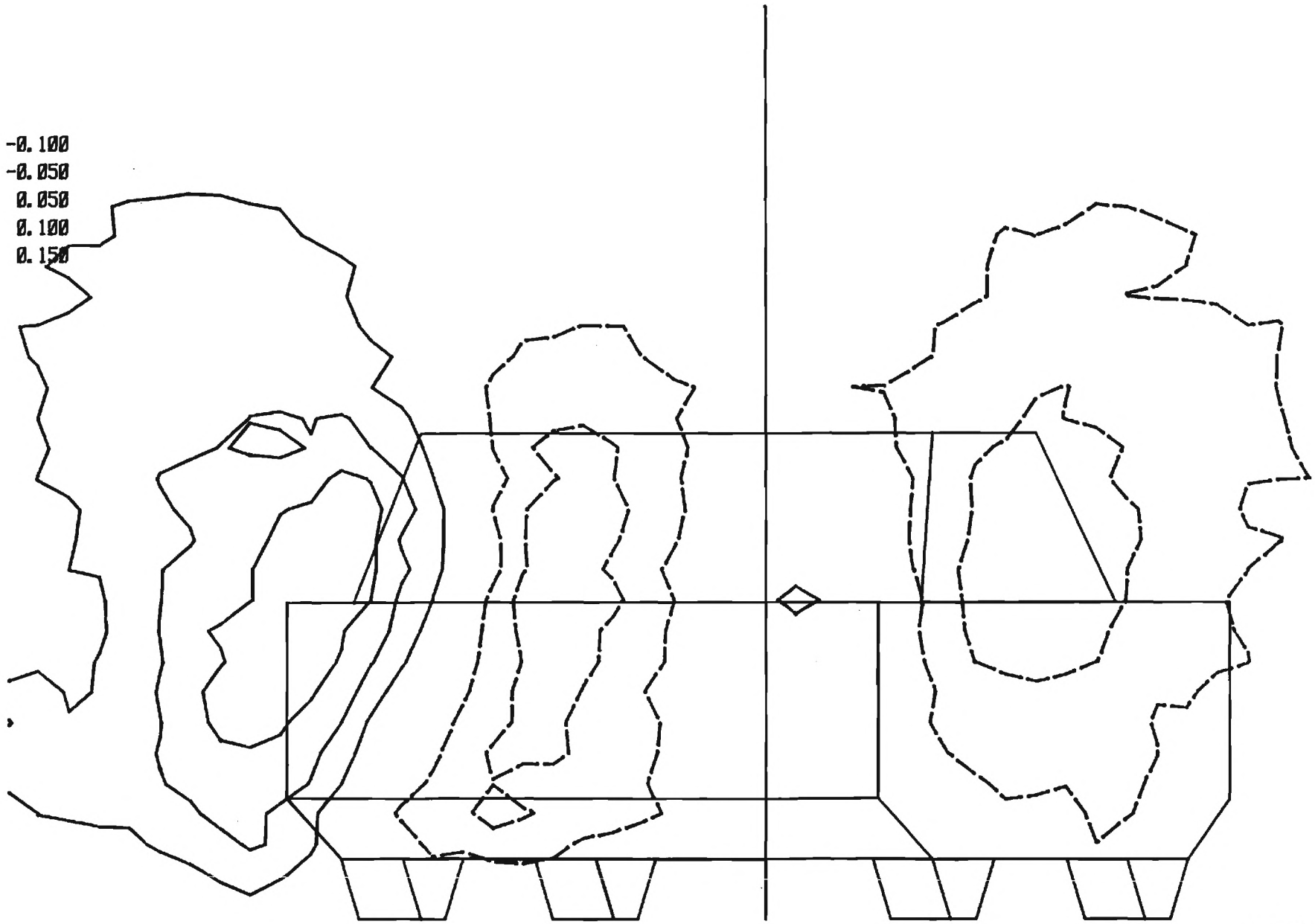

MP73

LOCKHEED-GEORGIA COMPANY -- RESEARCH CENTER -- TEST 64--08

S. A. S. - 12.5 DEG - 36 INS

AXIAL VELOCITY RATIO U/U0

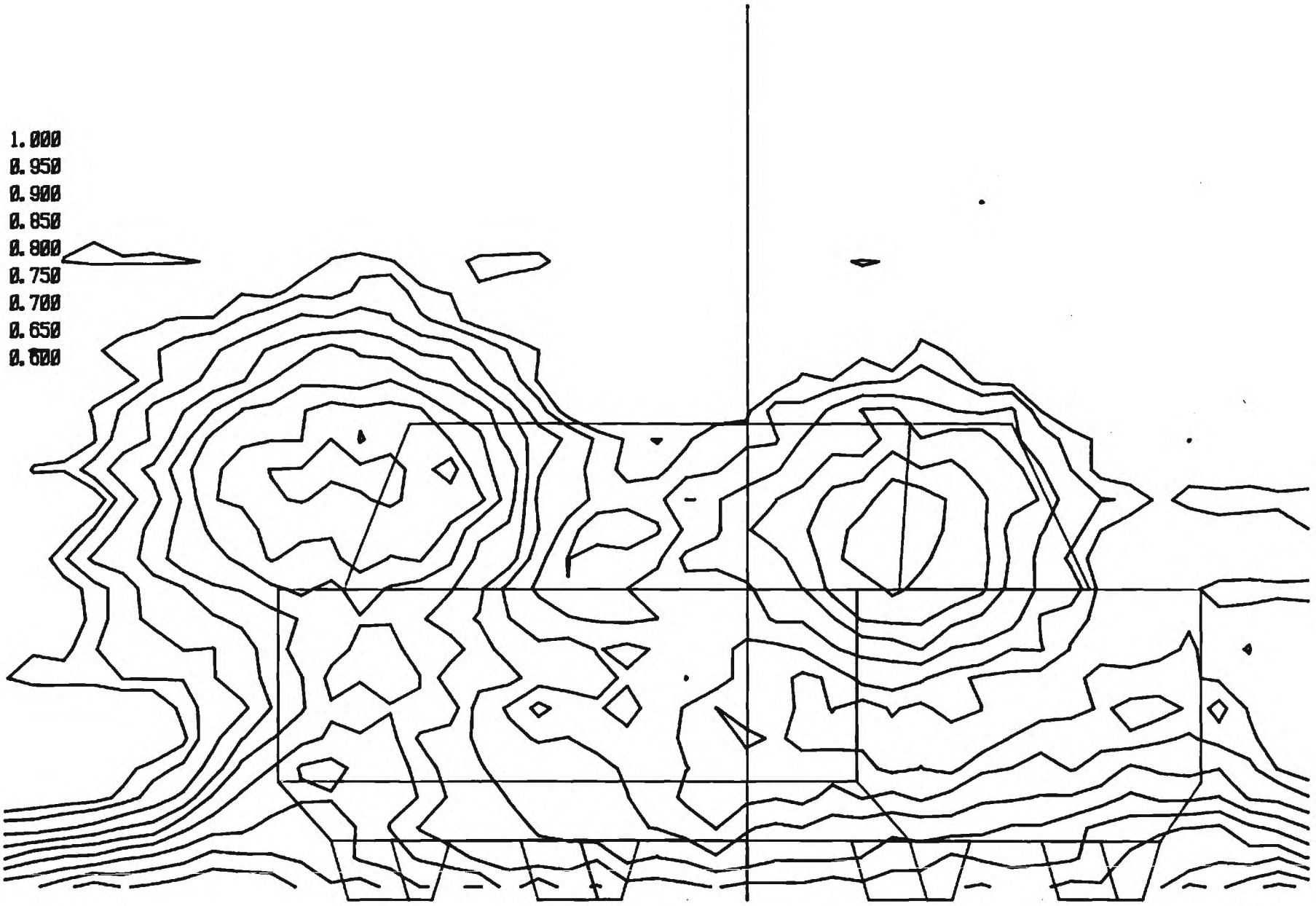

MP74

LOCKHEED-GEORGIA COMPANY - RESEARCH CENTER - TEST 64-08

S. A. S. - 12.5 DEG - 36 INS

TOTAL PRESSURE DEFICIT (HO-P)/QO

MP75

LOCKHEED-GEORGIA COMPANY - RESEARCH CENTER - TEST 64-08

S. A. S. - 12.5 DEG - 36 INS

CROSS-FLOW KINETIC ENERGY (VC*VC)/(UO*UO)

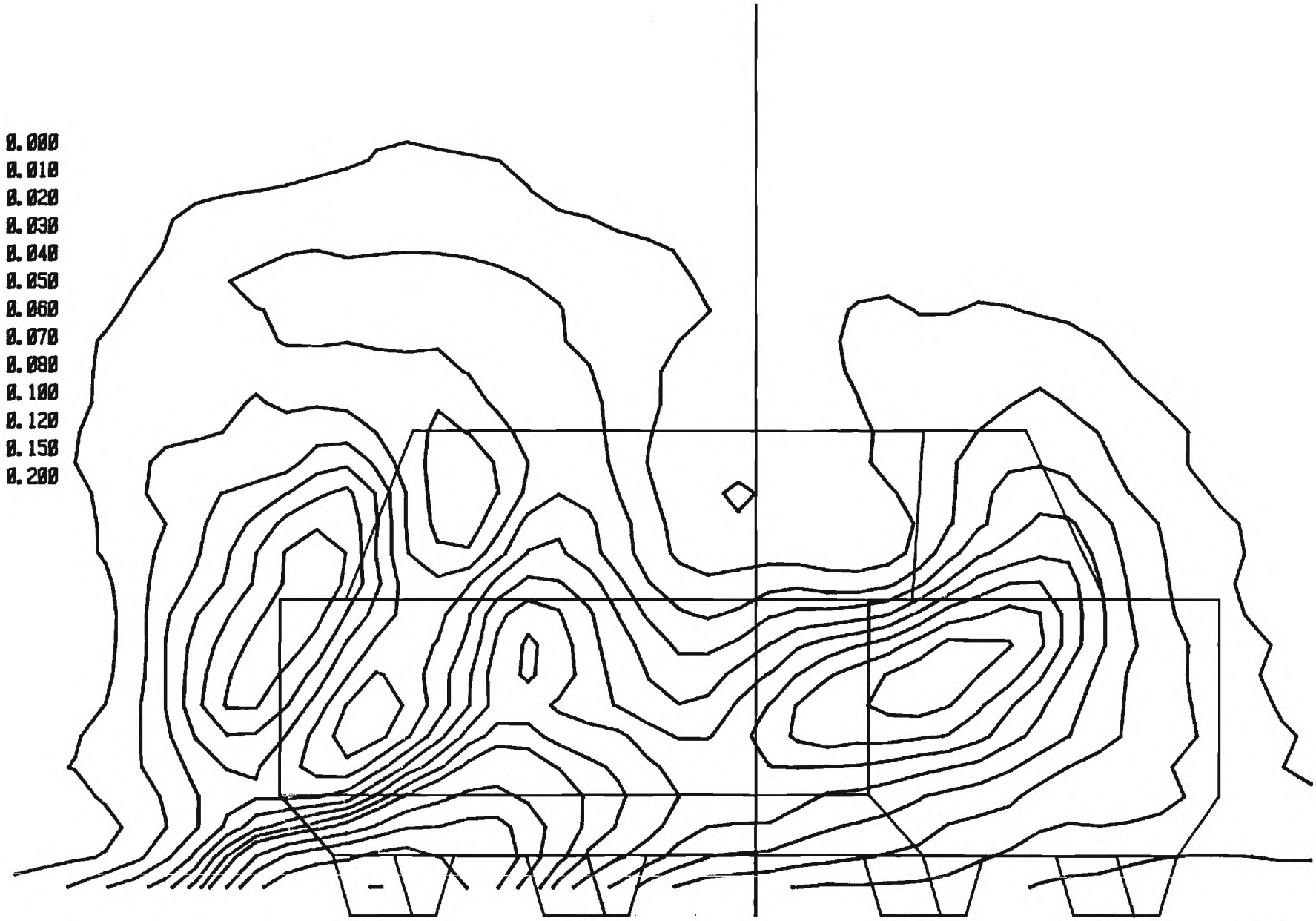

MP76

LOCKHEED-GEORGIA COMPANY - RESEARCH CENTER - TEST 64-Ø8

S. A. S. - 12.5 DEG - 36 INS

VORTICITY

NOTE

$(\frac{\xi \ell}{U_o})$ = (CONTOUR VALUE x 739.2

-Ø.ØØ3Ø
-Ø.ØØ25
-Ø.ØØ2Ø
-Ø.ØØ15
-Ø.ØØ1Ø
Ø.ØØ1Ø
Ø.ØØ15
Ø.ØØ2Ø
Ø.ØØ25
Ø.ØØ3Ø
Ø.ØØ35

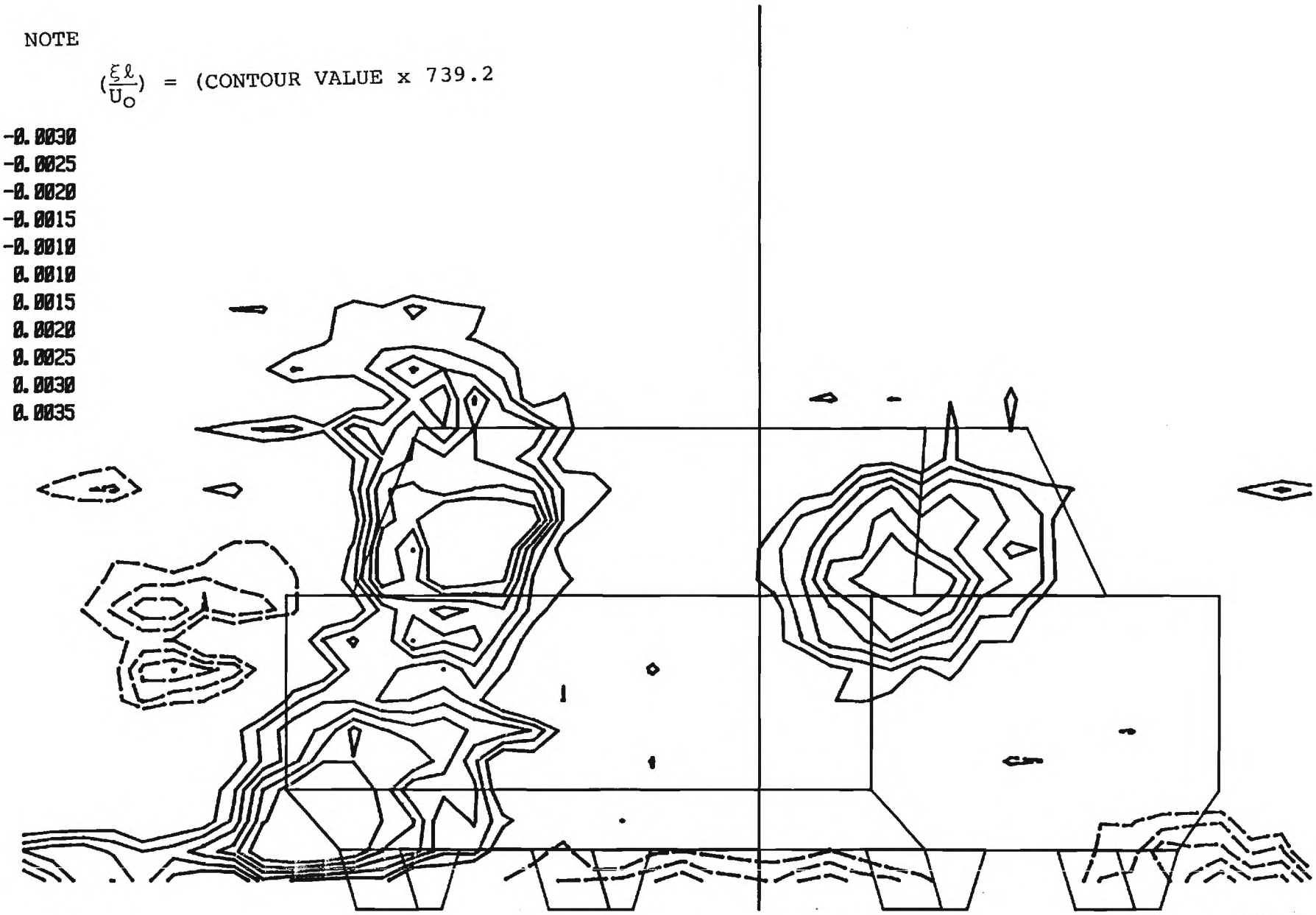

MP77

LOCKHEED-GEORGIA COMPANY - RESEARCH CENTER - TEST 64-Ø8

S. A. S. - 12.5 DEG - 36 INS

CORR LAT VELOCITY V/UO

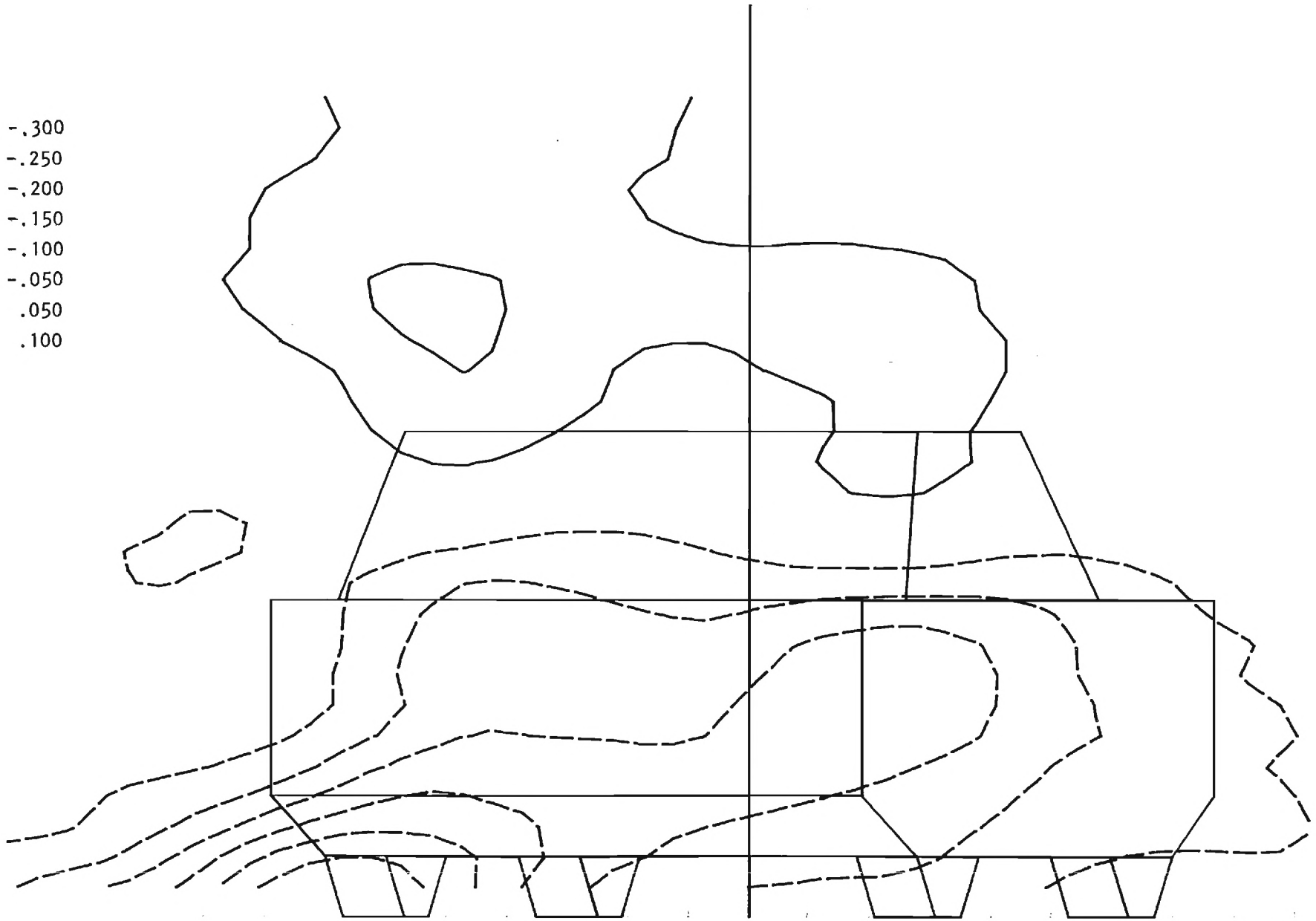

MP78

LOCKHEED-GEORGIA COMPANY - RESEARCH CENTER - TEST 64-08

S. A. S. - 12.5 DEG - 36 INS

CORR VERT VELOCITY W/UO

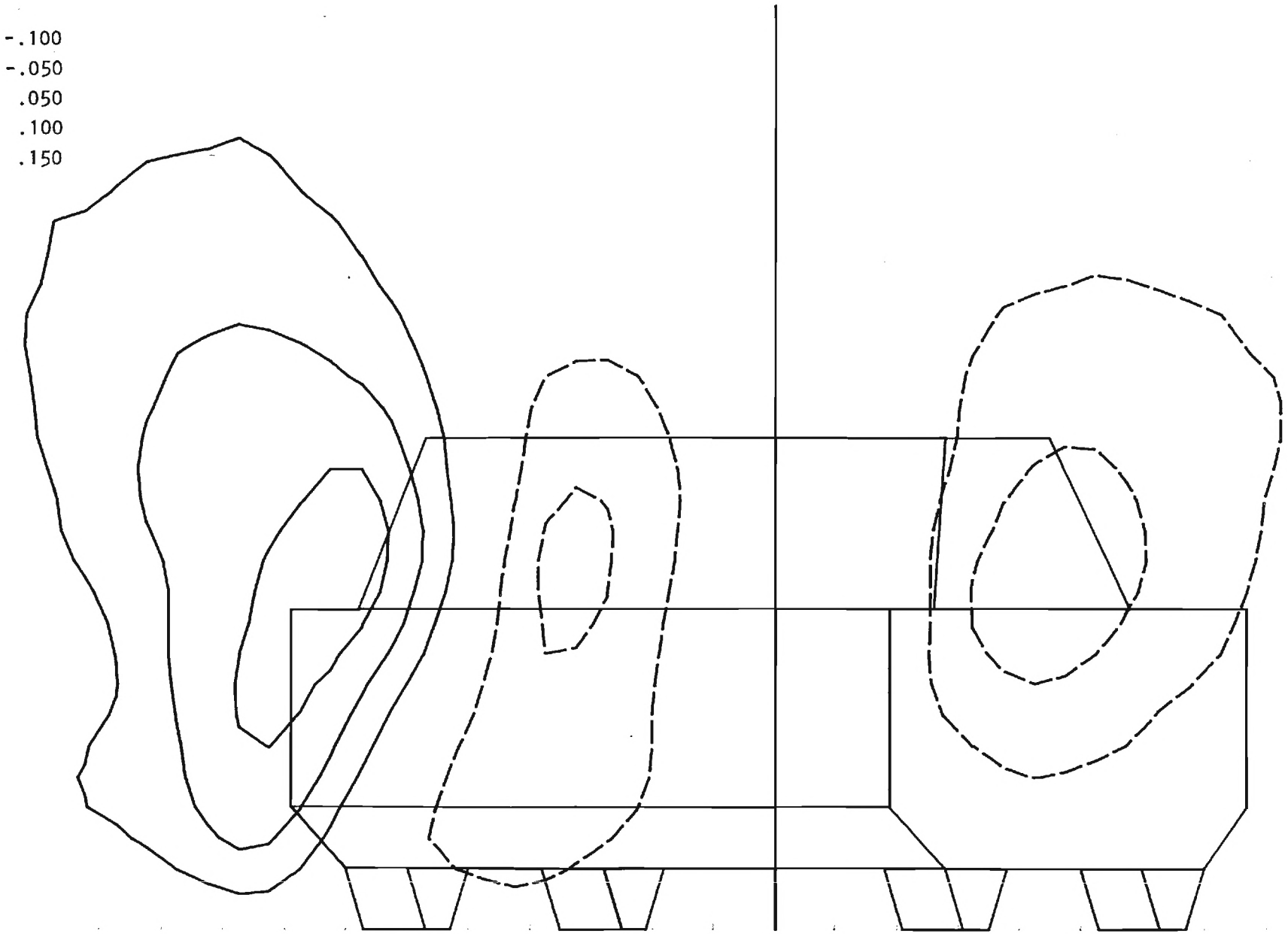

MP79

LOCKHEED-GEORGIA COMPANY - RESEARCH CENTER - TEST 64-Ø8

S. A. S. - 12.5 DEG - 36 INS

STREAM FUNCTIONS

NOTE

$(\frac{\psi}{U_o \ell})$ = (CONTOUR VALUE x 0.7792

where ℓ = wheelbase

0.000
0.010
0.020
0.030
0.040
0.050
0.060
0.070
0.080

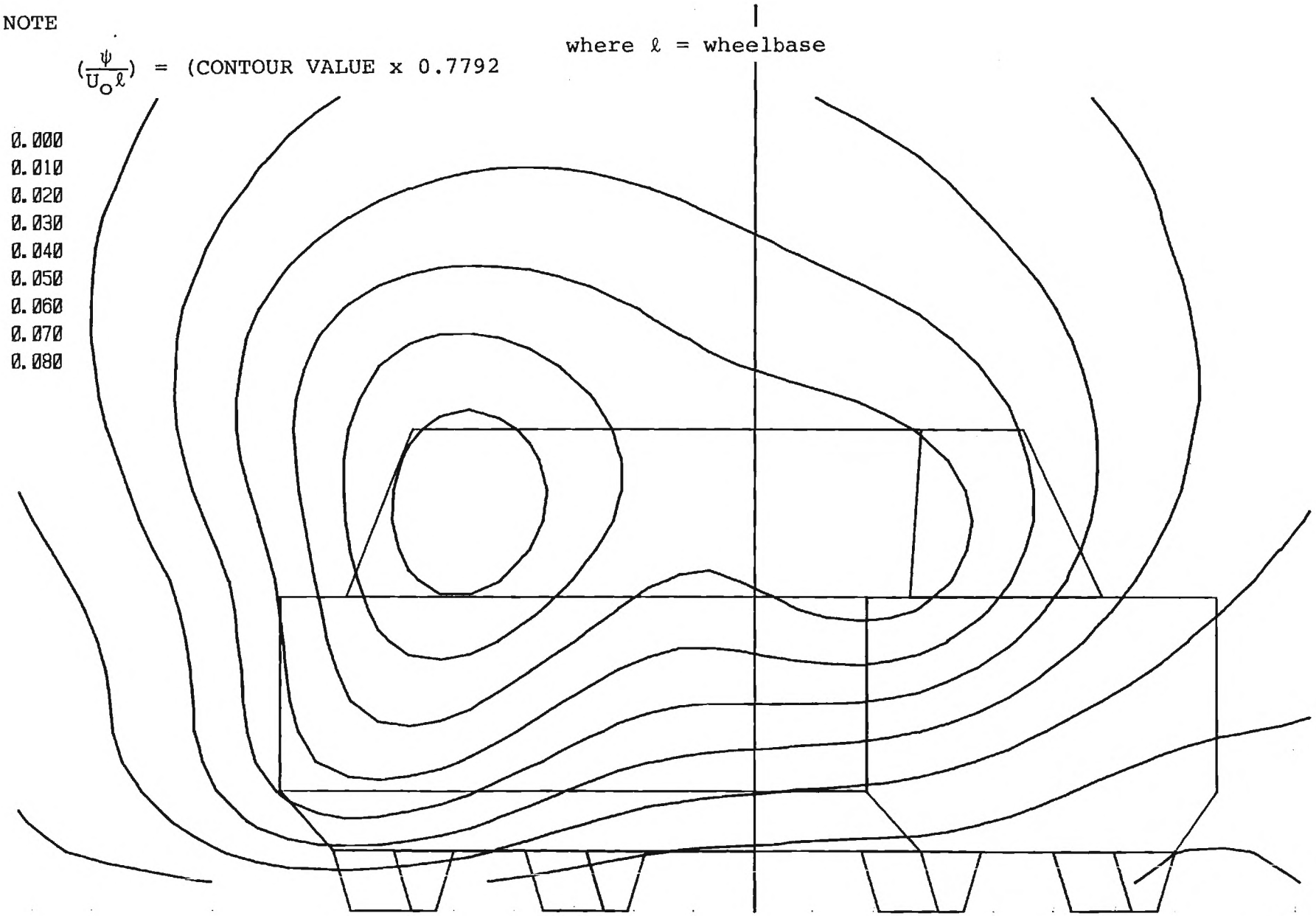

MP80